# lek. Filip Aleksander Garbicz

# Rola kinaz PIM w komórkach nowotworowych i mikrośrodowisku szpiczaka mnogiego

Rozprawa na stopień doktora nauk medycznych i nauk o zdrowiu w dyscyplinie nauki medyczne

Promotor: prof. dr hab. n. med. Przemysław Juszczyński



Obrona rozprawy doktorskiej przed Radą Dyscypliny Nauk Medycznych Warszawskiego Uniwersytetu Medycznego

Warszawa, 2025 r.

**Keywords:** myeloma, plasma cell, PIM, kinase, bone marrow, microenvironment, angiogenesis, vasculogenesis, small-molecule inhibitor

**Słowa kluczowe:** szpiczak, komórka plazmatyczna, PIM, kinaza, szpik kostny, mikrośrodowisko, angiogeneza, waskulogeneza, inhibitor małocząsteczkowy

This work was funded by Diamond Grant (0071/DIA/2016/45) from the Polish Ministry of Science and Higher Education, PRELUDIUM Grant (2018/31/N/NZ5/03214) and ExCELLent Grant edition 2022 supported by PBKM S.A. FamiCord Group.

The author was supported by ETIUDA Grant (2020/36/T/NZ5/00610) and OPUS Grant (2019/35/B/NZ5/02824) from the National Science Centre, Poland, Scholarship for Outstanding Young Scientists (SMN/16/1824/2020) from the Ministry of Education and Science, TEAM Project POIR.04.04.00-00-5C84/17-00 and TEAM-NET Project POIR.04.04.00-00-16ED/18 from the Foundation for Polish Science.

# Filip Aleksander Garbicz, M.D.

# Tumor cell-intrinsic and microenvironmental functions of PIM kinases in multiple myeloma

Dissertation submitted for the degree of

Doctor of Philosophy

in the Discipline of Medical Sciences

Supervisor: Przemysław Juszczyński, M.D., Ph.D.



Ph.D. dissertation presented to the

Medical Sciences Discipline Council of

Medical University of Warsaw



# **Declaration**

I hereby declare that except where specific reference is made to the work of others, the contents of this dissertation are original and have not been submitted in whole or in part for consideration for any other degree or qualification in this, or any other university. This dissertation is my own work and contains nothing which is the outcome of work done in collaboration with others, except as specified in the text and Acknowledgements. The research conducted for this dissertation involving human/animal subjects was carried out in accordance with ethical principles, and all necessary approvals and informed consent were obtained. Any sources, data, or ideas from external sources have been appropriately cited and referenced in accordance with the established academic conventions.

Filip A. Garbicz, M.D.

Warsaw, 2025

# **Acknowledgements**

I would like to express my deepest gratitude to Prof. Przemysław Juszczyński for the opportunity to pursue my PhD in his laboratory. His guidance, critical insight, and unwavering support throughout this project were invaluable. I am especially grateful for the freedom to pursue unconventional ideas, the encouragement to think independently, and the openness to broad institutional and international collaborations that made this work possible. Special thanks go to Prof. Maciej Szydłowski, whose advice, scientific rigor, and calm approach reminded me of the importance of patience, reproducibility, and focusing on the questions that truly matter. I am also thankful to Prof. Ewa Lech-Marańda, Director of the Institute of Hematology and Transfusion Medicine, for her support and for creating an environment that fosters translational research. I sincerely thank all the administrative staff - both at the Institute of Hematology and Transfusion Medicine and Dana-Farber Cancer Institute - whose work behind the scenes allowed me to complete this project smoothly. In particular, I thank Ms. Kamila Kuśmirowicz and Ms. Anna Kaczmarczyk for caring about my projects. I extend my sincere thanks to Prof. Ruben D. Carrasco, Tuyet Nguyen, Tomasz Sewastianik, Prof. Dominika Nowis, Prof. Jakub Gołąb, and Dr. Zofia Pilch for their input and help with *in vivo* work. I also wish to acknowledge Dr. Sonia Debek, Aleksandra Matrejek, Ewa Kurtz, Anna Rams, Paulina Laskowska, Dr. Mateusz Stoszko, and all other members of the Department of Experimental Hematology for their friendship and support. I thank Dr. Anna Szumera-Ciećkiewicz, and Prof. Monika Prochorec-Sobieszek for their expertise and support with myeloma pathology. I thank Dr. Dorota Komar for her constant encouragement, and Prof. Irena Misiewicz-Krzemińska, Dr. Joanna Barankiewicz, Dr. Aleksander Salomon-Perzyński, Dr. Agata Malenda, Prof. Michał Pawlak, and Dr. Marcin Kaszkowiak for insightful discussions. I am also grateful to our collaborators: Dr. Thorsten Stühmer, Dr. Teru Hideshima. Prof. David M. Dorfman. My thanks go to Monika Stańczak, Daria Owczarek, Mei Zhang, Dr. Urszula Bany-Łaszewicz, Magdalena Wojtas, Aleksandra Bluszcz, Agnieszka Krzywdzińska, Beata Krzymieniewska, Sylwia Radomska, and Dr. Eliza Głodkowska-Mrówka for their technical help and collaboration. I would like to thank all the medical staff, patients, and their families whose trust and participation made this research possible. I also thank the Prof. Paweł Włodarski Lab, Dr. Łukasz Hutnik, and Dr. Emir Sajjad, as well as Dr. Krzysztof Brzózka, Dr. Tomasz Rzymski (Ryvu Therapeutics), and Dr. Daniela Bellarosa (Menarini) for sharing valuable tools and insights. I am grateful to the Dana-Farber Cancer Institute Flow Cytometry Core, the Animal Facility of the Department of Immunology, and the Nencki Flow Cytometry Lab for essential experimental support. I thank my lab and office mates for their camaraderie and daily encouragement. On a personal note, I thank my parents, grandparents, sister, and friends for their unconditional support throughout this journey. Thank you to Aleksandra Grabalska and Dr. Magdalena Flaga-Łuczkiewicz for their help, kindness and compassion. I would like to thank Dr. Dawid Mehlich and Dr. Bartłomiej Tomasik for their scientific support and friendship. I am especially grateful to Prof. Tamara Kropiowska, my high school biology teacher, whose passion for science helped shape my path. Finally, I thank my wife, Julia, for her extraordinary patience, strength, and belief in me. Her support was the foundation that carried me through the most demanding phases of this work. I am deeply fortunate to have her by my side.

# **Contents**

i	List of figures	15
ii	List of tables	17
iii	Nomenclature	18
iν	Streszczenie	25
V	Summary	26
1	Introduction	
1	.1 Multiple myeloma: an overview	
	.2 Historical perspective	
	.3 Epidemiology	
	.4 Clinical presentation, diagnosis and treatment	30
1	.5 Treatment strategies	
	1.5.1 Proteasome inhibitors (PIs)	
	1.5.2 Immunomodulatory drugs (IMiDs)	
	1.5.3 Corticosteroids	
	1.5.4 Immunotherapy	
	1.5.5 Hematopoietic cell transplantation	
1	.6 Molecular pathogenesis of MM	
	1.6.1 Primary genetic events	
	1.6.2 Secondary genetic events	
	1.6.3 Subclonal heterogeneity	
	1.6.4 Mutation-generating mechanisms	
_	1.6.5 Clinical implications	
1	.7 Tumor microenvironment (TME)	
	1.7.1 T cells	
	1.7.1.1 Regulatory T cells	
	1.7.1.2 Exhausted and senescent T cells	
	1.7.1.3 Loss of naïve and stem-like T cells	
	1.7.1.4 Thelper cells	
	1.7.1.5 Clinical implications	
	1.7.2 Myeloid cells	
	1.7.2.1 Osteoclasts	
	1.7.2.2 Osteoblasts	
	1.7.2.3 Tumor-associated macrophages (TAMs)	47
	1.7.2.4 Myeloid-derived suppressor cells (MDSCs)	
	1.7.3 Plasmacytoid dendritic cells (pDCs)	
	1.7.4 NK cells	
	1.7.5 Bone marrow stromal cells	
	1.7.6 Endothelial cells	
	1.7.6.1 Origins of BMECs	
	1.7.6.2 BMEC heterogeneity	50
	1.7.6.3 MM-associated BMECs (MMECs)	
	1.7.6.4 Signaling pathways activated in MMECs	
	1.7.6.5 MMECs-mediated support of MM cells	
1	.8 PIM kinases	
	1.8.1 Physiological roles of PIM kinases	57

	1.8.2 PIN	1-dependent signaling	58
	1.8.2.1	JAK/STAT	58
	1.8.2.2	MYC	59
	1.8.2.3	NF-ĸB	59
	1.8.2.4	PI3K/AKT/mTOR	59
	1.8.2.5	MAPK	
	1.8.2.6	Cell cycle	60
	1.8.2.7	Role of PIM kinases in hematologic malignancies	61
	1.8.3 PIN	/I kinases in MM	
		A kinase inhibitors	
	1.9 Need	for further research	67
	1.10 Object	ctives of this thesis	68
2	Materials	and methods	69
	2.1 Mater	rials	69
	2.1.1 Cel	I lines and bacterial strains	69
	2.1.1.1	Human cell lines	69
	2.1.1.2	Primary cells	70
	2.1.1.3	Bacterial strains	70
	2.1.1.4	Genetically modified cell lines	70
	2.1.2 Ch	emicals and reagents	71
	2.1.2.1	Chemicals	71
	2.1.2.2	Kits	73
	2.1.3 But	fers and solutions	74
	2.1.4 Cel	I culture media and additives	81
	2.1.5 Nu	cleic acids	82
	2.1.5.1	5	
	2.1.5.2	Oligonucleotides for qPCR	83
	2.1.5.3		
		ibodies	
		nsumables	
	•	uipment	
		tware	
	2.2 Metho		
		I biology techniques	
	2.2.1.1		
	2.2.1.2	·	
		Lentivirus production and infection	
	2.2.1.4	Fluorescence microscopy	
	2.2.1.5	Flow cytometry	
	2.2.1.6	Isolation of cells from bone marrow aspiration biopsies	
	2.2.1.7	Magnetic sorting and culture of primary MM cells	
	2.2.1.8	Magnetic sorting and culture of primary MMECs and HD ECs	98
	2.2.1.9	Proliferation and viability assays by flow cytometry	
		MTS cell proliferation assay	
		Annexin V-based apoptosis assay	
		2 Caspase-Glo luminescent assay	
	2.2.1.13	B Cellular Thermal Shift Assay (CETSA)	101

	2.2.1.14	Comet assay	. 101
	2.2.1.15	Wound healing (scratch) assay	. 102
		Tube formation assay	
		Phalloidin-AF488 labeling of F-actin	
		Actin fractionation	
		RhoA GTPase activation assay	
		Conditioned media collection	
		Cell cycle analysis by Hoechst 34580 staining	
		ecular biology methods	
	2.2.2.1	Production of chemocompetent bacteria	. 105
		Transformation of competent bacteria with plasmid DNA and plasr	
		tion	
		Bacterial cryopreservation	
		Small-scale isolation of plasmid DNA from bacteria (Miniprep)	
		Large-scale isolation of plasmid DNA from bacteria (Maxiprep)	
		Restriction enzyme digestion	
		Gel electrophoresis separating DNA fragments	
		Extraction and purification of DNA fragments	
		Ligation of DNA fragments into plasmids	
		Colony PCR	
		Sanger sequencing	
		Cloning	
		Concentration quantification of nucleic acids	
		Mammalian cell RNA isolation	
		Complementary DNA (cDNA) synthesis	
		Quantitative real-time PCR (qPCR)	
		RNA-seq library preparation	
		ein biochemical methods	
		Quantification of protein using colorimetric methods	
		SDS-Polyacrylamide Gel Electrophoresis (SDS-PAGE) and weste	
		120	
		Immunohistochemistry	121
		ne studies	
		putation and data analysis	
		Statistical analysis	
		RNAseq data analysis	
		ChIPseq data analysis	
		scRNAseq data analysis	
3		of PIM kinases in multiple myeloma cells	
_		nase overexpression is essential for MM growth	
J		SPR/Cas9 cancer dependency screens identify PIM kinases as crit	
		in multiple myeloma	
		1/2/3 levels in healthy human and murine tissues	
		mRNA expression levels in MM and normal plasma cells	
		iomic datasets link PIM expression to specific MM-related features	
		staining and quantification of PIM1, PIM2 and PIM3 protein levels	
	iviivi and ne	althy bone marrow	. 134

		PIM kinase expression is linked to MM patient survival	
	3.2 S	Super-enhancer-mediated control of PIM expression in malignant plasma	1
		39	
		Pharmacological targeting of PIM kinases in MM	
	3.3.1	Systematic drug screening of pan-PIM inhibitors reveals heterogeneous	S
	sensit	tivity	.143
	3.3.2	MEN1703 sensitivity is associated with MYC-driven transcriptional	
	progra	ams	
		MEN1703 induces apoptosis in MM cell lines	
		MEN1703 induces apoptosis in primary MM cells	
	3.3.5	Time-course analysis reveals sustained anti-myeloma activity of MEN1 149	703
	3.3.6	Differential PIM2 engagement does not explain the superior cytotoxic	
		ty of MEN1703	
	3.4 C	Genetic silencing of PIM kinase expression in MM	. 151
		PIM2 is the dominant PIM family member supporting MM cell proliferation	
	and m	nTOR activity	.151
		Simultaneous silencing of PIM1, PIM2, and PIM3 results in more poten	
	anti-M	/IM effects	. 154
		ranscriptional and functional effects of pan-PIM inhibition in MM	
		MEN1703 suppresses MYC- and E2F-driven transcriptional programs a	
		ates stress responses	
		MEN1703 suppresses DNA repair gene networks	
		n vivo validation of MEN1703 efficacy in a disseminated MM model	
_		PIM inhibition synergizes with proteasome inhibition in MM	
4		tions of PIM kinases in MM microenvironment	
		Stromal expression of PIM kinases in MM bone marrow	
		Factors influencing PIM expression in MMECs	
		ranscriptional and functional consequences of pan-PIM inhibition in ECs	
		PIM kinase inhibition impairs angiogenic functions of ECs	
		Transcriptomic response to PIM kinase inhibition in ECs	
		MEN1703 reverses the MM-associated EC transcriptional state	
		PIM inhibition disrupts actin cytoskeletal architecture in ECs	
		Establishment of BM EC isolation and culture conditions	
_		nvestigation of MM-EC crosstalk in vitro	
5		lusions	
		Main results	
		PIMs in MM	
		PIMs in ECs	
		mpact	
		Discussion	
		imitations	
•		Outlook	
3 7		ences	
1		ndix Bioethical committee approval	
	7.1 E	ภบธนาเงลา งงเททแนธธ สมุมเงขลา	. ZZ4

# i List of figures

Figure number and title	Page
Fig. 1. Histopathologic features of MM cells.	28
Fig. 2. Clinical manifestations of MM.	31
Fig. 3. Diagnostic criteria for multiple myeloma, myeloma variants, and	
monoclonal gammopathy of unknown significance.	32
Fig. 4. Cytogenetic abnormalities and risk stratification in MM.	33
Fig. 5. Double IHC staining of multiple myeloma bone marrow sections.	51
Fig. 6. Vessel density in normal BM, MGUS and MM.	52
Fig. 7. Strategy for generation of single and triple PIM shRNA-expressing cells.	115
Fig. 8. Genome-wide CRISPR/Cas9 dropout screens identify genes	
preferentially essential for multiple myeloma cells compared to other types of	400
cancer.	128
Fig. 9. PIM1/2/3 expression levels across different levels of B cell maturation	129
Fig. 10. The distribution of PIM kinase mRNA expression in healthy human	120
tissues.	130
Fig. 11. PIM kinase expression in multiple myeloma patients, cell lines, and	131
normal plasma cells. Fig. 12. PIM expression across MM progression stages.	133
Fig. 13. Bulk RNA-seg analysis of <i>PIM</i> kinase gene expression during MM	100
progression.	134
Fig. 14. IHC optimization.	135
Fig. 15. Immunohistochemical analysis of PIM1/2/3 in healthy vs. newly	100
diagnosed MM bone marrow.	136
Fig. 16. Prognostic significance of <i>PIM1</i> , <i>PIM2</i> , and <i>PIM3</i> expression in MM	
from the MMRF CoMMpass cohort.	138
Fig. 17. Univariate and multivariate Cox regression analysis of overall survival	
in the MMRF CoMMpass cohort.	139
Fig. 18. Super-enhancer H3K27ac load at PIM loci in normal plasma cells, MM	
patient samples, and MM cell lines.	140
Fig. 19. H3K27ac ChIP-seq signal tracks.	142
Fig. 20. Effect of JQ1 treatment on PIM gene and MYC mRNA levels in MM1.S	
cells.	143
Fig. 21. Sensitivity of multiple myeloma cell lines to pan-PIM kinase inhibitors.	144
Fig. 22. Relationship between FLT3 expression and MEN1703 sensitivity in	
MM cell lines.	145
Fig. 23. Hallmark gene set enrichment analysis (GSEA) comparing resistant	4.40
versus sensitive multiple myeloma cell lines.	146
Fig. 24. MEN1703 induces apoptosis in MM cell lines.	147
Fig. 25. MEN1703 induces caspase activation in MM cells.	148
Fig. 26. Sensitivity of primary MM cells to MEN1703 and PIM447.	149
Fig. 27. Time-course analysis of PIM inhibitor efficacy in MM and DLBCL cell lines.	150
Fig. 28. Cellular thermal shift assay (CETSA) for assessment of target	130
engagement of PIM2 by MEN1703 and PIM447 in MM cells.	151
Fig. 29. Selective knockdown of individual PIM kinases reveals dominant role	101
of PIM2 in MM cell proliferation and S6 phosphorylation.	153
Fig. 30. Combined silencing of <i>PIM1</i> , <i>PIM2</i> , and <i>PIM3</i> impairs proliferation and	.00
induces cell death in MM cells.	155

Fig. 31. Transcriptomic effects of MEN1703 in MM1.S cells.	157
Fig. 32. MEN1703 reduces MYC, E2F1 and phosphorylation of S6 in MM1.S	
cells.	158
Fig. 33. MEN1703 downregulates DNA repair pathways and key repair genes	
in MM1.S cells.	159
Fig. 34. PIM inhibition induces DNA damage in MM cells.	160
Fig. 35. In vivo study design to assess MEN1703 activity in MM1.S-luc model.	161
Fig. 36. MEN1703 suppresses MM progression in vivo.	162
Fig. 37. MEN1703 decreases S6 phosphorylation in MM cells in vivo.	163
Fig. 38. MEN1703 synergizes with bortezomib in JJN3 cells.	164
Fig. 39. PIM1 and PIM3 protein expression in non-PC bone marrow cells.	165
Fig. 40. scRNA-seq analysis of PIM kinase expression in the multiple myeloma	
(MM) microenvironment.	166
Fig. 41. Cell type-specific expression of <i>PIM1</i> , <i>PIM2</i> , and <i>PIM3</i> in the MM	
stromal compartment.	167
Fig. 42. PIM1 and PIM3 are highly expressed in the MM vascular niche.	167
Fig. 43. IHC quantification of PIM1/2/3 in HD and MMECs.	168
Fig. 44. The effect of VEGFA stimulation of HUVEC-TERT2 cells on PIM	
kinase expression.	168
Fig. 45. PIM3 kinase expression in HUVEC-TERT2 cells stimulated with	
proangiogenic cytokines.	169
Fig. 46. PIM3 protein is upregulated in HUVEC-TERT2 cells by MM-derived	
conditioned medium (CM).	169
Fig. 47. MEN1703 impairs angiogenic functions of HUVEC-TERT2 endothelial	
cells without inducing apoptosis.	170
Fig. 48. Transcriptomic response to PIM kinase inhibition in HUVEC-TERT2	
cells.	171
Fig. 49. PIM inhibition with MEN1703 reverses the MMEC transcriptional	
signature.	173
Fig. 50. PIM inhibition disrupts actin cytoskeletal architecture and RhoA	
signaling in endothelial cells.	174
Fig. 51. Isolation and characterization of endothelial progenitor cells (EPCs)	
and mature endothelial cells (ECs) from bone marrow of MM patients.	176
Fig. 52. Characterization of endothelial and stromal cell populations and their	
influence on MM cell proliferation.	178
Fig. 53. BMEC-derived conditioned media induces PIM2 expression in MM1.S	
cells.	179
Fig. 54. PIM inhibition suppresses MMEC-mediated paracrine support of MM	
cell survival.	180

# ii List of tables

Table number and title	Page
Table 1. Key compounds targeting the PIM kinase family that have advanced	
to late-stage preclinical or clinical studies.	66
Table 2. Mammalian cell lines used in this thesis.	69
Table 3. Primary cells used in this thesis.	70
Table 4. Bacterial strains used in this thesis.	70
Table 5. Genetically modified mammalian cell lines used in this thesis.	70
Table 6. Chemicals and reagents used in this study.	71
Table 7. Kits used in this study.	73
Table 8. Compositions of buffers and solutions used in this study.	74
Table 9. Cell culture media and additives used in this study.	81
Table 10. Oligonucleotide sequences used for cloning, colony PCR and	
Sanger sequencing.	82
Table 11. Oligonucleotide sequences used for qPCR.	83
Table 12. Plasmids used in this study.	84
Table 13. Antibodies used in this study.	86
Table 14. Consumables used in this study.	88
Table 15. Machines and instruments used in this study.	89
Table 16. Software used in this study.	90
Table 17. Plasmids used for lentiviral production.	95
Table 18. DNA ligation setup.	110
Table 19. BigDye sequencing reaction composition.	111
Table 20. BigDye thermal cycling protocol.	112
Table 21. Reaction components for phosphorylation and annealing of	
oligonucleotides.	113
Table 22. Reaction conditions for phosphorylation and annealing of	
oligonucleotides.	113
Table 23. Reaction components for vector DNA dephosphorylation with	
FastAP.	114
Table 24. Antibiotic concentrations used in this study for JJN3 cells.	116
Table 25. Reverse transcription reaction components.	118
Table 26. Reverse transcription reaction thermal cycling protocol.	118
Table 27. qPCR thermal cycling protocol.	119
Table 28. MMEC gene signature extracted from Garbicz et al. [221].	173

## iii Nomenclature

**7-AAD** - 7-Aminoactinomycin D

**4EBP1** - Eukaryotic translation initiation factor 4E-binding protein 1

2B4 - CD244 (natural killer cell receptor)

#### <u>A</u>

ADCC - Antibody-dependent cellular cytotoxicity

AID - Activation-induced cytidine deaminase

AGM - Aorta-gonad-mesonephros

AKT - AKT serine/threonine kinase

AMDR - Adhesion-mediated drug resistance

ANGPT2 (Ang-2) - Angiopoietin-2

Ang-1 - Angiopoietin-1

APOBEC - Apolipoprotein B mRNA editing enzyme catalytic polypeptide

APOBEC3B - Apolipoprotein B mRNA editing enzyme catalytic polypeptide 3B

**APRIL** - A Proliferation-Inducing Ligand (TNFSF13)

ARG1 - Arginase-1

**ASK1** - Apoptosis Signal-Regulating Kinase 1 (MAP3K5)

ATR - Ataxia telangiectasia and Rad3-related

auto-HCT - Autologous hematopoietic cell transplantation

#### <u>B</u>

BAD - BCL2-Associated Agonist of Cell Death

BCL2 - B-cell lymphoma 2

BCL6 - B-cell lymphoma 6

BCL-xL - BCL-extra large

**BCMA** - B-cell maturation antigen

BCR - B-cell receptor

**BFU-E** - Burst-forming unit-erythroid

**BIM** - BCL2-interacting mediator of cell death

**BLI** - Bioluminescence imaging

**BM** - Bone marrow

BMECs - Bone marrow endothelial cells

**BMSCs** - Bone marrow stromal cells

BRAF - v-Raf murine sarcoma viral oncogene homolog B1

**BTK** - Bruton tyrosine kinase

#### C

CAM-DR - Cell adhesion-mediated drug resistance

**CAR T-cells** - Chimeric antigen receptor T cells

CCL3 - C-C motif chemokine ligand 3

CD4 - Cluster of differentiation 4

**CD8** - Cluster of differentiation 8

CD11a/CD18 - LFA-1 (lymphocyte function-associated antigen-1)

CD16 – Cluster of differentiation 16, Fc Gamma Receptor IIIa (FCGR3A)

**CD18** - Integrin β2 (part of LFA-1)

CD20 - Cluster of differentiation 20

**CD25** - IL-2 receptor  $\alpha$  chain

CD27 - Cluster of differentiation 27

CD28 - Cluster of differentiation 28

**CD31** - PECAM-1

CD34 - Hematopoietic/endothelial progenitor marker

CD38 - Cluster of differentiation 38

CD40 - Tumor necrosis factor receptor superfamily member 5

CD40L (CD154) - CD40 ligand

CD44 - Homing/adhesion receptor

CD57 - HNK-1 (NK/T-cell marker)

CD105 - Endoglin

CD138 - Syndecan-1 (plasma cell marker)

CD144 - VE-cadherin

**CD147** - Basigin (EMMPRIN)

CD160 - Immunoglobulin-like activating receptor

**CD163** - Scavenger receptor on macrophages

CD200 - OX-2 membrane glycoprotein

CD206 - Mannose receptor (MRC1)

CDC25 - Cell division cycle 25 phosphatase

**CETSA** - Cellular thermal shift assay

CFU-GEMM - Colony-forming unit-granulocyte, erythrocyte, macrophage, megakaryocyte

CFU-GM - Colony-forming unit-granulocyte, macrophage

CLL - Chronic lymphocytic leukemia

**CM** - Conditioned medium

**CRAB** - HyperCalcemia, Renal failure, Anemia, Bone lesions (MM features)

**CRBN** – Cereblon

**CRS** - Cytokine release syndrome

**CSR** - Class-switch recombination

**CT** - Computed tomography

CTLA-4 - Cytotoxic T-lymphocyte-associated protein 4

**CXCL8** - C-X-C motif chemokine ligand 8 (IL-8)

**CXCR3** - C-X-C chemokine receptor 3

**CYLD** - Cylindromatosis (deubiquitinase)

#### D

DC - Dendritic cell

**DDR** - DNA damage response

**ddH2O** - Double-distilled water

**DKK1** - Dickkopf-1

**DLBCL** - Diffuse large B-cell lymphoma

**DIS3** - RNA exosome catalytic subunit

**DMSO** - Dimethyl sulfoxide

**DOX** - Doxycycline

**DSBs** - Double-strand breaks

#### <u>E</u>

E2F1 - E2F transcription factor 1

EC - Endothelial cell

**ECM** - Extracellular matrix

**EGF** - Epidermal growth factor

EHT - Endothelial-to-hematopoietic transition

eIF4B - Eukaryotic translation initiation factor 4B

eIF4E - Eukaryotic translation initiation factor 4E

eCyPA - Extracellular cyclophilin A

EMT - Epithelial-to-mesenchymal transition

**EOC** - Early outgrowth endothelial cell

**EPC** - Endothelial progenitor cell

**ER** - Endoplasmic reticulum

**ERAD** - ER-associated degradation

**ERMM** - Early-relapse multiple myeloma

#### F

F-actin - Filamentous actin

FAM46C - Family with sequence similarity 46 member C

FDR - False discovery rate

**FGF2** - Fibroblast growth factor 2

**FGFR3** - Fibroblast growth factor receptor 3

FL - Follicular lymphoma

FLC - Free light chain

FLT3-ITD - Fms-like tyrosine kinase 3, internal tandem duplication

FOXO1 - Forkhead box O1

FOXO3 - Forkhead box O3

FOXP3 - Forkhead box P3 (Treg factor)

#### G

G-actin - Globular actin

**GEP** - Gene expression profiling

GC - Germinal center

GI<sub>50</sub> - Growth-inhibitory concentration 50%

**GM-CSF** - Granulocyte-macrophage colony-stimulating factor

**GPRC5D** - G protein-coupled receptor class C group 5 member D

**GR** - Glucocorticoid receptor

**GSEA** - Gene set enrichment analysis

#### Н

H3K27ac - Histone H3 lysine 27 acetylation

**HD** - Healthy donor

**HE** - Hemogenic endothelium

**HGF** - Hepatocyte growth factor

HIF-1α - Hypoxia-inducible factor 1 alpha

HIV - Human immunodeficiency virus

```
HSPCs - Hematopoietic stem and progenitor cells
IC<sub>50</sub> - Inhibitory concentration 50%
ICANS - Immune effector cell-associated neurotoxicity syndrome
ICAM-1 - Intercellular adhesion molecule-1
IFN-γ - Interferon-gamma
IGF1 - Insulin-like growth factor 1
IgG - Immunoglobulin G
IgM - Immunoglobulin M
IgL - Immunoglobulin light chain lambda
IGH - Immunoglobulin heavy chain locus
IKZF1 - Ikaros zinc finger protein 1
IKZF3 (Aiolos) - Ikaros zinc finger protein 3
IL-1β - Interleukin-1 beta
IL-2 - Interleukin-2
IL-6 - Interleukin-6
IL-7 - Interleukin-7
IL-8 - Interleukin-8 (CXCL8)
IL-10 - Interleukin-10
IL-10R - Interleukin-10 receptor
IL-12 - Interleukin-12
IL-17 - Interleukin-17
IMiDs - Immunomodulatory drugs
IMWG - International Myeloma Working Group
ING4 - Inhibitor of growth family member 4
IRF4 - Interferon regulatory factor 4
IV - Intravenous
JAK - Janus kinase
JAK1/2 - Janus kinase 1 / Janus kinase 2
JAM-A - Junctional adhesion molecule A
KDM1A - Lysine-specific demethylase 1A
KIRs - Killer immunoglobulin-like receptors
KLRG-1 - Killer cell lectin-like receptor subfamily G member 1
KRAS - Kirsten rat sarcoma viral oncogene homolog
LAG-3 - Lymphocyte-activation gene 3
LC<sub>50</sub> - Lethal concentration 50%
LEPR - Leptin receptor
LFA-1 - Lymphocyte function-associated antigen-1 (CD11a/CD18)
```

**HLA-I** - Human leukocyte antigen class I

**HSC** - Hematopoietic stem cell

LRP5/6 - Low-density lipoprotein receptor-related protein 5/6

**LRMM** - Late-relapse multiple myeloma

#### M

MAF - Musculoaponeurotic fibrosarcoma oncogene

MAFB - Musculoaponeurotic fibrosarcoma oncogene B

MAPK - Mitogen-activated protein kinase

MCH - Mean corpuscular hemoglobin

MCL - Mantle cell lymphoma

MCL1 - Myeloid cell leukemia 1

MCV - Mean corpuscular volume

**MDSCs** - Myeloid-derived suppressor cells

MGUS - Monoclonal gammopathy of undetermined significance

MM - Multiple myeloma

**MMP** - Matrix metalloproteinase

MMP-2 - Matrix metalloproteinase-2

MMP-9 - Matrix metalloproteinase-9

MMECs - MM-associated bone marrow endothelial cells

**MOMP** - Mitochondrial outer membrane permeabilization

MRI - Magnetic resonance imaging

MRD - Minimal residual disease

MSC - Mesenchymal stromal cell

mSMART - Mayo Stratification of Myeloma and Risk-Adapted Therapy

mTOR - Mechanistic target of rapamycin

mTORC1 - Mechanistic target of rapamycin complex 1

**MVD** - Microvessel density

MYC - MYC proto-oncogene

#### N

NDMM - Newly diagnosed multiple myeloma

**NES** - Normalized enrichment score

NF-κB - Nuclear factor kappa-B

**NG2** - Neural/glial antigen 2 (CSPG4)

NK cells - Natural killer cells

**NO** - Nitric oxide

NRAS - Neuroblastoma RAS viral oncogene homolog

**NSD2** - Nuclear receptor-binding SET domain protein 2

#### О

OLC - Osteolineage cells

**OPG** - Osteoprotegerin

**OPN** - Osteopontin

#### P

PCA - Principal component analysis

PC - Plasma cell

PD-1 - Programmed cell death-1

PD-L1 - Programmed death-ligand 1

**PET-CT** - Positron emission tomography-computed tomography

**PFS** - Progression-free survival

PI3K/AKT - Phosphoinositide 3-kinase/AKT pathway

PI - Proteasome inhibitor

PIM - Proviral integration site for Moloney murine leukemia virus kinases

PIM TKO - PIM triple knockout

PMBCL - Primary mediastinal B-cell lymphoma

**PO** - *Per os* (oral)

pPCL - Primary plasma cell leukemia

**PSGL-1** - P-selectin glycoprotein ligand-1

PUMA - p53-upregulated modulator of apoptosis

p70S6K - Ribosomal protein S6 kinase beta-1

#### Q

**QD** - *Quaque die* (once daily)

**qPCR** - Quantitative real-time polymerase chain reaction

#### R

RANK/RANKL - Receptor activator of NF-κB / its ligand

**RAS** - Rat sarcoma family of small GTPases

**RB1** - Retinoblastoma 1

RhoA - Ras homolog family member A

**RISS** - Revised International Staging System (for MM)

RNA-seq - RNA sequencing

**ROS** - Reactive oxygen species

RRMM - Relapsed/refractory multiple myeloma

**RUNX2** - Runt-related transcription factor 2

#### S

Sca-1 - Stem cell antigen-1

**SCF** - Stem cell factor (KIT ligand)

SDF-1 - Stromal cell-derived factor-1 (CXCL12)

**SELP** - P-selectin gene (Selectin P)

**SHM** - Somatic hypermutation

**SKP2** - S-phase kinase-associated protein 2

SMM - Smoldering multiple myeloma

SP - Solitary plasmacytoma

**STAT3** - Signal transducer and activator of transcription 3

#### Τ

**TAM** - Tumor-associated macrophage(s)

**TCEs** - T-cell engagers

TCF1 - T-cell factor 1 (TCF7)

TCR - T-cell receptor

**TGF-β** - Transforming growth factor beta

Th1 - T helper 1

Th2 - T helper 2

**Th17** - T helper 17

**TIGIT** - T cell immunoreceptor with Ig and ITIM domains

TIM-3 - T cell immunoglobulin and mucin domain-3

TLR - Toll-like receptor

TME - Tumor microenvironment

TNF-α - Tumor necrosis factor alpha

**TP53** - Tumor protein p53

**TRAF3** - TNF receptor-associated factor 3

**Treg** - Regulatory T cell

**TSC1** - Tuberous sclerosis complex 1

**TSC2** - Tuberous sclerosis complex 2

#### U

UPR - Unfolded protein response

**UPS** - Ubiquitin-proteasome system

#### <u>V</u>

VCAM-1 - Vascular cell adhesion molecule-1

VE-Cadherin - Vascular endothelial cadherin

**VEGF** - Vascular endothelial growth factor

**VEGFA** - Vascular endothelial growth factor A

**VEGFB** - Vascular endothelial growth factor B

VEGFR1 - Vascular endothelial growth factor receptor 1

**VEGFR2** - Vascular endothelial growth factor receptor 2

VGPR - Very good partial response

VLA-4 - Very late antigen-4 (integrin  $\alpha 4\beta 1$ )

VLA-5 - Very late antigen-5 (integrin  $\alpha$ 5 $\beta$ 1)

#### W-Z

WCE - Whole-cell extract

Wnt - Wingless/INT signaling pathway

**ZNF683** - Zinc finger protein 683 (Hobit)

# iv Streszczenie

# Rola kinaz PIM w komórkach nowotworowych i mikrośrodowisku szpiczaka mnogiego

lek. Filip A. Garbicz

Szpiczak mnogi (MM, ang. Multiple myeloma) to nieuleczalny nowotwór komórek plazmatycznych, którego rozwój zależy od złożonych interakcji genetycznych i mikrośrodowiskowych. Celem pracy była analiza funkcji kinaz PIM zarówno w samych komórkach nowotworowych, jak i w ich środowisku szpiku kostnego. Analizy transkryptomiczne, proteomiczne oraz na poziomie pojedynczych komórek wykazały nadekspresję PIM1, PIM2 i PIM3 w MM, z dominującą rolą PIM2. Wysoka ekspresja kinaz PIM korelowała z gorszym rokowaniem i zaawansowaną chorobą. Badania funkcjonalne wykazały, że farmakologiczna inhibicja kinaz PIM związkami takimi jak MEN1703 prowadziła do apoptozy i zahamowania proliferacji komórek MM zarówno in vitro, jak i in vivo. Efekty te zostały potwierdzone również po jednoczesnym wyciszeniu wszystkich trzech paralogów PIM. Inhibicja PIM zmniejszała aktywność czynników transkrypcyjnych MYC i E2F1, hamowała mTOR oraz zaburzała procesy naprawy DNA. Co istotne, MEN1703 zachowywał skuteczność w obecności komórek zrębowych i działał synergistycznie z inhibitorami proteasomu. Badania wykazały również znaczenie PIM w komórkach śródbłonka szpiku chorych na MM. Komórki te wykazywały wysoką ekspresję PIM1 i PIM3. Inhibicja PIM zaburzała ich funkcje angiogenne, organizację cytoszkieletu oraz sygnalizację parakrynną wspierającą komórki nowotworowe. Wyniki pracy wskazują kinazy PIM jako obiecujące cele terapeutyczne w MM. Jednoczesne działanie na komórki nowotworowe i ich mikrośrodowisko może stanowić podstawę do opracowania nowych strategii terapeutycznych. Uzyskane dane stanowią podstawę do dalszego rozwoju terapii celowanych przeciwko PIM oraz projektowania badań klinicznych z uwzględnieniem biomarkerów i strategii skojarzonych.

# v Summary

# Tumor cell-intrinsic and microenvironmental functions of PIM kinases in multiple myeloma

Filip A. Garbicz, M.D.

Multiple myeloma (MM) is a plasma cell malignancy driven by complex genetic and microenvironmental interactions, for which there is currently no cure. This thesis investigates the dual role of PIM kinases in MM biology - within malignant plasma cells and their bone marrow niche. Transcriptomic, proteomic, and single-cell analyses demonstrated that PIM1, PIM2, and PIM3 are overexpressed in MM, with PIM2 being the most dominant paralog. High PIM expression correlated with adverse prognosis. Functional studies revealed that pharmacologic inhibition of PIMs with the small-molecule compound MEN1703 induced apoptosis and suppressed proliferation of MM cells in vitro and in vivo, including patient-derived samples. Genetic knockdown of all three PIMs recapitulated these findings, confirming their essential role in myeloma cell survival. Mechanistically, PIM inhibition impaired MYC and E2F1 transcriptional programs, reduced mTOR activity, and suppressed multiple DNA repair pathways. Importantly, MEN1703 retained its efficacy in the presence of stromal cells and synergized with proteasome inhibition. This study also identifies a tumor-extrinsic role of PIMs in MM endothelial cells (MMECs). MMECs expressed high levels of PIM1 and PIM3. MEN1703 treatment disrupted angiogenic function, actin cytoskeleton dynamics, and tumorsupportive signaling in ECs. Blocking PIMs in ECs also diminished their paracrine support of myeloma cells. Together, these results support PIM kinases as actionable targets in MM. Combined inhibition of PIM activity in both tumor and stromal compartments may represent a rational therapeutic strategy. These findings support the clinical development of PIM-targeting therapies and open future directions including biomarker-driven patient stratification and rational combination regimens in MM.

# 1 Introduction

## 1.1 Multiple myeloma: an overview

Multiple myeloma (MM) is a hematological malignancy characterized by the accumulation of a clonal plasma cell population in the bone marrow (Fig. 1). It is the second most common blood cancer after non-Hodgkin lymphoma [1]. Although the disease primarily involves the bone marrow, advanced MM is able to spread to the peripheral blood, soft tissues and organs [2]. MM belongs to a broader group of plasma cell dyscrasias, a term encompassing a spectrum of conditions involving plasma cells, including solitary plasmacytoma of bone [3], extraosseous plasmacytoma [4], light chain amyloidosis [5], monoclonal light and heavy chain deposition diseases [6,7], osteosclerotic myeloma [8], and MM itself. A defining feature of multiple myeloma is the production of a monoclonal immunoglobulin (M protein) by the malignant plasma cells. Most cases involve M protein production, although some patients only produce monoclonal free light chains, and a small subset (<3%) are non-secretory [9]. The clinical manifestations of MM result from both the effects of monoclonal protein and malignant plasma cells, leading to hypercalcemia, kidney dysfunction, anemia, and bone disease with lytic lesions or pathological fractures, collectively known as the CRAB criteria (calcium elevation, renal failure, anemia, and bone lesions). MM is typically preceded by monoclonal gammopathy of undetermined significance (MGUS) [10], a precursor state defined by the presence of clonal plasma cells in the bone marrow and M protein production but no CRAB features. MGUS can evolve into MM or related disorders over time. Traditionally, MM treatment was initiated at the time of CRAB symptoms detection. However, with the discovery of biomarkers that identify high risk of disease progression, the diagnostic criteria have been updated to allow earlier treatment initiation in some cases [11]. Over the past decade, major progress has been made in understanding and treating plasma cell dyscrasias, including insights into disease biology, the development of more effective therapies, and genomic studies revealing MM as a spectrum of diseases with a shared clinical presentation [12]. Despite these advances, new treatment strategies targeting MM vulnerabilities are still needed to improve patient outcomes and transform MM from a treatable to a curable disease.

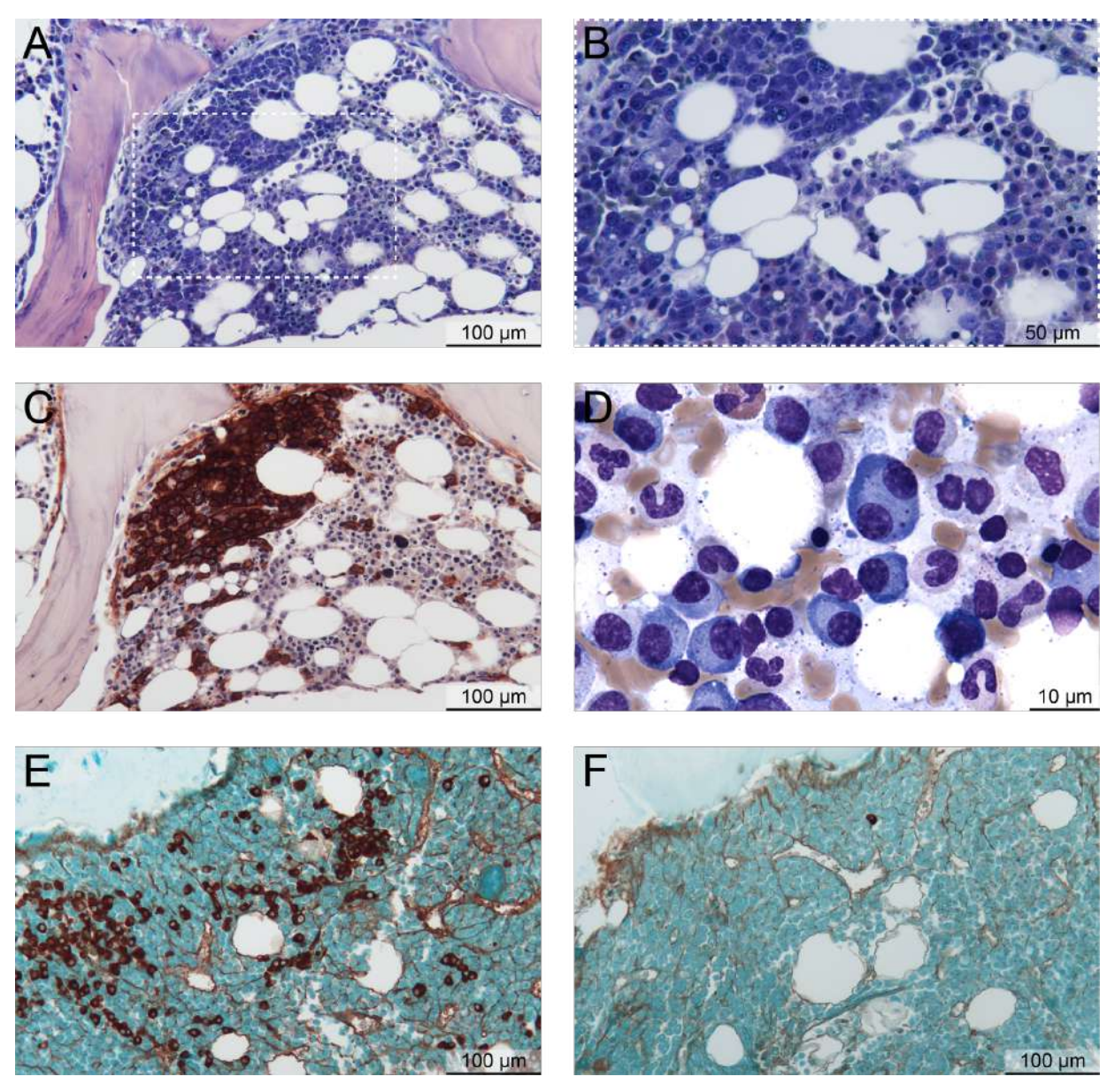


**Fig. 1. Histopathologic features of MM cells.** Representative images showing the morphology and immunophenotype of myeloma cells. (A-B) Giemsa-stained sections highlighting cellular and nuclear details. (C) CD138 immunostain showing strong membrane staining indicative of plasma cell lineage. (D) High-power smear view showing atypical plasma cell morphology. (E) Kappa and (F) Lambda light chain immunohistochemical stains illustrate light chain restriction characteristic for clonal plasma cells. In normal plasma cells, the Kappa/Lambda light chain ratio is approximately 3:1; however, in MM plasma cells, this ratio is skewed, corresponding to clonal light chain restriction.

## 1.2 Historical perspective

The first known case of MM (at that time called *mollities ossium* - softening of the bone) was reported in 1844 by Solly [13]. He described the case of Sarah Newbury, a housewife suffering from severe back pain. She died four years later and her autopsy revealed extensive bone damage.

The first well-documented MM case was published a year later, in 1845, when a London tradesman named Mr. McBean fell ill [14]. His physician, Dr. William Macintyre, along with chemical pathologist Henry Bence Jones, discovered an unusual protein in his urine, now known as Bence Jones protein [15]. This discovery later became a key diagnostic marker for MM.

The name "multiple myeloma" was introduced in 1873 by von Rustizky after he observed eight tumors in a patient's bone marrow during an autopsy [16]. In 1889 Kahler described the case of a 46-year-old physician with skeletal pain, albuminuria, pallor, anemia, and a precipitable urinary protein [17]. The patient survived for eight years after the diagnosis despite limited treatment options at that time. The autopsy report revealed characteristic findings suggesting extensive bone involvement. In 1928, Geschickter and Copeland described a series of 425 MM cases, providing the first estimate of MM's incidence [18].

In 1956, Korngold and Lipari demonstrated a relationship between Bence Jones protein and the serum proteins of MM, marking the first major advancement in understanding the disease at a molecular level [19]. They found that light chains from serum IgG myeloma protein and Bence Jones protein were identical, which was a significant breakthrough. Today, the identification of Bence Jones proteins in urine is a standard diagnostic criterion of MM, as these proteins are indicative of the abnormal proliferation of plasma cells characteristic of this disease [20].

# 1.3 Epidemiology

MM constitutes 1.8% of all cancer types and is the second most common hematologic malignancy. In 2019, there were an estimated 155,688 new cases and 113,474 deaths worldwide [21]. Age is a major risk factor, not only for MM but also for its precursors, smoldering myeloma (SMM) and MGUS [22]. The disease primarily affects older adults, with a median diagnosis age of 69, while cases in individuals under 40 are rare, accounting for only 2% to 5%.

MM is more common in men than women and is diagnosed more frequently in African Americans than White Americans in the United States. Its rising incidence is largely due to better detection, increased screening, an aging population, and improved survival rates thanks to modern treatments [22]. MGUS and SMM are considered obligatory MM precursors [23]. Other risk factors include HIV infection, obesity, occupational exposures, and contact with carcinogens

like Agent Orange [24]. Familial occurrences of MM are documented but constitute a minimal component of overall MM incidence [25,26].

## 1.4 Clinical presentation, diagnosis and treatment

MM typically manifests with clinical features attributable to marrow infiltration by aberrant plasma cells and the resultant disruption of normal hematopoiesis, or by end-organ damage. The latter is evidenced by renal dysfunction, osteolytic lesions, hypercalcemia, and compromised immune function [27]. However, a subset of patients may display neither symptoms nor overt end-organ damage and are often diagnosed incidentally through laboratory or radiological findings obtained during routine evaluations for other conditions. In certain cases, the clinical presentation may be complicated by the deposition of paraproteins in organs like the heart, kidneys, or the nervous system, in the form of light chains, amyloid, or heavy chain deposits. First symptoms may also arise from the effects of cytokines secreted by MM, such as IL-6 or Vascular Endothelial Growth Factor (VEGF). The spectrum of clinical manifestations associated with MM is presented in Fig. 2.

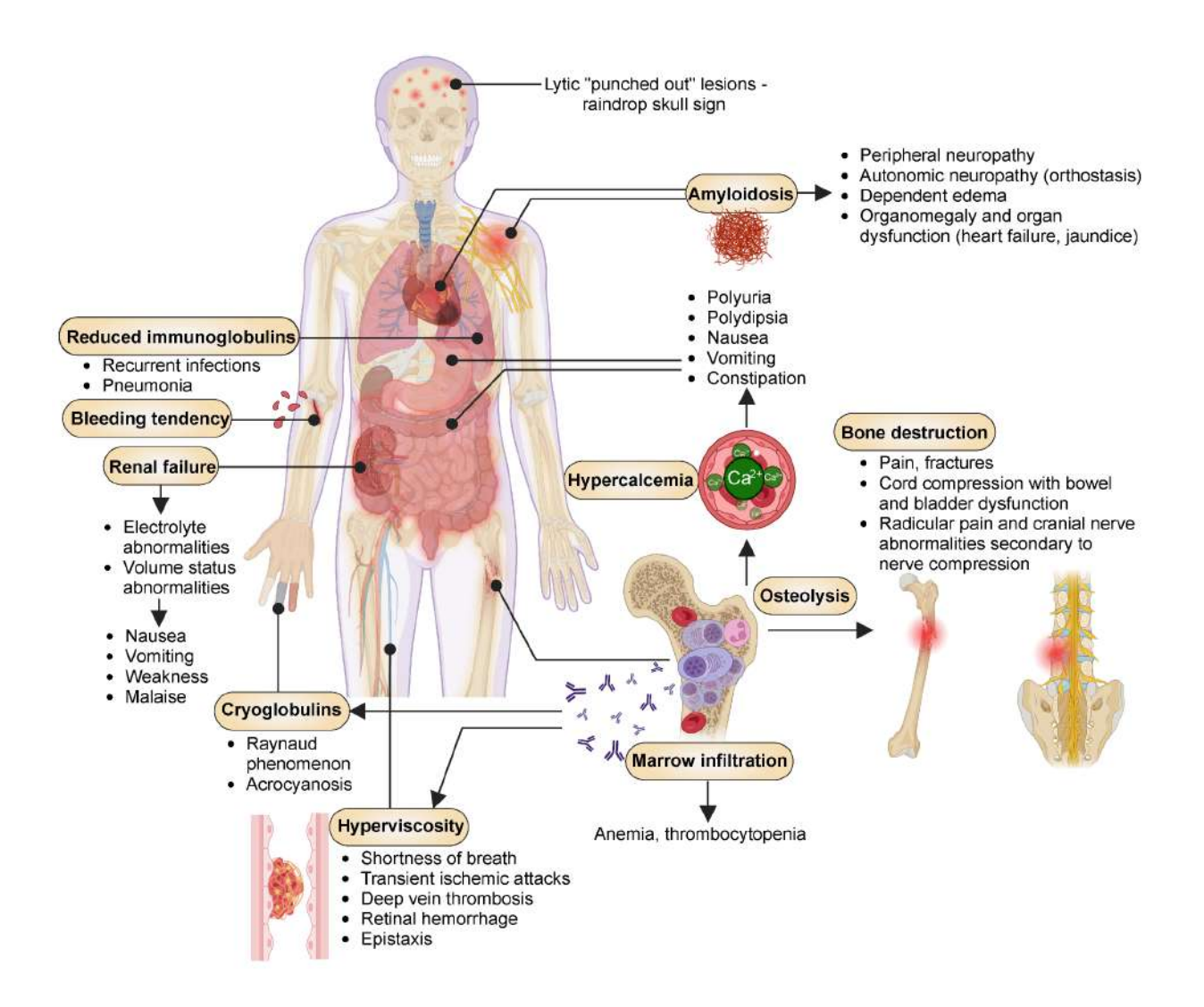


**Fig. 2. Clinical manifestations of MM.** Key symptoms involve the skeletal system (lytic lesions, osteolysis, and bone pain due to bone destruction), the renal system (renal failure with associated electrolyte imbalances and volume status abnormalities), the lymphoid and myeloid systems (anemia, thrombocytopenia, and reduced immunoglobulins leading to increased infection risk), the nervous system (peripheral neuropathy, autonomic neuropathy, and radicular pain). Additionally, symptoms may include metabolic disturbances (hypercalcemia with resultant polyuria, polydipsia, and constipation), paraprotein-related complications (hyperviscosity syndrome, cryoglobulinemia, and amyloidosis) [28].

Patients with MM often experience symptoms summarized by the acronym CRAB: hyperCalcemia, Renal dysfunction, Anemia, and Bone lesions. However, in the early stages, the disease often has no symptoms, which can delay diagnosis. Diagnostic criteria include the presence of monoclonal protein in the blood or urine, more than 10% of clonal plasma cells in the bone marrow, and evidence of end-organ damage. Advanced imaging techniques like MRI (Magnetic Resonance Imaging) and PET-CT (Positron Emission Tomography/Computed Tomography), along with bone marrow biopsy, are essential for proper staging. This thesis

adheres to the revised International Myeloma Working Group (IMWG) criteria for diagnosing MM and related disorders, as outlined in Fig. 3.

#### IgM Monoclonal gammopathy of undetermined significance (IgM MGUS)

All 3 criteria must be met:

- Serum IgM monoclonal protein <3gm/dL</li>
- Bone marrow lymphoplasmacytic infiltration <10%</li>
- No evidence of anemia, constitutional symptoms, hyperviscosity, lymphadenopathy, or hepatosplenomegaly that can be attributed to the underlying lymphoproliferative disorder.

# Smoldering multiple myeloma

Both criteria must be met:

- •Serum monoclonal protein (IgG or IgA) ≥3gm/dL, or urinary monoclonal protein ≥500 mg per 24h and/or clonal bone marrow plasma cells 10-60%
- Absence of myeloma defining events or amyloidosis

#### Plasma cell leukemia

Both criteria must be met:

- Meets diagnostic criteria for multiple myeloma
- Presence of 5% or more plasma cells in conventional peripheral blood smear white blood cell differential count

# Non-IgM monoclonal gammopathy of undetermined significance (MGUS)

All 3 criteria must be met:

- Serum monoclonal protein (non-IgM type) <3gm/dL</li>
- Clonal bone marrow plasma cells
   <10%</li>
- Absence of end-organ damage such as hypercalcemia, renal insufficiency, anemia, and bone lesions (CRAB) that can be attributed to the plasma cell proliferative disorder

#### Light chain MGUS

All criteria must be met:

- Abnormal FLC ratio (<0.26 or >1.65)
- Increased level of the appropriate involved light chain (increased kappa FLC in patients with ratio > 1.65 and increased lambda FLC in patients with ratio < 0.26)</li>
- No immunoglobulin heavy chain expression on immunofixation
- Absence of end-organ damage that can be attributed to the plasma cell proliferative disorder
- Clonal bone marrow plasma cells <10%</li>
- ·Urinary monoclonal protein <500 mg/24h

#### Multiple myeloma

Both criteria must be met:

- •Clonal bone marrow plasma cells ≥10% or biopsy-proven bony or extramedullary plasmacytoma
- ·Any one or more of the following myeloma defining events:
  - Evidence of end organ damage that can be attributed to the underlying plasma cell proliferative disorder, specifically:
    - Hypercalcemia: serum calcium >0.25 mmol/L (>1 mg/dL) higher than the upper limit of normal or >2.75 mmol/L (>11 mg/dL)
    - Renal insufficiency: creatinine clearance <40 mL per minute or serum creatinine >177 μmol/L (>2 mg/dL)
    - Anemia: hemoglobin value of >2 g/dL below the lower limit of normal, or a hemoglobin value <10 g/dL</li>
    - Bone lesions: one or more osteolytic lesions on skeletal radiography, computed tomography (CT), or positron emission tomography-CT (PET-CT)
  - Clonal bone marrow plasma cell percentage ≥60%
  - Involved: uninvolved serum free light chain (FLC) ratio ≥100 (involved free light chain level must be ≥100 mg/L)
  - >1 focal lesions on magnetic resonance imaging (MRI) studies (at least 5mm in size)

#### Solitary Plasmacytoma (SP)

All 4 criteria must be met

- Biopsy proven solitary lesion of bone or soft tissue with evidence of clonal plasma cells
- Normal bone marrow with no evidence of clonal plasma cells
- Normal skeletal survey and MRI (or CT) of spine and pelvis (except for the primary solitary lesion)
- Absence of end-organ damage such as hypercalcemia, renal insufficiency, anemia, or bone lesions (CRAB) that can be attributed to a lympho-plasma cell proliferative disorder

#### SP with minimal marrow involvement

All 4 criteria must be met

- Biopsy proven solitary lesion of bone or soft tissue with evidence of clonal plasma cells
- •Clonal bone marrow plasma cells <10%
- Normal skeletal survey and MRI (or CT) of spine and pelvis (except for the primary solitary lesion)
- Absence of end-organ damage such as hypercalcemia, renal insufficiency, anemia, or bone lesions (CRAB) that can be attributed to a lympho-plasma cell proliferative disorder

Fig. 3. Diagnostic criteria for multiple myeloma, myeloma variants, and monoclonal gammopathy of unknown significance. Based on [29] MRI, Magnetic Resonance Imaging; PET-CT, Positron Emission Tomography/Computed Tomography.

## 1.5 Treatment strategies

Over the past two decades, treatment options for MM have significantly expanded, moving beyond traditional chemotherapy to include targeted therapies such as proteasome inhibitors (e.g., bortezomib, carfilzomib) [30], immunomodulatory drugs (e.g., lenalidomide, pomalidomide) [31], and, more recently, monoclonal antibodies [32] and CAR T-cell (Chimeric antigen receptor T-cell) therapies [33]. While these treatments have improved patient outcomes, resistance mechanisms often emerge, and relapsed or refractory MM continues to pose a therapeutic challenge. Currently, treatment selection is guided by risk assessment according to the Mayo Stratification of Myeloma and Risk-Adapted Therapy (mSMART) consensus guidelines, which emphasize the cytogenetic background of the patient's disease. Most MM patients harbor standard-risk cytogenetic abnormalities (Fig. 4A), while approximately 40% are classified as high-risk (Fig. 4B).

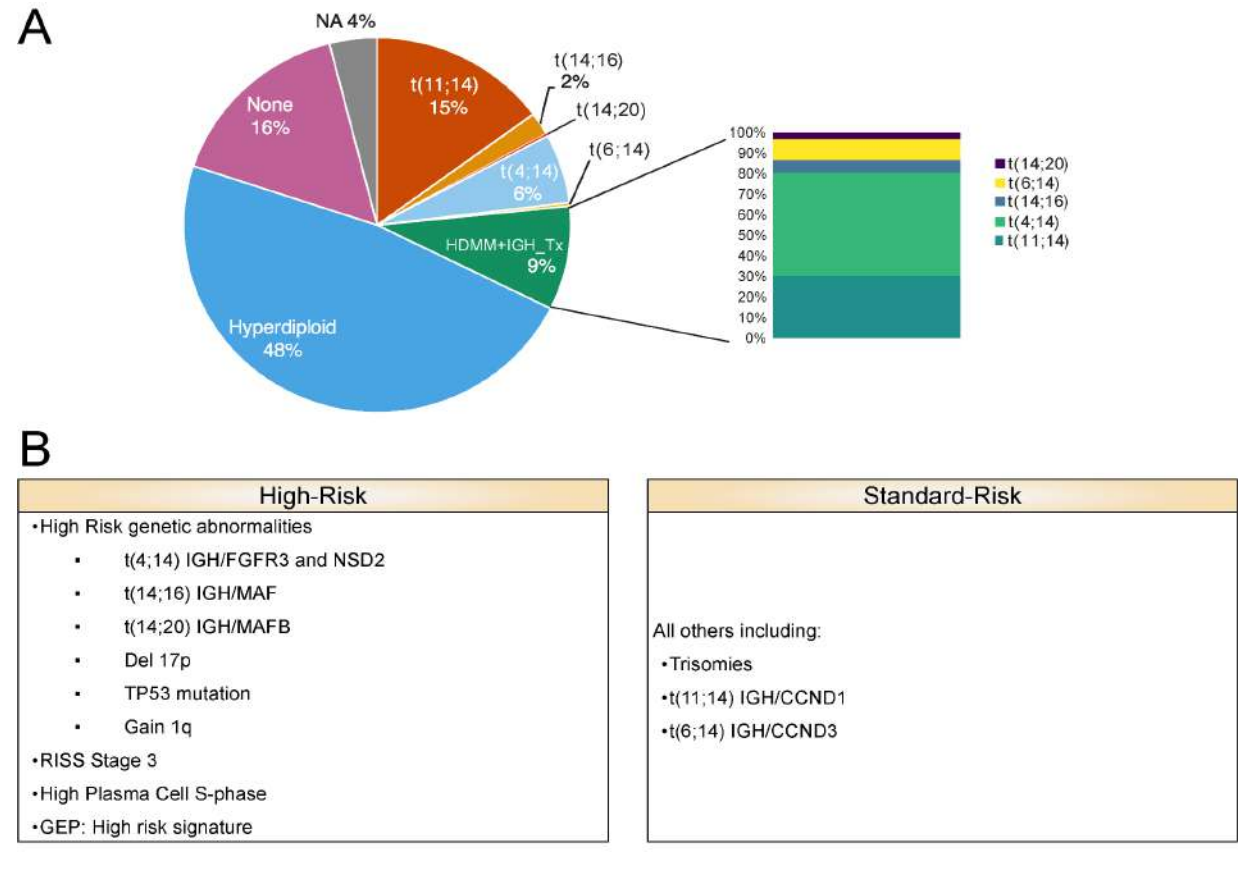


**Fig. 4. Cytogenetic abnormalities and risk stratification in MM.** (A) distribution of various genetic abnormalities in MM, adapted from [34]. (B) Specific disease features associated with high-risk and standard-risk MM [35].

Induction therapy for both transplant-eligible and -ineligible MM patients typically includes a combination of steroids (prednisone or dexamethasone), immunomodulatory drugs, and proteasome inhibitors. In some cases, alkylating agents or monoclonal antibodies are added. Therapy selection depends on patient-specific factors such as renal function and neuropathy, as well as patient age and frailty. Post-induction therapy response is monitored after each cycle. In transplant-eligible patients, stem cell harvesting is recommended by cycle 6 to prevent treatment-related stem cell damage. If a patient achieves a very good partial response (VGPR) or better, and there are no signs of active disease, minimal residual disease (MRD) testing may be performed. Those patients who do not achieve VGPR or who test positive for MRD may receive additional induction therapy or proceed to autologous stem cell transplantation, with tandem or auto-allo transplants restricted to clinical trial settings.

Maintenance therapy usually involves an oral immunomodulatory agent, proteasome inhibitor, or anti-CD38 antibody, particularly for patients at high-risk or with sub-optimal response. The primary goals of maintenance therapy are to slow disease progression, prolong the time to next treatment, and deepen the response to therapy. Achieving MRD-negative status is a marker of favorable prognosis, and this status can be attained during induction, post-autologous transplant, or maintenance phases.

## 1.5.1 Proteasome inhibitors (PIs)

PIs target the ubiquitin-proteasome system (UPS), a fundamental cellular mechanism responsible for protein degradation [36]. Malignant plasma cells are highly dependent on this system due to their increased production of immunoglobulin chains. Unlike most other cancer types, MM cells are constantly synthesizing and folding extremely large amounts of immunoglobulins, which must be properly assembled, post-translationally modified, and secreted. Any imbalance in this tightly regulated process results in the accumulation of misfolded or unassembled proteins, which are typically cleared through the ER-associated degradation (ERAD) pathway. The proteasome is a critical component of ERAD responsible for degrading excess or misfolded proteins which decreases proteotoxic stress.

When PIs block proteasomal function, misfolded and unassembled proteins accumulate within the endoplasmic reticulum (ER), overwhelming the cell's capacity to degrade proteins [37]. This

accumulation triggers ER stress and activates the unfolded protein response (UPR), a cellular mechanism designed to restore proteostasis by reducing protein synthesis, increasing chaperone expression, and enhancing protein degradation. Unresolved, prolonged ER stress leads to a shift from adaptive responses to pro-apoptotic signaling [38].

Bortezomib, the first clinically approved proteasome inhibitor [39,40], acts by blocking the proteasome's chymotrypsin-like activity [30]. This results in accumulation of misfolded proteins and induction of endoplasmic reticulum (ER) stress, ultimately activating apoptosis [41]. However, resistance to PIs remains a significant clinical challenge, necessitating the development of next-generation inhibitors such as carfilzomib and ixazomib, as well as synergistic drug combinations [30].

#### 1.5.2 Immunomodulatory drugs (IMiDs)

The first-generation IMiD, thalidomide [42], was initially introduced for its anti-angiogenic properties [43] but was later found to have potent immunomodulatory and tumor-suppressive effects in MM. However, its clinical utility was limited by severe toxicities, such as peripheral neuropathy [44]. To address this problem, second-generation IMiDs, such as lenalidomide and pomalidomide, were developed, offering greater potency and a more favorable safety profile compared to thalidomide [45].

IMiDs exert their anti-myeloma effects pleiotropically. They promote anti-tumor immune response by enhancing the function of T cells [46] and natural killer (NK) cells [47,48]. These effects are mediated mainly through the proteasomal degradation of transcription factors Ikaros (IKZF1) and Aiolos (IKZF3) via their interaction with cereblon (CRBN), a component of the E3 ubiquitin ligase complex [49,50]. This degradation reduces the suppression of IL-2 production, leading to enhanced T-cell activation and increased immune surveillance against MM cells [51]. In addition, IMiDs induce apoptotic cell death and cell cycle arrest in MM cells by downregulation of *MYC* and *IRF4* [52,53]. Despite their clinical success, IMiD resistance remains a major challenge [54]. Additionally, prolonged IMiD therapy has been linked to an increased risk of secondary primary malignancies, particularly *TP53*-mutated myeloid neoplasms [55].

#### 1.5.3 Corticosteroids

Corticosteroids, particularly dexamethasone, have long been included in MM treatment regimens due to their potent anti-inflammatory, immunosuppressive, and pro-apoptotic effects [56,57]. Dexamethasone binds to glucocorticoid receptor (GR), a transcriptional regulatory factor [58]. It induces apoptosis in malignant plasma cells [59] and suppresses cytokine production in the tumor microenvironment.

The pro-apoptotic effects of dexamethasone in MM are mediated by mitochondrial-dependent and independent pathways. Upon glucocorticoid receptor activation, dexamethasone downregulates anti-apoptotic proteins, while simultaneously increasing the expression of pro-apoptotic proteins such as BIM and PUMA [60]. This shift in the balance of pro- and anti-apoptotic signals leads to mitochondrial outer membrane permeabilization (MOMP) and activation of caspase-dependent cell death pathways [61]. Dexamethasone's anti-inflammatory effects may weaken anti-myeloma immune responses, which limited its effectiveness when used as monotherapy [62]. However, low-dose dexamethasone, when combined with PIs, IMiDs, and monoclonal antibodies, enhances the efficacy of these agents by increasing MM mitochondrial apoptotic priming [63,64].

## 1.5.4 Immunotherapy

Immunotherapy has revolutionized the treatment landscape of MM [65]. Daratumomab, a monoclonal anti-CD38 antibody, has been approved for MM treatment due to the significant extension of patients' overall survival [66–68]. Chimeric antigen receptor (CAR) T-cell therapies [69] and bispecific T-cell engagers (TCEs) [70] have demonstrated remarkable efficacy, particularly in relapsed or refractory multiple myeloma (RRMM). These therapies predominantly target B-cell maturation antigen (BCMA), though newer strategies are exploring alternative antigens such as G protein-coupled receptor class C group 5 member D (GPRC5D) [71]. CAR T-cell therapy involves genetically engineering patient's own T-cells to recognize and eliminate cancer cells [72]. The first approved BCMA-targeting CAR T-cell therapies, idecabtagene vicleucel (ide-cel) [73] and ciltacabtagene autoleucel (cilta-cel) [74], have yielded deep and durable responses, with complete remission rates exceeding 80% in select trials. Despite this success, there is still a risk of relapse due to antigen escape, T-cell exhaustion and systemic

toxicity, as well as potential long-term complications in the form of CAR+ T cell lymphoma [75].

T cell engagers (TCEs), such as teclistamab [76] and elranatamab [77], bridge T-cells to MM cells, leading to immune-mediated cytotoxicity [78]. These agents are particularly valuable for patients who relapse after CAR T-cell therapy or are ineligible for autologous T-cell collection. However, TCEs also pose challenges, including high rates of CRS (cytokine release syndrome) and immune effector cell-associated neurotoxicity syndrome (ICANS) [79].

# 1.5.5 Hematopoietic cell transplantation

Autologous hematopoietic cell transplantation (auto-HCT) continues to be recommended as a standard-of-care consolidation strategy following induction therapy in newly diagnosed multiple myeloma (NDMM) [80]. Studies such as the IFM 2009 trial have consistently demonstrated that auto-HCT provides a significant PFS (progression-free survival) benefit in the modern treatment era, despite the emergence of potent novel agents [81]. However, the role of transplantation has evolved with the advent of new immunotherapeutic approaches, necessitating a reassessment of its optimal timing during MM patients' disease course.

# 1.6 Molecular pathogenesis of MM

MM is a genetically heterogeneous plasma cell malignancy that arises through a multistep process involving both genetic alterations and bone marrow microenvironmental changes [82]. It typically originates from antigen-experienced post-germinal center B cells, progressing from precursor conditions such as MGUS and SMM to symptomatic MM. The transformation is primarily driven by errors during processes like class switch recombination (CSR) and somatic hypermutation (SHM) of the B cell receptor (BCR), which occur within germinal centers (GCs) of lymph nodes.

When antigens stimulate B cells in the splenic marginal zone or mature circulating follicular B cells, they proliferate and differentiate into short-lived plasma cells that secrete low-affinity immunoglobulin M (IgM) [83]. These plasma cells lack somatic hypermutations in their immunoglobulin genes, limiting their longevity. However, a subset of naïve follicular B cells,

upon activation by antigens and antigen-specific T helper cells, initiate a GC reaction within lymph nodes or other lymphoid tissues [84]. Within the GC, these B cells undergo proliferation, somatic hypermutation, antigen selection, and immunoglobulin heavy-chain class switching. This process generates both memory B cells and long-lived, terminally differentiated plasma cells secreting antibodies. Some of these plasma cells migrate to and persist in the bone marrow (BM), where they can survive for years, providing long-term immunity against previously encountered pathogens.

MM plasma cells exhibit somatically hypermutated immunoglobulin gene sequences that remain stable throughout the disease, indicating that both MGUS, SMM and MM originate from terminally differentiated, post-GC plasma cells [85,86]. These cells have undergone multiple rounds of proliferation, affinity maturation, somatic hypermutation, and class-switch recombination, acquiring characteristics of long-lived plasma cells and localizing to various sites within the bone marrow.

During CSR, B cells switch immunoglobulin production (from IgM to IgG, IgE, or IgA), and SHM enhances antigen specificity. Both processes are mediated by activation-induced cytidine deaminase (AID), which introduces DNA double-strand breaks (DSBs). Engagement of the error-prone DSB repair mechanisms can result in off-target mutations, chromosomal rearrangements and initiation of oncogenic transformation of B cells. MM pathogenesis is driven by primary and secondary genetic events, which influence disease initiation, progression, and response to therapy [87–89].

Approximately 2% of MM cases exhibit familial clustering, with germline mutations in KDM1A, ARID1A, and DIS3 conferring increased risk. These alleles may impair DNA repair or epigenetic regulation, lowering the threshold for B cell activation and malignant transformation [90]. Antigenic stimulation plays a dual role: chronic infections (Epstein-Barr virus, hepatitis C) or endogenous antigens (lysosomal GL-1 in Gaucher disease) drive B-cell proliferation while promoting genomic instability through prolonged AID activity [91–93]. Notably, 25% of monoclonal immunoglobulins in MM patients show specificity for viral or bacterial antigens, implicating pathogen-driven clonal selection in early pathogenesis [94].

Mathematical modeling of mutation accumulation suggests the first oncogenic hits occur decades before clinical diagnosis [95]. By analyzing clock-like mutational signatures, Rustad et al. estimated that hyperdiploid trisomies and IGH translocations arise as early as the second decade of life, followed by incremental genomic changes over 20-30 years [96]. This prolonged precursor phase underscores the importance of microenvironmental interactions in sustaining dormant clones until secondary alterations progress into overt malignancy.

## 1.6.1 Primary genetic events

The initiation and progression of MM rely on a combination of primary and secondary genetic events [97]. Primary genetic events are early alterations that initiate disease development [12,98,99]. These include:

- **IgH translocations** (40-50% of cases): Chromosomal rearrangements involving the immunoglobulin heavy chain (IGH) locus on chromosome 14. These translocations originate in GC B-cells, as evidenced by AID-mediated breakpoint signatures [100]. These translocations place oncogenes under the control of strong IGH enhancers, leading to their overexpression:
  - **t(4;14)**: Upregulates *NSD2* (a histone methyltransferase) and *FGFR3*, deregulating epigenetic homeostasis and RAS pathway [101]. Associated with poor prognosis.
  - **t(11;14)**: Upregulates *CCND1*, promoting G1/S cell cycle progression. Associated with CD20 expression and sensitivity to BCL2 inhibitors [12].
  - **t(14;16)** and **t(14;20)**: Overexpression of *MAF* and *MAFB*, respectively, associated with high-risk disease and activation of super-enhancers regulating migratory potential of plasma cells [102].
  - t(6;14), t(8;14): Dysregulation of CCND3 and MYC, respectively.
- IgL translocations: Rearrangements involving the immunoglobulin light chain locus (Igλ), present in ~10% of patients, often associated with poor prognosis. For instance, IgL-MYC translocations result in enhancer amplification and MYC overexpression [103].
- **Hyperdiploidy** (50-60% of cases): Present in approximately 50-60% of MM cases and involves trisomies of odd-numbered chromosomes (e.g., 3, 5, 7, 9, 11, 15, and 19)

through sequential duplication events initiated in the GC [98,99]. Hyperdiploid MM exhibits distinct biological behavior and is generally associated with a better prognosis compared to non-hyperdiploid MM. Unlike IGH translocations, hyperdiploidy shows incremental chromosomal gains during progression from MGUS to MM, suggesting ongoing genomic adaptation [95].

- **MYC overexpression**. MYC is one of the central oncogenes in MM [104,105]. It regulates cellular proliferation, survival, and anti-apoptotic pathways. Its overexpression is a common feature in most MM cases and is strongly linked to poor outcomes. While rarely mutated in early disease, MYC becomes deregulated in 70% of MM through:
  - Secondary translocations involving IGH, IGL, or non-immunoglobulin partners (e.g., FAM46C) [106].
  - Super-enhancer hijacking via focal amplifications at 8q24 [107].

These early genetic alterations occur during B cell maturation and play a central role in MM initiation [108].

## 1.6.2 Secondary genetic events

Secondary genetic events, which occur later in disease progression, are typically more complex and contribute to clonal evolution, therapeutic resistance, and relapse. These events include:

- **Copy number abnormalities**: Common alterations include losses (e.g., 13q, 1p32, 17p) and gains (e.g., 1q21). Amplifications of 1q21 and deletions of 17p (affecting TP53) are associated with poor prognosis and treatment resistance [99,107,109].
- Somatic mutations in key driver genes: These include mutations in KRAS, NRAS, BRAF, TP53, CYLD, TRAF3 and DIS3, which disrupt pathways like RAS-MAPK, PI3K-AKT, NF-κB and RNA metabolism [12,110–112]. Such mutations often lead to uncontrolled cell proliferation and survival [113,114].
- **Loss of cell cycle checkpoint genes**, such as RB1 or CDKN2C, leading to uncontrolled proliferation.
- Complex chromosomal events: These include chromothripsis (catastrophic chromosomal shattering), chromoplexy (concatenated translocations), and templated insertions [95,115,116]. Chromothripsis and templated insertions are involved in early

disease phases, while chromoplexy and focal deletions emerge later and are linked to relapse and drug resistance.

# 1.6.3 Subclonal heterogeneity

Single-cell studies revealed significant subclonal diversity in MM. Many secondary alterations are detectable at diagnosis but remain in minor subclones. These aggressive subclones expand during disease progression or under treatment pressure, leading to relapse. For example:

- **TP53 bi-allelic inactivation**: Combination of mutation and chromosome 17p deletion leads to poor outcomes [117].
- **1q21 amplification**: Associated with resistance to modern therapies and poor survival [118].

# 1.6.4 Mutation-generating mechanisms

Distinct mutational processes shape MM pathogenesis:

- APOBEC [119] (apolipoprotein B mRNA-editing enzyme): APOBEC enzymes, particularly APOBEC3B [120], introduce cytosine-to-uracil deaminations in single-stranded DNA, leading to characteristic mutational signatures. Associated with high mutation burdens and poor prognosis, particularly in MAF-translocation subtypes. The contribution of APOBEC activity increases during disease progression from MGUS to MM to primary plasma cell leukemia (pPCL) [121].
- AID activity [122]: Drives mutations in patients with IGH translocations.
- DNA repair deficiencies [123]: Result in genomic instability and are linked to t(11;14) and t(4;14).
- Age-related mutational processes, often referred to as "clock-like" signatures, are prevalent in hyperdiploid MM subtypes. These processes are characterized by the accumulation of mutations over time and correlate with the patient's age at diagnosis [96].

## 1.6.5 Clinical implications

The molecular heterogeneity of MM complicates selection of appropriate therapeutic interventions according to the principles of precision medicine. Patients with t(11;14) benefit significantly from venetoclax-based regimens due to their cancer's dependence on BCL-2 [124], while patients with high-risk 1q21 gains or TP53 deletions may require an early introduction of CAR-Ts or bispecific antibodies. In addition, the frequent RAS pathway mutations might be targeted therapeutically [125]. Finally, recent discoveries into the evolutionary timeline of multiple myeloma raise the possibility of early detection strategies and preventative therapeutic interventions in precursor conditions like MGUS and SMM, aiming to stop disease progression and prevent the onset of symptomatic MM [126].

# 1.7 Tumor microenvironment (TME)

The bone marrow microenvironment forms a specialized niche that promotes the growth, survival, and drug resistance of MM plasma cells [127,128]. This dynamic environment includes extracellular matrix (ECM) proteins and a diverse array of cell types, such as stromal cells [129], osteoblasts [130], osteoclasts [131], endothelial cells [132], and immune cells [133] (e.g., T cells, neutrophils, natural killer [NK] cells, monocytes, macrophages and myeloid-derived suppressor cells [MDSCs]). These cellular and molecular interactions drive MM evolution by promoting tumor growth, immune evasion, and resistance to therapy [82].

Malignant plasma cells interact with the microenvironment through cell-cell and cell-matrix adhesion, mediated by ECM components like fibronectin, laminin, and proteoglycans, as well as adhesion molecules, including integrins, N-cadherins, and hyaluronan receptors. These interactions lead to the activation of key intracellular signaling pathways, such as NF-κB, PI3K-AKT-mTOR, JAK-STAT, and MAPK, promoting proliferation, survival, and migration of plasma cells. This process also facilitates cell adhesion-mediated drug resistance (CAM-DR), a major obstacle in MM treatment [134–137].

## 1.7.1 T cells

Increasing evidence indicates that dysfunction within the T cell compartment plays a central role in this immune escape [133]. T cell abnormalities in MM include altered CD4<sup>+</sup> and CD8<sup>+</sup> T cell subsets, accumulation of exhausted and senescent T cells, and expansion of regulatory T cells (Tregs).

## 1.7.1.1 Regulatory T cells

A key mechanism of immune dysfunction in MM is the expansion of regulatory T cells (Tregs), which suppress effective anti-tumor responses [138]. There is a significant increase in Tregs in both the bone marrow and peripheral blood of MM patients compared to healthy donors, particularly in patients with active disease [139]. Tregs in MM display an activated phenotype, expressing high levels of CD25, PD-1, and LAG-3, which are associated with suppressive activity and poor prognosis [138]. Tregs in MM are highly suppressive, inhibiting the proliferation and cytokine production of conventional T cells. Mechanistically, they can act through PD-1/PD-L1 signaling, CTLA-4 engagement, and cytokine-mediated immune suppression [140–143].

#### 1.7.1.2 Exhausted and senescent T cells

In addition to Treg expansion, MM is associated with a marked increase in exhausted and senescent T cell populations. Bone marrow-infiltrating CD4<sup>+</sup> and CD8<sup>+</sup> T cells in MM exhibit high levels of exhaustion markers, such as PD-1, LAG-3, and CTLA-4 [144,145]. These dysfunctional T cells exhibit reduced cytokine production and impaired proliferation in response to antigenic stimulation [144]. CD8<sup>+</sup> T cells, in particular, undergo extensive functional decline during MM progression. They express molecules associated with T cell exhaustion (PD-1, CTLA-4, CD160, 2B4, LAG-3) and T cell senescence (CD57, KLRG-1, loss of CD28), impairing their tumor-specific response [146]. These dysfunctional T cells are also associated with a diminished response to TCEs. Patients with pre-existing immune exhaustion exhibit poor outcomes to TCE therapy, whereas responders show robust and sustained T cell receptor (TCR) clonotypic expansion, beginning as early as the first cycle of treatment [147].

#### 1.7.1.3 Loss of naïve and stem-like T cells

Another hallmark of T cell dysregulation in MM is the loss of naïve and stem-like T cells. Single-cell transcriptomic studies have shown that the transition from MGUS to MM is associated with a decline in CD4<sup>+</sup> and CD8<sup>+</sup> T cells with memory and stem-like phenotypes (TCF1<sup>high</sup>) [148]. Simultaneously, there is an increase in terminal effector CD8<sup>+</sup> T cells (granzyme B<sup>+</sup>) and monocytes (CD14<sup>+</sup> and CD16<sup>+</sup>) within the bone marrow [148]. The loss of stem-like TCF1/7<sup>+</sup> memory T cells in MM correlates with poor immune surveillance and decreased response to immune-based therapies. Mechanistically, this loss may be driven by chronic antigen stimulation, metabolic stress, and tumor-derived inhibitory signals such as Dickkopf-1 (DKK1), which has been shown to negatively regulate WNT signaling and TCF1 expression [148,149].

#### 1.7.1.4 T helper cells

The elevated levels of cytokines such as IL-6 and TGF-β in the bone marrow of MM patients significantly impair CD4<sup>+</sup> T cell proliferation and disrupt the balance of T helper cell subsets. This imbalance reduces Th1-mediated immune responses, promotes Th2 skewing, and increases the number of Th17 cells, which secrete IL-17 and IL-10 [150]. These cytokines suppress immune surveillance and activate osteoclastogenesis, which exacerbates MM-related bone lysis [151].

### 1.7.1.5 Clinical implications

MM long-term survivors exhibit sustained immune alterations driven by both reversible and irreversible mechanisms, even decades after their first-line therapy [152]. These changes persisted in patients with no detectable residual disease, suggesting a process of "immunological scarring". This scarring likely results from chronic exposure to malignant plasma cells and the inflammatory environment induced by initial therapy. A central mechanism identified in this remodeling involves an inflammatory circuit maintained by cytokine and chemokine interactions. Aberrant CD14<sup>+</sup> monocytes and CD8<sup>+</sup> T cells are key players in the pathogenesis of immune dysfunction in MM. Monocytes produce inflammatory mediators such as CXCL8, IL1B, and CCL3, promoting the recruitment and activation of CXCR3<sup>+</sup> CD8<sup>+</sup> T cells to the BM. The chronic inflammatory signaling not only sustains immune dysregulation but also serves as a biomarker of disease activity, as the abundance of CXCR3<sup>+</sup> T cells in the BM correlates with

residual malignant plasma cells and predicts relapse. This persistent inflammatory state appears to be tumor-driven but is also shaped by the long-term effects of therapy, particularly high-dose regimens followed by autologous stem cell transplantation. Even in patients considered "functionally cured", transcriptional and functional deficits, such as reduced cytokine production by T cells, persist [152].

The unique T-cell biology in MM has implications for designing therapeutic strategies. Checkpoint blockade therapies targeting PD-1/PD-L1 have shown promise [153] but have been limited by the presence of exhausted T cells that not able to respond to stimulation [154]. Strategies aimed at depleting Tregs, such as anti-CD25 antibodies, or reprogramming exhausted T cells through metabolic and epigenetic modulation are being explored. Combinatorial approaches targeting other components of the MM microenvironment along with immune checkpoint inhibitors or Treg-depleting agents may offer a way to overcome T cell dysfunction in MM.

## 1.7.2 Myeloid cells

The contribution of myeloid cells (osteoclasts, osteoblasts, macrophages, myeloid-derived suppressor cells (MDSCs), and dendritic cells) to MM pathophysiology has gained increasing recognition, despite lack of clinical translation to date. Myeloid cells within the TME can foster MM progression by promoting immune suppression, angiogenesis, and resistance to chemotherapy.

#### 1.7.2.1 Osteoclasts

Osteoclasts are specialized multinucleated cells derived from the monocyte-macrophage lineage, and their primary role in normal bone remodeling is to resorb bone. Under physiological conditions, osteoclast activity precisely balances osteoblast-mediated bone formation to continuously renew bone tissue. Osteoclast differentiation and activation are tightly regulated by the RANK/RANKL/OPG signaling axis. RANKL (Receptor Activator of NF-κB Ligand) is expressed on osteoblasts and bone marrow stromal cells and binds to its receptor RANK on osteoclast precursors, driving their maturation into active bone-resorbing cells [155]. In multiple myeloma, osteoclast function becomes pathologically hyperactive. Bone biopsies and

histomorphometric studies of MM patients consistently show a significant increase in osteoclast numbers and activity in affected bone areas [156–158]. Myeloma cells typically localize to areas of active bone resorption, indicating that osteoclast activation is a locally mediated process in MM. MM cells stimulate osteoclasts [159], and activated osteoclasts in turn secrete factors (e.g. IL-6, APRIL) that promote myeloma cell growth and survival [160]. This positive feedback loop exacerbates bone destruction and tumor expansion. Osteoclast activity is a central pathological feature and a therapeutic target in myeloma bone disease. Clinically, bisphosphonates and denosumab are used to inhibit osteoclast-mediated bone resorption.

#### 1.7.2.2 Osteoblasts

Osteoblasts are the bone-forming cells of the body. In normal bone remodeling, osteoblasts refill the cavities created by osteoclasts, thus maintaining bone mass and strength. Osteoblasts are responsible for synthesizing bone matrix and orchestrating its mineralization. They produce collagen and other proteins (osteocalcin, alkaline phosphatase, etc.) that form the scaffold for mineral deposition, and they regulate the deposition of calcium/phosphate (hydroxyapatite) crystals into this matrix [161]. Multiple myeloma causes a profound suppression of osteoblast differentiation and function. The presence of myeloma in the marrow skews mesenchymal stem cell (MSC) differentiation away from the osteoblast lineage. Bone marrow MSCs from myeloma patients are often abnormal - they have impaired osteogenic potential and a tendency to undergo adipogenic differentiation rather than osteogenesis [162]. MM cells inhibit osteoblast differentiation by releasing Wnt signaling antagonists, primarily DKK1 and, indirectly, sclerostin [163,164]. DKK1 blocks Wnt co-receptors (LRP5/6) on osteoblast precursors, preventing Wnt-induced RUNX2 activation and shutting down osteoblast maturation. Sclerostin, mainly produced by osteocytes, also inhibits Wnt signaling. Some agents like bisphosphonates or denosumab reduce osteoclast activity and slow bone loss, but they do not address the lack of bone formation. Even with anti-resorptive therapy, myeloma patients may not regain lost bone. Bortezomib has been shown to increase osteoblast numbers and bone formation markers in myeloma patients [165]. Therefore, more therapeutic agents stimulating bone formation should be tested. Notably, certain novel small-molecule inhibitors, including PIM kinase inhibitors, have been shown to promote osteoblastic differentiation while suppressing osteoclastogenesis [166].

### 1.7.2.3 Tumor-associated macrophages (TAMs)

TAMs represent a major myeloid component within the MM BM niche, with a predominant M2-like phenotype (CD163<sup>+</sup> CD206<sup>+</sup>) that supports tumor growth and immune suppression by inhibiting T cell and NK cell activity [167–170]. These macrophages are recruited and polarized by MM-derived cytokines such as IL-10 and IL-6, which drive their immunosuppressive activity [170]. TAMs secrete pro-tumorigenic factors such as vascular endothelial growth factor (VEGF), transforming growth factor-β (TGF-β), and matrix metalloproteinases (MMPs), which enhance angiogenesis and extracellular matrix remodeling. They also contribute to drug resistance by interacting with MM cells via adhesion molecules such as PSGL-1/P-selectin and ICAM-1/CD18, which activate survival pathways [171].

Recent studies have demonstrated that inhibiting TAM function can restore anti-tumor immunity. Studies utilizing disseminated murine MM models have shown that depletion of macrophages prevents homing of malignant plasma cells and slows down progression of the disease [172,173]. Other studies showed that blockade of the IL-10 receptor (IL-10R) reprograms TAMs to a pro-inflammatory M1 phenotype, enhances T cell activation and reverses MM drug resistance [174]. Similarly, targeting the tyrosine kinases JAK1/2 disrupts TAM recruitment and polarization, reducing MM cell survival [168].

## 1.7.2.4 Myeloid-derived suppressor cells (MDSCs)

These immature myeloid cells are expanded in MM patients and exert immunosuppressive effects by inhibiting T cell and NK cell activity [175]. MDSCs accomplish this through the production of nitric oxide (NO), arginase-1 (ARG1), and reactive oxygen species (ROS), which suppress T cell proliferation and function [176]. Additionally, MDSCs promote the differentiation of Tregs [177].

MM cells induce MDSC expansion through secretion of IL-6 and GM-CSF, which stimulate myelopoiesis while preventing terminal myeloid differentiation [175]. MDSCs have been implicated in MM progression by fostering a tumor-permissive niche, promoting angiogenesis and osteolysis [176].

# 1.7.3 Plasmacytoid dendritic cells (pDCs)

Unlike conventional antigen-presenting DCs, MM-associated pDCs are functionally impaired and promote MM cell survival rather than eliciting effective immune responses [178]. Interventions aimed at restoring DC function include the use of TLR agonists such as CpG oligodeoxynucleotides, which reinvigorate pDC activity and restore their ability to prime cytotoxic T cells. The role of these cells in MM remains largely unexplored.

### 1.7.4 NK cells

NK cells recognize and eliminate malignant cells without prior sensitization [179]. MM cells modulate the expression of NK cell ligands and induce NK cell exhaustion, which drives immune escape. Single-cell transcriptomic profiling identified a subset of exhausted ZNF683+ NK cells in MM patients, which show decreased expression of activating receptors such as SLAMF7 and SH2D1B. Loss of these molecules weakens NK cell activation and promotes their dysfunction [180]. Additionally, increased surface expression of TIM-3 and TIGIT further blocks NK cell responses [181]. NK cells from MM patients display reduced degranulation and low production of IFN-γ, granzyme B and perforin, limiting MM cell killing [182]. MM cells overexpress HLA-I molecules, which engage inhibitory killer immunoglobulin-like receptors (KIRs), further preventing NK-mediated lysis [183]. In the clinical setting, IMiDs enhance NK cell function by promoting IL-2 secretion by T cells and increasing NK cell activation markers [184]. The anti-CD38 monoclonal antibody daratumumab relies on NK cell-mediated antibody-dependent cellular cytotoxicity (ADCC) for its efficacy. However, daratumumab treatment leads to rapid NK cell depletion due to their CD38 positivity. Notably, patients with lower baseline CD16<sup>+</sup> NK cell frequencies exhibit poorer responses to therapy [185]. Strategies to restore NK cell populations, such as adoptive NK cell transfer, are under investigation [186].

## 1.7.5 Bone marrow stromal cells

Bone marrow stromal cells (BMSCs) are the non-hematopoietic supportive cells within the bone marrow microenvironment. A major component of BMSCs are mesenchymal stem/stromal cells (MSCs), multipotent cells capable of differentiating into osteoblasts, adipocytes, and chondrocytes. Historically, experiments using myeloma-associated BMSCs identified them as

the CD138<sup>-</sup> fraction, leading to the inclusion of a heterogeneous mix of cell types cultured in an adherent monolayer. However, most of these cells are of mesenchymal morphology and, as they have significantly higher proliferative potential than other bone marrow cell types when cultured *ex vivo* [187]. In normal physiology, BMSCs form the structural and functional foundation of the hematopoietic niche. They provide physical scaffolding and produce essential cytokines and growth factors that regulate hematopoietic stem cell (HSC) maintenance, self-renewal, and differentiation [188,189]. BMSCs secrete factors such as stem cell factor (SCF) and CXCL12 (also known as SDF-1) which promote HSC survival and retention in the marrow niche [190,191]. They also express cell-surface molecules (e.g., VCAM-1, ICAM-1) that mediate adhesion with HSCs or progenitors [192].

MM cells and bone marrow stromal cells engage in extensive bidirectional interactions that create a supportive microenvironment or "soil" for the tumor "seed." These interactions occur through direct cell-cell contact and soluble factors. The result is a vicious cycle - myeloma cells alter the phenotype and secretory profile of BMSCs, and in turn BMSCs produce signals that enhance myeloma cell survival, proliferation, and drug resistance [193,194] MM cells express various adhesion molecules (e.g., integrins VLA-4/VLA-5, LFA-1, CD44, syndecan-1/CD138) that bind to their ligands on BMSCs or the ECM (e.g., VCAM-1, ICAM-1, fibronectin) [195]. One well-studied adhesion-mediated loop involves CD40 on MM cells and CD40L (CD154) on stromal cells. When myeloma cells bind to BMSCs via CD40-CD40L, MM cells upregulate adhesion molecules (like LFA-1, VLA-4) on the stromal cells, further increasing the adhesion of tumor cells. This tight adhesion then triggers BMSCs to secrete higher levels of cytokines such as IL-6 and VEGF, which in turn promote tumor growth.

BMSCs are major contributors to therapy resistance through a phenomenon known as adhesion-mediated drug resistance (AMDR) or cell adhesion-mediated drug resistance (CAM-DR) [136]. Essentially, the same interactions that promote myeloma cell survival in the marrow also shield them from the cytotoxic effects of chemotherapy. One mechanism of CAM-DR involves physical adhesion of myeloma cells to stromal cells or ECM, which triggers anti-apoptotic signaling in the tumor cells. Binding of integrins (like VLA-4) on MM cells to fibronectin or BMSC-derived VCAM-1 can activate intracellular pathways (such as PI3K/AKT and NF-κB) in the myeloma cells that block chemotherapy-induced apoptosis.

## 1.7.6 Endothelial cells

## 1.7.6.1 Origins of BMECs

Bone marrow endothelial cells (BMECs) are crucial components of the bone marrow microenvironment, thanks to maintenance of hematopoietic stem cell homeostasis and participation in bone remodeling [196]. BMECs share a common developmental origin with hematopoietic cells. Both arise from mesodermal progenitors known as hemangioblasts, which can give rise to endothelial cells (ECs) and blood cells [197]. During embryonic development specialized endothelial cells with hemogenic potential - hemogenic endothelium (HE) - undergo an endothelial-to-hematopoietic transition (EHT) to form HSCs. EHT occurs in the aorta-gonad-mesonephros (AGM) region around mid-gestation, where a subset of embryonic endothelial cells activates hematopoietic genes and buds off HSCs. A heterogenous subset of ECs, BMECs, line the blood vessels within the bone marrow, and form a dynamic interface regulating the trafficking and engraftment of hematopoietic stem and progenitor cells (HSPCs) [198].

## 1.7.6.2 BMEC heterogeneity

The bone marrow vasculature displays remarkable structural and functional heterogeneity. Arteriolar vessels enter the bone and branch into capillaries and sinusoids that create distinct microvascular domains. Small arterioles give rise to transition capillaries (also known as type H capillaries) marked by high CD31 and endomucin expression as well as Notch signaling [199,200]. These transition vessels drain into wide, fenestrated sinusoids (type L vessels) that fill the marrow cavity. Arteriolar BMECs express markers like Sca-1, Nestin, and CD200, whereas sinusoidal BMECs express E-selectin, ICAM-1, podoplanin, and CD105 [201–204]. Arteriolar endothelium is ensheathed by smooth muscle and NG2+ pericytes, and is surrounded by Nestin+ MSCs, whereas sinusoids are loosely associated with Nestinlow, LEPR+ MSCs. These structural differences translate into distinct functions: arteriolar BMECs form a tight, high-flow, low-permeability circuit, while sinusoidal BMECs form a slow-flow, highly permeable network for cell trafficking [205]. Arteriolar BMECs also reside in relatively oxygen-rich niches, whereas the sinusoidal core of the marrow is more hypoxic [206]. MM cells are frequently found near sinusoidal vessels, often arranging themselves in rosette-like formations (Fig. 5) [207–209].

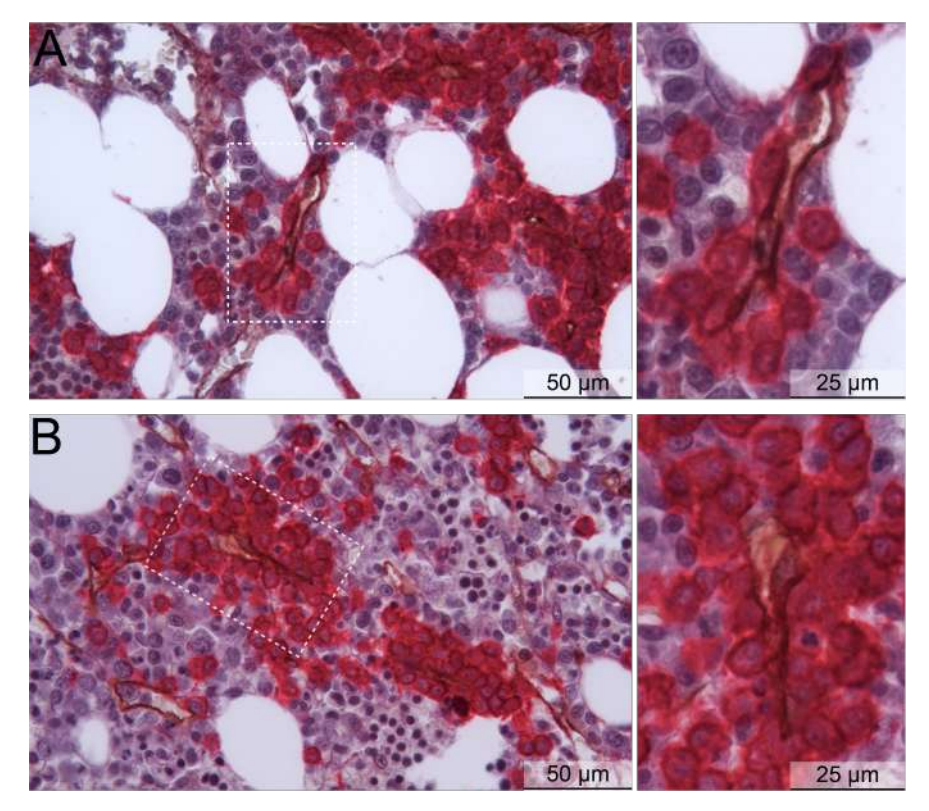


Fig. 5. Double IHC staining of multiple myeloma bone marrow sections. (A and B represent different patients). CD34 (brown) marks endothelial cells, while CD138 (red) identifies plasma cells.

## 1.7.6.3 MM-associated BMECs (MMECs)

Angiogenesis accompanies and supports the growth of virtually all types of human cancer [210–212]. In MM, BMECs are not merely passive bystanders but active participants in disease progression. Pathological angiogenesis is one of the hallmarks of MM [213–218]. Studies isolating ECs from MM patient bone marrow have shown that these cells exhibit an altered, tumor-supportive phenotype distinct from normal endothelium [219]. Single-cell RNA sequencing has identified distinct transcriptional alterations in MMECs, including upregulation of proangiogenic pathways, epithelial-to-mesenchymal transition (EMT) markers, and inflammatory cytokines [220,221]. MMECs express specific antigenic markers indicating ongoing angiogenesis and even embryonic vasculogenesis, suggesting that they are in an activated state akin to tumor endothelial cells [219]. They can form capillary-like networks rapidly *in vitro* and significantly contribute to new vessel formation *in vivo*. This means that new blood vessels in MM may arise both by sprouting from existing vessels (angiogenesis) and by incorporation of endothelial progenitors (vasculogenesis) recruited by or even originating from the tumor milieu [219,222].

The microvessels in MM bone marrow often show abnormal ultrastructure and chaotic organization (a hallmark of pathological angiogenesis) [217,219]. Frequent physical interactions are observed between ECs and myeloma cells, indicating that ECs provide scaffolding for plasma cell adhesion and dissemination within the marrow and possibly into circulation [219,223].

MMECs actively secrete various growth factors, chemokines, and proteases that promote myeloma cell proliferation, survival, and invasion. For example, they produce IL-6 - a known growth factor for myeloma - as well as matrix metalloproteinases, which fuel tumor expansion and bone marrow niche remodeling [224]. This creates a vicious cycle: myeloma cells induce ECs to become pro-angiogenic and pro-tumoral, and in turn ECs secrete factors that further stimulate the myeloma cells proliferation and survival [225].

MM exemplifies the "angiogenic switch" during tumor progression. In the benign precursor stage, bone marrow angiogenesis is minimal - the balance of angiogenic regulators is maintained such that new vessel formation is still relatively slow [216]. As MGUS evolves into active myeloma, myeloma cells (along with microenvironment cells) tip this balance by increasing production of pro-angiogenic factors and suppressing angiogenesis inhibitors [215]. This results in a marked increase in bone marrow microvessel density (MVD). Clinically, studies have shown MVD correlates with disease status: MGUS and smoldering myeloma have low MVD, whereas active MM has high MVD, which can further rise in advanced or relapsed disease [215]. Moreover, successful treatment of MM often reduces bone marrow MVD, whereas relapse is accompanied by revascularization - showing that angiogenesis is dynamically linked to disease activity (Fig. 6).



**Fig. 6. Vessel density in normal BM, MGUS and MM.** Representative images showing CD34 vascular staining in representative tissue sections of normal bone marrow, MGUS patient and MM patient.

### 1.7.6.4 Signaling pathways activated in MMECs

MMECs signal through activated kinases and pathways typically associated with angiogenesis and cell survival. For instance, they often show activation of the PI3K/AKT and mTOR pathways [226] as well as elevated activity of AP-1 and BACH1/2 target genes [221]. They also upregulate adhesion molecules and receptors (e.g., VEGF receptors, integrins), increasing their responsiveness to pro-angiogenic stimuli. A notable finding is the overexpression of JAM-A (Junctional Adhesion Molecule-A) on MM bone marrow ECs, which is not seen at high levels on normal marrow endothelium [225]. Elevated JAM-A on ECs appears to facilitate interactions with myeloma cells and endothelial motility, driving angiogenesis and correlating with worse patient outcomes.

The endothelial compartment in MM is heterogeneous. While most ECs are normal host-derived, a subset might be directly derived from the tumor clone or co-opted progenitors. Evidence of this comes from detection of myeloma-specific genetic markers (e.g., clonal immunoglobulin gene rearrangements or cytogenetic abnormalities) in endothelial progenitor cells of some patients [227].

The pro-angiogenic drive in MM is multifactorial. The malignant plasma cells themselves are a major source of angiogenic factors. They autonomously produce growth factors and cytokines that can directly act on endothelial cells. Key among these are vascular endothelial growth factor (VEGFA, VEGFB) and basic fibroblast growth factor (bFGF) [221,228]. Myeloma cells also secrete interleukin-8 (IL-8) [229], a cytokine that serves as a chemoattractant and mitogen for endothelial cells, and hepatocyte growth factor (HGF) [230], which can stimulate angiogenesis and plasma cell growth. Other tumor-derived pro-angiogenic molecules include osteopontin (OPN) [231], metalloproteinases (MMP-2, MMP-9) [232] which remodel the extracellular matrix to facilitate vessel sprouting, and angiopoietin-1 (Ang-1) [213]. Hypoxia also plays a role in sustaining angiogenesis by upregulating hypoxia-inducible factor-1α (HIF-1α), which further induces VEGF and other angiogenic cytokines [214]. Myeloma cells can also release exosomes containing microRNAs (e.g., miR-135b) under hypoxic conditions, which have been shown to enhance angiogenesis by reprogramming surrounding cells [233]. Notably, as the MM clone acquires these angiogenic features, it simultaneously often loses expression of angiogenesis

inhibitors. Endogenous inhibitors like thrombospondin-1 or interferons are found at lower levels in active MM, removing constraints on vessel growth [215,234–236].

The bone marrow microenvironment in active MM is often hypoxic, partly due to rapid cellular proliferation and abnormal vasculature. Hypoxia is a powerful inducer of angiogenesis through the HIF-1α pathway. In MM, HIF-1α is frequently overexpressed in the plasma cells [215]. HIF-1α drives the transcription of pro-angiogenic genes VEGF, IL-8, ANGPT2 (Ang-2), and SDF-1, switching on an angiogenic program in hypoxic marrow niches [237]. ING4, a tumor suppressor, normally interacts with NF-κB and HIF pathways to restrain angiogenesis. In MM cells, ING4 is commonly downregulated; as a result, myeloma cells with low ING4 produce excess IL-8 and osteopontin and show heightened HIF-1α activity, further accelerating angiogenesis [238].

MM cells "educate" other cells in the bone marrow to secrete angiogenic factors. BMSCs increase their production of VEGF, IL-6, and SDF-1 under the influence of myeloma [216]. MM cells express Jagged1/2 ligands which activate Notch signaling in BMSCs, causing the BMSCs to release more VEGF and SDF-1 $\alpha$  and become pro-angiogenic. In addition, inflammatory cells like mast cells [239] and macrophages [240] in the myeloma marrow secrete angiogenic mediators (TNF- $\alpha$ , bFGF, IL-1 $\beta$ ) when stimulated by tumor-derived signals. Osteoclasts (bone-resorbing cells often increased in MM) contribute by secreting VEGF and degrading bone matrix to release stored growth factors [241].

An interesting mechanism in MM angiogenesis is the involvement of circulating endothelial progenitor cells (EPCs). In many solid tumors, EPCs from the bone marrow are mobilized to help form new blood vessels. In MM, patients often have elevated levels of circulating EPCs and circulating endothelial cells, which correlate with disease activity[242]. These progenitors home to the bone marrow in response to gradients of CXCL12 and other chemokines released by the hypoxic, angiogenic niche. Research indicates that after therapy, a decrease in EPCs is associated with tumor regression, whereas a rebound or rise in EPC count can herald relapse or refractory disease. EPCs are mobilized from marrow into circulation at the smoldering MM stage and are actively recruited to MM-colonized BM niches, where they differentiate into endothelial cells [222]. Using EPC-deficient mice, researchers demonstrated that MM progression is dependent on EPC trafficking, as tumor burden and microvessel density were significantly reduced in these models. Early inhibition of EPC function with a VEGFR2 blocking antibody (DC101) delayed

MM progression and improved survival, whereas late-stage treatment was ineffective. This suggests that vasculogenesis targeting might need to be timed correctly, and such anti-angiogenic therapy should be tested as frontline therapy in early-stage MM. No clinical studies have been initiated to investigate this approach yet.

### 1.7.6.5 MMECs-mediated support of MM cells

The interactions between myeloma cells and ECs form a positive feedback loop (angiogenic loop) [218,243,244]. Myeloma cells secrete VEGF which acts on endothelial cells; endothelial cells, when stimulated by VEGF, in turn release IL-6, IGF-1 and other cytokines that feed back to myeloma cells, enhancing their growth and survival [223,245]. This creates a self-reinforcing circuit where more myeloma cells lead to more angiogenesis, and more vessels and EC-derived factors support more myeloma cells. Disrupting this loop can have therapeutic benefit, as demonstrated by agents that break the communication (for example, bortezomib can inhibit both VEGF and IL-6 production by ECs) [245]. Additionally, cell-cell contact between myeloma cells and ECs via adhesion molecules (like VLA-4/VCAM-1 or JAM-A) can activate signaling in both cell types that favor tumor proliferation and vessel formation [136,225]. The bidirectional crosstalk between MM cells and ECs involves adhesion molecules such as integrins (αVβ3, α4β1), syndecan-1 (CD138), and CD44, which mediate MM cell adhesion to ECs and the ECM [136]. MMECs support MM progression by secreting extracellular cyclophilin A (eCyPA), which binds to CD147 on MM cells, enhancing their migration, proliferation, and survival [223]. Compared to BMSCs, BMECs are a more potent source of eCyPA, driving stronger MM bone marrow homing and activation of chemoresistance pathways, including MAPK, PI3K/AKT, and STAT3 signaling. Thus, angiogenesis in MM is a part of an integrated network of signals that also involve tumor growth, migration and resistance to therapy.

Having explored the complex interactions within the bone marrow microenvironment that sustain MM progression, it is evident that malignant plasma cells exploit stromal, immune, and endothelial components to thrive, evade immune surveillance, resist therapy, and drive bone destruction and further dissemination. Among the molecular pathways that orchestrate these tumor-supportive mechanisms, serine/threonine kinases play a pivotal role in integrating signals that promote MM development. One such family of kinases, PIM (Proviral Integration site for Moloney murine leukemia virus) kinases, has emerged as a critical player in MM pathobiology

[246]. Their activity is largely dependent on the tumor microenvironment, where external cues such as IL-6 and CXCL12 sustain PIM expression, reinforcing MM cell survival. Given their role as downstream mediators of key survival pathways like JAK/STAT and NF-κB, targeting PIM kinases with small molecule inhibitors presents a promising strategy to disrupt these protumorigenic signals and was therefore explored in this thesis. The next chapter will describe the biology of PIM kinases, their functional significance in MM and TME, and the current state of knowledge about the therapeutic potential of PIM kinase inhibition in MM.

## 1.8 PIM kinases

Kinases are a large family of enzymes that play a critical role in regulating cellular processes by phosphorylating specific substrates [247]. This process modulates the activity, localization, and interactions of proteins, acting as a molecular switch to control various biological pathways. The PIM (Proviral Integration of Moloney virus) kinase family comprises three highly homologous serine/threonine kinases: PIM1, PIM2, and PIM3 [248]. They are important regulators of cellular processes such as cell cycle progression, apoptosis, and metabolism [249]. PIMs are constitutively active without the need for phosphorylation thanks to their unique structural configuration [250]. In kinases, activation generally involves forming a conserved lysineglutamate salt bridge (e.g., Lys67 and Glu89 in PIM1), adopting a closed-lobe conformation, and structuring the activation segment. For many kinases, this segment remains unstructured until phosphorylation, which induces folding onto the lower lobe, stabilizing the peptide-binding site and enabling enzymatic activity. PIM kinases, however, are unique in being catalytically active without phosphorylation. Their unphosphorylated activation segment establishes multiple polar interactions with the lower lobe, maintaining the active conformation [248]. While PIM kinases can undergo autophosphorylation, the functional significance of these modifications remains unclear [250]. The non-canonical binding conformation of the ATP-binding pocket and activation loop provides unique structural features that facilitate the design of PIM kinasespecific small-molecule inhibitors.

The "always-on" state of PIM kinases, which become active immediately following translation, benefits cancer cells by enhancing virtually all of the canonical cancer hallmarks [251,252]. Persistent overexpression of these kinases has been often described in various hematologic

malignancies [248,253] and some solid tumors [248]. Normally, PIM kinase expression is tightly controlled by transient cytokine pulses, such as IL-6 [254] and IL-7 [255], and regulated by shortlived growth factor signals or other inflammatory mediators.

## 1.8.1 Physiological roles of PIM kinases

PIM kinases are vital for certain physiological processes, such as HSC maintenance and immune cell function. Nonetheless, mice deficient in all 3 PIMs (Pim TKO mice) are viable and fertile [256]. These mice exhibit significantly reduced platelet counts and smaller hypochromic erythrocytes with decreased mean corpuscular volume (MCV) and mean corpuscular hemoglobin (MCH). CD4<sup>+</sup> T cells, granulocytes, and overall T-cell population counts are decreased in the peripheral blood of TKO animals [257]. However, peripheral B-cell numbers are less consistently affected, with slight reductions observed only in young animals [256]. Pim TKO mice have a reduced total bone marrow cellularity and splenocyte count. Their bone marrow cells demonstrate decreased capacity for granulocyte/macrophage (CFU-GM), erythrocyte (BFU-E), and multilineage (CFU-GEMM) colony formation, indicating impaired hematopoietic progenitor activity. These findings are highly relevant for the design of clinical trials involving pan-PIM inhibitors. Patients receiving these inhibitors may be at risk of significantly reduced granulocyte and monocyte levels, potentially compromising their immune response and increasing susceptibility to infections.

PIM1 is a significant factor in early B-cell development, influencing hematopoiesis through its effects on cytokine signaling pathways [258]. PIM2, on the other hand, has been shown to be important for plasma cell development [259]. PIM1 and PIM2 are required for efficient T-lymphocyte proliferation. In primed CD8<sup>+</sup> T cells, the costimulatory receptor CD27 drives PIM1 expression, enhancing T-cell survival independently of mTOR and IL-2 signaling [260]. T cells from Pim1/2-deficient mice have blunted expansion to T-cell receptor (TCR) stimulation and IL-2 [261]. The expression of PIM1/2 is upregulated by Th1-polarizing cytokines (IL-12, IFN-α), but not Th2 cytokines, and PIM activity drives Th1 lineage commitment [262,263]. PIM1/PIM2 directly phosphorylate FOXP3 (the master regulator in Tregs), which weakens Treg suppressive function [264,265]. These findings show PIM kinases boost immune responses (T and B cell growth, Th1 immunity, NF-κB activity) and, when overactive, can contribute to inflammatory pathology, while at the same time fostering immune tolerance.

Beyond their roles in hematopoiesis and immune function, PIM kinases contribute to skeletal and cardiac muscle regeneration [266,267] and vascular tube formation [268–272]. Renal expression of PIM3 appears to play a role in arterial blood pressure control [273], while neuronal PIM1 affects synaptic plasticity [274]. In addition, PIM kinases, especially PIM2, are expressed in adipocytes, and interfering with their function prevents lipid accumulation [275]. Finally, PIM1 had been found to regulate osteoclastogenesis [276]. Understanding these physiological functions of PIM kinases provides both opportunities and cautions for therapeutic targeting. However, the lack of a clear phenotype in single or triple knockout mice suggests that PIM kinases are not only functionally redundant but also that compensatory pathways may take over in their absence. This redundancy suggests the presence of a therapeutic window for PIM inhibitors, potentially allowing their use in patients without severe side effects.

# 1.8.2 PIM-dependent signaling

#### 1.8.2.1 JAK/STAT

PIM genes are classic downstream targets of the JAK/STAT pathway. In response to cytokines or growth factors, activated STAT3 and STAT5 translocate to the nucleus and bind the PIM1 promoter, driving its transcription [277]. PIM1 forms part of a negative feedback loop in the JAK/STAT pathway. PIM1 can bind and activate SOCS (Suppressor of Cytokine Signaling) proteins, which are negative regulators of JAK/STAT signaling [277]. In some contexts, however, PIM kinase activity is able to amplify JAK activity, however no mechanistic explanation has been reported yet [278]. One key outcome of JAK/STAT-mediated PIM induction is enhanced expression or activity of pro-survival genes. PIM kinases promote cell survival by upregulating anti-apoptotic members of the BCL2 family and inhibiting pro-apoptotic factors. For example, PIM1 activity is known to maintain high BCL2 levels in growth-factor-deprived cells [279]. PIM1 directly phosphorylates the pro-apoptotic BH3-only protein BAD on Ser112 (a gatekeeper inhibitory site), causing BAD to bind 14-3-3 and preventing it from neutralizing BCL2. By inactivating BAD and sustaining BCL2, PIM kinases tip the balance towards cell survival under cytokine withdrawal.

#### 1.8.2.2 MYC

PIM kinases cooperate with the MYC oncogene [280]. PIM1 was first discovered as a common proviral insertion [281] in T cell lymphomagenesis as well as oncogenic partner acting in synergy with Myc in murine lymphoma models [282]. PIM2 can phosphorylate MYC at Ser329, which prolongs MYC protein half-life [280]. PIM1, on the other hand, has been shown to decrease MYC Thr58 phosphorylation while increasing Ser62 phosphorylation, therefore preventing MYC proteasomal degradation. Stabilized MYC acts as a more potent transcription factor, driving the expression of genes involved in cell growth (ribosome biogenesis, metabolism) and cell cycle progression (cyclins, cyclin-dependent kinases). PIM-mediated MYC stabilization has been linked to increased MYC transcriptional activity and transformative ability [280,283].

#### 1.8.2.3 NF-κB

PIM kinases intersect with the NF-κB pathway, a central regulator of inflammation and cell survival. PIM1 directly phosphorylates the NF-κB subunit RelA/p65 at Ser276 [284]. In the absence of this phosphorylation, RelA is more readily ubiquitinated and targeted for degradation, limiting NF-κB activity. Thus, PIM1 acts as a positive regulator of NF-κB by safeguarding p65 from turnover. Stabilized p65/RelA can accumulate in the nucleus and drive transcription of NF-κB target genes, many of which are pro-survival or pro-proliferative. For instance, PIM1 enhancement of NF-κB leads to sustained expression of cytokines (like IL-6) and anti-apoptotic proteins (like Bcl-xL or survivin) that NF-κB controls [284,285]. Notably, NF-κB itself can upregulate PIM expression (e.g. CD40 signaling in B-cells induces PIM1 via NF-κB, suggesting a feed-forward loop [286]). This makes NF-κB and PIM targets of interest in cancers with significant inflammatory signature, such as MM.

#### 1.8.2.4 PI3K/AKT/mTOR

The PI3K/AKT pathway is another master regulator of growth and survival that largely functionally overlaps with PIM signaling. PIM and Akt kinases are often co-activated in tumors and phosphorylate an overlapping set of substrates [277]. PIM kinases help maintain the activity of mTOR Complex 1 (mTORC1, mammalian target of rapamycin complex 1), a central nutrient sensor and growth regulator. PIMs phosphorylate inhibitory nodes upstream of mTORC1. Akt phosphorylates TSC2 (Tuberous Sclerosis Complex 2) on Ser939/Thr1462, and PIM2

phosphorylates TSC2 on Ser1798, each of which inactivates TSC2 and relieves its suppression of mTORC1 [287]. PIMs can phosphorylate PRAS40 (Proline-Rich Akt Substrate of 40 kDa) at Thr246, causing PRAS40 to dissociate from mTORC1 [288]. Freed from PRAS40 inhibition, mTORC1 becomes more active, leading to increased phosphorylation of its targets 4EBP1 (Eukaryotic Translation Initiation Factor 4E Binding Protein 1) and p70S6K (Ribosomal Protein S6 Kinase B1), key nodes controlling protein synthesis. Beyond mTORC1 activation, PIM kinases directly regulate the protein synthesis machinery. PIM kinases can maintain translation initiation even when mTORC1 is inhibited. PIM1/2 directly phosphorylate 4E-BP1, the capbinding repressor, thus preventing it from sequestering eIF4E (Eukaryotic Translation Initiation Factor 4E) [289]. Furthermore, PIM1 phosphorylates eIF4B (Eukaryotic Translation Initiation Factor 4B) on Ser406, and promotes eIF4B's association with the translation pre-initiation complex [290].

#### 1.8.2.5 MAPK

Normal fibroblasts engineered to express KRAS G12V oncogene undergo hyper-proliferative signaling through ERK, but if they lack PIM kinases, they die to metabolic stress and ROS accumulation [291]. This suggests that PIMs function as critical "fitness" factors for Ras-driven proliferation, limiting oxidative stress and adjusting energy production so that ERK-activated growth program can be sustained. PIM1 phosphorylates the MAP3K ASK1 (Apoptosis Signal-Regulating Kinase 1) at Ser83, impairing ASK1's ability to phosphorylate its downstream targets MKK4/7 and, subsequently, JNK/p38 MAPKs. Since JNK/p38 pathways can induce apoptosis or cell cycle arrest (for instance, through upregulation of pro-apoptotic BIM [Bcl2-Interacting Mediator Of Cell Death] or cell cycle inhibitor p21), PIM's suppression of this cascade tilts the balance toward survival [292].

#### 1.8.2.6 Cell cycle

PIM1/2 phosphorylate FOXO1 and FOXO3 (Forkhead Box O1/3), leading to their inactivation and downregulation of target genes, such as p27 [293]. PIM kinases not only suppress p27 transcription via FOXO but also promote p27 protein degradation. PIM1/2 phosphorylate p27 at Thr157 and Thr198, which causes p27 to bind 14-3-3 and be exported from the nucleus for proteasomal degradation [294]. PIM1 also phosphorylates and stabilizes SKP2 (S-Phase Kinase

Associated Protein 2), the F-box protein that ubiquitylates p27, further enhancing p27's downregulation [295]. PIM kinases directly activate the CDC25 (Cell Division Cycle 25) family of cell cycle phosphatases, which remove inhibitory phosphates on CDKs. PIM1 phosphorylates CDC25A and CDC25C, enhancing their phosphatase activity [296]. PIM1 also inactivates the CDC25A inhibitory kinase MARK3 (Microtubule Affinity Regulating Kinase 3) [297]. By phosphorylating and activating CDC25, PIM promotes the activation of CDKs that drive cell cycle transitions (CDC25A acts in G1/S to activate CDK2, while CDC25C acts in G2/M to activate CDK1). This shortens checkpoint pauses and accelerates cell cycle progression.

Due to their broad substrate specificity, PIM kinases phosphorylate and modulate components of multiple additional signaling pathways, such as hypoxia [298], cell metabolism [299,300], ROS detoxification [301], DNA damage response [302], MDM2/TP53 [303], drug efflux [304,305].

## 1.8.2.7 Role of PIM kinases in hematologic malignancies

In acute myeloid leukemia (AML), PIM kinases are overexpressed primarily through mutation-triggered activation of signaling pathways associated with FLT3-ITD (Fms-like Tyrosine Kinase 3 - Internal Tandem Duplication), JAK2, and STAT5 [306,307]. PIM kinases in AML cells drive survival pathways, prevent apoptosis, and foster chemoresistance by stabilizing anti-apoptotic proteins such as MCL1 (Myeloid Cell Leukemia Sequence 1) and by phosphorylating prosurvival factors. High PIM expression correlates with a poorer prognosis in AML patients, especially those with FLT3-ITD mutations. PIM2 promotes metabolic reprogramming, sustaining glycolysis and mitochondrial function in leukemic blasts, thus supporting their survival under metabolic stress. Preclinical studies show that PIM inhibition in AML cell lines can disrupt STAT5 activity, reduce c-MYC stability, and promote apoptotic pathways. PIM inhibition sensitizes AML cells to standard chemotherapy (cytarabine, doxorubicin) and targeted therapies (FLT3 inhibitors). PIMs are also crucial for survival of MPN (myeloproliferative neoplasm) cells, and targeting them, in combination with JAK and CDK4/6 inhibitors is effective in MPN patients [308,309].

PIM kinases, particularly PIM1 and PIM2, are overexpressed in both B-cell and T-cell acute lymphoblastic leukemia (B-ALL and T-ALL). [310–313]. Their expression is partially driven by

IL-7/STAT5 signaling, which promotes leukemic cell survival and expansion. PIMs have been shown to be essential for pre-B-cell transformation [314]. PIM kinases in ALL confer glucocorticoid resistance [312]. PIM1 inhibition has been investigated as a strategy to enhance the efficacy of tyrosine kinase inhibitors in Ph+ B-ALL [315].

PIM1 and PIM2 are frequently upregulated in chronic lymphocytic leukemia (CLL) cells, particularly in the presence of cytokine-secreting microenvironmental cells. PIM kinases in CLL enhance chemotactic responses via the CXCR4 (C-X-C Motif Chemokine Receptor 4) pathway, increasing cell homing to protective niches. Additionally, PIM's effects on BCL2 (B-Cell CLL/Lymphoma 2) family members provide anti-apoptotic advantages. Targeting PIM kinases in CLL is of high therapeutic interest as it may disrupt interactions within the microenvironment and render CLL cells more susceptible to apoptosis [316–318]. PIM inhibitors are being tested in combination with BTK (Bruton Tyrosine Kinase) inhibitors (ibrutinib) and BCL2 inhibitors to overcome therapy resistance in CLL [319].

PIM1 is highly expressed in mantle cell lymphoma (MCL), especially in cases with aggressive disease phenotypes [320,321]. PIM kinases regulate cyclin D1 levels, a hallmark driver of MCL proliferation. Targeting PIMs in MCL is a currently investigated therapeutic strategy [322,323]. PIM kinases are expressed in follicular lymphoma (FL) [324], but their role is still unknown. In Hodgkin lymphoma (HL), PIMs contribute to the activation of pro-survival NF-κB and JAK/STAT pathways [278], promoting Reed-Sternberg cell survival and immune escape. In primary mediastinal B-cell lymphoma (PMBCL) PIM kinases are promoting cancer cell survival via a similar mechanism [325].

In diffuse large B-cell lymphoma (DLBCL), PIM kinases often work in conjunction with other oncogenes, including MYC and BCL6 (B-Cell Lymphoma 6) [249]. The *PIM1* gene, located at 6p21, is frequently mutated in DLBCL, where it is associated with higher proliferative indices and an aggressive disease course [326]. PIM1 is overexpressed in DLBCL subtypes with an "activated B-cell" (ABC) phenotype, where it enhances NF-κB activity, cell survival, motility and growth [327–329]. The degree of PIM expression often correlates with disease severity, making it a useful prognostic marker in some lymphoma cases [330,331].

## 1.8.3 PIM kinases in MM

PIM kinases, especially PIM2, have been linked with differentiation of B cells into plasmablasts, and their expression is crucial for plasma cell survival [332]. PIM2 is significantly overexpressed in MM cells compared to other hematologic malignancies, and its expression is further induced by interactions with the bone marrow microenvironment [333]. BMSCs and osteoclasts upregulate PIM2 through cytokines such as IL-6, TNF-α, BAFF, and APRIL, most likely via the JAK/STAT3 and NF-κB pathways [334]. This upregulation confers resistance to apoptosis and promotes myeloma cell survival.

PIM2 enhances the survival of MM cells by phosphorylating key pro-apoptotic proteins such as BAD (BCL2 Associated Agonist Of Cell Death), thereby preventing its interaction with BCL2 and BCL-xL [335]. This phosphorylation event results in the inhibition of apoptosis, making MM cells more resilient to stress and therapeutic interventions [334]. Additionally, PIM2 reduces apoptotic priming in MM, and PIM inhibition promotes MCL1 dependency [336]. PIM2 plays a significant role in metabolic adaptation in MM cells. It regulates glycolysis and oxidative phosphorylation to sustain energy production [337]. PIM2 also modulates the DNA damage response (DDR) in MM cells. It acts as a negative regulator of DDR by suppressing ATR (Ataxia Telangiectasia And Rad3 Related) signaling, thereby allowing MM cells to continue proliferating despite accumulating genomic instability [338]. Inhibition of PIM2 results in increased activation of DDR markers.

In addition to promoting MM cell survival, PIM2 is involved in MM-associated bone disease by negatively regulating osteoblastogenesis and enhancing osteoclast activity [339]. PIM2 expression is upregulated in osteoclast lineage cells, promoting RANKL-induced osteoclastogenesis and bone resorption [340]. Inhibition of PIM2 restores osteoblast differentiation and reduces MM-associated bone destruction [339].

PIM kinases, particularly PIM2, play an important role in multiple myeloma by promoting cell survival, metabolic adaptation, DNA damage tolerance, and MM bone disease. Targeting PIM kinases with small-molecule inhibitors represents a promising therapeutic approach, particularly in combination with existing MM treatments.

## 1.8.4 PIM kinase inhibitors

Given their involvement in many types of cancer, PIM kinases are considered good targets for therapeutic intervention. Their unique ATP-binding pocket and lack of regulatory phosphorylation make PIM kinases suitable for small molecule inhibition. PIM2 has a low ATP  $K_m$  (Michaelis Constant), meaning it binds ATP with high affinity, necessitating a highly potent inhibitor to effectively suppress its kinase activity at the ATP concentrations present in cells. Table 1 summarizes the current landscape of PIM inhibitors.

Several PIM inhibitors have been evaluated in preclinical and clinical studies for multiple myeloma or other blood cancers.

SGI-1776 is one of the first pan-PIM inhibitors tested in MM in preclinical studies. It induces mainly autophagy rather than apoptosis, reducing MM viability [341]. However, this compound did not suceed in clinical trials due to severe cardiac adverse effects [342]. INCB053914, another pan-PIM inhibitor, has demonstrated efficacy against MM cell lines in preclinical studies [343] and has a favorable safety profile when administered to humans. A phase 1/2 study in blood cancer patients is currently ongoing, however limited clinical efficacy has been reported when the compound was used in monotherapy, despite achieving pharmacodynamic target inhibition [344]. Similarly, no objective clinical responses were observed in AML patients treated with AZD1208, another pan-PIM inhibitor, although some patients experienced reductions in peripheral blast counts [345]. Pharmacodynamic assessments indicated biological activity of AZD1208, but these did not translate into significant clinical efficacy as a monotherapy.

PIM447 (LGH447), a potent pan-PIM inhibitor, has been shown to induce apoptosis, reduce tumor burden *in vivo*, and exert its effects primarily through mTOR inhibition and suppression of protein translation [346,347]. A phase 1 trial demonstrated disease control in 72.2% of patients with relapsed/refractory MM, while overall response rate was 8.9% [348]. Unfortunately, the bone marrow examination showed lack of reduction of plasma cell count, suggesting cytostatic, rather than cytotoxic response to PIM447. A similar concurrent trial conducted in Japan has been terminated early due to lack of clinical efficacy in MM [349]. Despite potential synergistic effect of PIM447 with PIs and IMiDs, clinical development of PIM447 in MM has been suspended [347].

TP-3654, a mostly PIM1-selective kinase inhibitor, has been investigated in a Phase 1/2 study for patients with relapsed or refractory myelofibrosis. Preliminary data indicate that TP-3654 is well tolerated, with no dose-limiting toxicities reported [350]. No data on its anti-MM efficacy are currently available.

Clinical trials of MEN1703/SEL24 (dapolsertib), an oral dual PIM/FLT3 kinase inhibitor, have demonstrated a manageable safety profile and preliminary efficacy in patients with relapsed or refractory acute myeloid leukemia (AML) [351,352]. In the DIAMOND-01 trial, the recommended dose was established at 125 mg/day, with common adverse events including asthenia, nausea, and vomiting. Among AML patients harboring IDH1/2 mutations, an objective response rate of 13% was observed, with some achieving complete responses or partial responses, and one patient proceeding to HSC transplantation. Based on our prior preclinical studies in DLBCL [353], MEN1703 is now being evaluated in a Phase 2 trial (JASPIS-01, NCT06534437) in combination with glofitamab [354].

Developing safe and effective PIM kinase inhibitors has been challenging. Despite promising preclinical results, these inhibitors have shown limited success in the clinic so far. This gap may be due to the complex role of PIM kinases in cancer and the ability of cells to compensate when these kinases are blocked. To overcome these hurdles, more in-depth preclinical studies are needed in order to pave the way for more effective, next generation PIM inhibitors.

Table 1. Key compounds targeting the PIM kinase family that have advanced to late-stage preclinical or clinical studies.  $IC_{50}$  - Half-maximal Inhibitory Concentration; Ki - Inhibition Constant; Kd - Dissociation Constant.

Name(s)	Chemical structure	Binding affinities	Tested indication
SMI-4a	F ONH S	IC <sub>50</sub> : PIM1: 24 nM PIM2: 100 nM PIM3: NA	-
SGI-1776	N N N N F F F F F F F F F F F F F F F F	Half-maximal inhibitory concentration (IC <sub>50</sub> ): PIM1: 7nM PIM2 363 nM PIM3: 69nM	Phase 1: Prostate cancer and Non-Hodgkin lymphoma (NCT00848601) Phase 1: Leukemia (NCT01239108)
	~	Inhibition constant (Ki): PIM1: 12 nM PIM2: 980 nM PIM3: 20 nM	
TP-3654/ Nuvisertib	HO N N F F F F F	Ki: PIM1: 5 nM PIM2: 239 nM PIM3: 42 nM	Phase 1: Healthy volunteers (NCT06389955) Phase 1: Myelofibrosis (NCT04176198) Phase 1: Solid tumors (NCT03715504)
AZD1208	HN O S NH <sub>2</sub>	IC <sub>50</sub> : PIM1: 0.4 nM PIM2: 5 nM PIM3: 1.9 nM	Phase 1: Solid tumors and lymphoma (NCT01588548) Phase 1: AML (NCT01489722)
LGB321	NH <sub>2</sub> OH NH F H-CI	Ki: PIM1: 1 pM PIM2: 2.1 pM PIM3: 0.8 pM	-
LGH447/ PIM447	H <sub>2</sub> N F F F	Ki: PIM1: 6 pM PIM2: 18 pM PIM3: 9 pM	Phase 1: MM (NCT01456689, NCT02144038, NCT02160951) Phase 1: AML and MDS (NCT02078609) Phase 1: Myelofibrosis (NCT02370706)
INCB053914/ Uzansertib	OH HO-P-OH OH	IC <sub>50</sub> : PIM1: 0.24 nM PIM2: 30 nM PIM3: 0.12 nM	Phase 1: MM (NCT04355039) Phase 1: DLBCL (NCT03688152) Phase 1/2: AML and myelofibrosis (NCT02587598)

CX-6258		IC <sub>50</sub> : PIM1: 5 nM PIM2: 25 nM PIM3: 16 nM	-	
MEN1703/ SEL24/ Dapolsertib	Br NH NH	Dissociation constants (Kd): PIM1: 2 nM PIM2: 2 nM PIM3 :3 nM	Phase 1/2: (NCT03008187) Phase 2: (NCT06534437)	AML DLBCL

## 1.9 Need for further research

MM is a genetically diverse and complex disease. Complex relationships between tumor cells and the TME contribute to failure of monotherapies to achieve lasting disease control [355]. While advancements in the available treatment options have improved patient survival, high-risk patients continue to face poor prognoses [356]. Current therapies also cause significant side effects like peripheral neuropathy and immunosuppression, emphasizing the need for novel therapeutic strategies. Therefore, MM remains a chronic, incurable and debilitating disease. For this reason, the identification and validation of new drug targets, as well as the optimization of existing therapies, are crucial for improving patient outcomes. MM treatment strategies often focus on introducing new drug classes into subsequent therapeutic lines, which can reduce cross-resistance and expand treatment options, improving disease management [357]. New drug classes engaging novel therapeutic targets carry a particular therapeutic potential to broaden the available treatment arsenal.

Despite transformative advances (proteasome inhibitors, IMiDs, anti-CD38 mAbs, CAR T-cells), MM remains incurable. Resistance emerges both through cell-intrinsic adaptations and through protective signals originating from the bone marrow microenvironment. PIM kinases are serine/threonine kinases that integrate growth, survival, and stress tolerance pathways and are upregulated in MM. We hypothesized that: (i) MM cells are addicted to PIM signaling, and (ii) MM-associated endothelial cells also depend on PIM activity to create a tumor-supportive niche. This thesis addresses these two hypotheses.

# 1.10 Objectives of this thesis

This thesis aims to investigate the roles of PIM kinases in multiple myeloma, examining their effects both on malignant plasma cells and the surrounding microenvironment, particularly MM-associated endothelial cells. While PIM kinases are known to promote oncogenic signaling and survival in hematologic cancers, their specific contributions to MM pathogenesis and progression remain incompletely understood.

The core objectives of this thesis are as follows:

- 1. To define the expression and activation patterns of PIM1, PIM2, and PIM3 in MM. This includes comparing protein expression in malignant versus normal plasma cells and determining the prevalence of PIM-positive MM cases using immunohistochemistry and validated tissue microarrays.
- To evaluate the functional dependency of MM cells on PIM kinases. Using genetic
  and pharmacological approaches, we aimed to assess how MM cells respond to selective
  or pan-PIM inhibition.
- To characterize the transcriptional and mechanistic consequences of PIM inhibition in MM. We aimed to apply transcriptomic profiling to identify key pathways disrupted by PIM blockade.
- 4. To investigate the role of PIM kinases in the MM-associated microenvironment. This includes examining how PIM signaling affects bone marrow endothelial cells, angiogenesis, and the MM-EC crosstalk.
- 5. To evaluate the therapeutic potential of PIM inhibition in preclinical MM models. We aimed to test the efficacy of PIM inhibitors *in vitro* and *in vivo* using MM cell lines, primary patient samples, and murine xenograft models.

# 2 Materials and methods

# 2.1 Materials

### 2.1.1 Cell lines and bacterial strains

#### 2.1.1.1 Human cell lines

Table 2. Mammalian cell lines used in this thesis. F, female; M, male; nons, nonsecretory; DSMZ, German Collection of Microorganisms and Cell Cultures; ATCC, American Type Culture Collection; JCRB, Japanese Collection of Research Bioresources; DFCI, Dana-Farber Cancer Institute; MM, multiple myeloma; DLBCL, diffuse large B-cell lymphoma; nd, no data.

Cell line	Disease type	Cytokine dependence	Sex	Ancestry	Heavy chain	Light chain	Source
AMO1	MM	-	F	East Asia	ΙgΑ	Kappa	DSMZ
ANBL6	MM	IL6	F	Europe	nd	Lambda	Keats Lab
BMEC60	-	VEGFA, FGF2, IGF1, EGF	nd	nd	-	-	van der Schoot Lab
DP6	MM	IL6	F	Europe	IgA	Lambda	Keats Lab
H929	MM	-	F	Europe	ΙgΑ	Kappa	ATCC
HBL1	DLBCL	-	М	East Asia	-	-	DSMZ
HEK293T	-	-	F	Europe	-	-	Chowdhury Lab
HUVEC- TERT2	-	VEGFA, FGF2, IGF1, EGF	F	Europe	-	-	ATCC
INA6	MM	IL6	М	Europe	IgG	Карра	Gramatzki Lab
JJN3	MM	-	F	Europe	IgA1	Kappa	DSMZ
KJON	MM	IL6, human serum	F	Europe	nd	Карра	Holien Lab
KMM1	MM	-	М	East Asia	nd	Lambda	JCRB
KMS11	MM	-	F	East Asia	IgG	Kappa	JCRB
KMS12BM	MM	-	F	East Asia	nons	nons	DSMZ
KMS12PE	MM	-	F	East Asia	nons	nons	DSMZ
KMS18	MM	-	М	East Asia	IgA	Lambda	Carrasco Lab
KMS20	MM	-	F	East Asia	IgG	Kappa	JCRB
KMS26	MM		М	East Asia	IgG	Kappa	JCRB
KP6	MM	-	М	Europe	IgG	Карра	Keats Lab
L363	MM	-	F	Europe	IgG	Lambda	DSMZ
MM1.S	MM	-	F	Africa	ΙgΑ	Lambda	ATCC
MOLP8	MM	-	nd	East Asia	nd	Lambda	DSMZ
OCI-Ly1	DLBCL	-	М	nd	-	-	DSMZ

OCI-My5	MM	-	nd	Europe	nd	Lambda	Carrasco Lab
OCI-My7	MM	-	nd	Europe	nd	Карра	Carrasco Lab
OH2	MM	IL6	F	Europe	IgGl	Kappa	Keats Lab
OPM1	MM	_	F	East Asia	nd	Lambda	Carrasco
	101101		ı	Lastrisia	i i d	Lambda	Lab
OPM2	MM		F	East Asia	nd	Lambda	DSMZ
RPMI8226	MM	•	М	Africa	IgG	Lambda	ATCC
U266	MM	-	М	Europe	IgE	Lambda	ATCC
XG1	MM	IL6	М	Europe	ΙgΑ	Карра	Tonon Lab

## 2.1.1.2 Primary cells

Table 3. Primary cells used in this thesis. MM, multiple myeloma, HD, healthy donor; IRB, Institutional Review Board.

Cell type	Origin
MM patient bone marrow cells	Department of Hematology, Institute of Hematology and Transfusion Medicine, Warsaw, Poland (IRB approval 43/2016)
	Department of Pathology, Brigham and Women's Hospital, Boston, Massachusetts, USA (IRB approval #01-206)
HD bone marrow cells	BioIVT, Cat. No. HUMANHLBM-0002228 (Westbury, New York, USA)

### 2.1.1.3 Bacterial strains

Table 4. Bacterial strains used in this thesis.

Strain	Source
E. coli MAX Efficiency DH5α	Thermo Fisher Scientific
	(Massachusetts, USA)
One Shot Stbl3 Chemically Competent E. coli	Thermo Fisher Scientific
	(Massachusetts, USA)

## 2.1.1.4 Genetically modified cell lines

Table 5. Genetically modified mammalian cell lines used in this thesis.

Cell line	Description	Source
JJN3-TST209	JJN3 with tetracycline repressor (pTST209)	This work
JJN3-shPIM1.2	JJN3 with pTST201-shPIM1.2 for inducible KD of PIM1	This work
JJN3-shPIM1.3	JJN3 with pTST201-shPIM1.3 for inducible KD of PIM1	This work
JJN3-shPIM1.4	JJN3 with pTST201-shPIM1.4 for inducible KD of PIM1	This work
JJN3-shPIM1.5	JJN3 with pTST201-shPIM1.5 for inducible KD of PIM1	This work
JJN3-shPIM2.1	JJN3 with pTST201-shPIM2.1 for inducible KD of PIM2	This work
JJN3-shPIM2.2	JJN3 with pTST201-shPIM2.2 for inducible KD of PIM2	This work
JJN3-shPIM2.3	JJN3 with pTST201-shPIM2.3 for inducible KD of PIM2	This work

JJN3-shPIM2.4	JJN3 with pTST201-shPIM2.4 for inducible KD of PIM2	This work
JJN3-shPIM2.5	JJN3 with pTST201-shPIM2.5 for inducible KD of PIM2	This work
JJN3-shPIM3.1	JJN3 with pTST201-shPIM3.1 for inducible KD of PIM3	This work
JJN3-shPIM3.2	JJN3 with pTST201-shPIM3.2 for inducible KD of PIM3	This work
JJN3-shPIM3.3	JJN3 with pTST201-shPIM3.3 for inducible KD of PIM3	This work
JJN3-shPIM3.4	JJN3 with pTST201-shPIM3.4 for inducible KD of PIM3	This work
JJN3-shPIM3.5	JJN3 with pTST201-shPIM3.5 for inducible KD of PIM3	This work
JJN3-shSCR	JJN3 with pTST201-shSCR, control cell line	This work
JJN3-sh3xPIM	JJN3 with pTST201-shTRIPLE for inducible KD of PIM1,	This work
	PIM2, PIM3	
MM1.S-luc	MM1.S stably expressing firefly luciferase	This work

# 2.1.2 Chemicals and reagents

# 2.1.2.1 Chemicals

Table 6. Chemicals and reagents used in this study.

Name	Manufacturer		
Acrylamide/Bis-acrylamide, 37.5:1, 30% mix	Bio-Rad (Hercules, CA, USA)		
Agar	ROTH (Karlsruhe, Germany)		
Agarose	ROTH (Karlsruhe, Germany)		
Alexa Fluor 488-phalloidin	Cell Signaling Technology (Danvers, MA, USA)		
Ampicillin	Sigma-Aldrich (St. Louis, MO, USA)		
APS	Sigma-Aldrich (St. Louis, MO, USA)		
ATP	PamGene (Hertogenbosch, The Netherlands)		
AZD1208	SelleckChem (Houston, TX, USA)		
BgIII	Thermo Fisher Scientific (Waltham, MA, USA)		
Bortezomib	SelleckChem (Houston, TX, USA)		
Bromophenol blue	ROTH (Karlsruhe, Germany)		
BSA (bovine serum albumin), heat shock fraction, protease free (A3294)	Sigma-Aldrich (St. Louis, MO, USA)		
BstXI	Thermo Fisher Scientific (Waltham, MA, USA)		
CaCl <sub>2</sub> ·2H <sub>2</sub> O	ROTH (Karlsruhe, Germany)		
CD138 microbeads	Miltenyi Biotec (Bergisch Gladbach, Germany)		
CD31 MicroBeads	Miltenyi Biotec (Bergisch Gladbach, Germany)		
Chloramphenicol	Sigma-Aldrich (St. Louis, MO, USA)		
Citric acid	Sigma-Aldrich (St. Louis, MO, USA)		
CytoFlex Isoflow Sheath Fluid	Beckman Coulter (Brea, CA, USA)		
D-Glucose	Sigma-Aldrich (St. Louis, MO, USA)		
DMSO	Sigma-Aldrich (St. Louis, MO, USA)		
DNA Gel Loading Dye (6x)	Thermo Fisher Scientific (Waltham, MA, USA)		

dNTPs	oligo.pl (Warsaw, Poland)
Doxycycline hyclate	Sigma-Aldrich (St. Louis, MO, USA)
EDTA	ROTH (Karlsruhe, Germany)
Ethanol	Sigma-Aldrich (St. Louis, MO, USA)
Ethidium bromide	ROTH (Karlsruhe, Germany)
Fibronectin (F2006)	Sigma-Aldrich (St. Louis, MO, USA)
G418 (Geneticin)	Sigma-Aldrich (St. Louis, MO, USA)
Gelatin (porcine)	Sigma-Aldrich (St. Louis, MO, USA)
GeneRuler 1 kb DNA ladder	Thermo Fisher Scientific (Waltham, MA, USA)
Glacial acetic acid	Pol-Aura (Dywity, Polska)
Glycerol	ROTH (Karlsruhe, Germany)
Glycine	Sigma-Aldrich (St. Louis, MO, USA)
Guanidine hydrochloride	Pol-Aura (Dywity, Polska)
HCI (concentrated 37%)	Pol-Aura (Dywity, Polska)
Hoechst 34580	BD (Franklin Lakes, NJ, USA)
Hydrogen peroxide (3%)	Sigma-Aldrich (St. Louis, MO, USA)
INCB053914	SelleckChem (Houston, TX, USA)
Isopropanol	ROTH (Karlsruhe, Germany)
IVISbrite D-Luciferin Potassium Salt Bioluminescent Substrate	Revvity (Waltham, MA, USA)
KCI	ROTH (Karlsruhe, Germany)
KH <sub>2</sub> PO <sub>4</sub>	ROTH (Karlsruhe, Germany)
Matrigel (Growth Factor-Reduced)	Corning (Corning, NY, USA)
MEN1703	Menarini Ricerche SpA (Florence, Italy)
Methanol	ROTH (Karlsruhe, Germany)
MgCl <sub>2</sub> ·6H <sub>2</sub> O	ROTH (Karlsruhe, Germany)
MgSO <sub>4</sub> ·7H <sub>2</sub> O	ROTH (Karlsruhe, Germany)
MnCl <sub>2</sub> ·4H <sub>2</sub> O	ROTH (Karlsruhe, Germany)
MOPS free acid	Pol-Aura (Dywity, Polska)
Na <sub>2</sub> HPO <sub>4</sub> ·2H <sub>2</sub> O	ROTH (Karlsruhe, Germany)
NaCl	ROTH (Karlsruhe, Germany)
NaHCO <sub>3</sub>	ROTH (Karlsruhe, Germany)
NaOH	ROTH (Karlsruhe, Germany)
Non-fat dry milk	ROTH (Karlsruhe, Germany)
NP-40	Sigma-Aldrich (St. Louis, MO, USA)
NucBlue Live	Thermo Fisher Scientific (Waltham, MA,
Naobiao Eivo	USA)
Nuclease-free water, DEPC treated	ROTH (Karlsruhe, Germany)
PageRuler Prestained Protein Ladder	Thermo Fisher Scientific (Waltham, MA,
	USA)
Paraformaldehyde 16% (Cell Signaling)	Cell Signaling Technology (Danvers, MA, USA)
PIM447	SelleckChem (Houston, TX, USA)
Ponceau S	Sigma-Aldrich (St. Louis, MO, USA)
Potassium acetate	Sigma-Aldrich (St. Louis, MO, USA)
ProLong Glass Antifade Mountant	Thermo Fisher Scientific (Waltham, MA, USA)
Propidium iodide	BD (Franklin Lakes, NJ, USA)

Puromycin	Thermo Fisher Scientific (Waltham, MA, USA)
PVDF membrane	Merck Millipore (Burlington, MA, USA)
Random hexamers	Thermo Fisher Scientific (Waltham, MA, USA)
RbCl (Rubidium chloride)	ROTH (Karlsruhe, Germany)
RNase A (DNase-free)	PanReac Applichem (Chicago, IL, USA)
RNaseOUT RNase Inhibitor	Thermo Fisher Scientific (Waltham, MA, USA)
Sacl	Thermo Fisher Scientific (Waltham, MA, USA)
SDS	ROTH (Karlsruhe, Germany)
SGI1776	SelleckChem (Houston, TX, USA)
Sodium acetate	Sigma-Aldrich (St. Louis, MO, USA)
Sodium citrate dihydrate	Sigma-Aldrich (St. Louis, MO, USA)
Sodium deoxycholate	Sigma-Aldrich (St. Louis, MO, USA)
SYBR Gold	Thermo Fisher Scientific (Waltham, MA, USA)
T4 DNA Ligase	Thermo Fisher Scientific (Waltham, MA, USA)
T4 Polynucleotide Kinase	Thermo Fisher Scientific (Waltham, MA, USA)
TEMED	Sigma-Aldrich (St. Louis, MO, USA)
Thymolphthalein	Pol-Aura (Dywity, Polska)
Tris base	ROTH (Karlsruhe, Germany)
Triton X-100	Sigma-Aldrich (St. Louis, MO, USA)
Triton X-114	Sigma-Aldrich (St. Louis, MO, USA)
Trypan blue	Thermo Fisher Scientific (Waltham, MA, USA)
Tryptone	ROTH (Karlsruhe, Germany)
Tween 20	Sigma-Aldrich (St. Louis, MO, USA)
Western Lightning Pro, Chemiluminescent Substrate	PerkinElmer (Shelton, CT, USA)
Western Lightning Ultra, Chemiluminescent Substrate	PerkinElmer (Shelton, CT, USA)
Yeast extract	ROTH (Karlsruhe, Germany)
β-mercaptoethanol	Sigma-Aldrich (St. Louis, MO, USA)

# 2.1.2.2 Kits

Table 7. Kits used in this study.

Name	Manufacturer	Catalog number
BigDye Terminator v3.1 Cycle	Applied Biosystems (Waltham,	4337455
Sequencing Kit	MA, USA)	
Caspase-Glo 3/7 Assay Kit	Promega (Madison, WI, USA)	G8090
Caspase-Glo 8 Assay Kit	Promega (Madison, WI, USA)	G8200
Caspase-Glo 9 Assay Kit	Promega (Madison, WI, USA)	G8210
CometAssay Single Cell Gel	Trevigen (Gaithersburg, MD, USA)	4250-050-K
Electrophoresis Assay		

Dual-Luciferase Reporter Assay System	Promega (Madison, WI, USA)	E1910
EnVision™ FLEX DAB+ Substrate Chromogen System	Dako (Glostrup, Denmark)	GV825
ExTerminator PCR Cleanup Kit	A&A Biotechnology (Gdańsk, Poland)	444-250
FITC Annexin V Apoptosis Detection Kit	BD Biosciences (San Jose, CA, USA)	556547
GeneMATRIX Plasmid Miniprep DNA Purification Kit	EURx (Gdańsk, Poland)	E3500
iTaq Universal SYBR Green Supermix	Bio-Rad (Hercules, CA, USA)	1725124
KAPA Library Quantification Kit	Roche (Pleasanton, CA, USA)	KK4824
Liquid Permanent Red, Substrate- Chromogen	Dako (Glostrup, Denmark)	GV825
MycoAlert Mycoplasma Detection Kit	Lonza (Walkersville, MD, USA)	LT07-318
NEBNext Dual Index UMI Adaptors	New England Biolabs (Ipswich, MA, USA)	E7395S
		E7400V
NEBNext rRNA Depletion Kit v2	New England Biolabs (Ipswich, MA, USA)	E7400X
NEBNext rRNA Depletion Kit v2  NEBNext Ultra II Directional RNA Library Prep Kit for Illumina	` ` ` ` ` ` ` ` ` ` ` ` ` ` ` ` ` ` ` `	E7400X E7765L
NEBNext Ultra II Directional RNA Library Prep Kit for Illumina NZYGelpure Gel Extraction Kit	MA, USA)  New England Biolabs (Ipswich, MA, USA)  NZYTech (Lisbon, Portugal)	E7765L MB011
NEBNext Ultra II Directional RNA Library Prep Kit for Illumina NZYGelpure Gel Extraction Kit PE Annexin V Apoptosis Detection Kit I	MA, USA)  New England Biolabs (Ipswich, MA, USA)  NZYTech (Lisbon, Portugal)  BD Biosciences (San Jose, CA, USA)	E7765L MB011 559763
NEBNext Ultra II Directional RNA Library Prep Kit for Illumina NZYGelpure Gel Extraction Kit PE Annexin V Apoptosis Detection	MA, USA)  New England Biolabs (Ipswich, MA, USA)  NZYTech (Lisbon, Portugal)  BD Biosciences (San Jose, CA, USA)  Thermo Fisher Scientific (Waltham, MA, USA)	E7765L MB011
NEBNext Ultra II Directional RNA Library Prep Kit for Illumina NZYGelpure Gel Extraction Kit PE Annexin V Apoptosis Detection Kit I	MA, USA)  New England Biolabs (Ipswich, MA, USA)  NZYTech (Lisbon, Portugal)  BD Biosciences (San Jose, CA, USA)  Thermo Fisher Scientific	E7765L MB011 559763
NEBNext Ultra II Directional RNA Library Prep Kit for Illumina  NZYGelpure Gel Extraction Kit  PE Annexin V Apoptosis Detection Kit I  Pierce BCA Protein Assay Kit	MA, USA)  New England Biolabs (Ipswich, MA, USA)  NZYTech (Lisbon, Portugal)  BD Biosciences (San Jose, CA, USA)  Thermo Fisher Scientific (Waltham, MA, USA)  Thermo Fisher Scientific (Waltham, MA, USA)  Thermo Fisher Scientific (Waltham, MA, USA)	E7765L  MB011 559763  23225  Q32851  Q32850
NEBNext Ultra II Directional RNA Library Prep Kit for Illumina NZYGelpure Gel Extraction Kit PE Annexin V Apoptosis Detection Kit I Pierce BCA Protein Assay Kit  Qubit DNA HS Assay Kit  Qubit dsDNA BR Assay Kit  Qubit RNA HS Assay Kit	MA, USA)  New England Biolabs (Ipswich, MA, USA)  NZYTech (Lisbon, Portugal)  BD Biosciences (San Jose, CA, USA)  Thermo Fisher Scientific (Waltham, MA, USA)  Thermo Fisher Scientific (Waltham, MA, USA)  Thermo Fisher Scientific (Waltham, MA, USA)	E7765L  MB011 559763  23225  Q32851  Q32850
NEBNext Ultra II Directional RNA Library Prep Kit for Illumina  NZYGelpure Gel Extraction Kit PE Annexin V Apoptosis Detection Kit I Pierce BCA Protein Assay Kit  Qubit DNA HS Assay Kit  Qubit dsDNA BR Assay Kit  Qubit RNA HS Assay Kit  QuickLoad Taq 2× Master Mix	MA, USA)  New England Biolabs (Ipswich, MA, USA)  NZYTech (Lisbon, Portugal)  BD Biosciences (San Jose, CA, USA)  Thermo Fisher Scientific (Waltham, MA, USA)  New England Biolabs (Ipswich, MA, USA)	E7765L  MB011 559763  23225  Q32851  Q32850  Q32852  M0271L
NEBNext Ultra II Directional RNA Library Prep Kit for Illumina NZYGelpure Gel Extraction Kit PE Annexin V Apoptosis Detection Kit I Pierce BCA Protein Assay Kit  Qubit DNA HS Assay Kit  Qubit dsDNA BR Assay Kit  Qubit RNA HS Assay Kit	MA, USA)  New England Biolabs (Ipswich, MA, USA)  NZYTech (Lisbon, Portugal)  BD Biosciences (San Jose, CA, USA)  Thermo Fisher Scientific (Waltham, MA, USA)  New England Biolabs (Ipswich,	E7765L  MB011 559763  23225  Q32851  Q32850  Q32852

# 2.1.3 Buffers and solutions

**Table 8. Compositions of buffers and solutions used in this study.** Warning - always handle concentrated acids and bases under fume hood and wear protective PPE.

Name	Recipe/Composition
Alkaline Electrophoresis Solution	200 mM NaOH + 1 mM EDTA; adjust pH >13
Alkaline Unwinding Solution	200 mM NaOH + 1 mM EDTA; adjust pH >13

Amnicillin Stock (0.1 g/ml.)	Dissolve 1 a Ampieillin in 10 ml storile H O	
Ampicillin Stock (0.1 g/mL)	Dissolve 1 g Ampicillin in 10 mL sterile H <sub>2</sub> O Adjust pH to ~10 with 1 M NaOH to help dissolve	
	Sterile-filter (0.22 µm)	
	Aliquot and store at -80 °C (stable for 1 year)	
	Dilute 1:1000 to reach the working concentration of	
	100 µg/mL	
APS (10%)	Weigh 1.0 g APS powder.	
,	Dissolve in 10 mL cold distilled water.	
	Mix gently until fully dissolved.	
	Aliquot if needed.	
	Store at -20 °C; prepare fresh every few weeks for best	
	activity.	
CaCl <sub>2</sub> (2.5 M)	Weigh 36.75 g CaCl₂·2H₂O	
	Dissolve in ~70 mL distilled water	
	Bring volume to 100 mL with distilled water	
	Filter-sterilize (0.22 µm) under laminar flow	
011 1 1 01 1 (05	Store at 4 °C	
Chloramphenicol Stock (25	Dissolve 250 mg chloramphenicol in 10 mL 100%	
mg/mL)	ethanol	
	Mix until fully dissolved Filter-sterilize (0.22 µm) if needed	
	Aliquot and store at -20 °C (light-protected)	
	Use at 1:1000 dilution for 25 µg/mL working	
	concentration	
Citrate Buffer, pH 6.0)	24.27 g Sodium Citrate dihydrate	
	3.36 g Citric Acid	
	Dissolve in ~800 mL deionized water	
	Adjust pH to 6.0 with 0.1 N HCI	
	Bring volume to 1 L	
Doxycycline Stock (10 mg/mL)	Dissolve 100 mg Doxycycline in 10 mL sterile water	
	Protect from light	
	Filter-sterilize (0.22 µm)	
	Aliquot and store at -20 °C	
	Working concentration: 0.5 µg/mL (1:20,000)	
EDTA, pH 8.0 (0.5 M)	Weigh 93.05 g EDTA disodium salt (MW 372.24 g/mol).	
	Add to 400 mL deionized water	
	Slowly add solid NaOH until EDTA fully dissolves and pH reaches 8.0	
	Adjust volume to 500 mL with water	
Endotoxin Removal (ER) Buffer	750 mM NaCl	
Endotoxin Nemovai (EN) Ballei	10% Triton X-114	
	40 mM MOPS, pH 7.0	
	Adjust pH to 7.0 with NaOH	
	Bring to 100 mL with ddH₂O	
	Store at 4 °C	
	Apply heat to resolubilize the contents before use.	
F-actin Extraction Buffer	0.75 µL 1 M Guanidine HCl	
	0.5 μL 1 M Sodium Acetate	
	0.2 μL 2.5 M CaCl <sub>2</sub>	
	5 μL 100 mM ATP	
	50 μL 1 M Tris-HCl, pH 7.5	

	443.55 μL ddH₂O
	Mix fresh; use immediately or store on ice
Fibronectin coating solution	Stock solution:
	Dissolve fibronectin in sterile PBS to a concentration of
	1 mg/mL
	Aliquot and store at -80 °C. Avoid repeated freeze-thaw
	cycles
	Working solution (50 μg/mL):
	Dilute the 1 mg/mL stock 1:20 in sterile PBS
G418 Stock (100 mg/mL)	Dissolve 1 g G418 in 10 mL sterile water
	Filter-sterilize (0.22 µm)
	Aliquot and store at -20 °C
	Working concentration: 1000 µg/mL (1:100 dilution)
Gelatin coating solution (0.2%)	1 g gelatin
	500 mL distilled water
	Autoclave, store at 4 °C for up to 1 month
Glucose Solution (2.5 M)	Dissolve 22.52 g Glucose (C <sub>6</sub> H <sub>12</sub> O <sub>6</sub> , 100% purity) in
	~40 mL distilled water
	Stir until fully dissolved
	Adjust volume to 50 mL with distilled water
	Filter-sterilize using a 0.22 µm filter under laminar flow
	Store at 4 °C
Guanidine-HCl (1 M)	Weigh 0.96 g guanidine hydrochloride
` ,	Add to ~7 mL distilled water
	Heat to 35 °C for 30 minutes with gentle stirring until
	dissolved
	Bring volume to 10 mL with distilled water
	Use immediately
HBSS (1×)	8 g NaCl (0.14 M)
,	0.4 g KCl (0.005 M)
	0.14 g CaCl <sub>2</sub> (0.001 M)
	0.1 g MgSO <sub>4</sub> ·7H <sub>2</sub> O (0.0004 M)
	0.1 g MgCl <sub>2</sub> ·6H <sub>2</sub> O (0.0005 M)
	$0.06 \text{ g Na}_2\text{HPO}_4 \cdot 2\text{H}_2\text{O} (0.0003 \text{ M})$
	0.06 g KH <sub>2</sub> PO <sub>4</sub> (0.0004 M)
	1 g D-Glucose (0.006 M)
	0.35 g NaHCO <sub>3</sub> (0.004 M)
	Add ddH <sub>2</sub> O to 1 L total volume
	Adjust pH to 7.4 if needed
	Sterile-filter or autoclave if required
	Dilute 1:10 for working solution.
Laemmli Buffer (4×)	12.5 mL 1 M Tris-HCl, pH 6.8 (Stacking Gel Buffer)
	2.5 g SDS (5%)
	20 mL Glycerol (40%)
	Tiny crystal Bromophenol Blue
	Add ddH <sub>2</sub> O to 50 mL
	Store at RT, stable 1-2 years
	Fresh β-mercaptoethanol should be added directly
	before use at 10% v/v.
LB Agar	5 g NaCl
<del>.g</del>	5 g Tryptone
	108 11750010

	2.5 g Yeast extract	
	7.5 g Agar	
	Add ddH <sub>2</sub> O to 500 mL, mix well	
	Autoclave; store at +4 °C or RT	
	Microwave until fully melted	
	Pour into 10 cm Petri dishes under laminar flow hood or	
I D Droth	near Bunsen burner	
LB Broth	5 g NaCl 5 g Tryptone	
	2.5 g Yeast extract	
	Add ddH₂O to 500 mL, mix well	
	Autoclave; store at +4 °C or RT	
LyseBlue (10,000×)	43 mg/mL thymolphthalein	
Lysobias (10,000*)	Solvent: 100% ethanol	
	Store at RT, protected from light	
MACS Buffer	PBS + 0.5% BSA + 2 mM EDTA; filter-sterilize and	
	degas	
Magnesium Chloride (MgCl <sub>2</sub> ) (2M)	Dissolve 9.52 g MgCl <sub>2</sub> (100% purity) in ~40 mL distilled	
· · · · · · · · · · · · · · · · · · ·	water (exothermic!)	
	Mix until fully dissolved	
	Bring volume to 50 mL with distilled water	
	Filter-sterilize through a 0.22 µm membrane under	
	laminar flow	
	Store at 4 °C	
Magnesium Sulfate (MgSO <sub>4</sub> ) (1 M)	Dissolve 6.02 g MgSO <sub>4</sub> (100% purity) in ~40 mL distilled	
	water	
	Stir until fully dissolved	
	Bring volume to 50 mL with distilled water	
	Filter-sterilize using a 0.22 µm filter under laminar flow Store at 4 °C	
Medium Stripping Buffer	15 g Glycine	
Modium Surpping Baner	1 g SDS	
	10 ml Tween 20	
	Adjust pH to 2.2 with conc. HCl (37%)	
	Add ddH <sub>2</sub> O to 1 L total volume	
	Store at 4 °C	
MOPS Buffer, pH 7.0-7.5 (1 M)	Dissolve 209.26 g MOPS free acid in 750 mL distilled	
	water.	
	Adjust pH with 10 M NaOH to desired value.	
	Bring volume to 1 L with distilled water.	
	Filter-sterilize (preferred) or autoclave.	
MODE Dunning Buffor (10v)	Store at 4 °C.	
MOPS Running Buffer (10×)	41.86 g MOPS free acid (0.2 M)	
	4.1 g Sodium Acetate (0.05 M)	
	3.72 g Disodium EDTA (0.01 M) Add ddH₂O to 800 mL	
	Adjust pH to 7.0 with NaOH	
	Bring to 1 L total volume	
	Store at RT	
	Dilute 1:10 for 1× working solution	
NaOH (1 M)	Weigh 4.00 g NaOH pellets	
,		

	Carefully dissolve in ~80 mL distilled water (exothermic!)
	Cool if needed, then bring volume to 100 mL with water
NaOH (10 M)	Weigh 40.00 g NaOH pellets.
	Carefully add to ~70 mL distilled water in a heat-
	resistant container (strongly exothermic!).
	Stir until fully dissolved and allow to cool.
	Bring volume to 100 mL with distilled water.
P1	Dissolve 6.06 g Tris base, 3.72 g Na2EDTA·2H2O in
	800 ml distilled water
	Adjust the pH to 8.0 with HCl
	Adjust the volume to 1 liter with distilled water
	Add 100 mg RNase A per liter of P1 just before use
	Add 0.1 µL of LyseBlye per liter of P1 just before use
P2	Dissolve 8.0 g NaOH pellets in 950 ml distilled water, 50
	ml 20% SDS (w/v) solution
P3	The final volume should be 1 liter
F3	Dissolve 294.5 g potassium acetate in 500 ml distilled water
	Adjust the pH to 5.5 with glacial acetic acid (~110 ml)
	Adjust the volume to 1 liter with distilled water
PBS (10×)	400 g NaCl (1.37 M)
. == (,	10 g KCI (0.027 M)
	72 g Na <sub>2</sub> HPO <sub>4</sub> ·2H <sub>2</sub> O (0.081 M)
	$12 \text{ g KH}_2\text{PO}_4 (0.018 \text{ M})$
	Dissolve in 5000 mL dH <sub>2</sub> O, pH should = 7.4
	Autoclave.
	Dilute 1:10 for 1× working solution.
Puromycin Stock (10 mg/mL)	Dissolve 100 mg Puromycin in 10 mL sterile water
	Filter-sterilize (0.22 µm)
	Aliquot and store at -20 °C
ODT	Working concentration: 1 µg/mL (1:10,000)
QBT	Dissolve 43.83 g NaCl, 10.46 g MOPS (free acid) in 800 ml distilled water
	Adjust the pH to 7.0 with NaOH Add 150 ml pure isopropanol and 15 ml 10% Triton X-
	100 solution (v/v)
	Adjust the volume to 1 liter with distilled water
QC	Dissolve 58.44 g NaCl and 10.46 g MOPS (free acid) in
	800 ml distilled water
	Adjust the pH to 7.0 with NaOH
	Add 150 ml pure isopropanol
	Adjust the volume to 1 liter with distilled water
QN	Dissolve 93.50 g NaCl and 10.46 g MOPS (free acid) in
	800 ml distilled water and adjust the pH to 7.0 with
	NaOH
	Add 150 ml pure isopropanol
	Adjust the volume to 1 liter with distilled water
RF1	12 g RbCl (100 mM)
	9.9 g MnCl <sub>2</sub> ·4H <sub>2</sub> O (50 mM)
	30 mL of 1 M Potassium Acetate, pH 7.5 (30 mM)

	1.5 g CaCl <sub>2</sub> ·2H <sub>2</sub> O (10 mM) 150 g Glycerol (15% w/v) Add ddH <sub>2</sub> O to ~900 mL Adjust pH to 5.8 with 0.2 M glacial acetic acid Bring to 1 L, sterile-filter (0.22 μm) Store at -20 °C
RF2	20 mL of 0.5 M MOPS, pH 6.8 (10 mM) 1.2 g RbCl (10 mM) 11 g CaCl <sub>2</sub> (75 mM) 150 g Glycerol (15% w/v) Add ddH <sub>2</sub> O to ~900 mL Adjust pH to 6.8 with NaOH Bring to 1 L, sterile-filter (0.22 μm) Store at -20 °C
RIPA (2×)	3 mL 5 M NaCl 1 mL NP-40 (100%) 0.5 g Sodium deoxycholate 1 mL 10% SDS 5 mL 1 M Tris (pH 8.0) 1 mL 0.5 M EDTA (pH 8.0) Add ddH <sub>2</sub> O to 50 mL total volume Store at 4 °C or aliquot and freeze
SDS (10%)	Weigh 10 g SDS powder. Add to 80-85 mL distilled water. Warm gently (40-50 °C) and stir until fully dissolved. Bring volume to 100 mL with distilled water.
SDS Running Buffer (Towbin) (10×)	60.6 g Tris (0.25 M) 288.8 g Glycine (1.92 M) 20 g SDS (0.035 M) or 200 mL of 10% SDS Add ddH <sub>2</sub> O to 2 L total volume Store at RT Dilute 1:10 for 1× working solution
SDS-PAGE 10% Separating Gel (50 mL)	Add 19.8 mL distilled water to a clean tube Add 16.7 mL of 30% acrylamide mix Add 12.5 mL of 1 M Tris, pH 8.8 Add 0.5 mL of 10% SDS Mix well, then add 0.5 mL of 10% APS Add 0.02 mL of TEMED Mix quickly and pour the gel immediately Let polymerize at room temperature for ~30 minutes
SDS-PAGE 12% Separating Gel (50 mL)	Add 16.5 mL distilled water to a clean tube Add 20.0 mL of 30% acrylamide mix Add 12.5 mL of 1 M Tris, pH 8.8 Add 0.5 mL of 10% SDS Mix well, then add 0.5 mL of 10% APS Add 0.02 mL of TEMED Mix quickly and pour the gel immediately Let polymerize at room temperature for ~30 minutes
SDS-PAGE 15% Separating Gel (50 mL)	Add 11.4 mL distilled water to a clean tube Add 25.0 mL of 30% acrylamide mix Add 12.5 mL of 1 M Tris, pH 8.8

	Add 0.5 mL of 10% SDS Mix well, then add 0.5 mL of 10% APS Add 0.02 mL of TEMED
	Mix quickly and pour the gel immediately
000000000000000000000000000000000000000	Let polymerize at room temperature for ~30 minutes
SDS-PAGE Separating Gel Buffer	90.8 g Tris base (1.5 M)
	20 mL of 10% SDS (final 0.4%) Add ddH <sub>2</sub> O to 400 mL
	Adjust pH to 8.8 with conc. HCI (37%)
	Bring to 500 mL with ddH <sub>2</sub> O
	Store at RT
SDS-PAGE Stacking Gel (10 mL)	Add 6.8 mL distilled water to a clean tube
<b>5</b> , ,	Add 1.7 mL of 30% acrylamide mix
	Add 1.25 mL of 1 M Tris, pH 6.8
	Add 0.1 mL of 10% SDS
	Mix well, then add 0.1 mL of 10% APS
	Add 0.01 mL (10 µL) of TEMED
	Mix quickly and pour the gel immediately
CDC DACE Stocking Cal Duffer	Let polymerize at room temperature for ~30 minutes
SDS-PAGE Stacking Gel Buffer	4.2 g Tris base (1 M) 8 mL of 10% SDS (final 0.4%)
	Add ddH <sub>2</sub> O to 150 mL
	Adjust pH to 6.8 with conc. HCI (37%)
	Bring to 200 mL with ddH <sub>2</sub> O
	Store at RT
SOB Medium	10 g Tryptone
	2.5 g Yeast extract
	0.25 g NaCl
	0.093 g KCl
	Add ddH <sub>2</sub> O to 500 mL total volume
SOC Medium	Autoclave, then add 5 mL sterile 2 M MgCl <sub>2</sub> after cooling
SOC Medium	5 g Tryptone 1.25 g Yeast extract
	0.125 g NaCl
	0.045 g KCl
	Add ddH <sub>2</sub> O to $\sim$ 200 mL, adjust pH to 6.8-7.0 with $\sim$ 0.25-
	0.5 mL 1 M NaOH
	Bring to 250 mL, autoclave
	Cool to RT, then add:
	1.25 mL 2 M MgCl <sub>2</sub>
	2.5 mL 1 M MgSO <sub>4</sub>
	2 mL 2.5 M Glucose
Codium Acetata nU 5 5 / 7 0 /1 M	Mix well, aliquot, and store at -20 °C
Sodium Acetate, pH 5.5 / 7.0 (1 M)	Add 7.721 g Sodium Acetate to 800 mL distilled water Add 352.5 mg Acetic Acid
	Adjust pH to indicated level as needed with HCl or
	NaOH
	Bring volume to 1 L with distilled water
TAE (10×)	48.5 g Tris base
•	11.4 mL glacial acetic acid
	20 mL 0.5 M EDTA (pH 8.0)

	Dissolve in ~800 mL deionized water, adjust pH to ~8.3
	Bring volume to 1 L Dilute 1:10 for 1× working solution
TBS (10×)	30 g Tris base (250 mM)
100 (1011)	80 g NaCl (1.5 M)
	2g KCl
	Add ddH <sub>2</sub> O to 800 mL
	Adjust pH to 7.4 with ~15-20 mL conc. HCI (37%)
	Bring to 1 L with ddH <sub>2</sub> O
	Store at +4 °C (preferred) or RT
Transfer Buffer (1×)	100 mL of 10× Transfer Buffer
	200 mL Methanol (20%)
	700 mL ddH <sub>2</sub> O
	~1.6 L of 1× buffer is needed to fill one electrophoresis
Tu-u-f-u D. #- u (40)	tank.
Transfer Buffer (10×)	60.6 g Tris (0.25 M)
	288.8 g Glycine (1.92 M) Add ddH <sub>2</sub> O to 2 L total volume
	Store at 4 °C
Tris, pH 6.8 / 8.0 / 8.8 (1M)	Dissolve 12.11 g Tris base in ~80 mL distilled water
, p e.e / e.e //	Adjust pH to indicated level using concentrated HCl
	Bring volume to 100 mL with water
Tris-EDTA Buffer, pH 9.0	1.21 g Tris base
	0.37 g EDTA (disodium salt)
	Dissolve in ~800 mL deionized water
	Adjust pH to 9.0 with 1 N NaOH
	Add 0.5 mL Tween 20
Total V 400 (400/)	Bring volume to 1 L
Triton X-100 (10%)	Add 10 mL Triton X-100 to 80 mL distilled water.
	Warm gently and mix until fully dissolved. Bring volume to 100 mL with distilled water.
	Store at room temperature.
Triton X-114 (10%)	Add 10 mL Triton X-114 to 80 mL distilled water.
	Warm gently and mix until fully dissolved.
	Bring volume to 100 mL with distilled water.
	Store at room temperature.

# 2.1.4 Cell culture media and additives

Table 9. Cell culture media and additives used in this study.

Name	Manufacturer
RPMI-1640	Sigma-Aldrich (St. Louis, MO, USA)
IMDM	Sigma-Aldrich (St. Louis, MO, USA)
DMEM	Sigma-Aldrich (St. Louis, MO, USA)
EBM-2	Lonza (Walkersville, MD, USA)
EGM-2 SingleQuots	Lonza (Walkersville, MD, USA)
OptiMEM	Thermo Fisher Scientific (Waltham, MA, USA)
Penicillin/Streptomycin (10,000 U/mL)	Thermo Fisher Scientific (Waltham, MA, USA)

L-Glutamine (200 mM)	Thermo Fisher Scientific (Waltham, MA, USA)
HEPES (1M)	Thermo Fisher Scientific (Waltham, MA,
	USA)
Recombinant human IL6	Peprotech (Cranbury, NJ, USA)
Human Serum AB	GemCell (Lawrence, MA, USA)
Fetal Bovine Serum (Chile origin)	Sigma-Aldrich (St. Louis, MO, USA)

# 2.1.5 Nucleic acids

# 2.1.5.1 Oligonucleotides for cloning

Table 10. Oligonucleotide sequences used for cloning, colony PCR and Sanger sequencing.

Name	Sequence (5'-3')	Purpose
Oligo_shPIM _1.2_T	gatctGTGCAAGATCTCTTCGACTTTCAAGAG AAGTCGAAGAGATCTTGCACTTTTTTgagct	Top strand for shPIM1.2 insert for TST30
Oligo_shPIM 1.2_B	CAAAAAAGTGCAAGATCTCTTCGACTTCTCTT GAAAGTCGAAGAGATCTTGCACa	Bottom strand for shPIM1.2 insert for TST30
Oligo_shPIM 1.3_T	gatctGCAAGATCTCTTCGACTTCTTCAAGAG AGAAGTCGAAGAGATCTTGCTTTTTTgagct	Top strand for shPIM1.3 insert for TST30
Oligo_shPIM 1.3_B	CAAAAAAGCAAGATCTCTTCGACTTCTCTTT GAAGAAGTCGAAGAGATCTTGCa	Bottom strand for shPIM1.3 insert for TST30
Oligo_shPIM 1.4_T	gatctGAGTGAACTGGTCTTCCTTTTCAAGAG AAAGGAAGACCAGTTCACTCTTTTTTgagct	Top strand for shPIM1.4 insert for TST30
Oligo_shPIM 1.4_B	CAAAAAAGAGTGAACTGGTCTTCCTTTCTCTT GAAAAGGAAGACCAGTTCACTCa	Bottom strand for shPIM1.4 insert for TST30
Oligo_shPIM 1.5_T	gatctGCCTGGAGGTCAATGTTATGTTCAAGA GACATAACATTGACCTCCAGGTTTTTTgagct	Top strand for shPIM1.5 insert for TST30
Oligo_shPIM 1.5_B	CAAAAAACCTGGAGGTCAATGTTATGTCTCTT GAACATAACAT	Bottom strand for shPIM1.5 insert for TST30
Oligo_shPIM 2.1_T	gatctGCTTGACTGGTTTGAGACATTCAAGAG ATGTCTCAAACCAGTCAAGCTTTTTTgagct	Top strand for shPIM2.1 insert for TST30
Oligo_shPIM 2.1_B	CAAAAAAGCTTGACTGGTTTGAGACATCTCTT GAATGTCTCAAACCAGTCAAGCa	Bottom strand for shPIM2.1 insert for TST30
Oligo_shPIM 2.2_T	gatctGCTTCATGATGAACCCTACTTCAAGAG AGTAGGGTTCATCATGAAGCTTTTTTgagct	Top strand for shPIM2.2 insert for TST30
Oligo_shPIM 2.2_B	CAAAAAAGCTTCATGATGAACCCTACTCTTT GAAGTAGGGTTCATCATGAAGCa	Bottom strand for shPIM2.2 insert for TST30
Oligo_shPIM 2.3_T	gatctAGGAGATTCTGGAAGCTGATTCAAGAG ATCAGCTTCCAGAATCTCCTTTTTTTgagct	Top strand for shPIM2.3 insert for TST30
Oligo_shPIM 2.3_B	CAAAAAAAGGAGATTCTGGAAGCTGATCTCTT GAATCAGCTTCCAGAATCTCCTa	Bottom strand for shPIM2.3 insert for TST30
Oligo_shPIM 2.4_T	gatctGCCGGGACTCTTATTCTGATTTCAAGA GAATCAGAATAAGAGTCCCGGTTTTTTgagct	Top strand for shPIM2.4 insert for TST30
Oligo_shPIM 2.4_B	CAAAAAACCGGGACTCTTATTCTGATTCTCTT GAAATCAGAATAAGAGTCCCGGCa	Bottom strand for shPIM2.4 insert for TST30
Oligo_shPIM 2.5_T	gatctGCCAGGATCTCTTTGACTATTTCAAGA GAATAGTCAAAGAGATCCTGGTTTTTTgagct	Top strand for shPIM2.5 insert for TST30

Oligo_shPIM 2.5_B	CAAAAAACCAGGATCTCTTTGACTATTCTCTT GAAATAGTCAAAGAGATCCTGGCa	Bottom strand for shPIM2.5 insert for TST30
Oligo_shPIM 3.1_T	gatctGCGACATTAAGGACGAAAATTCAAGAG ATTTTCGTCCTTAATGTCGCTTTTTTgagct	Top strand for shPIM3.1 insert for TST30
Oligo_shPIM 3.1_B	CAAAAAAGCGACATTAAGGACGAAAATCTCTT GAATTTTCGTCCTTAATGTCGCa	Bottom strand for shPIM3.1 insert for TST30
Oligo_shPIM 3.2_T	gatctGCCGCCAACTCTGTTATTTATTCAAGA GATAAATAACAGAGTTGGCGGTTTTTTgagct	Top strand for shPIM3.2 insert for TST30
Oligo_shPIM 3.2_B	CAAAAAACCGCCAACTCTGTTATTTATCTCTT GAATAAATAACAGAGTTGGCGGCa	Bottom strand for shPIM3.2 insert for TST30
Oligo_shPIM 3.3_T	gatctGCTGTCAGAAGATGAACATGTTCAAGA GACATGTTCATCTTCTGACAGTTTTTTgagct	Top strand for shPIM3.3 insert for TST30
Oligo_shPIM 3.3_B	CAAAAAACTGTCAGAAGATGAACATGTCTCTT GAACATGTTCATCTTCTGACAGCA	Bottom strand for shPIM3.3 insert for TST30
Oligo_shPIM 3.4_T	gatctGCTGTGAAGCACGTGGTGAATTCAAGA GATTCACCACGTGCTTCACAGTTTTTTgagct	Top strand for shPIM3.4 insert for TST30
Oligo_shPIM 3.4_B	CAAAAAACTGTGAAGCACGTGGTGAATCTCTT GAATTCACCACGTGCTTCACAGCa	Bottom strand for shPIM3.4 insert for TST30
Oligo_shPIM 3.5_T	gatctGCAGGACCTCTTCGACTTTTTCAAGAG AAAAGTCGAAGAGGTCCTGCTTTTTTgagct	Top strand for shPIM3.5 insert for TST30
Oligo_shPIM 3.5_B	CAAAAAGCAGGACCTCTTCGACTTTTCTCTT GAAAAAGTCGAAGAGGTCCTGCa	Bottom strand for shPIM3.5 insert for TST30
Oligo_shSC R_T	gatctCCTAAGGTTAAGTCGCCCTCGCTCGAG CGAGGGCGACTTAACCTTAGGTTTTTTgagct	Top strand for shSCR insert for TST30
Oligo_shSC R_B	CAAAAAACCTAAGGTTAAGTCGCCCTCGCTCG AGCGAGGGCGACTTAACCTTAGGA	Bottom strand for shSCR insert for TST30
seq30	CAGGAAACAGCTATGAC	Sequencing TST30-sh
seq201F	GGCTTTAGAAGCTTCCCAC	Sequencing and colony PCR of TST201-sh
seq201R2	GCTGACTAATTGAGATGCATGC	Sequencing and colony PCR of TST201-sh

# 2.1.5.2 Oligonucleotides for qPCR

Table 11. Oligonucleotide sequences used for qPCR.

Gene	Forward primer (5'-3')	Reverse primer (5'-3')
RNA18S	CGTCTGCCCTATCAACTTTG	TGCCTTCCTTGGATGTGGTAG
YWHAZ	AGGAGATTACTACCGTTACTTGGC	AGCTTCTTGGTATGCTTGTTGTG
ACTB	CATGTACGTTGCTATCCAGGC	CTCCTTAATGTCACGCACGAT
PIM1	TCATTAGGCTCCTGGACTGG	GCGATTGAGGTCGATAAGGA
PIM2	CTCGAAGTCGCACTGCTATG	CTGGATGGCTGCCACTACTT
PIM3	TCTCTCCAGAGTGCCAGCA	GTGCACAGCCGCAGGTCA
MYC	GGCTCCTGGCAAAAGGTCA	CTGCGTAGTTGTGCTGATGT
PTPRC	ACCACAAGTTTACTAACGCAAGT	TTTGAGGGGGATTCCAGGTAAT
PECAM1	AACAGTGTTGACATGAAGAGCC	TGTAAAACAGCACGTCATCCTT
CD34	CTACAACACCTAGTACCCTTGGA	GGTGAACACTGTGCTGATTACA
KDR	GGCCCAATAATCAGAGTGGCA	CCAGTGTCATTTCCGATCACTTT
PROM1	AGTCGGAAACTGGCAGATAGC	GGTAGTGTTGTACTGGGCCAAT
CDH5	TTGGAACCAGATGCACATTGAT	TCTTGCGACTCACGCTTGAC
STAB2	GTGCCCGGATGGTTACACC	CTTCCTACAAATATGGCGGCAT

VCAM1	GGGAAGATGGTCGTGATCCTT	TCTGGGGTGGTCTCGATTTTA
APLNR	CTCTGGACCGTGTTTCGGAG	GGTACGTGTAGGTAGCCCACA
EFNB2	TATGCAGAACTGCGATTTCCAA	TGGGTATAGTACCAGTCCTTGTC
SOX17	GTGGACCGCACGGAATTTG	GGAGATTCACACCGGAGTCA
FLT1	TTTGCCTGAAATGGTGAGTAAGG	TGGTTTGCTTGAGCTGTGTTC
PDGFA	GCAAGACCAGGACGGTCATTT	GGCACTTGACACTGCTCGT

# **2.1.5.3 Plasmids**

Table 12. Plasmids used in this study.

Name	Backbone	Description	Source
TST209	pT2	Sleeping Beauty system plasmid encoding tetracycline-repressor and puromycin resistance gene.	Kindly provided by Thorsten Stühmer (University of Würzburg)
pCMV(CAT)T7- SB100	pCMV	Allows for transient expression of Sleeping Beauty transposase SB100X.	Gift from Zsuzsanna Izsvak (Addgene plasmid # 34879)
TST30	pSUSTER2	Sleeping Beauty system acceptor plasmid for shRNA duplex cloning. Contains H1 promoter followed by tet operator.	Kindly provided by Thorsten Stühmer (University of Würzburg)
TST30-shPIM1.2	TST30	TST30 plasmid for PIM1 silencing. shRNA target sequence: GTGCAAGATCTCTTCGACT	This work
TST30-shPIM1.3	TST30	TST30 plasmid for PIM1 silencing. shRNA target sequence: GCAAGATCTCTTCGACTTC	This work
TST30-shPIM1.4	TST30	TST30 plasmid for PIM1 silencing. shRNA target sequence: GAGTGAACTGGTCTTCCTT	This work
TST30-shPIM1.5	TST30	TST30 plasmid for PIM1 silencing. shRNA target sequence: CCTGGAGGTCAATGTTATG	This work
TST30-shPIM2.1	TST30	TST30 plasmid for PIM2 silencing. shRNA target sequence: GCTTGACTGGTTTGAGACA	This work
TST30-shPIM2.2	TST30	TST30 plasmid for PIM2 silencing. shRNA target sequence: GCTTCATGATGAACCCTAC	This work

TST30-shPIM2.3	TST30	TST30 plasmid for PIM2 silencing. shRNA target sequence:	This work
		AGGAGATTCTGGAAGCTGA	
TST30-shPIM2.4	TST30	TST30 plasmid for PIM2	This work
		silencing. shRNA target	
		sequence:	
TOTOO abDIMO E	TCT20	CCGGGACTCTTATTCTGAT	This work
TST30-shPIM2.5	TST30	TST30 plasmid for PIM2	This work
		silencing. shRNA target	
		sequence: CCAGGATCTCTTTGACTAT	
TST30-shPIM3.1	TST30	TST30 plasmid for PIM3	This work
10100 3111 11110.1	10100	silencing. shRNA target	THIS WOLK
		sequence:	
		GCGACATTAAGGACGAAAA	
TST30-shPIM3.2	TST30	TST30 plasmid for PIM3	This work
		silencing. shRNA target	
		sequence:	
		CCGCCAACTCTGTTATTTA	
TST30-shPIM3.3	TST30	TST30 plasmid for PIM3	This work
		silencing. shRNA target	
		sequence:	
		CTGTCAGAAGATGAACATG	
TST30-shPIM3.4	TST30	TST30 plasmid for PIM3	This work
		silencing. shRNA target	
		sequence:	
	<b>T0700</b>	CTGTGAAGCACGTGGTGAA	
TST30-shPIM3.5	TST30	TST30 plasmid for PIM3	This work
		silencing. shRNA target	
		sequence: GCAGGACCTCTTCGACTTT	
TST30-SCR	TST30	TST30 control plasmid with non-	This work
10100-0010	13130	targeting shRNA.	THIS WOLK
TST201	pT2	Sleeping Beauty system plasmid	Kindly provided
101201	PIZ	for doxycycline-induced PIM	
		silencing. Allows for	Stühmer
		concatenated cloning of multiple	(University of
		expression casettes derived from	Würzburg)
		TST30 plasmids.	3,
TST201-	TST201	TST201 plasmid with shPIM1.1	This work
shPIM1.1		sequence and H1 promoter.	
TST201-	TST201	TST201 plasmid with shPIM1.2	This work
shPIM1.2		sequence and H1 promoter.	
TST201-	TST201	TST201 plasmid with shPIM1.3	This work
shPIM1.3		sequence and H1 promoter.	
TST201-	TST201	TST201 plasmid with shPIM1.4	This work
shPIM1.4		sequence and H1 promoter.	
TST201-	TST201	TST201 plasmid with shPIM1.5	This work
shPIM1.5		sequence and H1 promoter.	
TST201-	TST201	TST201 plasmid with shPIM2.1	This work
shPIM2.1		sequence and H1 promoter.	

TST201- shPIM2.2	TST201	TST201 plasmid with shPIM2.2	This work
	TST201	sequence and H1 promoter.	This work
TST201-	131201	TST201 plasmid with shPIM2.3	THIS WOLK
shPIM2.3	TOTODA	sequence and H1 promoter.	This consult
TST201-	TST201	TST201 plasmid with shPIM2.4	This work
shPIM2.4		sequence and H1 promoter.	<del></del>
TST201-	TST201	TST201 plasmid with shPIM2.5	This work
shPIM2.5		sequence and H1 promoter.	
TST201-	TST201	TST201 plasmid with shPIM3.1	This work
shPIM3.1		sequence and H1 promoter.	
TST201-	TST201	TST201 plasmid with shPIM3.2	This work
shPIM3.2		sequence and H1 promoter.	
TST201-	TST201	TST201 plasmid with shPIM3.3	This work
shPIM3.3		sequence and H1 promoter.	
TST201-	TST201	TST201 plasmid with shPIM3.4	This work
shPIM3.4		sequence and H1 promoter.	
TST201-	TST201	TST201 plasmid with shPIM3.5	This work
shPIM3.5		sequence and H1 promoter.	
TST201-shSCR	TST201	TST201 plasmid with shSCR	This work
		sequence and H1 promoter.	
TST201-	TST201	TST201 plasmid with shPIM1.5,	This work
sh3xPIM	101201	shPIM2.4, shPIM3.4 casettes,	Time work
01107ti 1111		each driven by a separate	
		tetracycline-inducible H1	
		promoter.	
pSIREN-RetroQ-	pSIREN RetroQ	Allows transient flow cytometry-	Shipp Lab
ZsGreen-shLuc	POINTIN NOTION	based tracking of cells	Onipp Lab
23010011-311Eu0		successfully co-electroporated	
		with plasmid mixture (ZsGreen <sup>+</sup> ).	
pHIV-ZsGreen-	pHIV-Zsgreen	Allows for constitutive expression	Gift from Bryan
Luc	priiv-23green	of Firefly Luciferase for <i>in vivo</i>	Welm (Addgene
Luc		studies.	plasmid #
		studies.	39196)
pMDLg/pRRE	pMD	3rd generation lentiviral	Gift from Didier
piviDLg/pixixL	PIVID	I — — — — — — — — — — — — — — — — — — —	
		packaging plasmid. Contains Gag and Pol.	Trono (Addgene plasmid #
		Gag and Foi.	12251)
nDC\/ Doy/	nDCV/ Dov	2rd generation lentiviral	,
pRSV-Rev	pRSV-Rev	3rd generation lentiviral	Gift from Didier
		packaging plasmid. Contains	Trono (Addgene
		Rev.	plasmid #
·· MDO C	- MD0 0	1/0// 0	12253)
pMD2.G	pMD2.G	VSV-G envelope expressing	Gift from Didier
		plasmid.	Trono (Addgene
			plasmid # 12259

# 2.1.6 Antibodies

Table 13. Antibodies used in this study. R, rabbit; M, mouse; G, goat; H, horse; Hs, Human; FC, flow cytometry; IHC, immunohistochemistry; WB, western blot.

Target	Host	Application	Dilution	Clone/Cat. No.	Source
rarget	11031	Application	Dilation	Ololle/Oat. No.	Oource

CD138	М	FC	1:20	B-B4/130-081- 301	Miltenyi Biotec (Bergisch Gladbach, Germany)
CD31	М	FC	1:20	WM59/303106	BioLegend (San Diego, CA, USA)
VEGFR1	Hs	FC	1:20	REA569/A1608 3C	Miltenyi Biotec (Bergisch Gladbach, Germany)
CD144 (VE- Cadherin)	М	FC	1:20	BV9/348506	BioLegend (San Diego, CA, USA)
PIM1	R	IHC	1:100	ST0513/NBP2- 67528	Novus Biologicals (Centennial, CO, USA)
PIM1	R	WB	1:500	D8D7Y/54523	Cell Signaling Technology (Danvers, MA, USA)
PIM2	М	IHC	1:100	OTI5D5/NBP2- 02441	Novus Biologicals (Centennial, CO, USA)
PIM2	R	WB	1:500	D1D2/4730	Cell Signaling Technology (Danvers, MA, USA)
PIM3	R	IHC, WB	1:50 + linker, 1:500	D17C9/4165	Cell Signaling Technology (Danvers, MA, USA)
GAPDH	М	WB	1:2000	6C5/MAB374	Millipore (Burlington, MA, USA)
β-Actin	R	WB	1:2000	13E5/4970	Cell Signaling Technology (Danvers, MA, USA)
S6	R	WB	1:1000	5G10/2217	Cell Signaling Technology (Danvers, MA, USA)
pS6 (Ser235/2 36)	R	WB	1:1000	91B2/4857	Cell Signaling Technology (Danvers, MA, USA)
pAkt (Ser473)	R	WB	1:1000	193H12/4058	Cell Signaling Technology (Danvers, MA, USA)
Akt (pan)	R	WB	1:1000	11E7/4685	Cell Signaling Technology (Danvers, MA, USA)
pERK1/2 (Thr202/T yr204)	R	WB	1:1000	D13.14.4E/437	Cell Signaling Technology (Danvers, MA, USA)
ERK1/2	R	WB	1:1000	137F5/4695	Cell Signaling Technology (Danvers, MA, USA)
PARP	R	WB	1:1000	46D11/9532	Cell Signaling Technology (Danvers, MA, USA)
RhoA	M (IgM)	WB	1:500	ARH05	Cytoskeleton (Denver, CO, USA)

CD34	М	IHC	1:400	QBEnd 10/M7165	Dako (Glostrup, Denmark)
E2F1	R	WB	1:1000	3742	Cell Signaling Technology (Danvers, MA, USA)
MYC	R	WB	1:10,000	ab32072	Abcam (Waltham, MA, USA)
Mouse IgG + IgM (H+L)	G	WB secondary	1:10,000	15-035-068	Jackson Immunoresearch (West Grove, PA, USA)
Rabbit IgG	G	WB secondary	1:2000	7074	Cell Signaling Technology (Danvers, MA, USA)
Mouse IgG	Н	WB secondary	1:2000	7076	Cell Signaling Technology (Danvers, MA, USA)

# 2.1.7 Consumables

Table 14. Consumables used in this study.

Name	Manufacturer
0.2 mL PCR tubes	Sarstedt (Nümbrecht, Germany)
1 mL pipette tips	Sarstedt (Nümbrecht, Germany)
1.5 glass coverslips (22 × 22 mm)	Fisher Scientific (Waltham, MA, USA)
1.5 mL Safe-Lock microcentrifuge tubes	Eppendorf (Hamburg, Germany)
10 cm cell culture dishes (nontreated)	Sarstedt (Nümbrecht, Germany)
10 cm cell culture dishes (treated)	Sarstedt (Nümbrecht, Germany)
10 mL BD Luer-Lok Syringe	BD (Franklin Lakes, NJ, USA)
10 mL serological pipettes	Sarstedt (Nümbrecht, Germany)
10 μL pipette tips	Sarstedt (Nümbrecht, Germany)
100 µL pipette tips	Sarstedt (Nümbrecht, Germany)
15 cm cell culture dishes (nontreated)	Sarstedt (Nümbrecht, Germany)
15 cm cell culture dishes (treated)	Sarstedt (Nümbrecht, Germany)
15 mL conical tubes	Sarstedt (Nümbrecht, Germany)
2 mL serological pipettes	Sarstedt (Nümbrecht, Germany)
2 mm Gene Pulser electroporation cuvettes	Bio-Rad (Hercules, CA, USA)
2.0 mL Safe-Lock microcentrifuge tubes	Eppendorf (Hamburg, Germany)
200 µL pipette tips	Sarstedt (Nümbrecht, Germany)
24-well plates (nontreated)	Sarstedt (Nümbrecht, Germany)
24-well plates (treated)	Sarstedt (Nümbrecht, Germany)
25 mL serological pipettes	Sarstedt (Nümbrecht, Germany)
4 mm Gene Pulser electroporation cuvettes	Bio-Rad (Hercules, CA, USA)
5 mL serological pipettes	Sarstedt (Nümbrecht, Germany)
50 mL conical tubes	Sarstedt (Nümbrecht, Germany)
6-well plates (nontreated)	Sarstedt (Nümbrecht, Germany)
6-well plates (treated)	Sarstedt (Nümbrecht, Germany)
96-well plates (nontreated)	Sarstedt (Nümbrecht, Germany)

96-well Solid White Flat Bottom Polystyrene TC-treated Plate	Corning (Corning, NY, USA)	
BD Bard-Parker Disposable Scalpel with Handle, Size #15	BD (Franklin Lakes, NJ, USA)	
BD Lo-Dose U-100 Insulin Syringes 28G	BD (Franklin Lakes, NJ, USA)	
BD SafetyGlide Needle 18 G x 1 1/2 in.	BD (Franklin Lakes, NJ, USA)	
Cell scrapers	Sarstedt (Nümbrecht, Germany)	
Cryovials	Sarstedt (Nümbrecht, Germany)	
DNA LoBind tubes 0.5 mL	Eppendorf (Hamburg, Germany)	
GenCatch DEAE-Silica Anion Exchange Maxi Column	Epoch Life Science (Fort Bend County, TX, USA)	
Hemacytometer	Marienfeld (Lauda-Königshofen, Germany)	
Hemacytometer cover glass	WWR (Radnor, PA, USA)	
Heparin-coated blood collection tubes	BD (Franklin Lakes, NJ, USA)	
LS columns	Miltenyi Biotec (Bergisch Gladbach,	
L3 COIUITIIS	Germany)	
MicroAmp Optical 96-Well Reaction Plate	Thermo Fisher Scientific (Waltham, MA, USA)	
Microseal 'B' PCR Plate Sealing Film, adhesive, optical	Thermo Fisher Scientific (Waltham, MA, USA)	
MidiMACS Separator	Miltenyi Biotec (Bergisch Gladbach, Germany)	
Mr. Frosty freezing container	Thermo Fisher Scientific (Waltham, MA, USA)	
MultiStand	Miltenyi Biotec (Bergisch Gladbach, Germany)	
Paper coffee filters	Auchan (Croix, France)	
SuperFrost Plus microscope slides	Thermo Fisher Scientific (Waltham, MA, USA)	
Syringe Filter, PTFE, 0.45 µm, 30 mm	StemCELL (Vancouver, Canada)	
Syringe Filter, PVDF, 0.22 µm, 30 mm	StemCELL (Vancouver, Canada)	
T25 culture flask (treated)	Sarstedt (Nümbrecht, Germany)	
T25 culture flask (untreated)	Sarstedt (Nümbrecht, Germany)	
T75 culture flask (treated)	Sarstedt (Nümbrecht, Germany)	
T75 culture flask (untreated)	Sarstedt (Nümbrecht, Germany)	

# 2.1.8 Equipment

Table 15. Machines and instruments used in this study.

Name	Manufacturer
−20 °C Freezer	PHCbi (Tokyo, Japan)
4 °C Refrigerator	Liebherr (Ochsenhausen, Germany)
−80 °C Freezer	PHCbi (Tokyo, Japan)
ABI 3500 Genetic Analyzer	Applied Biosystems (Waltham, MA, USA)
Accumet pH meter	Thermo Fisher Scientific (Waltham, MA, USA)
Agarose Gel Electrophoresis System (Sub- Cell GT Cell, PowerPac)	Bio-Rad (Hercules, CA, USA)
Agilent TapeStation 4200	Agilent Technologies (Santa Clara, CA, USA)

Axio Imager.Z2 Fluorescence Microscope	Zeiss (Oberkochen, Germany)	
BD FACSCanto II Flow Cytometer	BD Biosciences (Franklin Lakes, NJ, USA)	
C1000 Touch™ Thermal Cycler	Bio-Rad (Hercules, CA, USA)	
CFX96 Touch Real-Time PCR System	Bio-Rad (Hercules, CA, USA)	
Class II Biosafety cabinet	Thermo Fisher Scientific (Waltham, MA, USA)	
Cole-Parmer Stuart Digital Tube Roller	Thermo Fisher Scientific (Waltham, MA, USA)	
CytoFLEX S V4-B2-Y4-R3 Analyzer	Beckman Coulter (Brea, CA, USA)	
CytoFLEX SRT V5-B2-Y5-R3 Cell Sorter	Beckman Coulter (Brea, CA, USA)	
Forma Direct Heat CO2 Incubator	Thermo Fisher Scientific (Waltham, MA, USA)	
G:BOX Imaging System	Syngene (Cambridge, UK)	
Gene Pulser Xcell Electroporation System	Bio-Rad (Hercules, CA, USA)	
Hot plate magnetic stirrer	Thermo Fisher Scientific (Waltham, MA, USA)	
Innova 42/44 Series Shaking Incubator	New Brunswick (Enfield, CT, USA)	
Lab digital scale	Radwag (Radom, Poland)	
Liquid Nitrogen Storage Tank	Thermo Fisher Scientific (Waltham, MA, USA)	
LP Vortex Mixer	Thermo Fisher Scientific (Waltham, MA, USA)	
Memmert IN110 Bacterial Incubator	Memmert (Schwabach, Germany)	
Microcentrifuge for 0.2 mL Tubes	USA Scientific (Ocala, FL, USA)	
Milli-Q Water Purification System	Millipore (Burlington, MA, USA)	
MiniSpin Centrifuge	Eppendorf (Hamburg, Germany)	
Mithras LB 940 Luminometer	Berthold Technologies (Bad Wildbad,	
	Germany)	
Multiskan Microplate Spectrophotometer	Thermo Fisher Scientific (Waltham, MA, USA)	
NextSeq 500 Sequencing System	Illumina (San Diego, CA, USA)	
Precision GP 10 Water Bath	Thermo Fisher Scientific (Waltham, MA, USA)	
PrimoVert Inverted Phase Contrast	Zeiss (Oberkochen, Germany)	
Microscope	,	
Qubit 4 Fluorometer	Thermo Fisher Scientific (Waltham, MA, USA)	
Refrigerated Centrifuge 5418R	Eppendorf (Hamburg, Germany)	
Refrigerated Centrifuge 5810R	Eppendorf (Hamburg, Germany)	
Rocking Platform Shaker	Thermo Fisher Scientific (Waltham, MA, USA)	
Tube Revolver Rotator	Thermo Fisher Scientific (Waltham, MA, USA)	

# 2.1.9 Software

Table 16. Software used in this study.

Name	Manufacturer/Source	Version
bcl2fastq	Illumina (San Diego, CA, USA)	2.20.0.422
Benchling	Benchling (San Francisco, CA, USA)	Online
Bio-Rad CFX Manager	Bio-Rad (Hercules, CA, USA)	2.1
BioRender	BioRender (Toronto, Canada)	Online
Bowtie2	Johns Hopkins University (Baltimore, MD, USA)	2.4.5
Clontech's shRNA design tool	Takara Bio (Otsu, Shiga, Japan)	Online, no longer available
ClusterProfiler	Bioconductor (Boston, MA, USA)	4.16.0
Conda	Anaconda (Austin, TX, USA)	25.3.1
Cutoff Finder	Charité (Berlin, Germany)	Online, no longer available

CytExpert	Beckman Coulter (Brea, CA, USA)	2.4.0.28
deepTools	Freiburg Galaxy Team (Freiburg, Germany)	3.5.6
DESeq2	Bioconductor (Boston, MA, USA)	1.48.1
Excel	Microsoft (Redmond, WA, USA)	365
FastQC	Babraham Bioinformatics (Cambridge, UK)	0.12.1
FlowJo	BD Biosciences (Franklin Lakes, NJ, USA)	10.10
Illustrator	Adobe (San Jose, CA, USA)	CC
ImageJ	NIH (Bethesda, MD, USA)	1.53
ISIS Fluorescence Imaging System	MetaSystems (Altlussheim, Germany)	5.3.1
LAS X Office	Leica Microsystems (Wetzlar, Germany)	1.4.6
Living Image Software	PerkinElmer (Waltham, MA, USA)	4.7.4
MACS2	Zhang Lab (St. Louis, MO)	2.2.9.1
MedCalc	MedCalc Software (Ostend, Belgium)	20
MikroWin	Berthold Technologies (Bad Wildbad, Germany)	4.41
NCBI BLAST	NCBI (Bethesda, MD, USA)	Online
NEBioCalculator	New England Biolabs (Ipswich, MA, USA)	Online, 1.16.24
Nextflow	Seqera Labs (Barcelona, Spain)	22.10.1
Photoshop	Adobe (San Jose, CA, USA)	CC
Prism	GraphPad (Boston, MA, USA)	10.0
R	R Core Team (Vienna, Austria)	4.4.3
R Studio	Posit (Boston, MA, USA)	2025.05.0
Sambamba	Artem Tarasov (St. Petersburg, Russia)	1.0.1
SAMtools	HTSlib team (Hinxton, UK)	1.21
Sciugo	Jonah Librah (Toronto, Canada)	Online
Sequencing Analysis Software	Applied Biosystems (Foster City, CA, USA)	6.0
Seurat	Satija Lab (New York, NY, USA)	5.1.0
STAR aligner	Alexander Dobin group (New York, NY, USA)	2.7.11
SynergyFinder	FIMM (Helsinki, Finland)	Online
Windows Subsystem for Linux	Microsoft (Redmond, WA, USA)	2.2.4

### 2.2 Methods

# 2.2.1 Cell biology techniques

#### 2.2.1.1 Culture of mammalian cell lines

All original cell lines used in this study are listed in Table 2, along with relevant metadata such as sex, geographic ancestry, immunoglobulin (Ig) isotype, and light chain expression. Cell lines were obtained from commercial sources (ATCC, DSMZ, JCRB) or academic collaborators.

All cells were cultured under standard conditions at 37 °C in a humidified incubator with 5% CO<sub>2</sub>. MM lines and HBL-1 were maintained in RPMI-1640 medium supplemented with 10% fetal bovine serum (FBS), 100 U/mL penicillin, 100 μg/mL streptomycin, and 2 mM L-glutamine as well as 10 mM HEPES. OCI-Ly1 was maintained in IMDM medium supplemented as described above. Interleukin-6 (IL-6) was added to a final concentration of 1-2 ng/mL where required (e.g., ANBL6, DP6, INA6, KJON, OH2, XG1). KJON cells additionally required 10% pooled human serum. All suspension cell lines were cultured in non-treated cell culture dishes.

HUVEC-TERT2 and BMEC60 endothelial cells were cultured in EBM-2 medium supplemented with EGM-2 SingleQuots Supplements and 10 mM HEPES. The final EBM-2 composition included 2% FBS, 5 ng/ml human EGF, 5 ng/ml human FGF, 50 μg/ml ascorbic acid, 1 μg/ml hydrocortisone hemisuccinate, 10 mM L-glutamine, 15 ng/ml human long R3 insulin-like growth factor (R3-IGF-1), 5 ng/ml human VEGF, 0.75 U/ml heparin sulfate, 30 mg/ml gentamicin, and 15 μg/ml amphotericin B. HUVEC-TERT2 cells were always cultured on tissue culture-treated dishes. Dishes were coated with 0.2% gelatin solution for 1 hour at 37 °C, then aspirated and air-dried for 10 minutes in a biosafety cabinet.

HEK293T cells were cultured in DMEM with 10% FBS, 100 U/mL penicillin, 100 μg/mL streptomycin, and 2 mM L-glutamine on tissue culture-treated dishes.

Cell identity was confirmed by STR profiling or obtained from authenticated sources. Cultures were regularly screened for mycoplasma contamination using MycoAlert Mycoplasma Detection Kit.

Cells were maintained below overconfluent conditions. Cells growing in suspension were passaged 24 hours before starting each experiment to achieve density of 0.5 million cells/mL. For each experiment, cells were seeded at 0.5 million cells/mL in fresh medium, except for long timecourse-based experiments, where cells were seeded at 0.1-0.2 million cells/mL depending on the cell line. Adherent cells were seeded into new dishes 24 h before starting each experiment at a density of 8000 cells/cm<sup>2</sup>. All cell lines were passaged 2-3 times per week. New vials were thawed and expanded every 3 months to maintain cell line stability.

Suspension cell lines were passaged by gentle pipetting to resuspend the cells, followed by counting with trypan blue exclusion. Cultures were then diluted in fresh pre-warmed medium to maintain a density of 0.5 million cells/mL. Semi-adherent MM cell lines (MM1.S, KMS11, RPMI8226) were scraped with a cell scraper to dislodge the adherent cell subpopulation. Adherent cell lines were washed once with PBS (without Ca²+/Mg²+), detached using 0.05% trypsin-EDTA for 2-5 minutes at 37 °C, and the detachment was monitored under a microscope. For endothelial cell lines, cells were frequently released by firmly striking the side of the culture dish with the palm of the hand to dislodge them after trypsinization. Detached cells were transferred to a tube, centrifuged at 300 × g for 5 minutes, and the supernatant was carefully aspirated to avoid disturbing the loose pellet. Cells were then resuspended in fresh medium and reseeded at densities appropriate for each experiment.

For cell line cryopreservation, 5-10 million cells were frozen per cryovial in freezing medium containing 90% FBS and 10% DMSO. Vials were placed in a Mr. Frosty container filled with isopropanol, cooled at -80 °C overnight, and then transferred to liquid nitrogen for long-term storage. The cryovials were thawed by warming the vial in 37 °C water bath, immediately followed by slow dilution of the freezing medium with 10 mL culture medium, centrifugation at  $100 \times g$  for 5 min, and resuspension of the cell pellet in appropriate culture medium. The cells were then cultured in a 6-well plate in 3-6 mL of medium, inspected and split accordingly. If several days after thawing the cell viability kept decreasing, the culture was subjected to gradient centrifugation with Histopaque 1077 (as described in 2.2.1.6).

#### 2.2.1.2 Electroporation of mammalian cell lines

JJN3 cells were harvested from routine cultures at a density of  $3 \times 10^5$ - $7 \times 10^5$  cells/mL, pelleted at  $300 \times g$ , and resuspended in additive-free, freshly opened RPMI-1640 medium. Medium stored in tightly filled, sealed tubes was used when freshly opened bottles were unavailable, to preserve pH.

Final electroporation mixtures contained  $2 \times 10^7$ -6  $\times$  10<sup>7</sup> cells/mL. For 2 mm cuvettes (200  $\mu$ L volume), this corresponded to  $0.4 \times 10^7$ -1.2  $\times$  10<sup>7</sup> cells per reaction; for 4 mm cuvettes (500  $\mu$ L volume),  $1 \times 10^7$ -3  $\times$  10<sup>7</sup> cells per reaction. Cells were mixed with plasmid DNA and/or siRNA directly in 1.5 mL tubes by gentle pipetting.

Electroporation was performed using a Gene Pulser (Bio-Rad) with a single exponential decay pulse at 960  $\mu$ F and voltages set to 300 V. Immediately after pulsing, cells were transferred into 500  $\mu$ L of fresh, RPMI medium without additives and kept at room temperature until all electroporations were completed. Cells were then plated in pre-warmed complete medium and returned to standard culture conditions.

Electroporation efficiency was monitored by co-transfection with a plasmid allowing for a transient expression of a fluorescent protein (pSIREN-RetroQ-ZsGreen-shLuc). Consistent use of fresh, pH-stable medium was critical for cell viability and transfection efficiency.

Reusable electroporation cuvettes were cleaned between runs with ddH<sub>2</sub>O and 70% ethanol, then air-dried and sterilized with UV light in a biosafety cabinet for 1 h. Reuse did not significantly impact transfection efficiency.

#### 2.2.1.3 Lentivirus production and infection

Lentivirus was produced using HEK293T cells seeded at  $6 \times 10^6$  per 10 cm tissue culture-treated dish in DMEM supplemented with 10% FBS (without penicillin/streptomycin) 24 hours prior to transfection.

For transfection, the following plasmids were used (Table 17):

Table 17. Plasmids used for lentiviral production.

Plasmid	Amount
pHIV-ZsGreen-Luc	5 μg
pMDLg/pRRE	5 μg
pRSV-Rev	5 μg
pMD2.G	5 µg

Plasmids were diluted in Opti-MEM to a total volume of 500  $\mu$ L. Separately, 40  $\mu$ L of Lipofectamine 2000 was diluted in 460  $\mu$ L of Opti-MEM and incubated at room temperature for 5 minutes. The DNA solution was added to the Lipofectamine mix, gently mixed, and incubated for 30 minutes at room temperature. The resulting 1 mL DNA-Lipofectamine complex was slowly added dropwise to HEK293T cells. After 6 hours, the media was replaced with fresh DMEM + 10% FBS.

Viral supernatants were collected at 48 and 72 h post-transfection. Each harvest was centrifuged at  $300 \times g$  for 5 minutes at 4 °C, filtered through a 0.45  $\mu m$  syringe filter, and stored at 4 °C until use on day 3 post-transfection.

MM1.S cells were plated at  $2 \times 10^6$  cells per well in 6-well plates (2 mL/well) with the filtered viral supernatant supplemented with polybrene (2  $\mu$ g/mL). Plates were centrifuged at  $600 \times g$  for 60 minutes at 37 °C (spinfection). After centrifugation, viral media was removed by pelleting the cells, and fresh complete RPMI-1640 medium was added.

Transduction efficiency was assessed by ZsGreen fluorescence using flow cytometry 72 hours post-infection. ZsGreen<sup>+</sup> cells were sorted to establish a stably transduced population.

Stable ZsGreen<sup>+</sup> cells were tested for luciferase activity using the Dual-Luciferase Reporter Assay System (Promega) on a Berthold luminometer. Cells were tested for mycoplasma contamination and cryopreserved in FBS + 10% DMSO.

#### 2.2.1.4 Fluorescence microscopy

Cells grown on 1.5 glass coverslips (22 × 22 mm) were fixed, stained, and mounted onto SuperFrost glass slides using ProLong Glass Antifade Mountant to preserve fluorescence. The mounting medium was allowed to cure for 24 hours at room temperature before imaging.

Imaging was performed using a Zeiss Axio Imager.Z2 fluorescence microscope equipped with appropriate filter sets and objectives. Image acquisition was carried out using the Isis Fluorescence Imaging System (MetaSystems). Exposure settings were kept constant within each experiment. Linear adjustments to brightness and contrast were applied uniformly across image sets when needed.

#### 2.2.1.5 Flow cytometry

Flow cytometry was performed using a CytoFLEX S V4-B2-Y4-R3 analyzer. Cells were stained with fluorescently labeled antibodies or dyes according to standard protocols and washed with PBS containing 2% FBS or another appropriate buffer.

Data acquisition was carried out using CytExpert software with compensation applied as needed. The same acquisition speed and gain settings were applied to all experimental conditions within one experiment. Forward and side scatter were used to exclude debris and doublets. A minimum of 10,000 events per sample were collected. Gating strategies were defined using unstained and single-stained controls. Data was analyzed using FlowJo. Fluorescence thresholds for positive populations were determined based on appropriate negative controls.

#### 2.2.1.6 Isolation of cells from bone marrow aspiration biopsies

Bone marrow aspirates were obtained from the newly diagnosed MM patients following informed consent and in accordance with the institutional ethical guidelines, as approved by the Institute of Hematology and Transfusion Medicine Bioethical Committee (43/2016) and DFCI IRB #01-206. Bone marrow aspirates were collected into sodium heparin-coated tubes immediately after the procedure. Only freshly collected samples were used in this thesis, since frozen MM samples exhibit low plasma cell viability. To obtain a single-cell suspension, the sample was gently homogenized using an 18G green needle and 10 mL syringe to disrupt marrow clumps, which often contain multiple myeloma cells. This step increases the yield of purified MM cells approximately twofold.

The homogenized sample was diluted 1:1 with RPMI-1640 complete medium, and 6 mL of this mixture was slowly layered over 3 mL of room temperature Histopaque-1077 in a 15 mL conical tube, taking care not to disturb the interface. Density gradient centrifugation was performed at

1500 rpm for 20 minutes at room temperature using an Eppendorf 5810R centrifuge with swing-bucket rotor. The corresponding relative centrifugal force (RCF) was approximately  $400 \times g$ . Acceleration was set to 3, and deceleration was set to 0 (brake off) to preserve gradient separation.

Following centrifugation, the mononuclear cell layer (buffy coat) was carefully aspirated, transferred to a new tube, and washed once with RPMI-1640 medium. We did not perform RBC lysis due to negative effect on cell viability and CD138 expression on the surface of plasma cells. Cells were counted using a hemocytometer with trypan blue exclusion to assess viability. Isolated cells were used immediately for downstream applications such as flow cytometry or drug treatment.

#### 2.2.1.7 Magnetic sorting and culture of primary MM cells

CD138<sup>+</sup> plasma cells were isolated from mononuclear cell fractions obtained after Histopaque separation of bone marrow aspirates using CD138 MicroBeads and MACS LS Columns. LS columns were chosen over MS columns to reduce the risk of clogging due to the high cellularity and viscosity of the myeloma cell suspension.

Mononuclear cells were washed with MACS buffer (PBS with 0.5% BSA and 2 mM EDTA, pre-cooled and degassed) and centrifuged at  $300 \times g$  for 10 minutes. Cells were then resuspended at a concentration of up to  $2 \times 10^7$  total cells per 80  $\mu$ L of MACS buffer. CD138 MicroBeads were added at 20  $\mu$ L per  $2 \times 10^7$  cells. The suspension was mixed gently and incubated for 15 minutes at 4 °C. After incubation, cells were washed with 1-2 mL of MACS buffer per  $2 \times 10^7$  cells and centrifuged again at  $300 \times g$  for 10 minutes. The pellet was resuspended in 500  $\mu$ L of MACS buffer for magnetic separation.

MACS LS columns were prepared by rinsing with 3 mL of MACS buffer and placed into a MidiMACS separator. The labeled cell suspension was loaded onto the column, and the flow-through containing unlabeled cells was saved as it contains the CD138<sup>-</sup> fraction. Columns were washed three times with 3 mL of MACS buffer. After removal from the magnetic field, CD138<sup>+</sup> cells were eluted with 5 mL of MACS buffer by firmly pushing the plunger into the column.

CD138<sup>+</sup> and CD138<sup>-</sup> cells were counted using trypan blue exclusion, assessed for purity using flow cytometry, and used for downstream assays immediately, since their viability decreases after 48 h. CD138<sup>+</sup> MM cells were cultured as described in 2.2.1.1.

#### 2.2.1.8 Magnetic sorting and culture of primary MMECs and HD ECs

Mononuclear cells were obtained from bone marrow aspirates via density gradient centrifugation as described in 2.2.1.7. The CD138<sup>-</sup> fraction was retained for endothelial culture.

The CD138<sup>-</sup> cells were seeded onto fibronectin-coated 24-well plates at a density of one bone marrow sample per 12 wells. Plates were coated with fibronectin at 50  $\mu$ g/mL in 300  $\mu$ L per well and incubated for 1 hour at 37 °C. The fibronectin solution was then aspirated, and wells were air-dried in a biosafety cabinet.

Cells were cultured in EBM-2 medium supplemented with the EGM-2 SingleQuots Supplement and 10% human AB serum. After 24 hours, non-adherent cells were gently removed by medium exchange. Subsequent media changes were performed every 48 hours. Early endothelial colony formation was typically observed between days 5-7, with larger, subconfluent sheets forming by day 10. The efficiency of colony generation was approximately 90%.

To enrich endothelial cells, adherent cultures were subjected to positive selection using CD31 MicroBeads, and CD31<sup>+</sup> cells were expanded under the same conditions on fibronectin-coated cultureware. Purity of endothelial cells was verified by flow cytometry for CD31, VEGFR1, and CD144. Cells were used for downstream applications before reaching 3 passages.

#### 2.2.1.9 Proliferation and viability assays by flow cytometry

All small-molecule compounds were reconstituted according to the manufacturer's instructions in DMSO from a freshly opened bottle, at a stock concentration of 20 mM and protected from light. Stocks were aliquoted and stored at -80 °C to minimize freeze-thaw cycles.

To assess drug effects on cell viability and proliferation, cells were seeded on day -1 at a density of 20,000 cells per well in 96-well flat-bottom plates in  $50 \,\mu\text{L}$  of complete medium. After overnight incubation at 37 °C, drugs were added in  $50 \,\mu\text{L}$  per well using serial dilutions. DMSO in control wells was maintained at <0.02% final concentration.

Cells were incubated for 4 days. On day 4, each well was gently pipetted up and down to resuspend the cells. Then,  $50 \,\mu\text{L}$  of the suspension was transferred into 1.5 mL Eppendorf tubes preloaded with  $50 \,\mu\text{L}$  of PBS containing propidium iodide (PI) at a final concentration of  $1 \,\mu\text{g/mL}$ . Samples were acquired immediately on a CytoFLEX S V4-B2-Y4-R3 flow cytometer.

Forward and side scatter gating was used to exclude small cellular debris and doublets. Cells were then classified as live (PI<sup>-</sup>) or dead (PI<sup>+</sup>). The percentage of PI<sup>-</sup> cells was used to calculate LC<sub>50</sub> values. The CytoFLEX's peristaltic pump allows for consistent volumetric acquisition, enabling direct quantification of absolute live cell counts from the PI<sup>-</sup> gate. These counts were used to compute GI<sub>50</sub> values.

Baseline (day 0) samples were stained and analyzed before drug addition using the same protocol. Data analysis was performed in R, and dose-response metrics (LC<sub>50</sub>, GI<sub>50</sub>) were derived using a four-parameter logistic (4PL) sigmoidal curve fitting model.

#### 2.2.1.10 MTS cell proliferation assay

For drug synergy studies, cell proliferation and metabolic activity were assessed using the CellTiter 96 AQueous One Solution Cell Proliferation Assay according to the manufacturer's instructions. The assay relies on the bioreduction of MTS (3-(4,5-dimethylthiazol-2-yl)-5-(3-carboxymethoxyphenyl)-2-(4-sulfophenyl)-2H-tetrazolium) in the presence of phenazine methosulfate (PMS) by NAD(P)H-dependent dehydrogenases active only in viable cells, generating a soluble purple formazan product. Cells were seeded in 96-well plates at 20,000 cells per well in 50  $\mu$ L of complete medium and allowed to recover overnight in cell incubator. The following day, 25  $\mu$ L of each drug (prepared at 4× final concentration) was added per well in a checkerboard format, bringing the total volume to 100  $\mu$ L per well. Serial dilutions were used to create concentration gradients for both drugs. This allows systematic testing of all possible pairwise combinations in a defined concentration range. Control wells received DMSO vehicle. Blank wells with medium and MTS reagent only were included for background subtraction. Plates were incubated at 37 °C for 2 hours. Absorbance was measured at 490 nm using a microplate reader. The absorbance signal was directly proportional to the number of metabolically active, viable cells. The results were analyzed using Excel and SynergyFinder.

#### 2.2.1.11 Annexin V-based apoptosis assay

Apoptosis was assessed using the PE (or in some cases FITC) Annexin V Apoptosis Detection Kit, following the manufacturer's protocol. This assay distinguishes viable, early apoptotic, and late apoptotic or necrotic cells based on phosphatidylserine exposure and membrane integrity. Cells were harvested and washed twice with cold phosphate-buffered saline (PBS). They were then resuspended in  $1\times$  Annexin V Binding Buffer at a concentration of  $1\times10^6$  cells/mL. An aliquot of  $100~\mu\text{L}$  of the cell suspension ( $1\times10^5$  cells) was transferred to a 5 mL polystyrene tube. To each tube,  $5~\mu\text{L}$  of PE Annexin V and  $5~\mu\text{L}$  of 7-Aminoactinomycin D (7-AAD) were added. The samples were gently mixed and incubated for 15 minutes at room temperature in the dark.

Following incubation,  $400 \,\mu\text{L}$  of 1X Annexin V Binding Buffer was added to each tube. Samples were analyzed by flow cytometry within one hour of staining. Compensation was calculated using single-stained controls. Cells were first gated to exclude debris and doublets based on forward and side scatter properties. The following populations were identified:

- 1. Viable cells: Annexin V<sup>-</sup> / 7-AAD<sup>-</sup>
- 2. Early apoptotic cells: Annexin V<sup>+</sup> / 7-AAD<sup>-</sup>
- 3. Late apoptotic or dead cells: Annexin V<sup>+</sup> / 7-AAD<sup>+</sup>
- 4. Necrotic cells: Annexin V<sup>-</sup> / 7-AAD<sup>+</sup>

#### 2.2.1.12 Caspase-Glo luminescent assay

Caspase activity was measured using Caspase-Glo 3/7, Caspase-Glo 8, and Caspase-Glo 9 Assay Kits according to the manufacturer's instructions. These assays use a luminogenic substrate cleaved by active caspases, producing a stable glow-type luminescent signal proportional to caspase activity.

Cells were harvested, counted using trypan blue exclusion, and seeded into white-walled 96-well plates at 20,000 total (live + dead) cells in 100 µL complete medium. Cell counting ensured normalization of caspase activity per cell across experimental conditions. Plates were equilibrated to room temperature for 10 minutes. Caspase-Glo reagent was prepared fresh by reconstituting lyophilized substrate with the provided buffer and equilibrated to room

temperature. An equal volume ( $100 \,\mu\text{L}$ ) of Caspase-Glo reagent was added to each well, resulting in a final volume of  $200 \,\mu\text{L}$ . Plates were mixed on a plate shaker at  $300\text{-}500 \,\text{rpm}$  for  $30 \,\text{seconds}$  and incubated at room temperature for 1 hour in the dark. Luminescence was recorded using a microplate luminometer. Blank values (medium + reagent, no cells) were subtracted, and caspase activity was expressed in relative light units (RLU).

#### 2.2.1.13 Cellular Thermal Shift Assay (CETSA)

Drug-protein target engagement in intact cells was assessed using the cellular thermal shift assay (CETSA), as described by Jafari et al. [358] with modifications. Cells were cultured in complete medium and harvested during logarithmic growth phase.

Cells were pelleted at  $300 \times g$  for 5 minutes, washed once in 15 mL of room temperature PBS, and resuspended in 5 mL PBS. Protease and phosphatase inhibitors (Roche) were added to 1 mL of PBS, which was used to resuspend the final pellet. Cells were counted and distributed to achieve  $1 \times 10^6$  cells per temperature condition. Each condition was aliquoted into four PCR tubes (100  $\mu$ L per well).

Cell suspensions were heated for 3 minutes in a thermal cycler preheated to target temperature gradient. For PIM kinases we have determined it to be 42-53°C. Following heating, samples were incubated at room temperature for 3 minutes and then immediately snap-frozen in liquid nitrogen.

Lysis was achieved via two freeze-thaw cycles between liquid nitrogen and 25 °C in a thermal cycler. Lysates were centrifuged at 20,000 × g for 20 minutes at 4 °C. The supernatant containing the soluble protein fraction was carefully aspirated without disturbing the pellet and transferred to new tubes. The samples underwent SDS-PAGE and western blotting as described in 2.2.3.2-2.2.3.3. Band intensities were quantified in ImageJ. Melting curves were generated in Prism using a four-parameter logistic (4PL) sigmoidal curve fitting model.

#### 2.2.1.14 Comet assay

DNA strand breaks were assessed using the alkaline CometAssay Silver Kit, following the manufacturer's instructions with minor modifications. The assay detects both single- and double-stranded DNA breaks in individual cells by gel electrophoresis under alkaline conditions.

Cells were harvested, washed once with cold PBS ( $Ca^{2+}/Mg^{2+}$ -free), and resuspended in PBS at  $1 \times 10^5$  cells/mL. Molten low melting point Comet LMAgarose was first melted at  $80^{\circ}$ C and then equilibrated to 37 °C and mixed with cells at a 10:1 ratio ( $500 \mu$ L agarose: $50 \mu$ L cells). Immediately,  $50 \mu$ L of this mixture was pipetted onto CometSlides (precoated glass microscope slides), and evenly spread across the well using the pipette tip edge. Slides were placed flat at 4 °C for  $10 \mu$ C minutes in the dark to solidify.

Slides were immersed in pre-chilled Lysis Solution for 1 hour at 4 °C. After lysis, they were incubated in freshly prepared Alkaline Unwinding for 20 minutes at room temperature in the dark to denature DNA and unwind damaged regions.

Electrophoresis was performed at 33 V (1 V/cm) for 30 minutes in cold Alkaline Electrophoresis Solution. After electrophoresis, slides were neutralized with two washes in deionized water (5 minutes each), followed by a 5-minute wash in 70% ethanol. Slides were air-dried at 37 °C for 15 minutes.

For visualization, slides were stained with 100 µL of diluted SYBR Gold. Comets were visualized using epifluorescence microscopy with a fluorescein filter. DNA damage was quantified using comet tail/head ratio calculated in ImageJ.

#### 2.2.1.15 Wound healing (scratch) assay

HUVEC-TERT2 cells were seeded in 6-well tissue culture-treated plates and cultured for 4 days in fully supplemented EBM-2 medium until reaching 95% confluence. The cells were then incubated with indicated compounds for 24h.

After 24h, a straight scratch was made across the cell monolayer in each well using a sterile 200 μL pipette tip. Detached cells and debris were removed by gently washing twice with PBS. Fresh medium containing indicated compounds was then added to each well. Plates were returned to the incubator (37 °C, 5% CO<sub>2</sub>), and cells were imaged after 8 hours using brightfield microscopy to assess wound closure. Scratch area was quantified using ImageJ. Healing was expressed as the percentage of wound closure relative to the initial scratch width.

#### 2.2.1.16 Tube formation assay

Endothelial tube formation was assessed using a Matrigel-based *in vitro* angiogenesis assay. Growth factor-reduced Matrigel was thawed on ice overnight and added (300 μL per well) to pre-chilled (-20°C) 24-well plates using pre-chilled pipette tips. Plates were incubated at 37 °C for 60 minutes to allow Matrigel polymerization. HUVEC-TERT2 cells were harvested, counted, and resuspended in complete EBM-2 medium. A total of 45,000 cells in 300 μL of medium were seeded onto each Matrigel-coated well. Cells were incubated at 37 °C and 5% CO<sub>2</sub> for 8 hours to allow tube formation. Brightfield images were acquired at multiple fields per well using an inverted microscope. Quantitative analysis of tube formation (including number of junctions, total tube length, meshes, and nodes) was performed using the Angiogenesis Analyzer plugin for ImageJ.

#### 2.2.1.17 Phalloidin-AF488 labeling of F-actin

F-actin structures were visualized using Alexa Fluor 488-conjugated phalloidin. Lyophilized reagent was reconstituted in 750 μL of anhydrous DMSO to create an 800× stock solution. To preserve cellular morphology during fixation, 3 mL of HBSS was added to each well of a 6-well plate, followed by 1 mL of freshly opened 16% paraformaldehyde (final concentration: 4%). Cells were fixed for 15 minutes at room temperature, then washed three times with PBS (5 minutes each). Alexa Fluor 488 phalloidin was diluted 1:800 in PBS and applied to cells for 15 minutes at room temperature in the dark. Cells were washed once in PBS following incubation. Nuclei were counterstained with NucBlue Live ReadyProbes Reagent at a dilution of 2 drops per 1 mL PBS for 15 minutes at room temperature, then washed three times with PBS.

Coverslips were mounted using ProLong Gold Antifade Mountant and imaged by fluorescence microscopy using appropriate filters. Formation of actin stress fibers, membrane ruffles and lamellipodia area was quantified using ImageJ and Photoshop.

#### 2.2.1.18 Actin fractionation

Cells were lysed directly in culture dishes using ice-cold RIPA buffer supplemented with protease and phosphatase inhibitors for 30 minutes on ice. Lysates were collected and centrifuged at  $15,000 \times g$  for 30 minutes at 4 °C. The supernatant (G-actin fraction) was

transferred to a new tube. The pellet (F-actin fraction) was washed twice with ice-cold PBS and centrifuged at  $15,000 \times g$  for 5 minutes after each wash. The pellet was resuspended in  $25 \,\mu L$  RIPA buffer and  $25 \,\mu L$  freshly prepared F-actin Extracting Solution. Resuspension was performed on ice with gentle mixing every 15 minutes for 1 hour. Samples were centrifuged at  $15,000 \times g$  for 30 minutes at 4 °C, and the supernatant containing solubilized F-actin was collected for SDS-PAGE, western blotting and detection using an anti- $\beta$ -actin primary antibody, as described in 2.2.3.3.

#### 2.2.1.19 RhoA GTPase activation assay

RhoA activation was assessed using a rhotekin-RBD pulldown assay (Rho Activation Assay Biochem Kit) following the manufacturer's instructions. This assay allows for isolation of the GTP-bound (active) form of RhoA from cell lysates using GST-tagged Rhotekin-RBD protein immobilized on colored sepharose beads.

Lyophilized rhotekin-RBD sepharose beads were rehydrated by adding the recommended volume of sterile water and allowing them to sit at room temperature for 5 min. Beads were fully dispersed by flicking the tube several times. After rehydration, the bead slurry was aliquoted using a wide-bore pipette tip (trimmed with scissors to prevent clogging). The slurry was mixed again after every two aliquots to prevent bead settling. Aliquots were snap-frozen in liquid nitrogen and stored at -80 °C for long-term use.

Cells were grown in 150 mm dishes under specified conditions for 24 h to modulate RhoA activity. Following treatment, cells were immediately placed on ice. Culture medium was aspirated, and cells were rinsed once with ice-cold PBS. Residual PBS was removed by tilting the plate on ice for 1 minute. Cells were lysed directly in the plate with 500  $\mu$ L Cell Lysis Buffer (supplemented with protease and phosphatase inhibitors). Lysates were harvested using a cell scraper and clarified by centrifugation at  $10,000 \times g$  for 1 minute at 4 °C. Protein concentrations were determined as described in 2.2.3.1. To validate assay performance, two control lysates were loaded with 200  $\mu$ M GTP $\gamma$ S or 1 mM GDP to create positive and negative controls, respectively.

Equal amounts of total protein (300-800  $\mu$ g) were incubated with 50  $\mu$ g rhotekin-RBD beads for 1 hour at 4 °C with constant rocking. Beads were washed once with 500  $\mu$ L Wash Buffer and pelleted by centrifugation at 3,000  $\times$  g for 3 minutes at 4 °C. Supernatants were carefully

removed, and beads were resuspended in 1× Laemmli buffer. Samples were boiled for 2 minutes and loaded directly onto SDS-PAGE as described in 2.2.3.3. His-tagged RhoA (30 kDa) was used as a Western blot standard.

#### 2.2.1.20 Conditioned media collection

Conditioned medium was collected by washing confluent adherent endothelial cells or MM cells with PBS and incubating them in for 24 hours. The supernatant was harvested and stored at -80°C for downstream applications.

#### 2.2.1.21 Cell cycle analysis by Hoechst 34580 staining

Cell cycle phase distribution was assessed using Hoechst 34580 DNA staining followed by flow cytometry. Cells were incubated with Hoechst 34580 at a final concentration of 10 µg/mL for 30 minutes at 37 °C. After incubation, cells were analyzed on a CytoFLEX flow cytometer using the PB-450 channel. Hoechst 34580 binds preferentially to adenine-thymine-rich regions of double-stranded DNA. The dominant peak in PB-450 fluorescence histograms was assigned to the G1 phase. A second peak with approximately double the intensity was labeled as the G2/M phase. The region between these peaks represented cells in S phase, characterized by ongoing DNA synthesis and intermediate DNA content (2n-4n). Fluorescence signals below the G1 peak were interpreted as sub-G1 events with fragmented DNA. Events above the G2/M fluorescence peak were polyploid cell populations.

# 2.2.2 Molecular biology methods

#### 2.2.2.1 Production of chemocompetent bacteria

Chemically competent  $E.\ coli$  cells were prepared using the RbCl-based two-step protocol involving cold treatment with RF1 and RF2 solutions. An overnight culture (50-100 mL) of  $E.\ coli$  was grown in LB medium at 37 °C with shaking (180 rpm). The following day, 5 mL of the overnight culture was used to inoculate 100 mL of fresh SOB medium in a 500 mL flask. Cells were grown at 37 °C with shaking until the optical density at 600 nm (OD600) reached 0.6 (approximately 2-3 hours). The culture was immediately transferred to two pre-chilled 50 mL Falcon tubes and incubated on ice for 15 minutes. Cells were pelleted by centrifugation at 600 ×

g for 15 minutes at 4 °C. The supernatant was carefully discarded. The cell pellet was gently resuspended in one-third the original culture volume of ice-cold RF1 solution (e.g., 16.7 mL RF1 for a 50 mL culture) by slow vortexing. The suspension was incubated on ice for 30 minutes. Cells were pelleted again by centrifugation at  $600 \times g$  for 15 minutes at 4 °C. The supernatant was discarded, and the pellet was resuspended in 1/12.5 of the original culture volume of ice-cold RF2 solution (e.g., 4 mL for a 50 mL culture) by gentle vortexing. The suspension was incubated on ice for an additional 15 minutes. Aliquots of 100 µL were prepared in pre-chilled 1.5 mL microcentrifuge tubes on ice. Tubes were snap-frozen in liquid nitrogen and stored at 80 °C.

# 2.2.2.2 Transformation of competent bacteria with plasmid DNA and plasmid amplification

Chemically competent E. coli cells were transformed using the heat shock method. Aliquots of  $100~\mu L$  competent cells were thawed on ice for 10-15 minutes. To each aliquot, either 10-50 ng of plasmid DNA or  $10~\mu L$  of a ligation reaction mixture was added. The tubes were gently flicked to mix and incubated on ice for 30~minutes. Cells were heat-shocked by transferring the tubes to a pre-warmed  $42~^{\circ}C$  water bath for 2~minutes, followed by immediate incubation on ice for 2~minutes additional minutes to stabilize the membrane. After heat shock,  $500~\mu L$  of pre-warmed SOC medium was added to each tube. Tubes were incubated at  $37~^{\circ}C$  for 1~h with shaking (180~rpm) to allow for recovery and antibiotic resistance gene expression. Following incubation, cells were pelleted by centrifugation at  $2000~\times~g$  for 5~minutes. The supernatant was removed, and the pellet was gently resuspended in  $100~\mu L$  sterile LB medium. The entire volume was plated onto dry 10~cm~LB-agar plates supplemented with the appropriate selective antibiotic. Plates were incubated overnight at  $37~^{\circ}C$ , and colonies were observed the next morning.

Single colonies were picked from LB-agar plates and inoculated into 15 mL conical tubes with loosely tightened caps containing 5 mL of LB medium with the appropriate antibiotic. Cultures were grown overnight at 37 °C with shaking at 180 rpm. For large-scale plasmid preparation, 1-2 mL of the overnight starter culture was used to inoculate 250-400 mL of LB medium with antibiotic in a sterile 500 mL Erlenmeyer flask and incubated at 37 °C with shaking for 12-16 hours. Cells were harvested by centrifugation at 4000 × g for 10 minutes at 4 °C. Pellets were either processed immediately for plasmid extraction or stored at -20 °C for later use.

#### 2.2.2.3 Bacterial cryopreservation

To preserve *E. coli* strains carrying plasmids, glycerol stocks were prepared from overnight LB cultures grown with appropriate antibiotics. A volume of 750 μL of the bacterial culture was mixed with 250 μL of sterile 80% glycerol in a 1.5 mL cryovial (final glycerol concentration: 20%). Tubes were mixed by pipetting up and down, labeled, and immediately stored at -80 °C. For recovery, frozen stocks were scraped with a sterile pipette tip and cultured in 5 mL LB medium overnight.

#### 2.2.2.4 Small-scale isolation of plasmid DNA from bacteria (Miniprep)

Plasmid DNA was extracted using the GeneMATRIX Plasmid Miniprep DNA Purification Kit following the manufacturer's protocol. The procedure is based on alkaline lysis followed by silica column purification. Each spin column was pre-wetted with 30 µL of Activation Buffer PL, which was applied directly to the membrane and allowed to sit at room temperature for at least 5 minutes prior to lysate application. An overnight culture (4 mL) of E. coli was pelleted by two consecutive centrifugation steps at 12,000 × g for 2 minutes in 2 mL microcentrifuge tubes. The supernatant was removed, and the pellet was very thoroughly resuspended in 250 µL of Cell R buffer (containing RNase A). Cells were lysed by adding 250 μL of Lysis Blue buffer and gently inverting the tube several times until a homogeneous blue lysate was formed. Neutralization was achieved by adding 350 µL of Neutral B buffer, followed by gentle inversion until the blue color disappeared and a white precipitate formed. Lysates were clarified by centrifugation at  $12,000 \times g$  for 7 minutes at room temperature. The clear supernatant ( $\sim 600 \,\mu\text{L}$ ) was applied in two rounds to the activated spin column and centrifuged at  $11,000 \times g$  for 1 minute per load. Flow-through was discarded between each step. The column was washed sequentially with 500 µL of Wash PLX1 buffer and 600 µL of Wash PLX2 buffer, each followed by 1-minute centrifugation at 11,000 × g. A final dry spin at 11,000 × g for 1 minute was performed to remove residual wash buffer. Spin columns were transferred to clean 1.5 mL microcentrifuge tubes. Plasmid DNA was eluted with 20-50 µL of Elution buffer, pre-warmed to 80 °C. Elution buffer was pipetted directly onto the center of the column membrane, incubated for 5 minutes at room temperature, and centrifuged at 11,000 × g for 1 minute. Eluted plasmid DNA was stored at -20 °C for long-term storage or at 2-8 °C for short-term use. DNA purity and concentration were assessed by spectrophotometry (2.2.2.13) and agarose gel electrophoresis (2.2.2.7).

#### 2.2.2.5 Large-scale isolation of plasmid DNA from bacteria (Maxiprep)

A single bacterial colony was inoculated into 5 mL LB medium containing the appropriate antibiotic and grown overnight at 37 °C with shaking. The culture was diluted 1:100 into 250-400 mL fresh LB medium and incubated overnight for 16 h at 37 °C with vigorous shaking. Bacterial pellets were harvested by centrifugation at 6,000 × g for 15 minutes at 4 °C, and resuspended in 10 mL Buffer P1 supplemented with RNase A (100 mg/L) and LyseBlue reagent (1:1000 v/v). Lysis was performed by adding 10 mL Buffer P2, gently mixing, and incubating at RT for 5 minutes. Lysis was neutralized by adding 10 mL of pre-chilled Buffer P3, followed by gentle inversion until the blue color cleared. The mixture was incubated on ice for 15 minutes.

The lysate was clarified by centrifugation at 20,000 × g for 30 minutes at 4 °C. The supernatant was first passed through a double layer of sterile medical gauze to remove large debris. It was then filtered through a QBT-prewetted coffee filter to remove residual particulates. To reduce endotoxin content, 3 mL of Buffer ER was added to the filtered lysate, mixed by inversion, and incubated for 30 minutes on ice. A GenCatch DEAE-Silica Anion Exchange Maxi Column was pre-equilibrated with 10 mL Buffer QBT, and the ER-treated lysate was applied by gravity flow. The column was washed twice with 30 mL Buffer QC, and plasmid DNA was eluted with 15 mL Buffer QN. DNA was precipitated by adding 10.5 mL (0.7×) isopropanol, mixed gently, and centrifuged at 15,000 × g for 30 minutes at 4 °C. The resulting pellet was washed with 5 mL endotoxin-free 70% ethanol, centrifuged again, and air-dried for 5-10 minutes. The DNA pellet was resuspended in endotoxin-free Buffer TE and stored at -20 °C. In some cases, the pellet was incubated at 60 °C for 10 min and at +4 °C overnight to increase solubility. Identity of each plasmid was confirmed using restriction enzyme digestion (2.2.2.6) followed by agarose gel electrophoresis (2.2.2.7).

#### 2.2.2.6 Restriction enzyme digestion

Restriction digests were performed to prepare plasmid DNA for cloning and to verify construct identity. Digestion reactions were carried out in a total volume of 20-50 μL using commercially available restriction enzymes and manufacturer-recommended buffers. For preparative digests used in cloning workflows, 5-10 μg of plasmid DNA were incubated with 10 units of each restriction enzyme at 37 °C for 1 hour. Reactions were adjusted to 1× buffer concentration. After

digestion, samples were separated by electrophoresis (2.2.2.7). For analytical digests to confirm plasmid structure or cloning success, 300-500 ng of plasmid DNA was digested with 1-2 units of restriction enzyme in a 20  $\mu$ L reaction volume. These digests were incubated for 1 hour at the enzyme's optimal temperature and analyzed by agarose gel electrophoresis (2.2.2.7). All digestion reactions were performed with high-fidelity (HF) enzymes when available to reduce star activity. Digested DNA was either used directly for downstream ligation or stored at -20 °C until further use.

#### 2.2.2.7 Gel electrophoresis separating DNA fragments

DNA fragments were separated using horizontal agarose gel electrophoresis in 1× TAE buffer. Agarose gels (1-2%, w/v) were prepared in-house by dissolving agarose in TAE buffer, heating until fully melted, and allowing the solution to cool to ~60 °C before adding 2 μL of ethidium bromide and pouring into a gel tray with combs. Gels were cast and run using Sub-Cell GT Cell. DNA samples were mixed with 6× loading dye and loaded into wells alongside a molecular weight marker (e.g. GeneRuler 1 kb DNA Ladder). Electrophoresis was performed at 120 V until sufficient separation was achieved. Gels were imaged under UV illumination using a gel documentation system. DNA band sizes were estimated by comparison with the molecular weight standard. For circular DNA samples, appropriate vectors of established MW were separated alongside experimental samples for more exact molecular weight reference.

#### 2.2.2.8 Extraction and purification of DNA fragments

DNA fragments were purified from agarose gels and enzymatic reactions using the NZYGelpure kit following the manufacturer's instructions.

DNA bands were excised from 1% TAE agarose gels using a clean scalpel under low-intensity UV illumination to prevent random mutagenesis. Gel slices were weighed, and 300  $\mu$ L of Binding Buffer was added per 100 mg of gel (or 500  $\mu$ L for high-concentration gels). Samples were incubated at 60 °C for 10 minutes until the agarose was fully dissolved. If the resulting solution appeared orange or violet, 10  $\mu$ L of 3 M sodium acetate (pH 5.0) was added to adjust pH for optimal binding. For fragments <500 bp or >10 kb, one gel volume of isopropanol was added prior to binding. The mixture was loaded onto NZYTech spin columns and centrifuged at 12,000 × g for 60 seconds. After pre-washing with 500  $\mu$ L Wash Buffer, columns were washed

with 600 μL Wash Buffer, followed by a 1-minute dry spin to remove residual ethanol. DNA was eluted in 50 μL Elution Buffer (prewarmed to 80°C), applied to the center of the column membrane, and incubated at room temperature for 2 minutes before centrifugation. This silica membrane-based method enables efficient recovery of DNA ranging from 50 bp to 20 kb.

For PCR or enzyme cleanup, five volumes of Binding Buffer were added to each reaction mixture. After mixing, the sample was loaded onto the spin column. Washing and elution steps were identical to the gel extraction protocol.

All centrifugations were carried out at room temperature at  $\geq$ 12,000  $\times$  g. Purified DNA was quantified and stored at -20 °C.

#### 2.2.2.9 Ligation of DNA fragments into plasmids

DNA fragments were ligated using T4 DNA Ligase in a 20 µL reaction volume. Insert-to-vector molar ratios of 3:1 or 5:1 were calculated using the NEBioCalculator tool.

Typical ligation reaction setup (20 μL total, Table 18):

Table 18. DNA ligation setup.

Component	Volume
Insert DNA (variable amount)	2 µL
Vector DNA (100 ng)	3 µL
10× T4 DNA Ligase Buffer	2 µL
T4 DNA Ligase	1 μL
Nuclease-free water	12 µL

DNA concentrations were determined by NanoDrop prior to setup.

Reactions were incubated in a thermocycler at 22 °C for 1 hour. In selected experiments, ligation was extended overnight at 16 °C to improve efficiency. Following ligation,  $10 \,\mu\text{L}$  of the reaction mixture was used to transform  $100 \,\mu\text{L}$  of chemically competent *E. coli* by heat shock. Transformed cells were plated on LB-agar containing the appropriate selective antibiotic and incubated overnight at 37 °C.

#### 2.2.2.10 Colony PCR

To quickly assess cloning efficiency after bacterial transformation, colony PCR was performed directly from individual colonies. Typically, 10-20 colonies were tested in parallel using the QuickLoad Taq  $2\times$  Master Mix (NEB) according to the manufacturer's protocol. A total reaction volume of 10  $\mu$ L was sufficient for robust amplification and was prepared by mixing 5  $\mu$ L of  $2\times$  Master Mix, 0.2  $\mu$ L of each primer (10  $\mu$ M), and 4.6  $\mu$ L of nuclease-free water. Individual colonies were picked with a pipette tip, streaked onto a replica agar plate containing the appropriate antibiotic (for backup), and then transferred into the PCR tube containing the reaction mix. The replica plate was incubated at 37 °C for several hours.

PCR conditions included an initial denaturation at 95 °C for 30 seconds, followed by 35 cycles of denaturation at 95 °C for 30 seconds, annealing at 45-68 °C for 15 seconds (depending on primer Tm calculated using the NEB online tool), and extension at 68 °C (1 minute per kb). A final elongation step was carried out at 68 °C for 8 minutes.

PCR products were directly analyzed by electrophoresis on 1% agarose gels containing ethidium bromide and visualized under UV light. Colonies yielding bands of the expected size were considered positive. These clones were retrieved from the replica plate and cultured overnight in selective media.

#### 2.2.2.11 Sanger sequencing

Sanger sequencing was performed using the BigDye Terminator v3.1 Cycle Sequencing Kit on an ABI 3500 Genetic Analyzer. Plasmid DNA and PCR products were sequenced using custom primers.

Sequencing reaction (10 µL total) and cycling protocols are presented in Tables 19 and 20.

Table 19. BigDye sequencing reaction composition.

Component	Volume
DNA template (100-500 ng plasmid or 5-	3 μL
20 ng PCR product)	
3.2 µM primer	1 μL
BigDye v3.1 mix	1 μL
5× sequencing buffer	2 μL
Nuclease-free water	3 µL

Table 20. BigDye thermal cycling protocol.

Cycles	Temperature	Time
1	96 °C	1 min
	96 °C	10 s
25	50 °C	5 s
	60 °C	4 min

Dye terminators were removed using the ExTerminator kit. Sequencing reactions were mixed with 5  $\mu$ L of Mix Blue and 100  $\mu$ L of WP Bind/Wash solution. The mixture was applied to a spin column and centrifuged at 15,000  $\times$  g for 30 s. After a wash with 400  $\mu$ L of WP solution and 2 min centrifugation, columns were transferred to fresh tubes. Elution was performed with 25  $\mu$ L of ultrapure water, applied directly to the resin, followed by 2 min incubation and 1 min centrifugation. Eluted samples were light blue. They were either sequenced on the same day or stored at -20 °C to be sequenced the following day. Sequencing was performed at the Laboratory of Molecular Biology, Institute of Hematology and Transfusion Medicine, Warsaw, Poland. Purified products were loaded onto the ABI 3500 and separated using POP-7 polymer with a 50 cm capillary array. Data were analyzed using Sequencing Analysis Software, and base calls were verified manually. Sequences were aligned to reference constructs using Benchling.

#### 2.2.2.12 Cloning

To enable doxycycline-inducible knockdown of the three PIM kinases (PIM1, PIM2, PIM3), a panel of 14 plasmids expressing individual shRNAs and 1 scrambled control (shSCR) was constructed using a modular Sleeping Beauty (SB) transposon system described previously by Fink et al. [359]. The cloning strategy has been presented in Fig. X. The backbone plasmid TST30 (pS2, pSUSTER2 derivative) contains a modified H1 promoter with two Tet-operator sites for tight inducible expression of shRNA. The transposon integration vector TST201 (pT2-neo-S2) was used to flank expression cassettes with inverted terminal repeats (ITRs) recognized by the SB transposase and carries a neomycin resistance cassette for stable selection. TST209 (pT2-CAG-puro-tTR) was used to establish stable expression of the tetracycline repressor (tetR) and puromycin resistance in target cell lines. Oligonucleotides used for shRNA duplex generation, colony PCR and Sanger sequencing (seq201F, seq201R2, seq30) are listed in 2.1.5.1.

Oligonucleotide sequences encoding shRNAs were designed using Clontech's online shRNA design tool. The shRNAs were designed to target PIM1 (four variants: shPIM1.2-1.5), PIM2 (shPIM2.1-2.5), and PIM3 (shPIM3.1-3.5), as well as a scrambled control (shSCR). All sequences have been checked for possible off-targets using NCBI Blast tool. Only shRNA sequences complimentary with individual PIM mRNA sites were selected, to avoid unintentional silencing of other PIM family members. The shRNA oligonucleotides were synthesized by oligo.pl (IBB PAN, Warsaw, Poland). Complementary top and bottom oligonucleotides encoding the shRNA sequences were phosphorylated and annealed in a single-step reaction using T4 Polynucleotide Kinase (PNK) and a thermocycler-controlled annealing ramp. Each single-stranded DNA oligo was resuspended in nuclease-free water to a final concentration of 100 µM and used in the annealing reaction (Tables 21 and 22).

Table 21. Reaction components for phosphorylation and annealing of oligonucleotides.

Component	Volume
Top strand oligo (100 μM)	1 μL
Bottom strand oligo (100 µM)	1 μL
10× T4 Ligation Buffer (with ATP)	1 μL
T4 Polynucleotide Kinase	1 μL
Nuclease-free water	6 µL

Table 22. Reaction conditions for phosphorylation and annealing of oligonucleotides.

Temperature	Time
37 °C	30 min
95 °C	5 min

Ramp down to 25 °C at 5 °C/min

TST30 plasmids were digested with BgIII and SacI, heat-inactivated and purified as described in 2.2.2.7 (since BgIII is not sensitive to heat inactivation). The annealed shRNA duplexes were ligated into the multiple cloning site downstream of the doxycycline-inducible H1 promoter. The resulting TST30-shRNA constructs were verified and named accordingly (e.g., TST30-shPIM1.2, TST30-shSCR, etc.).

To generate constructs suitable for transposition, the complete promoter-shRNA expression cassettes were excised from TST30 using BstXI and SacI. These were ligated into TST201, which had been pre-digested with BstXI, heat-inactivated, and dephosphorylated with FastAP to prevent vector self-ligation (Table 23). The mixture was gently mixed, briefly spun down, and

incubated at 37 °C for 10 minutes. Enzyme inactivation was performed by heating the reaction at 75 °C for 5 minutes. Ligation was carried out using protocol specified in 2.2.2.8.

Table 23. Reaction components for vector DNA dephosphorylation with FastAP.

Component	Volume
Linearized plasmid DNA (~1 µg)	1 μL
10× FastAP Reaction Buffer	2 µL
FastAP enzyme (1 U/μL)	1 μL
Nuclease-free water	to 20 µL

This step placed each shRNA cassette between Sleeping Beauty-compatible ITRs in TST201 (Fig. 7). In total, 15 functional TST201-shRNA plasmids were successfully constructed.

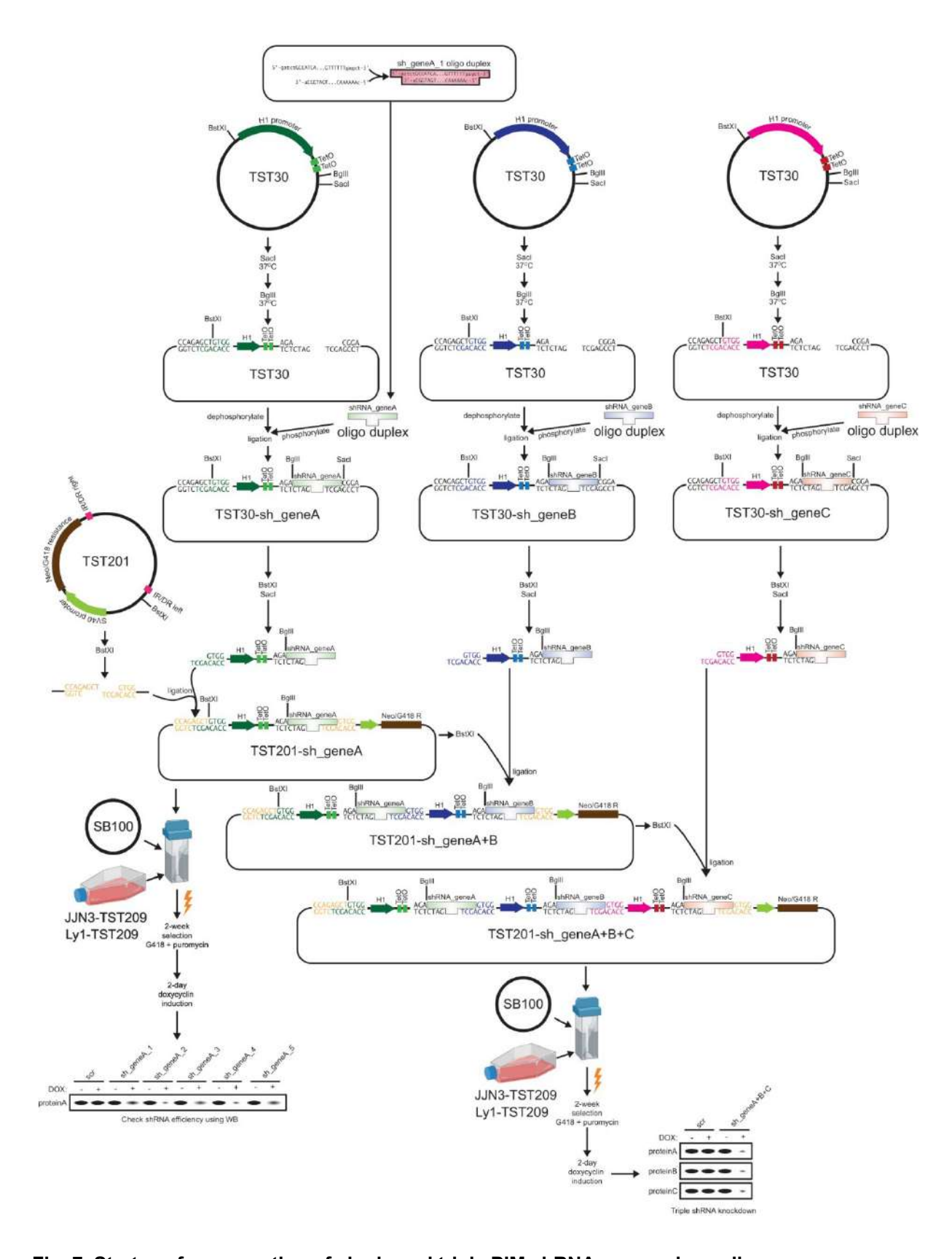


Fig. 7. Strategy for generation of single and triple PIM shRNA-expressing cells.

The TST201-shRNA plasmids were individually co-electroporated with pCMV(CAT)T7-SB100 into JJN3-TST209 cells, which had been previously co-electroporated with TST209 and pCMV(CAT)T7-SB100 and selected with puromycin to stably express the tetracycline repressor. Each resulting cell line was selected with G418 and puromycin and tested for doxycycline-inducible knockdown of its respective target by western blot.

To combine shRNA sequences targeting all three PIMs, the selected shRNAs (shPIM1.5, shPIM2.4, and shPIM3.4) were sequentially excised from their respective TST30 backbones and ligated into a TST201-shRNA plasmid using BstXI/SacI-compatible ligation. Each insert was added head-to-tail, maintaining the orientation and spacing of H1-TetO promoters. The resulting construct, TST201-sh3xPIM, expresses all three shRNAs from individual doxycycline-inducible units within a single SB transposon cassette.

TST201-sh3xPIM was co-electroporated with pCMV(CAT)T7-SB100 into JJN3-TST209 cells. Stable integrants were selected with G418 and puromycin and evaluated for inducible PIM1-3 silencing by immunoblotting following doxycycline treatment. The creation of this plasmid panel was a joint project executed together with Dr. Sonia Dębek.

Optimal concentrations of antibiotics were determined by titration experiments and are presented in Table 24.

Table 24. Antibiotic concentrations used in this study for JJN3 cells.

Antibiotic	Stock concentration	Final concentration
G418 (Geneticin)	100 mg/mL	1000 μg/mL
Puromycin	10 mg/mL	1 μg/mL
Doxycycline	10 mg/mL	0.5 μg/mL

#### 2.2.2.13 Concentration quantification of nucleic acids

Quantification of DNA and RNA was performed using two complementary methods, depending on sample type and downstream application. For routine assessment of nucleic acid concentration and purity, absorbance was measured using a Multiskan Microplate Spectrophotometer. Samples were diluted in nuclease-free water and loaded into  $\mu$ Drop plate (2  $\mu$ L/sample). Absorbance was read at 260 nm (for nucleic acid concentration), 280 nm (protein contamination), and 230 nm (salt/phenol contamination). Purity was assessed based on standard absorbance ratios:

DNA: acceptable A260/A280 = 1.8-2.0; A260/A230 > 1.8

RNA: acceptable A260/A280 =  $\sim$ 2.0; A260/A230 > 1.8

During RNA-seq library preparation, concentrations of RNA and amplified libraries were quantified using the Qubit Fluorometer (Thermo Fisher Scientific) with Qubit RNA HS, DNA HS, or dsDNA BR Assay Kits, depending on sample type and concentration range. All Qubit measurements were performed according to the manufacturer's protocol using low-binding tubes.

#### 2.2.2.14 Mammalian cell RNA isolation

Total RNA was isolated using TRIzol Reagent following Chomczynski's phenol-chloroform extraction protocol [360]. Samples were homogenized in 1 mL of TRIzol reagent per sample. For frozen samples stored in TRIzol, tubes were first thawed to room temperature. After homogenization, 200 µL of chloroform was added per 1 mL of TRIzol. Tubes were sealed and shaken vigorously by hand for 15 seconds, followed by incubation at RT for 2-3 minutes. Phase separation was achieved by centrifugation at 12,000 × g for 15 minutes at 4 °C. The mixture separated into three phases: a lower red phenol-chloroform phase, a middle interphase, and a clear upper aqueous phase containing RNA. The aqueous phase was carefully transferred to a new tube (~500 μL) without disturbing the interphase. To precipitate RNA, 0.5 mL of 100% isopropanol was added per 1 mL of initial TRIzol volume. Samples were incubated for 10 minutes at RT and centrifuged at 12,000 × g for 10 minutes at 4 °C. The RNA pellet, often invisible, formed at the bottom or side of the tube. The supernatant was gently removed, and the pellet was washed with 1 mL of 75% ethanol (prepared in RNase-free water). After gentle flicking to dislodge the pellet, tubes were centrifuged at 7,500 × g for 5 minutes at 4 °C. The wash was carefully discarded, and a brief spin at max speed (~12,000 × g for 30-60 seconds at RT) was used to collect any residual liquid, which was removed with a P20 pipette. The pellet was air-dried until translucent or white (not over-dried) and resuspended in 20 µL of RNase-free water. Tubes were flicked gently and incubated at 4 °C to aid resuspension. The RNA solution was gently mixed and briefly pipetted up and down to ensure homogeneity. RNA concentration and purity were assessed as described in 2.2.2.12. Samples were stored at -80 °C until further use.

#### 2.2.2.15 Complementary DNA (cDNA) synthesis

First-strand cDNA synthesis was performed using SuperScript IV Reverse Transcriptase according to the manufacturer's instructions. Total RNA (0.1-1  $\mu$ g) was used as the template in a 20  $\mu$ L reaction. RNA was combined with 1  $\mu$ L of 50  $\mu$ M random hexamer primers and 1  $\mu$ L of 10 mM dNTP mix. The total volume was adjusted to 13  $\mu$ L with nuclease-free water. The mixture was heated to 65 °C for 5 minutes, then placed on ice for 1 minute to allow primer annealing.

In a separate tube, the following were combined to a total of 7  $\mu$ L (Table 25):

Table 25. Reverse transcription reaction components.

Component	Volume
5× SSIV Reaction Buffer (pre-warmed to	4 μL
room temperature)	
100 mM DTT	1 μL
RNaseOUT Recombinant RNase Inhibitor	1 μL
_(40 U/μL)	·
SuperScript IV Reverse Transcriptase	1 μL
(200 U/µL)	·

The reverse transcription mix was gently mixed, briefly centrifuged and added to the annealed RNA-primer mixture (13  $\mu$ L) for a final volume of 20  $\mu$ L. The tubes were incubated in a thermocycler according to the protocol in Table 26.

Table 26. Reverse transcription reaction thermal cycling protocol.

Temperature	Time
23 °C	10 min
50 °C	10 min
80 °C	10 min

The resulting cDNA was used immediately for PCR or stored at -80 °C.

#### 2.2.2.16 Quantitative real-time PCR (qPCR)

Quantitative real-time PCR (qRT-PCR, qPCR) was performed using iTaq Universal SYBR Green Supermix on a CFX96 Touch Real-Time PCR Detection System. Reactions were carried out in a  $10 \,\mu\text{L}$  volume according to the manufacturer's protocol, using gene-specific primers at a final concentration of  $200 \,\text{nM}$  (Table 27).

Table 27. qPCR thermal cycling protocol.

Cycles	Temperature	Time
1	95 °C	30 s
40	95 °C	5 s
40	60 °C (plate read)	30 s

Melt curve analysis 65-95 °C with 0.5 °C increments at 5 s/step

Gene expression was normalized to the geometric mean of three housekeeping genes: YWHAZ, ACTB, and RNA18S. Relative expression levels were calculated using the  $2^{-\Delta Ct}$  method, where  $\Delta Ct = Ct_{target gene}$  -  $Ct_{reference genes}$ . All reactions were performed in technical duplicates or triplicates, and data was analyzed using Bio-Rad CFX Manager software and Excel.

#### 2.2.2.17 RNA-seq library preparation

Total RNA was quantified using the Qubit RNA HS Assay Kit and RNA integrity was assessed using the Agilent TapeStation 4200 with RNA ScreenTape. Only samples with RIN > 8 were selected for library preparation. RNA-seq libraries were prepared using the NEBNext rRNA Depletion Kit v2 (Human/Mouse/Rat) followed by the NEBNext Ultra II Directional RNA Library Prep Kit for Illumina, according to the manufacturer's instructions. 100-500 ng of total RNA was subjected to rRNA depletion via probe-based hybridization, RNase H digestion, and DNase I treatment. The depleted RNA was purified using NEBNext Sample Purification Beads and fragmented at 94 °C for 15 minutes. First-strand cDNA synthesis was performed using random priming. Strand specificity was introduced during second-strand synthesis using dUTP. After end-repair and A-tailing, NEBNext Dual Index UMI Adaptors were ligated. USER enzyme treatment was then applied to selectively degrade the dUTP-containing strand, preserving strand specificity. Libraries were PCR-amplified (8 cycles) using Ultra II Q5 Master Mix and purified using SPRIselect beads. Final libraries were eluted in 0.1× TE buffer. Library size distribution and quality were verified using the TapeStation D1000 ScreenTape, and concentrations were measured with KAPA Library Quantification Kit Complete Kit according to manufacturer's manual. Libraries with an average size of ~300 bp and no adaptor dimers were used for sequencing on Illumina NextSeq 500 at the Laboratory of Next-Generation Sequencing, Institute of Hematology and Transfusion, Warsaw, Poland by Magdalena Skrzypczak and Sylwia Radomska.

#### 2.2.3 Protein biochemical methods

#### 2.2.3.1 Quantification of protein using colorimetric methods

Protein concentrations were determined using the Pierce BCA Protein Assay Kit following the manufacturer's microplate protocol. Samples and standards were prepared in a 96-well flat-bottom clear plate. A BSA standard curve was included in each run, ranging from 125 μg/mL to 2000 μg/mL. Working reagent (WR) was freshly prepared by mixing Reagent A and Reagent B at a 50:1 ratio. 200 μL of WR was added to 2 μL of each sample or standard. Plates were incubated at 37 °C for 30 minutes, protected from light. Absorbance was measured at 562 nm using a microplate reader. Sample concentrations were interpolated from the standard curve using linear regression in Excel. All samples were measured in triplicates.

### 2.2.3.2 SDS-Polyacrylamide Gel Electrophoresis (SDS-PAGE) and western blotting

Sodium dodecyl sulfate-polyacrylamide gel electrophoresis (SDS-PAGE) was performed to separate proteins under denaturing conditions. Polyacrylamide gels were cast in-house, consisting of a resolving gel (8-12%, depending on protein size) and a 4% stacking gel, using standard acrylamide:bis-acrylamide mixtures and Tris-HCl buffer systems with SDS. In some cases, commercially prepared SDS-PAGE gels (stored at 4 °C) were used. Samples were denatured by boiling at 95 °C for 5 minutes in Laemmli buffer, followed by cooling on ice for 2 minutes and centrifugation at maximum speed for 1 minute. Samples were vortexed before gel loading. Equal amounts of protein lysates (10-40  $\mu$ g protein/lane) were loaded into gel wells along with molecular weight standards (typically 3  $\mu$ L). Electrophoresis was carried out in 1× SDS Running Buffer. Gels were initially run at 80 V to allow proteins to migrate through the stacking gel, followed by 120 V for separation in the resolving gel. Electrophoresis continued until the dye front reached the bottom of the gel (~60-90 min). In some cases, Bis-Tris precast gels were used and run with 1× MOPS running buffer according to the manufacturer's instructions, typically at 150 V of constant voltage.

Following electrophoresis, proteins were transferred to a PVDF membrane using a wet transfer system. The membrane was pre-wetted in methanol for at least 1 min. Transfer was performed in 1× Transfer Buffer (prepared from 10× stock with methanol and ddH<sub>2</sub>O in a 1:2:7 ratio) for 1

hour at 400 mA constant current ( $\sim$ 140-160 V) at 4  $^{\circ}$ C or in a cooled Styrofoam container with ice.

Membranes were stained with Ponceau S for 5 minutes and washed with ddH<sub>2</sub>O to verify protein transfer, imaged, and then destained with TBST. Membranes were blocked for 1 h at RT on a shaker in 5% non-fat dry milk or 5% BSA in TBST (1×) to reduce nonspecific binding. BSA was used when probing for phosphorylated proteins or to reduce background in sensitive applications. In some cases the blocking has been performed overnight at 4 °C to further reduce unspecific binding. For especially sensitive applications, the 5% BSA blocking solution was passed through a 0.22 µm filter to remove particulates and prevent background signal. Blocked membranes were incubated overnight at 4 °C with primary antibodies diluted in 5% BSA or, in case of PIM1/2/3 antibodies, in TBST. Following incubation, membranes were washed 3 times for 15 minutes with 20 mL TBST. Secondary antibodies conjugated to horseradish peroxidase (HRP) were diluted in TBST and incubated with the membranes for 1 h at RT with gentle agitation. This was followed by 3 washes of 15 minutes each in 20 mL TBST.

Signal detection was performed using enhanced chemiluminescence (ECL) reagents, and membranes were exposed to X-ray film or imaged with G:BOX digital detection system. All blots were quantified using densitometric analysis in ImageJ when applicable. Primary antibody solutions were saved for later reuse at -20 °C.

To enable sequential immunoblotting of different proteins on the same membrane, Medium Stripping Buffer was applied to remove primary and secondary antibodies after initial detection. Membranes were incubated in the stripping buffer  $2 \times 7$  minutes, followed by  $2 \times 10$  minutes in PBS, then washed in TBST  $2 \times 5$  minutes. Methanol-based rehydration was not used. After stripping, the membrane was blocked for 1 h as described above.

After the final stripping or detection step, membranes were air-dried at RT and stored for archival purposes.

#### 2.2.3.3 Immunohistochemistry

Immunohistochemical staining was performed on a tissue microarray (TMA) constructed from formalin-fixed paraffin-embedded (FFPE) bone marrow trephine biopsies from patients with

MM or healthy donors. The samples were anonymized and retrieved from the Department of Pathology, Brigham and Women's Hospital, Boston, Massachusetts, USA. Due to the observed loss of PIM2 antigenicity from decalcification, staining for PIM2 was performed using a TMA composed of bone marrow clot sections, which had not been subjected to decalcification. Sections were cut at 4 µm thickness, mounted onto charged glass slides, and dried. After deparaffinization and rehydration, slides underwent heat-induced epitope retrieval (HIER) using either citrate buffer (pH 6.0) or Tris-EDTA buffer (pH 9.0), depending on the target antigen. Endogenous peroxidase activity was blocked with 3% hydrogen peroxide, and nonspecific binding was minimized using appropriate blocking buffer. The following primary antibodies were used: PIM1 (Novus ST0513, NBP2-67528; 1:100; HIER pH 9.0), PIM2 (Novus OTI5D5, NBP2-02441; 1:100; HIER pH 6.0), PIM3 (Cell Signaling D17C9; 1:50 with antibody linker; HIER pH 9.0), CD34 (M71165, DAKO, 1:400).

Control tissues were selected based on known antigen expression: testis for PIM1, lymph node for PIM2, and kidney for PIM3. Slides were incubated with primary antibodies for 1 hour at room temperature, followed by detection using an HRP-conjugated secondary antibody. Visualization was performed using a DAB chromogen substrate. Slides were lightly counterstained with hematoxylin, dehydrated, and mounted. To localize PIM1 and PIM3 expression in vascular structures, double IHC staining was performed using CD34 as an endothelial marker. After initial antigen retrieval, slides were incubated sequentially with: Anti-PIM1 or anti-PIM3 as the first primary antibody, HRP-conjugated secondary antibody and developed with DAB chromogen (brown). After appropriate blocking and washing, slides were incubated with anti-CD34 antibody detected with an alkaline phosphatase-conjugated secondary antibody and visualized using red chromogen. Slides were counterstained lightly with hematoxylin, dehydrated, and mounted.

In all cases staining was evaluated using a Leica DM2000 microscope. Microphotographs were taken on the same day, using the same light intensity, magnification, brightness and exposure settings. Co-expression of PIM1 or PIM3 with CD34<sup>+</sup> endothelial structures was confirmed by overlay of brown and red signals. All slides were assessed together with a board-certified pathologist (Dr. Ruben Carrasco).

#### 2.2.4 Murine studies

To evaluate the in vivo efficacy of MEN1703, we used a luciferase-tagged disseminated MM model in immunodeficient mice. 6-8 weeks old female NSG mice (NOD.Cg-Prkdcscid Il2rgtmlWjl/SzJ, Jackson Lab, Bar Harbor, ME, USA) were injected intravenously via tail vein with 1×106 MM1.S-luciferase (MM1.S-luc) cells suspended in sterile PBS using 28G syringes. Tumor progression was monitored by bioluminescence imaging (BLI) using the IVIS Spectrum Imaging System (PerkinElmer) following intraperitoneal injection of D-luciferin (150 mg/kg). On day 7 post-injection, upon confirmation of establishment of MM in the skeletal system, mice were randomized into treatment groups to ensure comparable tumor burden based on total BLI signal. Mice received either MEN1703 (50 mg/kg) or vehicle (water) administered per os (PO), once daily (QD) by oral gavage. MEN1703 was supplied as dry powder by Menarini Ricerche SpA and stored at +4 °C. Dosing volume was standardized at 10 µL per gram of mouse body weight (e.g., 200 µL for a 20 g mouse). To prepare the dosing solution, sterile water was added to the powder 15-30 minutes before administration. Tubes were then incubated in a 42 °C water bath for 15 minutes with intermittent vigorous vortexing to enhance drug solubility. Tumor burden was monitored weekly by BLI throughout the study. Bioluminescence signal was quantified using Living Image Software (PerkinElmer) and expressed as total flux (photons/second). Statistical comparisons between treatment groups at individual time points were made using the Mann-Whitney U test. Mice were monitored daily for signs of distress or treatment-related toxicity. All mouse procedures were approved by the appropriate institutional animal care and use committee (IACUC) and were conducted in accordance with institutional and national guidelines.

### 2.2.5 Computation and data analysis

#### 2.2.5.1 Statistical analysis

Statistical analysis was performed using GraphPad Prism (versions 9.0-10.0), R (v4.2.3) with dedicated packages, and MedCalc Statistical Software (v23.2.1) for selected multivariate analyses. For all *in vitro* and *in vivo* experiments, results are presented as mean  $\pm$  standard deviation (SD) or standard error of the mean (SEM) as indicated. Group comparisons were evaluated using unpaired two-tailed Student's t-test or one-way ANOVA with appropriate post

hoc correction (Tukey's or Dunnett's test), depending on the experimental design. For non-normally distributed data, non-parametric tests (Mann-Whitney or Kruskal-Wallis) were used. Survival curves were plotted using Kaplan-Meier estimates and compared by log-rank test. All statistical tests were two-sided. A p-value < 0.05 was considered statistically significant unless noted otherwise. The following notation was used to denote significance:  $p < 0.05 = *; p < 0.01 = **; p < 0.001 = ***; p < 0.0001 = ***; p-values <math>\ge 0.05$  were considered not statistically significant (ns).

#### 2.2.5.2 RNAseq data analysis

Demultiplexing of raw Illumina sequencing output was performed using bcl2fastq with default settings to generate per-sample FASTQ files, which were stored on the IHIT-NGS computational cluster. Primary data processing was performed using the nf-core/rnaseq pipeline (v1.4.2) implemented through Nextflow, with a workflow configuration stored in the IHIT-ZHE GitHub repository https://github.com/zhe-lab-ihit/. Quality control, adapter trimming, and alignment were carried out according to nf-core default settings. Read alignment was performed using the STAR aligner, mapping reads to the GRCh38 (hg38) human genome assembly for RNA-seq data. Gene quantification was based on Gencode annotations corresponding to the genome build used. These initial steps have been performed by experienced bioinformaticians, Drs. Michał Pawlak and Marcin Kaszkowiak. Differential gene expression analysis was performed using DESeq2. Raw read counts were imported into RStudio, filtered, normalized, and analyzed using the default DESeq2 workflow. Each cell line was processed and analyzed separately. Genes with adjusted p-value < 0.05 and  $|log_2FC| \ge 1$  were considered significant. Gene Set Enrichment Analysis (GSEA) was performed using ClusterProfiler. Ranked gene lists (based on Wald statistic) were used to identify enriched biological pathways or signatures. Additional exploratory and visualization analyses (e.g. PCA, volcano plots, heatmaps) were performed in R.

#### 2.2.5.3 ChIPseq data analysis

ChIP-seq data were downloaded from the NCBI SRA repository (https://www.ncbi.nlm.nih.gov/Traces/study/?acc=PRJNA608768) and processed in a custom pipeline implemented in a Linux environment using the Ubuntu Subsystem for Windows. All

steps were performed in Conda-managed environments to ensure reproducibility. FASTQ files were first assessed for quality using FastQC. Reads were aligned to the GRCh38 human genome reference using Bowtie2. The reference genome was indexed prior to alignment. After alignment, SAM files were converted to BAM, and BAM files were sorted and filtered to remove unmapped, duplicate, or multi-mapped reads using SAMtools and Sambamba. For peak calling, filtered BAM files were analyzed with MACS2, using the corresponding input control samples and the effective genome size for GRCh38. Peaks were called with default parameters optimized for broad H3K27Ac signal detection. Post-alignment quality control was conducted in R, and all BAM files were indexed for downstream visualization. To generate genome browser tracks, bigWig files were created from filtered BAM files using deepTools (bamCoverage), applying normalization to BPM (bins per million mapped reads) and enabling read centering and extension. Input normalization was intentionally omitted from bigWig generation to avoid potential bias, based on current best practices in the field. The input samples were used strictly for peak calling.

#### 2.2.5.4 scRNAseq data analysis

Publicly available single-cell RNA-seq datasets were retrieved from the study by de Jong et al. [220], comprising bone marrow samples from both multiple myeloma (MM) patients and healthy donors (HDs). The datasets included sorted subpopulations: CD45<sup>-</sup> cells, CD45<sup>+</sup>CD38<sup>+</sup> (nonplasma cells), CD45+CD38- cells, and CD45+CD38+ malignant plasma cells. Data were provided as pre-processed Seurat objects and integrated using Seurat version 5.1.0. Low-quality cells were excluded based on filtering parameters reported in the source publication. Remaining cells were normalized using Seurat's NormalizeData() function with default settings. Dimensionality reduction was performed using Uniform Manifold Approximation and Projection (UMAP) via the RunUMAP() function. Clustering was performed based on canonical markers and existing cell-type annotations from the original dataset. Endothelial cells (ECs) were defined by expression of CDH5, PECAM1, and FLT1, and absence of the pan-hematopoietic marker PTPRC (CD45). ECs from MM and HD samples were subsetted and analyzed separately. To compare gene expression between MM-derived and HD-derived ECs, we used a pseudobulk strategy, aggregating transcript counts per donor using Seurat's AggregateExpression() function, grouped by sample origin and disease state. Differential gene expression analysis was performed with DESeq2, applying Benjamini-Hochberg correction for multiple testing. Differential expression was computed using the FindMarkers() function with pseudobulked input. Genes with adjusted p-value < 0.05 and  $|log_2FC| \ge 1$  were considered significant. GSEA was conducted using the fgsea and clusterProfiler R packages. Reference gene sets were obtained from the Molecular Signatures Database (MSigDB). Gene ranking was based on DESeq2 Wald statistics, and enrichment scores were computed using 10,000 permutations. Only gene sets with at least 10 genes were retained for analysis.

# 3 Functions of PIM kinases in multiple myeloma cells

### 3.1 PIM kinase overexpression is essential for MM growth

# 3.1.1 CRISPR/Cas9 cancer dependency screens identify PIM kinases as critical oncogenes in multiple myeloma

To investigate the role of PIM kinases in multiple myeloma (MM), we initially analyzed two independent, publicly available datasets generated from CRISPR/Cas9 drop-out screens using a panel of MM cell lines (Cancer Dependency Map (DepMap) [361] and Yang et al. [125]. PIM2 kinase ranked at the top of oncogenic dependencies in MM cells in both datasets, thus confirming the critical role of PIM kinases in MM pathogenesis (Fig. 8A). Notably, no such dependency was detected for PIM1 or PIM3. The reliance of malignant plasma cells on PIM2 was either similar to or exceeded that of established MM oncogenes (e.g., MYC, IRF4, MAF, IKZF1, IKZF3) and previously recognized drug targets (e.g., PSMB5, BCL2, BRD4). Additionally, a comprehensive analysis of DepMap cancer cell lines showed that MM cell lines uniquely overexpress PIM2 compared to all other cell lines, even those from other hematologic malignancies like lymphoma and leukemia (Fig. 8B). Intriguingly, PIM2 expression did not correlate with PIM2 dependency in MM cell lines (Fig. 8B-C), suggesting the need to identify alternative biomarkers for more effective patient selection during clinical trials of PIM inhibitors. PIM2 dependency was particularly evident in MM cell lines and a subset of B-cell lymphoma lines, suggesting that these neoplasms are likely the most responsive to PIM depletion or pharmacological inhibition.

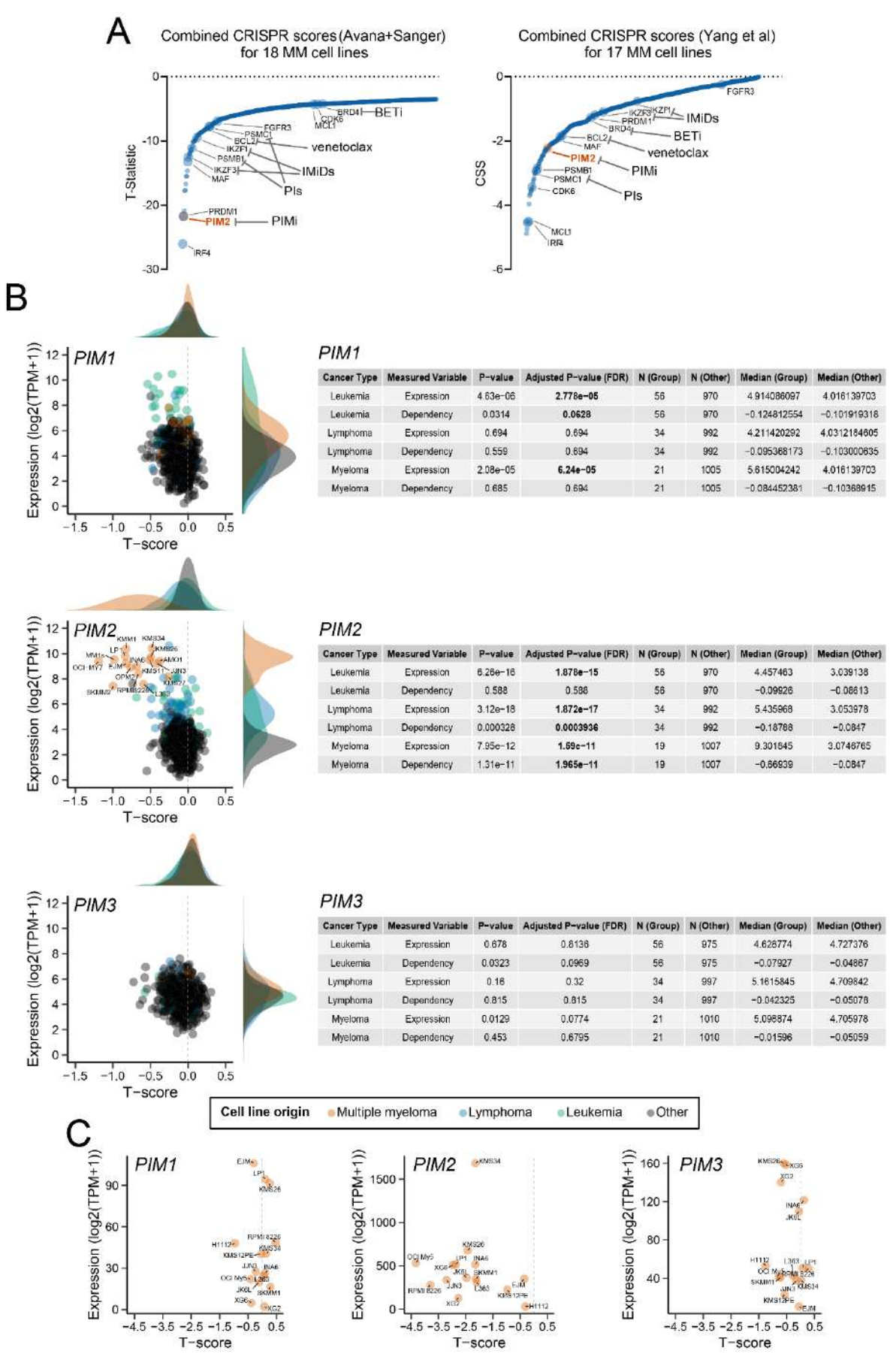


### Fig. 8. Genome-wide CRISPR/Cas9 dropout screens identify genes preferentially essential for multiple myeloma cells compared to other types of cancer.

A - Combined CRISPR scores (Avana+Sanger) for plasma cell-specific dependencies across 18 MM cell lines from DepMap and Yang et al. [125]. PIM1/2/3 dependency scores and expression levels in all cell lines included in the (B) DepMap database and (C) Yang et al. [125] datasets. P-values were calculated using the Wilcoxon rank-sum test to compare each cancer type (leukemia, lymphoma, myeloma) against all other samples. Adjusted P-values were computed using the Benjamini-Hochberg method.

#### 3.1.2 PIM1/2/3 levels in healthy human and murine tissues

While the CRISPR/Cas9 screen results offer promising leads, it's important to note that such hits frequently result in clinical trial failures due to off-tumor, on-target drug effects. To address this, we examined PIM kinase expression in healthy murine tissues [362] as well as in human tissues [363]. Notably, in murine lymphoid cells, PIM1 and PIM2 were predominantly expressed in plasmablasts and plasma cells (Fig. 9). PIM3, on the other hand, showed more uniform expression, with elevated expression levels primarily at the B-cell progenitor stage.

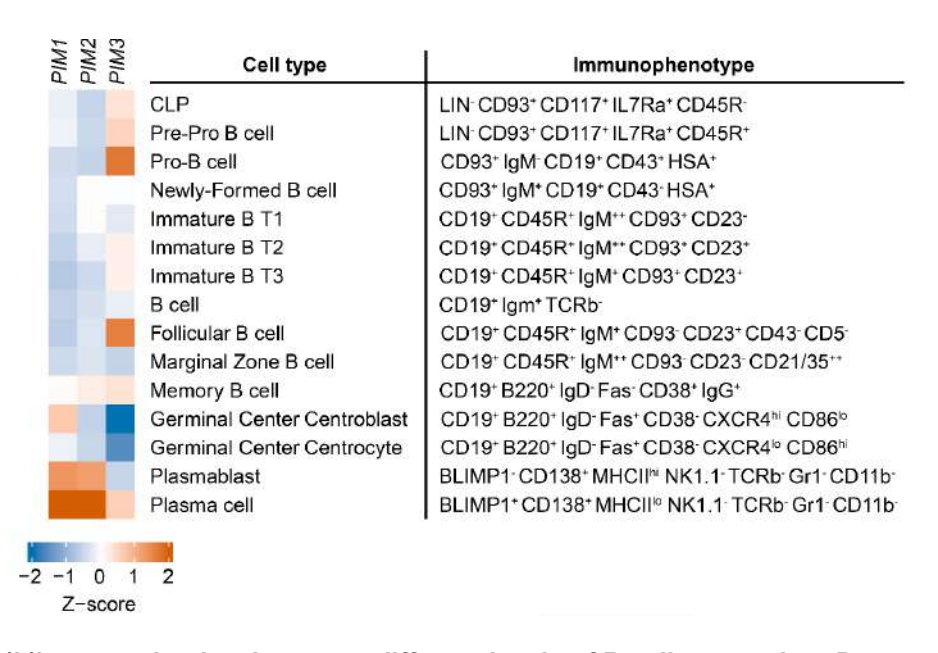
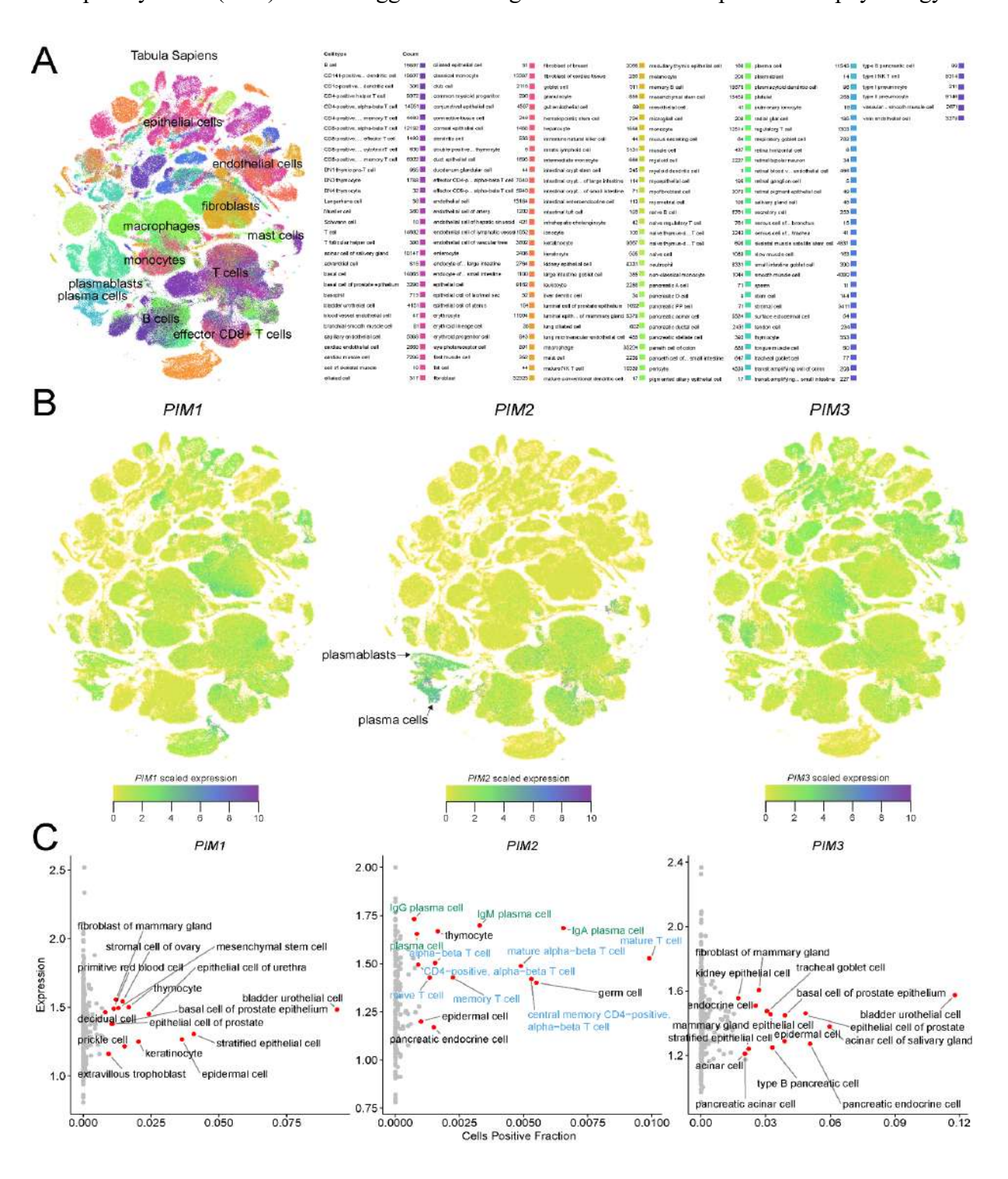


Fig. 9. PIM1/2/3 expression levels across different levels of B cell maturation. Data source: [362].

In the Tabula Sapiens dataset, a single-cell transcriptomic atlas spanning multiple human organs [364], *PIM2* showed significant enrichment in plasma cells compared to other cell types (Fig. 10A-C). This suggests likely functional relevance in both normal and malignant plasma cells. Notably, *PIM2* was also abundant in various T cell subsets, such as CD4+ and memory T cells, indicating possible immunomodulatory consequences of *PIM2* inhibition in T cells. In contrast, *PIM1* and *PIM3* were predominantly expressed in epithelial and mesenchymal cells, albeit with notable distinctions. *PIM1* was broadly present in various fibroblast subtypes, while *PIM3* was

particularly enriched in endothelial cells compared to *PIM1*. These patterns suggest potential functions of PIMs in the tumor microenvironment, The preferential expression of PIM2 in plasma cells relative to other healthy tissues identifies it as a promising therapeutic target for multiple myeloma (MM). It also suggests an integral role for PIM2 in plasma cell physiology.



**Fig. 10.** The distribution of PIM kinase mRNA expression in healthy human tissues. Data sourced from scRNAseq studies within the Tabula Sapiens project [364]. (A) UMAP visualization of single-cell clusters from the Tabula Sapiens dataset used in this study. (B) UMAP dimensional reduction plot (dimplot) representing the expression levels of PIM1, PIM2, and PIM3 across various human cell types. (C) Analysis of both expression levels and the fraction of cells expressing PIM1, PIM2, and PIM3 in healthy human tisues. The color-coded labeling highlights plasma cells (green) and T cells (blue) as the primary cell types with significant PIM2 expression. Red-colored points identify the top 15 cell types for each gene based on weighted gene expression.

#### 3.1.3 PIM mRNA expression levels in MM and normal plasma cells

To evaluate the expression of PIM kinases in multiple myeloma (MM), we first analyzed transcriptomic datasets from primary patient samples and MM cell lines. In a large MM patient cohort (n = 881)[12], *PIM2* showed the highest median expression among the three paralogs, followed by *PIM1* and (Fig. 11, top left). Similar trends were observed in MM cell lines (n = 66), with *PIM2* consistently exhibiting higher transcript levels (Fig. 11, top right, \*\*\*\*p < 0.0001).

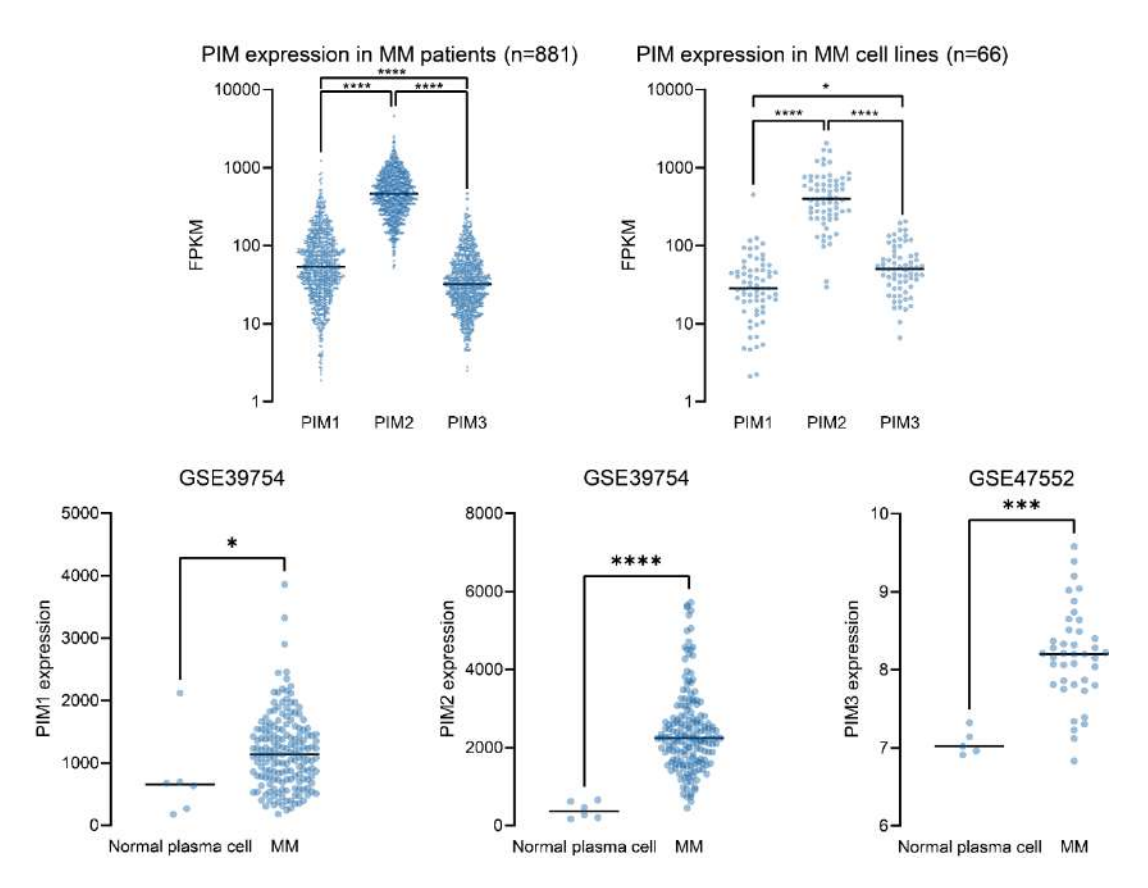


**Fig. 11. PIM kinase expression in multiple myeloma patients, cell lines, and normal plasma cells.** (Top) Expression of PIM1, PIM2, and PIM3 in MM patients (n = 881, left) and MM cell lines (n = 66, right). Data derived from MMRF CoMMpass study and Keats Lab MM Cell Line Characterization Project. (Bottom) Comparison of PIM expression in MM versus normal plasma cells. Statistical significance was determined using two-sided Student's t-test.

To determine whether these expression patterns were specific to malignant plasma cells, we compared MM samples with normal plasma cells using publicly available datasets (Fig. 10, bottom). In GSE39754, both *PIM1* and *PIM2* expression were significantly increased in MM compared to normal counterparts (\*p < 0.05 and \*\*\*\*p < 0.0001, respectively). Additionally, *PIM3* expression was significantly higher in MM in the GSE47552 dataset (\*\*\*p < 0.001), while other PIMs did not display such a trend in this dataset (data not shown).

These data suggest that all three PIM kinases are transcriptionally upregulated in MM, with *PIM2* showing the highest expression, supporting its potential as a therapeutic target.

### 3.1.4 Multiomic datasets link PIM expression to specific MM-related features

To further confirm PIM kinase expression in MM and evaluate the putative association of PIM expression with clinical features of the disease, we first examined a publicly available scRNAseq dataset including cells from patients at various stages of MM: IgM MGUS, MGUS, SMM, NDMM, and RRMM (Fig. 12). *PIM1* showed elevated expression predominantly in IgM MGUS cases (Fig. 12A, D), which commonly precede the onset of non-Hodgkin lymphomas such as Waldenström macroglobulinemia. *PIM2* expression remained relatively stable across all MM stages, and 100% of sequenced cells expressed *PIM2* mRNA (Fig. 12B, D). Notably, *PIM3* expression was significantly higher in RRMM cells compared to NDMM cells (Fig.12C, D), hinting at a possible role of PIM3 in late-stage disease or chemotherapy resistance.

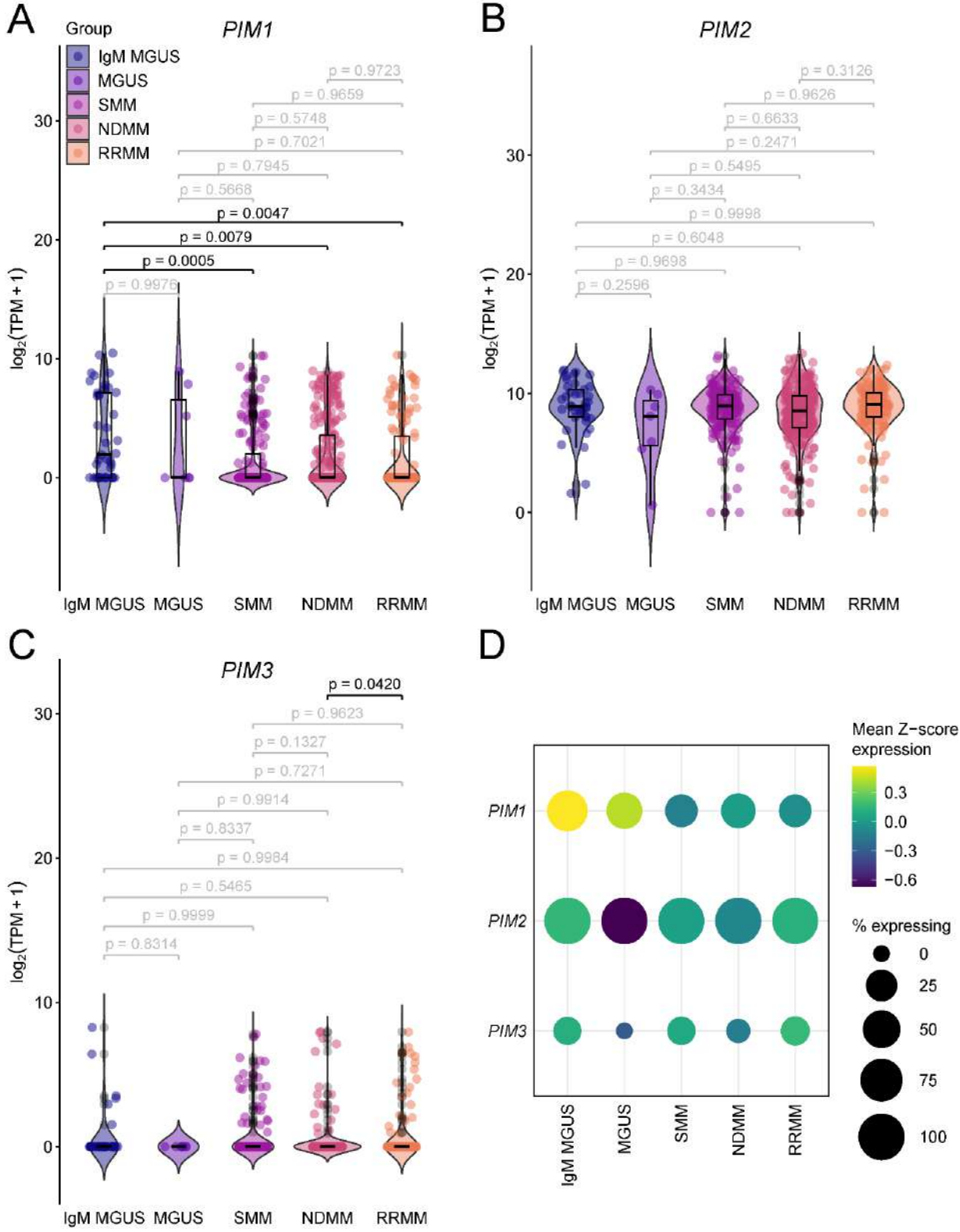


**Fig. 12. PIM expression across MM progression stages.** A, B, C - Expression levels of PIM1, PIM2, and PIM3, respectively, at distinct MM stages, sourced from scRNAseq data [365]. Significance assessed using ANOVA with Tukey's post-hoc test; p-values in black denote significance (p < 0.05). D - Bubble plot illustrating PIM1/2/3 expression levels and the percentage of cells expressing respective PIM kinase transcripts across various stages of plasma cell neoplasia.

Because scRNAseq can underestimate low-abundance transcripts, we next analyzed a bulk RNA-seq dataset from Silva et al.[366], which includes samples across MM stages. Differential expression analysis confirmed that *PIM1* is upregulated in MGUS compared to SMM, consistent with early-stage expression. In contrast, *PIM2* was significantly upregulated in RRMM compared to NDMM, suggesting a possible role in relapsed disease. *PIM3* showed only modest increases in RRMM compared to NDMM (Fig. 13). No changes in PIM1/2/3 expression were detected when comparing early versus late relapsed MM. These findings support stage-specific regulation of PIM kinases, with *PIM1* induced early and *PIM2* enriched in late-stage, treatment-exposed myeloma.

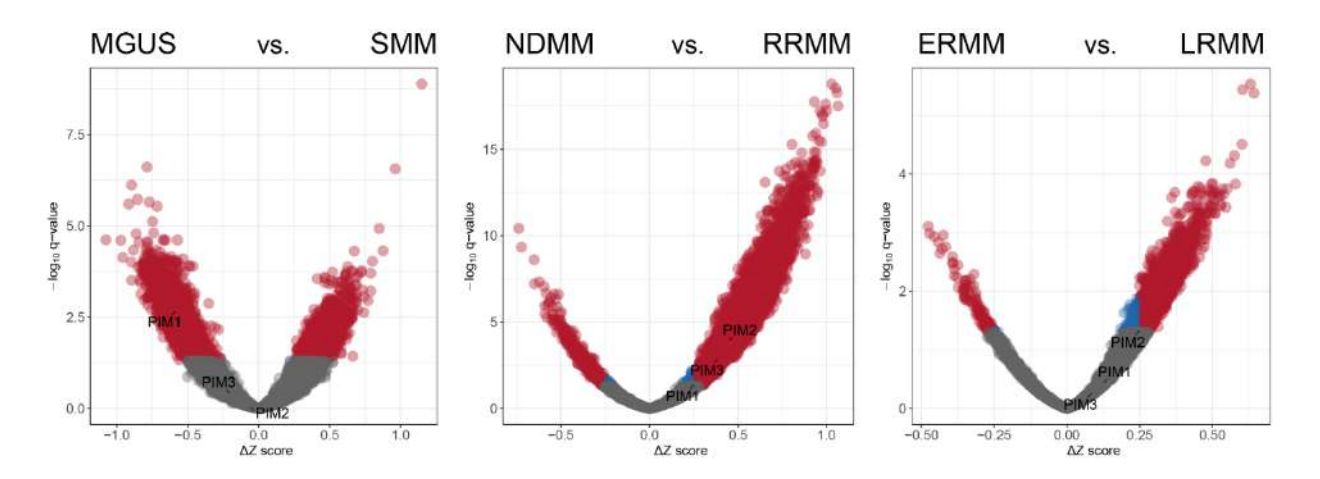
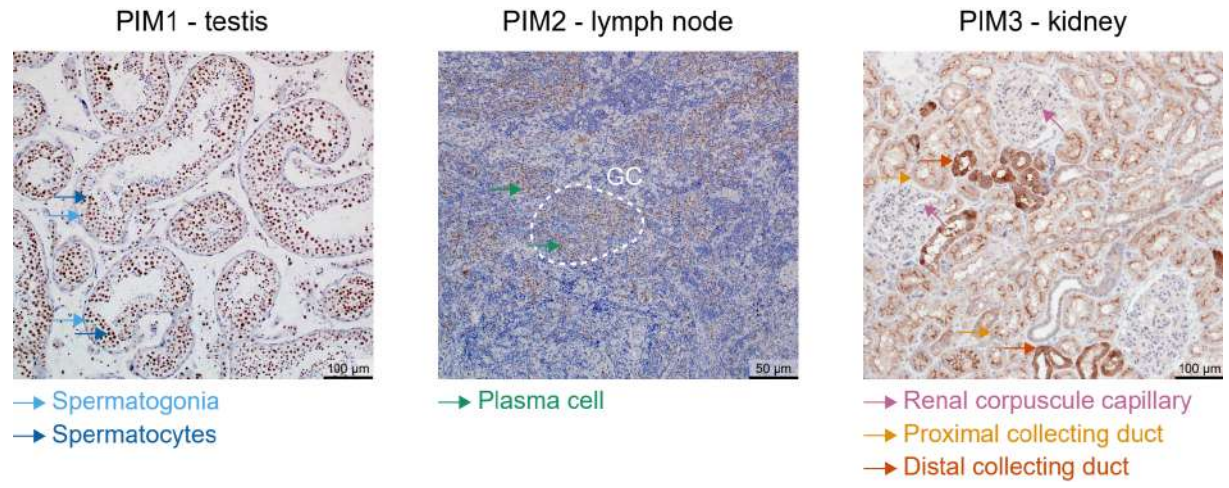


Fig. 13. Bulk RNA-seq analysis of PIM kinase gene expression during MM progression. Data source: Silva et al. [366]. Genes significantly upregulated ( $|\Delta Z| > 0.25$ , padj < 0.05) are red; non-significant are blue ( $|\Delta Z| \le 0.25$ , padj < 0.05) or grey. PIM1, PIM2, and PIM3 are highlighted. ERMM - early relapse MM, LRMM - late relapse MM.

## 3.1.5 IHC staining and quantification of PIM1, PIM2 and PIM3 protein levels in MM and healthy bone marrow

Given the strong dependency of MM cells on PIM2, we decided to pursue PIM kinases as therapeutic targets in this disease. Recognizing that mRNA levels do not always correlate with protein levels [367,368], we evaluated PIM kinase protein expression using immunohistochemical staining. We used a panel of rigorously validated antibodies (Fig. 14) compatible with decalcified bone marrow (PIM1, PIM3) or bone marrow clot sections (PIM2). These assays were conducted on tissue microarrays (TMAs) combining trephine bone marrow samples from MM patients as well as bone marrow from healthy donors (Fig. 15).



**Fig. 14. IHC optimization.** PIM1 (Novus ST0513 NBP2-67528; antigen retrieval pH 9.0; dilution 1:100) stains spermatogonia and spermatocytes. PIM2 (Novus OTI5D5 NBP2-02441; antigen retrieval pH 6.0; dilution 1:100) is prominent in germinal center B cells and lymph node plasma cells. PIM3 (Cell Signaling D17C9; antigen retrieval pH 9.0; dilution 1:50 plus Linker) stains kidney epithelium, predominantly the distal collecting ducts.

Quantification of DAB staining intensity demonstrated a statistically significant increase in PIM1, PIM2, and PIM3 expression in malignant plasma cells (MM PC) compared to normal plasma cells (Normal PC), with p-values of 0.0396, 0.0098, and 0.0012, respectively. The majority of MM samples were positive for PIM1 (17/18, 94.4%), PIM2 (21/23, 91.3%), and PIM3 (18/18, 100%), as assessed by a pathologist. PIM1 displayed predominantly nuclear staining in MM cells, often with a speckled appearance. PIM2 was restricted to the cytoplasm and strongly expressed in MM cells but not in normal plasma cells. PIM3 showed diffuse cytoplasmic staining in most MM cases, with frequent moderate nuclear localization.

Together, these findings confirm that all three PIM kinases are overexpressed at the protein level in MM compared to normal plasma cells, and that they display distinct subcellular localization patterns suggestive of different functions of each PIM family member.

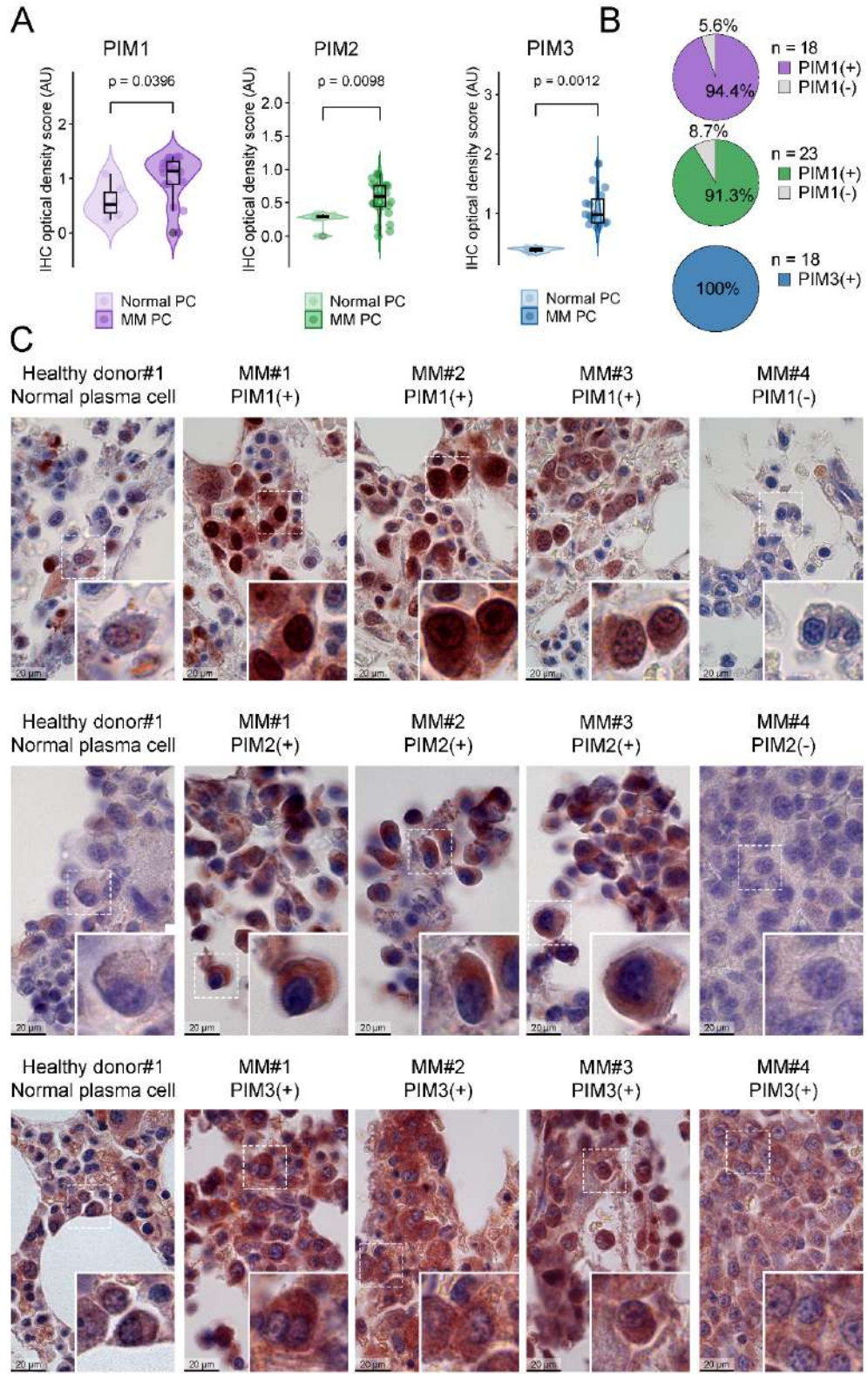


**Fig. 15.** Immunohistochemical analysis of PIM1/2/3 in healthy vs. newly diagnosed MM bone marrow. \*A) IHC optical density scores determined via IHC Profiler, quantified within regions of interest (ROIs) containing cells displaying plasma cell morphology for each case. (B) Distribution of PIM1/2/3-positive and -negative cases within the studied cohorts. (C) Selected microphotographs illustrating differences in PIM expression between healthy bone marrow (far left) and bone marrow samples from MM patients.

#### 3.1.6 PIM kinase expression is linked to MM patient survival

To assess the clinical impact of PIM kinase expression in multiple myeloma, we analyzed RNA-seq data from the MMRF CoMMpass study [12]. We used Cutoff Finder [369] to stratify patients into high and low expression groups for each PIM. Survival outcomes were evaluated using overall survival (OS) and progression-free survival (PFS) as endpoints (Fig. 16)

Cutoffs for each PIM gene were selected based on the method that maximized the significance of survival separation. For *PIM1*, a log-rank test was used to identify the most prognostically relevant threshold. This test was appropriate because the survival hazard associated with PIM1 expression showed a smooth gradient, allowing for estimation of a split point based on time-to-event data. In contrast, for *PIM2* and *PIM3*, we observed more bimodal distributions of expression and sharper separations in group sizes. Therefore, we applied Fisher's exact test to identify optimal cutoffs based on dichotomous association with survival status at specific time points.

Kaplan-Meier curves for OS and PFS illustrate that high expression of any PIM gene is associated with worse outcomes.

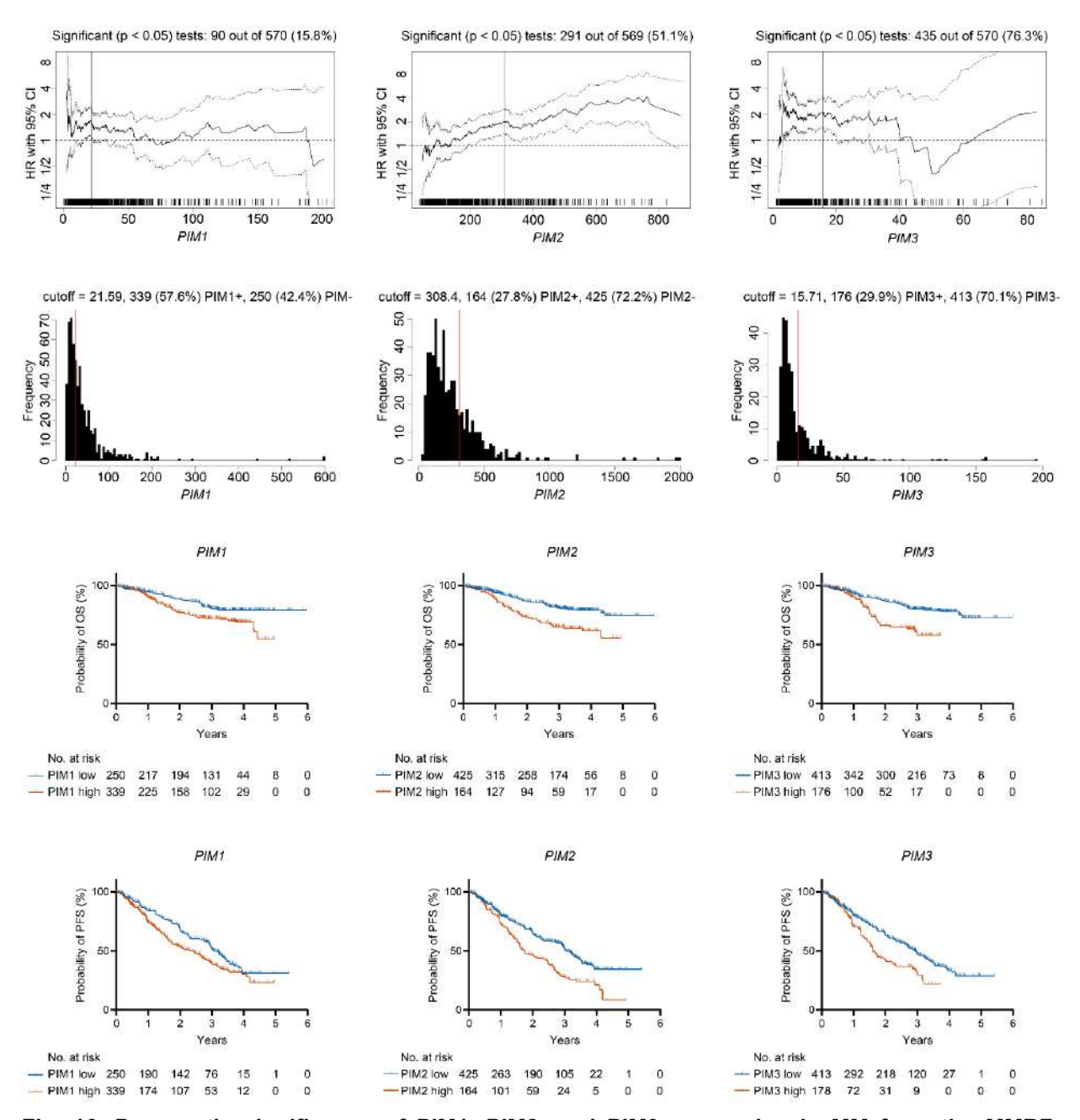
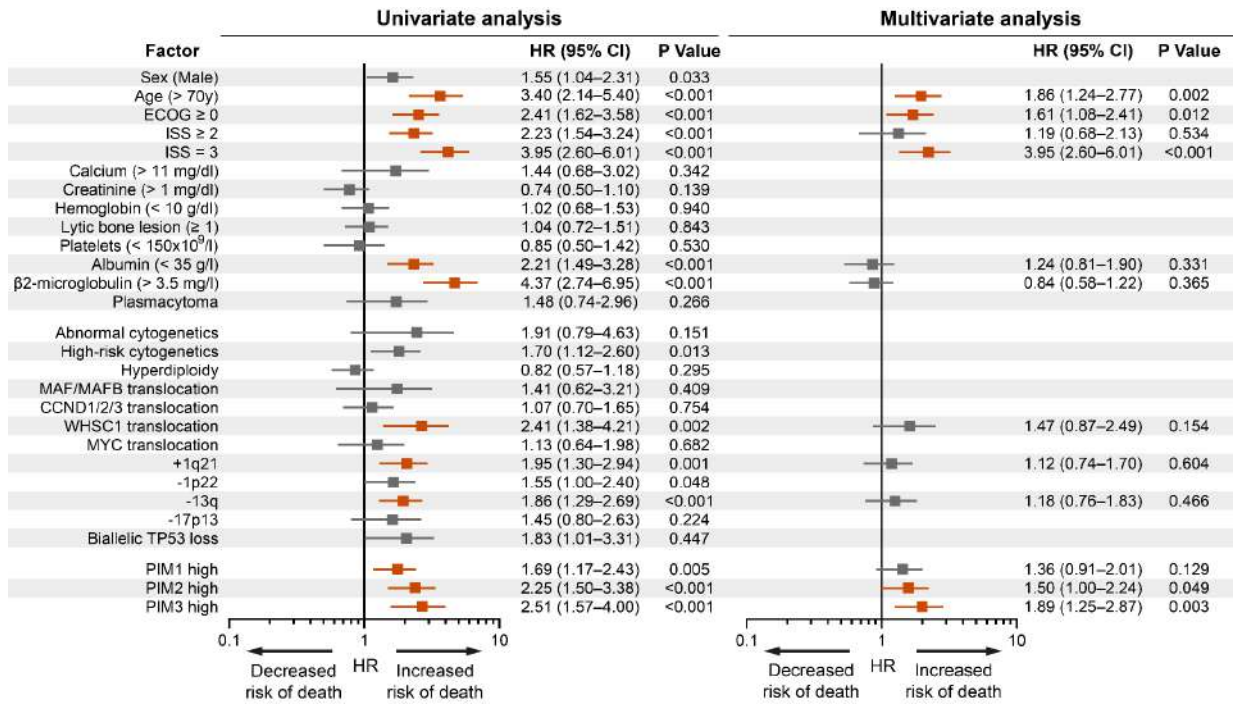


Fig. 16. Prognostic significance of PIM1, PIM2, and PIM3 expression in MM from the MMRF CoMMpass cohort. (Top row) Hazard ratio plots with 95% confidence intervals show the association between gene expression levels and OS, as determined by Cutoff Finder. (Middle row) Histograms of gene expression values and the corresponding cutoff points (red lines). (Bottom two rows) Kaplan-Meier survival curves for OS and PFS, comparing patients with high vs. low expression of each PIM gene. Number at risk is shown below each plot.

To further evaluate the prognostic relevance of PIM kinase expression, we performed univariate and multivariate Cox regression analyses using clinical and molecular data from the MMRF CoMMpass dataset (Fig. 17). This included OS and PFS data, as well as baseline variables such as age, sex, ECOG status, ISS stage, laboratory parameters, cytogenetic features, and key genetic

lesions. In univariate analysis, high expression of *PIM1*, *PIM2*, or *PIM3* was associated with significantly increased risk of death. In multivariate analysis adjusting for established risk factors, high *PIM2* or *PIM3* expression remained independent predictors of poor OS, with hazard ratios of 1.50 and 1.89, respectively. These results support the independent prognostic value of PIM kinase expression in MM.



**Fig. 17. Univariate and multivariate Cox regression analysis of overall survival in the MMRF CoMMpass cohort.** Hazard ratios (HR) and 95% confidence intervals (CI) are shown for clinical, cytogenetic, and molecular variables. In univariate analysis (left panel), high expression of *PIM1*, *PIM2*, and *PIM3* was significantly associated with increased risk of death. For the multivariate model (right panel), only variables with univariate P < 0.01 were included. High expression of *PIM2* and *PIM3* remained independently associated with shorter overall survival. Variables with statistically significant hazard ratios are shown in orange.

# 3.2 Super-enhancer-mediated control of PIM expression in malignant plasma cells

Given the strong link between high *PIM1/2/3* expression and poor prognosis in MM, we next investigated the mechanisms underlying this elevated expression. Transcriptional regulation by enhancers, and particularly super-enhancers, is a well-known driver of high and lineage-restricted gene expression in cancer and in normal hematopoietic cells [370]. Super-enhancers are large genomic regions marked by dense clusters of active enhancer elements, characterized by high levels of H3K27 acetylation (H3K27ac).

To explore whether super-enhancer activity might explain high PIM2 expression in MM, we reanalyzed H3K27ac ChIP-seq data from Jia et al [371]. This dataset includes B-cell lymphoma cell lines (Raji, Daudi), primary MM patient samples (CD138+ plasma cells), healthy donor BM CD138+ plasma cells, and established MM cell lines. H3K27ac is a robust marker of active enhancers and super-enhancers, making it ideal for identifying regulatory elements linked to gene activation. Using peak calling and super-enhancer identification algorithm ROSE [372,373], we detected super-enhancers near the *PIM2* locus in several MM cell lines, but not in normal plasma cells. This supports the hypothesis that aberrant enhancer activation, and acquisition of super-enhancers, is a major contributor to pathological *PIM2* expression in multiple myeloma.

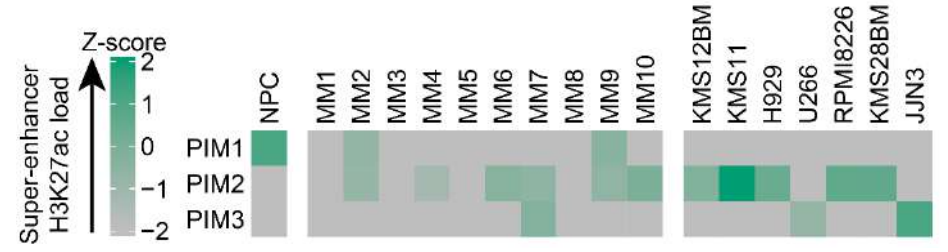


Fig. 18. Super-enhancer H3K27ac load at PIM loci in normal plasma cells, MM patient samples, and MM cell lines. Heatmap shows Z-scored H3K27ac ChIP-seq signal over super-enhancer regions assigned to PIM1, PIM2, and PIM3. Each column represents a sample or cell line from the Jia et al. Dataset [371].

To visualize the enhancer landscape at each PIM locus, we plotted H3K27ac ChIP-seq tracks across representative normal and malignant plasma cell samples (Fig. 19). Regions identified as super-enhancers by ROSE are highlighted in blue. For PIM2, a broad and intense H3K27ac signal was observed in several MM samples (MM10, JJN3, H929), consistent with strong enhancer activity. In contrast, normal plasma cells showed lower enrichment, suggesting that this regulatory element is undergoing epigenetic remodeling during transformation or disease progression.

A similar, though less consistent, pattern was observed at the PIM1 and PIM3 loci. Overall, these findings suggest that PIM2 is more consistently and strongly regulated by super-enhancer elements than PIM1 or PIM3 in MM. This enhancer-driven mechanism may explain the dominant role of PIM2 in MM pathobiology and its strong association with poor prognosis in our cohort.

To experimentally confirm that *PIM* gene expression in MM is driven by super-enhancer activity, we treated MM1.s cells with JQ1, a selective BET bromodomain inhibitor that blocks BRD4-dependent transcription. BET proteins, including BRD4, are critical for the maintenance of super-enhancer activity and drive the transcription of associated oncogenes [372]. JQ1 displaces BRD4 from chromatin, leading to rapid transcriptional repression of super-enhancer-regulated genes. *MYC*, a known super-enhancer-regulated oncogene, was included as a positive control to validate assay sensitivity.

Following JQ1 treatment, we observed a significant downregulation of *PIM2* mRNA levels compared to DMSO controls (Fig. 20). *PIM1* and *PIM3* expression also decreased, although the effect was slightly less pronounced than for *PIM2*. As expected, *MYC* expression was robustly suppressed.

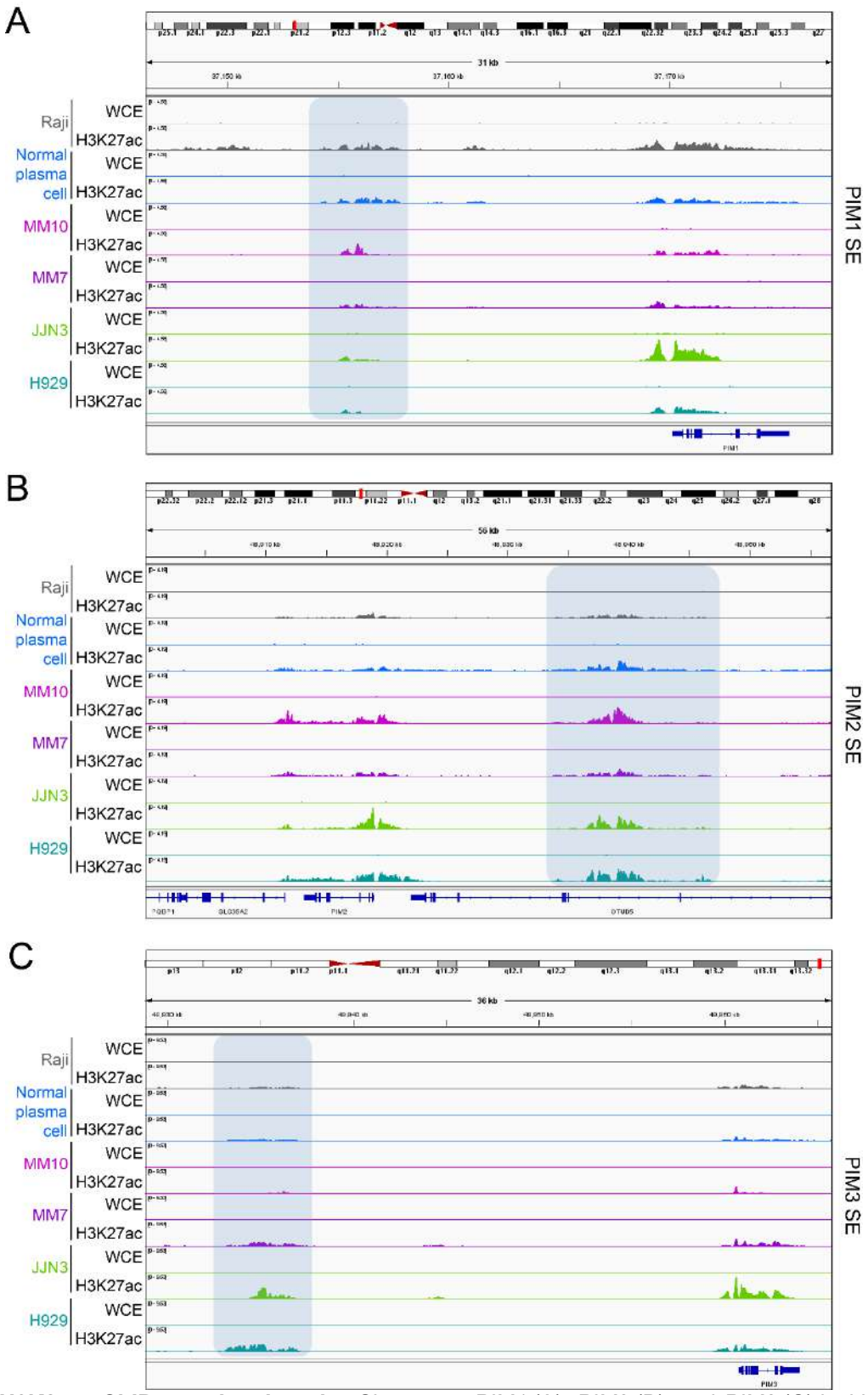


**Fig. 19. H3K27ac ChIP-seq signal tracks.** Shown are *PIM1* (A), *PIM2* (B), and *PIM3* (C) loci in normal plasma cells, B-cell lymphoma (Raji), and multiple myeloma samples. Whole-cell extract (WCE) and H3K27ac signals are shown for each sample. Blue-shaded areas indicate regions identified as superenhancers using the ROSE algorithm.

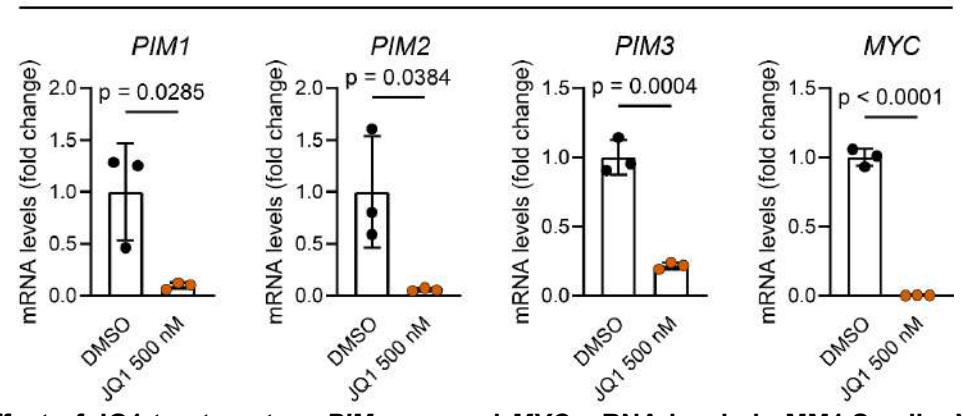


Fig. 20. Effect of JQ1 treatment on *PIM* gene and *MYC* mRNA levels in MM1.S cells. MM1.s cells were treated with DMSO (control) or 500 nM JQ1 for 24 hours. mRNA levels of *PIM1*, *PIM2*, *PIM3*, and *MYC* were measured by qRT-PCR and are shown as fold change relative to DMSO. MYC was included as a positive control for BRD4-dependent super-enhancer regulation. Data are shown as mean  $\pm$  SD; each dot represents an independent biological replicate.

### 3.3 Pharmacological targeting of PIM kinases in MM

# 3.3.1 Systematic drug screening of pan-PIM inhibitors reveals heterogeneous sensitivity

To evaluate the therapeutic potential of PIM kinase inhibition in MM, we performed a systematic drug screen using five pan-PIM inhibitors (MEN1703, PIM447, INCB053914, AZD1208, and SGI1776) across a panel of MM cell lines (Fig. 21). Both growth inhibitory (GI<sub>50</sub>) and lethal (LC<sub>50</sub>) concentrations were determined based on flow cytometry-based cell counting coupled with live cell detection via propidium iodide (PI) staining. Cells were treated with nine serial drug concentrations (0.05-12.8 μM) and analyzed at baseline (day 0) and after 4 days of drug treatment. This approach was prompted by conflicting preclinical data and recent disappointing clinical outcomes for PIM447 [348] and AZD1208 [345]. Our aim was to establish whether PIM kinases represent a consistent and targetable vulnerability in MM, and whether differences in drug response could be linked to underlying genetic features or the type of inhibitor used.

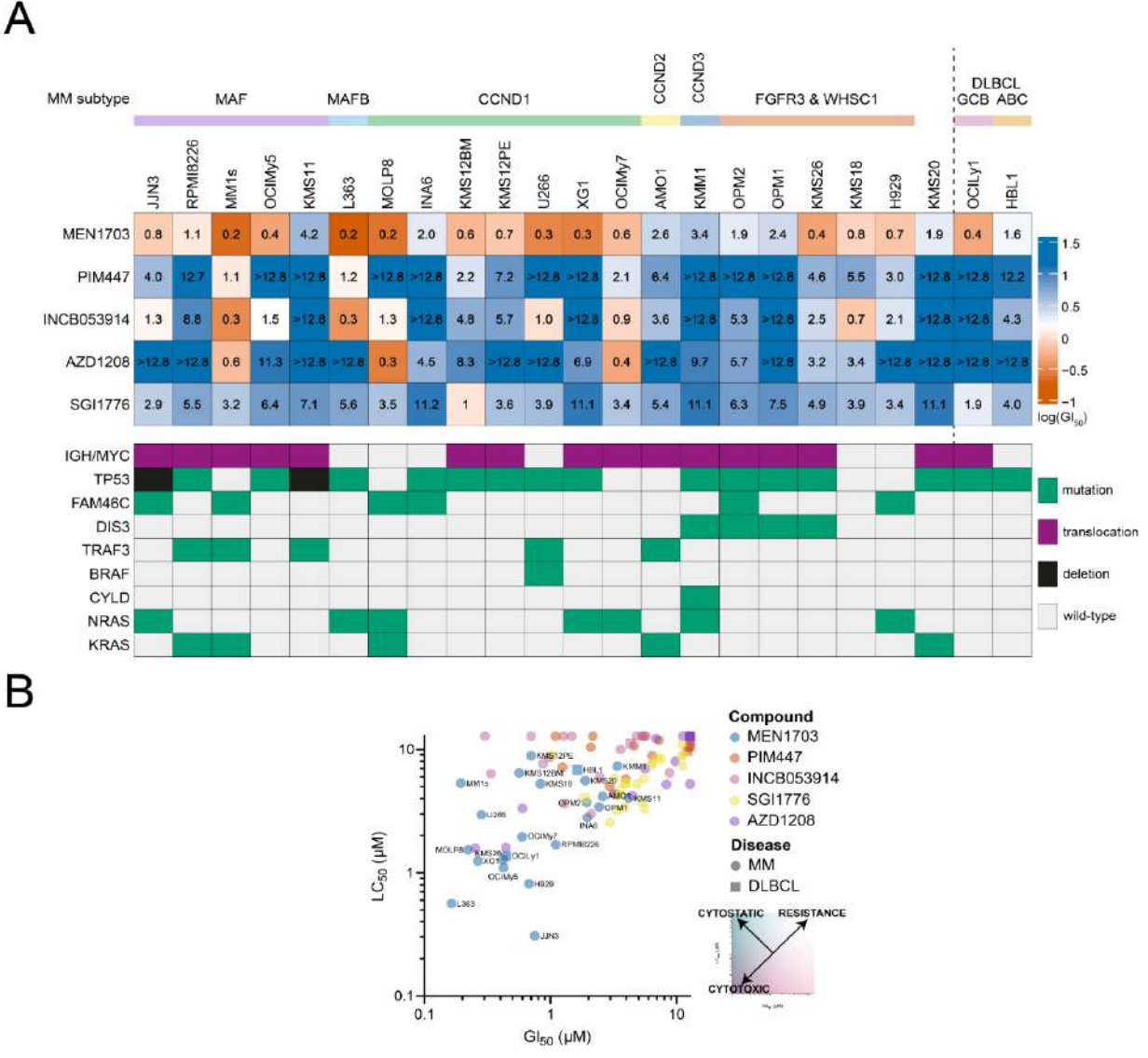


Fig. 21. Sensitivity of multiple myeloma cell lines to pan-PIM kinase inhibitors. (A) Heatmap showing  $Gl_{50}$  values ( $\mu$ M) for five pan-PIM inhibitors (MEN1703, PIM447, INCB053914, AZD1208, SGI1776) across a panel of MM and DLBCL cell lines. Values are color-coded by  $log_{10}(Gl_{50})$ , with higher sensitivity shown in blue. Cell lines are annotated by genetic subtype (top bar) and key oncogenic alterations (middle panel), including translocations (purple), mutations (green), and deletions (black). (B)  $Gl_{50}$  and  $LC_{50}$  values for all compounds and cell lines. Each point represents one cell line-drug combination, colored by compound and shaped by disease type.

The five pan-PIM inhibitors showed variable efficacy across MM cell lines. MEN1703 and INCB053914 exhibited the most potent activity, with low micromolar GI<sub>50</sub> values in several lines such as MM1.S, L363 and OCI-My7. In contrast, PIM447 and AZD1208 were less effective overall, consistent with prior clinical trial reports. SGI1776 showed intermediate activity. Notably, sensitivity patterns did not strictly correlate across inhibitors, suggesting differing off-target effects or cellular uptake or efflux. Some cell lines, such as KMS11 and KMM1, were broadly resistant to all compounds, while others, including MM1.S, were more sensitive. Drug

response was partially associated with genetic background: for instance, cell lines with MAF or FGFR3/WHSC1 translocations tended to be less sensitive.

Among the compounds tested, MEN1703 consistently demonstrated the highest potency across MM cell lines. Given its known activity against FLT3 [307], we investigated whether FLT3 mRNA expression correlated with increased MEN1703 sensitivity (Fig. 22). No such association was observed, suggesting that the cytotoxic effects of MEN1703 are primarily mediated through on-target inhibition of PIM kinases rather than FLT3 engagement.

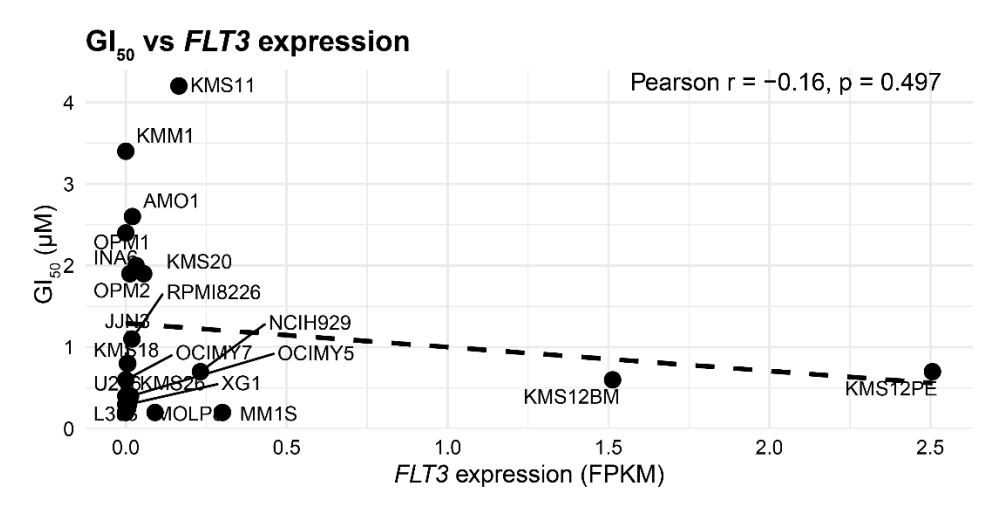


Fig. 22. Relationship between FLT3 expression and MEN1703 sensitivity in MM cell lines.

## 3.3.2 MEN1703 sensitivity is associated with MYC-driven transcriptional programs

To investigate potential mechanisms of MEN1703 sensitivity, we stratified MM cell lines into two groups using a GI<sub>50</sub> threshold of 1.5 μM to define resistant lines. Comparative transcriptomic analysis revealed that MEN1703-sensitive cell lines exhibited significantly higher expression of MYC and E2F1 target genes and genes associated with G2M checkpoint and glycolysis (Fig. 23). These findings suggest that MYC-driven transcriptional activity may enhance susceptibility to PIM inhibition and could serve as a predictive biomarker for MEN1703 response. MM cases harboring *IGH*::*MYC* translocations or relapsed/refractory disease (both associated with elevated MYC signaling [12,366]) may represent rational patient populations for clinical testing. Moreover, the data support the existence of a functional interaction between PIM kinase activity and MYC-driven oncogenic program.

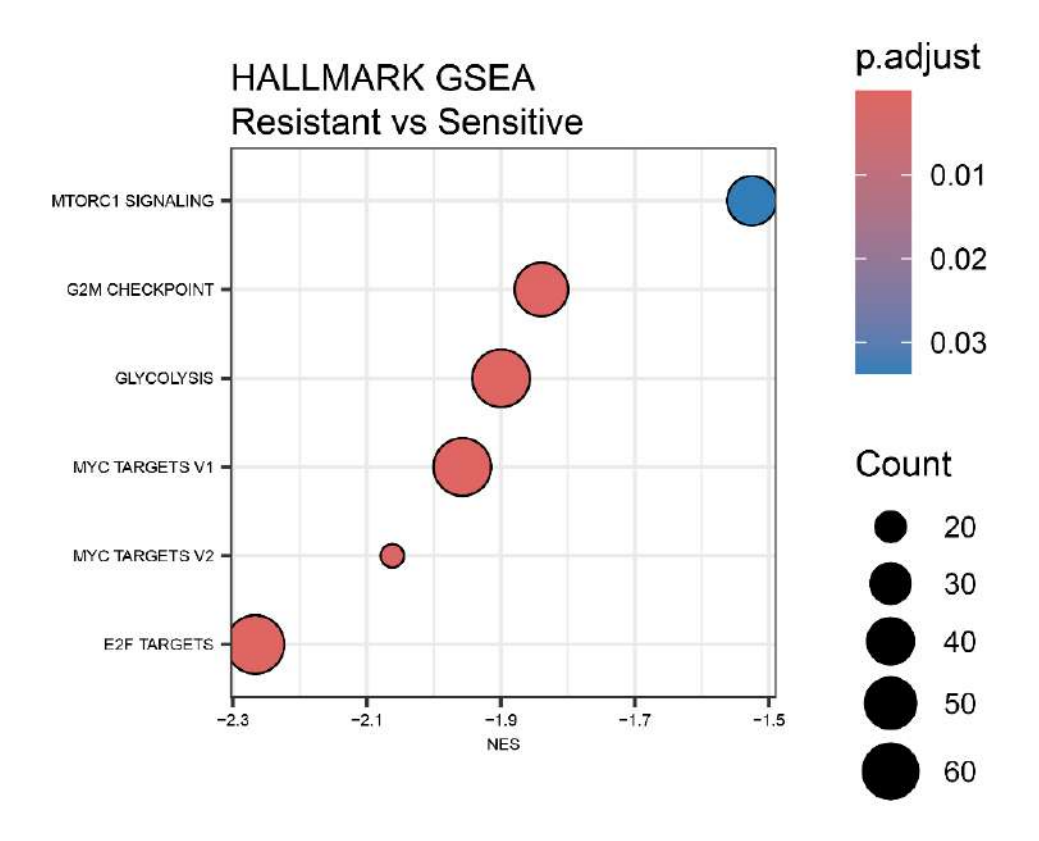
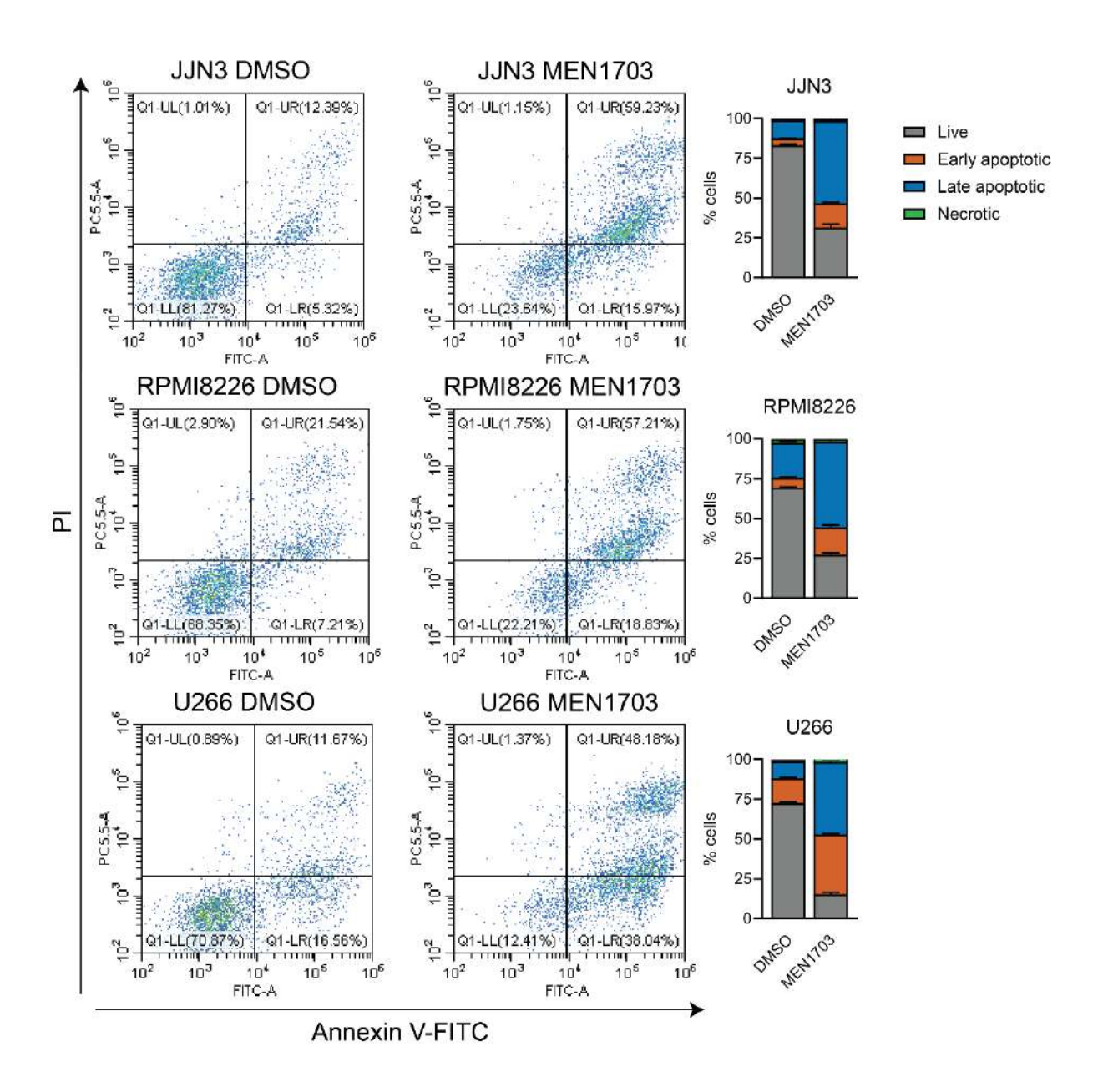


Fig. 23. Hallmark gene set enrichment analysis (GSEA) comparing resistant versus sensitive multiple myeloma cell lines.

### 3.3.3 MEN1703 induces apoptosis in MM cell lines

To determine whether MEN1703 suppresses MM cell viability through induction of apoptosis, we performed Annexin V-FITC/PI staining followed by flow cytometric analysis. Three representative MM cell lines (JJN3, RPMI8226, and U266) were treated with MEN1703 (1.5 μM) for 96 hours. MEN1703 markedly increased the proportion of apoptotic cells in all three lines, with a shift from the live (Annexin V<sup>-</sup>/PI<sup>-</sup>) population to early (Annexin V<sup>+</sup>/PI<sup>-</sup>) and late apoptotic/necrotic (Annexin V<sup>+</sup>/PI<sup>+</sup>) fractions (Fig. 24). In JJN3 cells, over 59% of the population shifted to late apoptosis/necrosis, compared to ~12% in DMSO-treated controls. Similar increases were observed in RPMI8226 and U266, indicating a consistent pro-apoptotic effect of MEN1703.



**Fig. 24. MEN1703 induces apoptosis in MM cell lines.** Annexin V-FITC and propidium iodide (PI) staining followed by flow cytometric analysis was used to assess apoptosis in JJN3, RPMI8226, and U266 cells after 96 h treatment with MEN1703 (1.5  $\mu$ M) or DMSO. Dot plots show the distribution of live (Annexin V<sup>+</sup>/PI<sup>-</sup>), early apoptotic (Annexin V<sup>+</sup>/PI<sup>-</sup>), late apoptotic (Annexin V<sup>+</sup>/PI<sup>+</sup>), and necrotic (Annexin V<sup>-</sup>/PI<sup>+</sup>) cells. Bar plots display the mean proportion of each population.

To further confirm the induction of apoptosis, we assessed the activity of caspase 3/7, caspase 8 and caspase 9 using the CaspGlo luminescence assay. MEN1703 treatment significantly elevated caspase activity in all tested cell lines, supporting the engagement of the intrinsic apoptotic cascade (Fig. 25A). Activity of caspase 8 was also increased following MEN1703 treatment, suggesting either activation secondary to cleavage mediated by caspase 3 or 9 [374] or activation of extrinsic apoptotic cascade. Western blot analysis revealed robust cleavage of PARP, a

hallmark of caspase-mediated apoptosis, in MEN1703-treated MM1.s and U266 cells, and to a lesser extent in RPMI8226 cells (Fig. 25B). These data demonstrate that MEN1703 induces apoptotic cell death in MM cells.

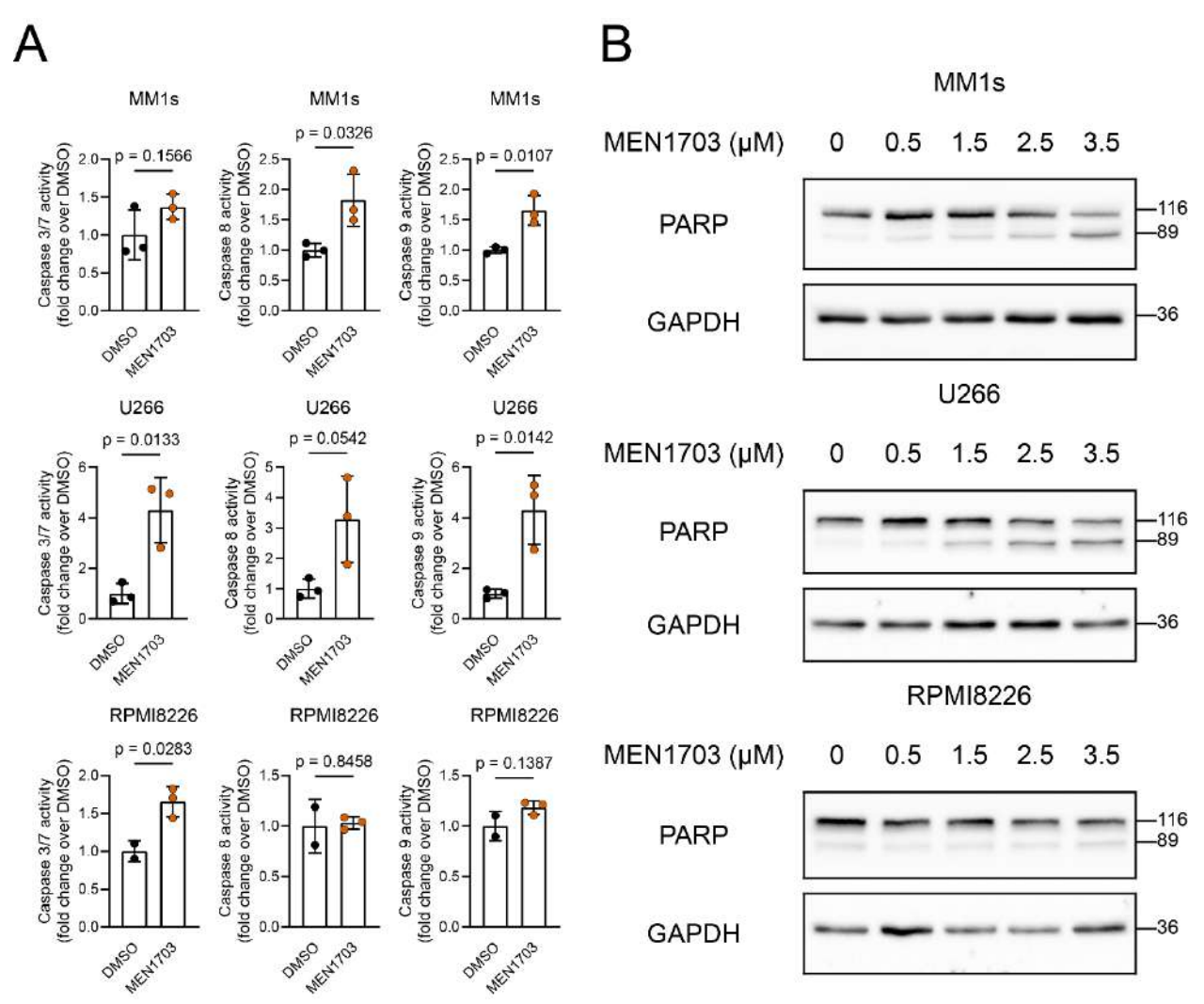


**Fig. 25. MEN1703 induces caspase activation in MM cells.** (A) Luminescence-based caspase activity assays were performed following 24 h treatment with MEN1703 (1.5  $\mu$ M) or DMSO. Data are shown as fold change over DMSO-treated controls (mean  $\pm$  SD). P values were determined by unpaired two-tailed t-test. (B) Western blot analysis of PARP cleavage in MM1.S, U266, and RPMI8226 cells treated with increasing concentrations of MEN1703 (0-3.5  $\mu$ M) for 24 hours. Cleaved PARP (89 kDa) serves as a marker of apoptosis. GAPDH was used as a loading control.

### 3.3.4 MEN1703 induces apoptosis in primary MM cells

To validate the anti-myeloma activity of PIM inhibition in primary samples, we treated freshly isolated bone marrow aspirates from MM patients with MEN1703 or PIM447 for 48 hours. The myeloma cells were magnetically separated from the rest of the bone marrow using anti-CD138

beads. Apoptosis was quantified by Annexin V-PE/7AAD staining and subsequent flow cytometric acquistion. The percentage of viable CD138+ MM cells (Annexin V- 7AAD-) was normalized to DMSO-treated controls. MEN1703 induced a marked reduction in viable MM cells in most samples, while sparing non-malignant CD138- cells (Fig. 26A). MEN1703 was effective even against MM cells cocultured directly with CD138- stromal cells, demonstrating that it could overcome the protective effect of bone marrow microenvironment. Caspase-3/7 activity assays using the CaspGlo kit confirmed apoptosis induction following MEN1703 treatment (Fig. 26B). In contrast, PIM447 demonstrated limited cytotoxic activity in these primary cells (Fig. 26C). To distinguish tumor from stromal compartments, CD138+ cells were pre-labeled with CFSE prior to drug exposure, allowing for reliable tracking despite time-dependent loss of CD138 surface expression.

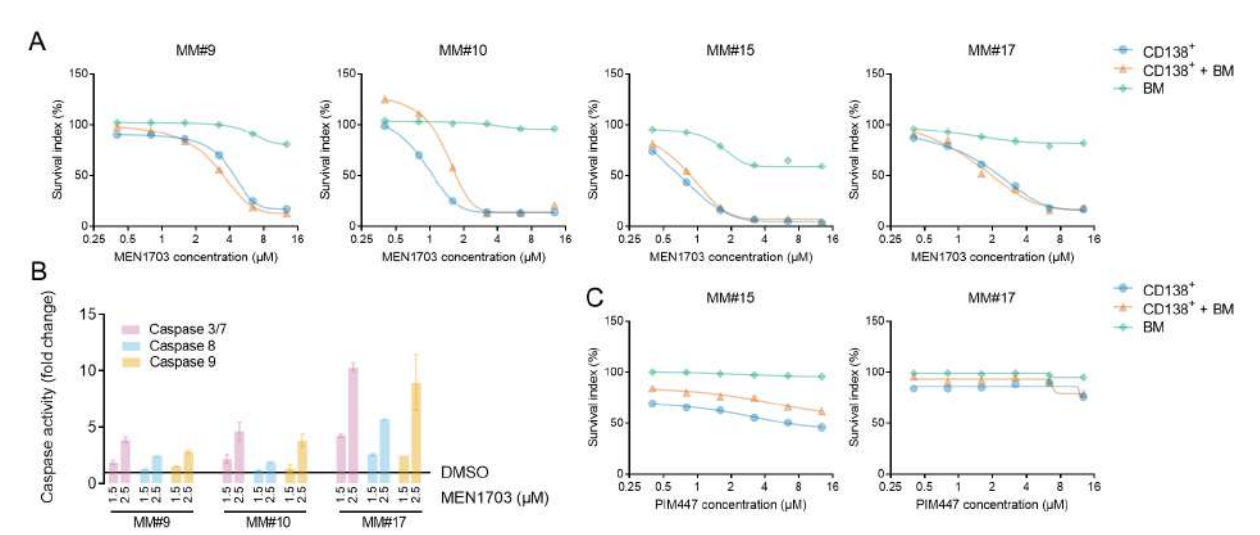


**Fig. 26. Sensitivity of primary MM cells to MEN1703 and PIM447.** (A) Bone marrow aspirates from MM patients were treated with MEN1703 or PIM447 for 48h. Apoptosis was assessed by Annexin V-PE/7AAD staining. Viable CD138<sup>+</sup> (CFSE<sup>+</sup>) MM cells were quantified as Annexin V-PE<sup>-</sup> 7AAD<sup>-</sup> and normalized to DMSO-treated controls. CD138<sup>-</sup> non-malignant cells and mixed cultures (CD138<sup>+</sup> + CD138<sup>-</sup>) were analyzed in parallel. (B) Caspase-3/7 activity in CD138<sup>+</sup> MM cells treated as in (A), measured using a luminescent CaspGlo assay. (C) PIM447 exhibited minimal cytotoxicity across primary MM samples.

## 3.3.5 Time-course analysis reveals sustained anti-myeloma activity of MEN1703

To evaluate the time-dependent effects of PIM kinase inhibition, we monitored MM and DLBCL cell line viability over a 12-day period following exposure to 1.5  $\mu$ M MEN1703, PIM447, or INCB053914 (Fig. 27). Viable cell counts were normalized to DMSO-treated controls at each

time point. MEN1703 induced a rapid and sustained decrease in viability across nearly all MM cell lines, with no evidence of rebound growth by day 12. INCB053914 exhibited intermediate efficacy, with a gradual reduction in viability observed in several lines, though the extent of suppression was less consistent than with MEN1703. In contrast, PIM447 failed to induce a meaningful decrease in cell viability in most lines, and, in several cases, cell numbers increased over time, indicating continued proliferation.

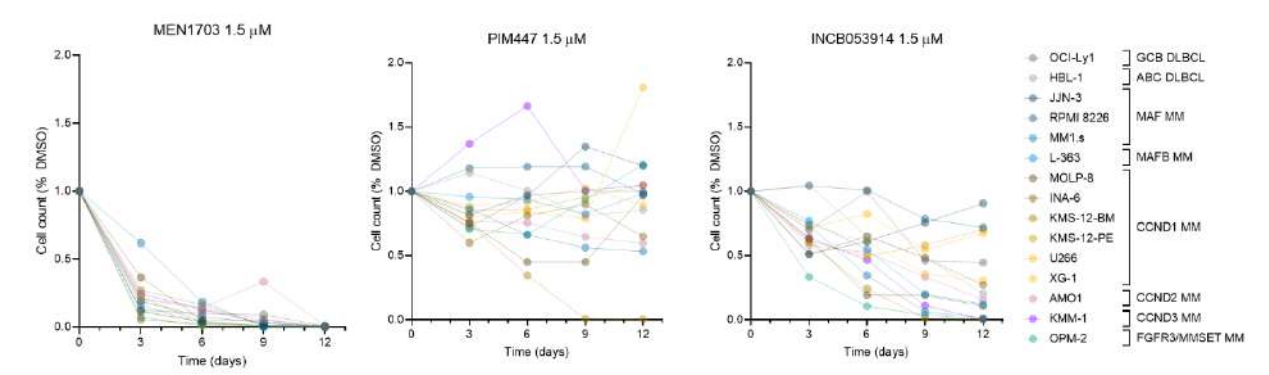


Fig. 27. Time-course analysis of PIM inhibitor efficacy in MM and DLBCL cell lines. Cell lines were treated with 1.5  $\mu$ M of MEN1703, PIM447, or INCB053914 and viable cell counts were assessed over 12 days using flow cytometry. Cell numbers were normalized to DMSO-treated controls at each time point. Each line represents an individual cell line, color-coded by name and grouped by genetic subtype (right).

## 3.3.6 Differential PIM2 engagement does not explain the superior cytotoxic activity of MEN1703

To assess whether differences in PIM2 binding affinity contribute to the superior cytotoxic activity of MEN1703 compared to PIM447, we performed a cellular thermal shift assay (CETSA) in MM cell lines (Fig. 28). JJN3 and U266 cells were treated with either MEN1703 or PIM447 (5  $\mu$ M dissolved in HBSS, t = 30 min), followed by heating across a temperature gradient. This assay measures thermal stability of endogenous PIM2 protein in intact cells. Upon heating, unbound PIM2 denatures at its characteristic melting temperature (Tm), while ligand binding stabilizes the protein, resulting in a rightward shift of the melting curve. Following heat treatment, soluble (non-denatured) PIM2 levels were quantified by immunoblotting.

Despite MEN1703 exhibiting potent pro-apoptotic activity in MM cells, CETSA showed that PIM447 induced a significantly greater thermal stabilization of PIM2 protein in both JJN3 and U266 lines (Fig. 28A), with melting temperatures (Tm) of 65.7 °C and 56.3 °C, respectively (Fig. 28B). In contrast, MEN1703-treated cells displayed lower Tm values (47.6 °C in JJN3 and

49.1 °C in U266), only modestly shifted relative to DMSO controls. These results indicate that the greater anti-myeloma activity of MEN1703 is not due to stronger intracellular engagement of PIM2.

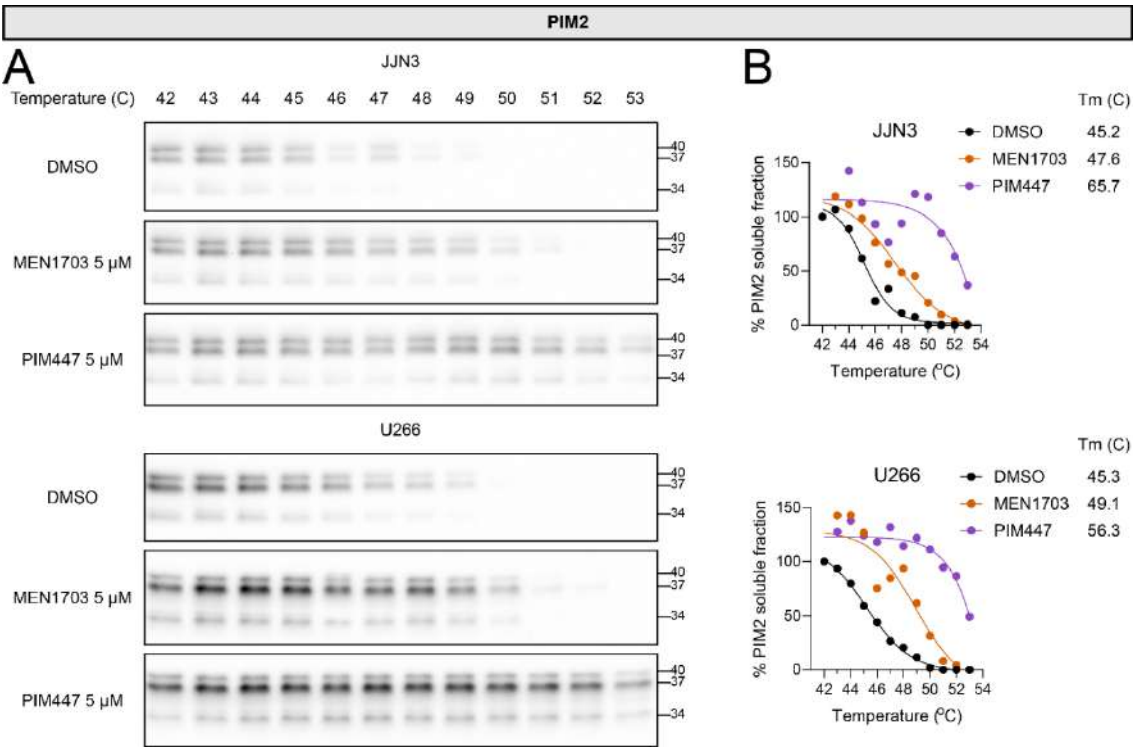


Fig. 28. Cellular thermal shift assay (CETSA) for assessment of target engagement of PIM2 by MEN1703 and PIM447 in MM cells. (A) Western blot analysis of PIM2 thermal stability in JJN3 and U266 cells treated with DMSO, MEN1703 ( $5\,\mu\text{M}$ ), or PIM447 ( $5\,\mu\text{M}$ ) for 1 hour. Cells were subjected to a temperature gradient (42-53 °C), and the soluble protein fraction was analyzed by SDS-PAGE and immunoblotting for PIM2. (B) Quantification of PIM2 stability curves based on densitometric analysis of the immunoblots. Calculated melting temperatures (Tm) are shown for each condition.

### 3.4 Genetic silencing of PIM kinase expression in MM

## 3.4.1 PIM2 is the dominant PIM family member supporting MM cell proliferation and mTOR activity

Although CETSA revealed that PIM447 binds PIM2 more efficiently than MEN1703, only MEN1703 consistently induced apoptosis and loss of viability in MM cells. To test whether the superior activity of MEN1703 is due to its functional inhibition of PIM kinase activity rather than binding affinity, we asked whether genetic depletion of PIM expression could phenocopy the effects of MEN1703. To address this, we developed a Sleeping Beauty-based doxycycline (DOX)-inducible system enabling shRNA-mediated silencing of each PIM (*PIM1*, *PIM2*, *PIM3*)

individually. The shRNAs were designed to be paralog-specific with no predicted off-target effects on the other PIMs.

We selected the JJN3 cell line for functional validation, as it displayed selective sensitivity to MEN1703 but remained resistant to PIM447 (Fig. 29A). Multiple shRNAs with different binding sites were tested per gene (4 for *PIM1*, 5 for *PIM2*, and 5 for *PIM3*). All stable lines selected with puromycin and G418 for at least 3 weeks were treated with 0.5 μg/mL doxycycline to induce knockdown.

In flow cytometry-based proliferation assays, shPIM2-transfected cells exhibited the most prominent growth disadvantage compared to scrambled control (shSCR), with effects emerging at day 6 and persisting through day 10 (Fig. 29B). Silencing of *PIM1* and *PIM3* had milder effects, with a moderate proliferative delay evident at day 10. Cell viability measured by PI staining and flow cytometry after 96 hours of DOX exposure showed a small but significant (~8%) reduction in the viability of shPIM2 cells relative to controls (Fig. 29C).

To confirm effective gene silencing, we performed immunoblotting for each PIM protein after 12 h (Fig. 29D) and 120 h (Fig. 29E) of DOX treatment. Importantly, *PIM2* knockdown led to a decrease in phosphorylation of ribosomal protein S6 at Ser235/236, a PIM target shared with mTORC1 pathway. A significant suppression of pS6 was evident at 12 hours and more pronounced at 120 hours, but this effect was unique to DOX-induced shPIM2 cells. This suggests PIM2 is a primary contributor to pS6 signaling in JJN3 cells, given that knockdown of either *PIM1* or *PIM3* had minimal impact.

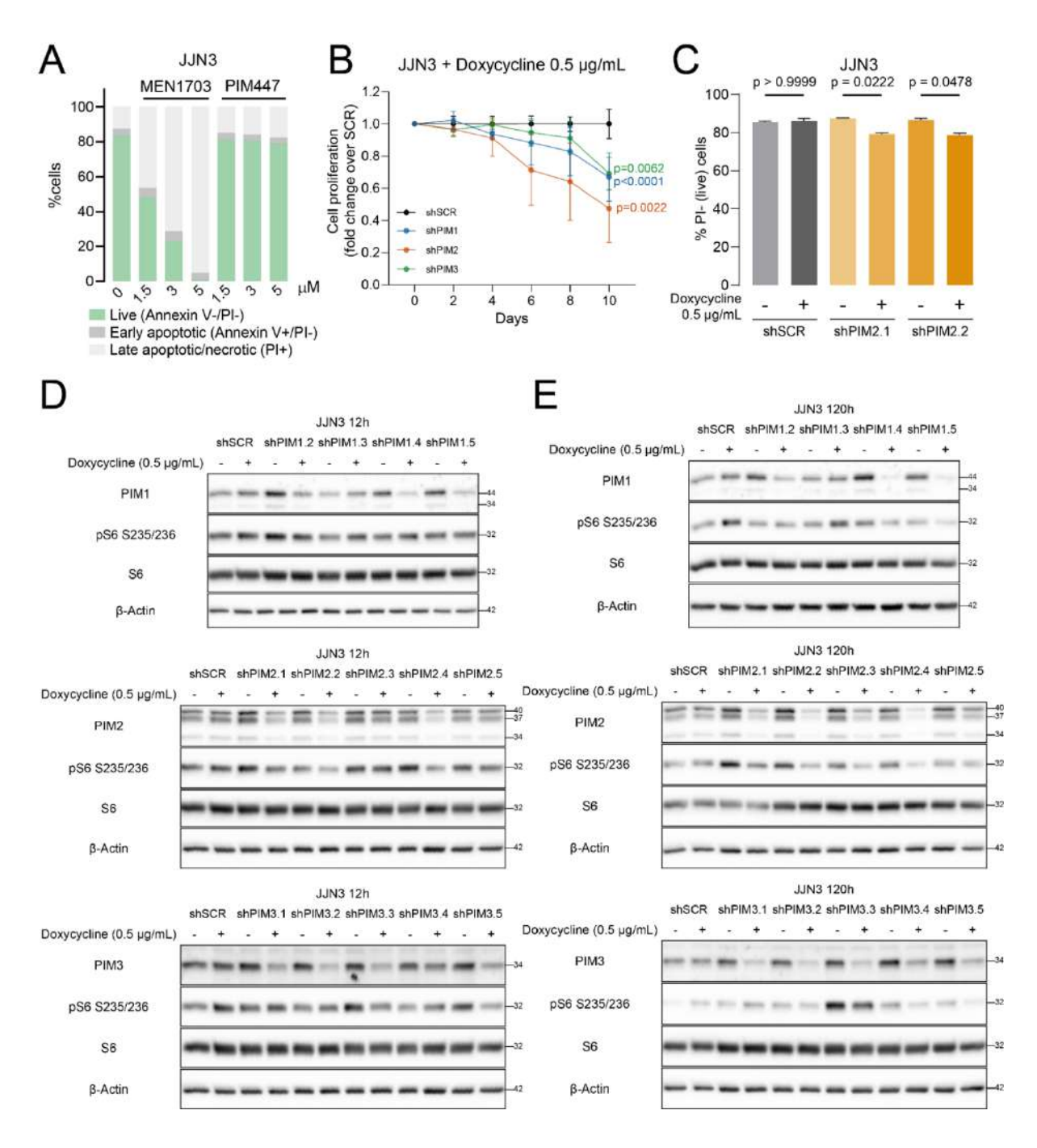


Fig. 29. Selective knockdown of individual PIM kinases reveals dominant role of PIM2 in MM cell proliferation and S6 phosphorylation. (A) Flow cytometry-based quantification of cell death in JJN3 cells treated for 96h with MEN1703 or PIM447. (B) Proliferation assay of doxycycline-inducible shPIM1, shPIM2, shPIM3 and control shSCR JJN3 cells treated with 0.5 μg/mL doxycycline. Doxycycline was readded with fresh medium every 2 days. Proliferation was expressed as fold change over shSCR at each time point. Data are mean±SD. Statistical analysis was performed using two-way repeated measures ANOVA comparing each shPIM condition to shSCR across the time course. (C) Viability assay using PI exclusion in shPIM2 clones after 5 days of DOX treatment. Data are mean±SD. Cell viability was analyzed using the Kruskal-Wallis test with Dunn's post hoc correction for multiple comparisons. (D-E) Western blot validation of shRNA knockdown after 12 h (D) and 120 h (E) of DOX induction. *PIM1*, *PIM2*, and *PIM3* were efficiently silenced by their respective shRNAs. pS6 (S235/236) levels were reduced in shPIM2 clones, consistent with impaired PIM signaling. β-Actin was used as a loading control.

These results are consistent with a model in which PIM2 plays a dominant, non-redundant role in sustaining MM cell growth and PIM-mediated S6 activation. However, the modest phenotypic effects of single PIM knockdowns suggest potential functional compensation between different PIMs. To overcome this redundancy, we next generated concatenated multi-shRNA constructs enabling simultaneous silencing of all three PIM kinases in a DOX-inducible fashion. This system was designed to genetically mimic pan-PIM inhibition, providing a more specific alternative to small-molecule inhibitors, which often exhibit off-target activity against other kinases.

## 3.4.2 Simultaneous silencing of PIM1, PIM2, and PIM3 results in more potent anti-MM effects

To test whether combined depletion of all three PIM kinases more closely copies the phenotype observed with pharmacologic inhibition using MEN1703, we used our Sleeping Beauty-based doxycycline-inducible system to generate a triple shRNA construct (sh3xPIM) targeting *PIM1*, *PIM2*, and *PIM3*. For construction of the triple knockdown plasmid, we selected the most effective shRNAs based on individual silencing efficiency: shPIM1.5, shPIM2.4, and shPIM3.4. The sh3xPIM vector allows for these shRNAs to be driven by separate tetracycline-responsive promoters to ensure efficient silencing upon doxycycline addition.

JJN3 cells were transfected with the sh3xPIM or shSCR vector, selected using puromycin and G418 for at least 3 weeks and cultured in the presence of 0.5 μg/mL doxycycline. Triple PIM silencing resulted in a robust inhibition of proliferation, beginning on day 4 and continuing through day 9 (Fig. 30A). This phenotype was more pronounced than that seen with individual PIM knockdowns. By day 9, cell proliferation was reduced to ~25% of the control (shSCR) level. Western blot analysis confirmed effective knockdown of *PIM1*, *PIM2*, and *PIM3* after 96 h of doxycycline exposure (Fig. 30B), with a corresponding decrease in phosphorylation of the PIM target substrate S6 at Ser235/236. The reduction in pS6 was more substantial than with single PIM knockdowns. Cell viability assays performed at 96 h post DOX addition revealed a ~16% increase in cell death in sh3xPIM cells compared to the non-induced control (Fig. 30C). These data show that genetic suppression of all three PIM kinases is sufficient to impair proliferation

and survival of MM cells, partially phenocopying the effects of MEN1703 treatment and reinforcing the concept that pan-PIM inhibition is necessary to fully target the PIM axis in MM.

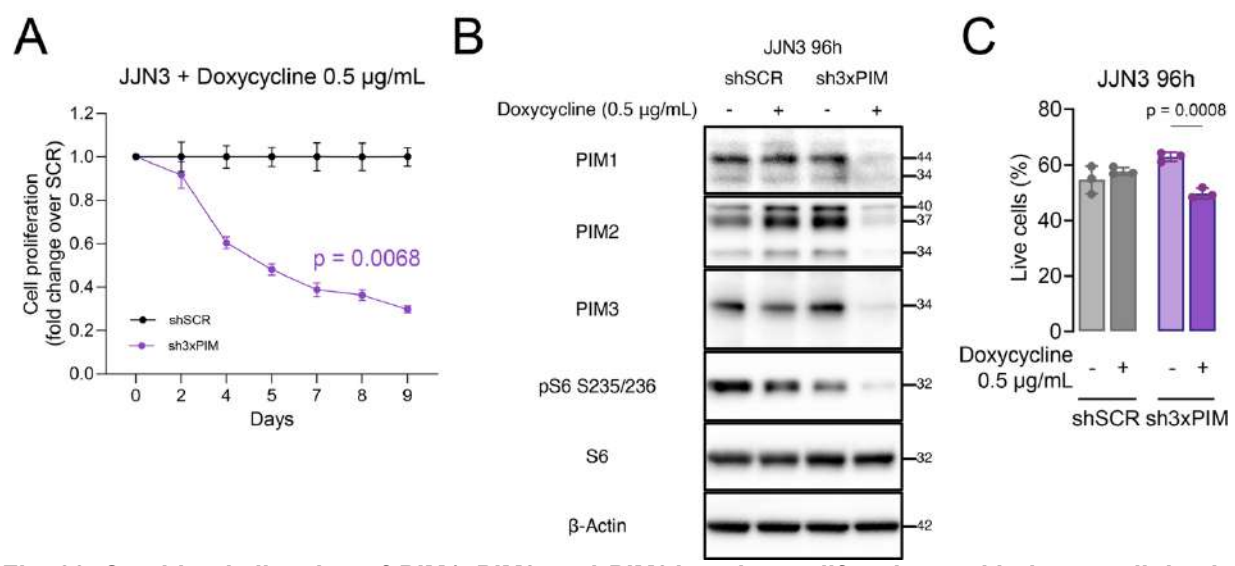


Fig. 30. Combined silencing of *PIM1*, *PIM2*, and *PIM3* impairs proliferation and induces cell death in MM cells. (A) Cell proliferation assay of JJN3 cells expressing doxycycline-inducible shSCR or triple PIM shRNAs (sh3xPIM) over 9 days. Doxycycline was added at 0.5 μg/mL and readded with fresh medium ever 2 days. Cell counts were normalized to shSCR. Data represent mean  $\pm$  SD. Statistical analysis was performed using two-way repeated measures ANOVA .(B) Immunoblot analysis of JJN3 cells 96 hours after doxycycline treatment showing effective knockdown of *PIM1*, *PIM2*, and *PIM3*, accompanied by reduced phosphorylation of S6 at Ser235/236. β-Actin was used as a loading control. (C) Viability assay of shSCR and sh3xPIM JJN3 cells treated with or without doxycycline for 96 h. Data represent mean  $\pm$  SD. Statistical analysis was performed using unpaired t-test.

# 3.5 Transcriptional and functional effects of pan-PIM inhibition in MM

## 3.5.1 MEN1703 suppresses MYC- and E2F-driven transcriptional programs and activates stress responses

To understand the transcriptional consequences of PIM inhibition using MEN1703, we performed bulk RNA-seq on MM1.S cells treated with MEN1703 for 24 hours. Principal component analysis (PCA) showed clear separation between MEN1703-treated and DMSO-treated samples (Fig. 31A), indicating distinct transcriptional profiles. MEN1703 treatment induced robust transcriptional changes, with 589 upregulated and 642 downregulated genes (FDR < 0.05). Differential expression analysis identified numerous upregulated and downregulated genes, with several involved in cell cycle regulation, DNA replication, RNA processing, and stress signaling (Fig. 31B).

Gene set enrichment analysis (GSEA) across HALLMARK, REACTOME, GO-Biological Process, and TFT collections revealed marked downregulation of MYC targets, E2F-regulated genes, G2/M checkpoint components, and mitotic regulators following MEN1703 treatment (Fig. 31C). Consistent with the observed growth arrest and impaired biosynthetic capacity, pathways essential for proliferation, including DNA replication, RNA splicing, ribosome biogenesis, and DNA repair, were significantly suppressed. These processes are canonical targets of the MYC oncogene, a master regulator of transcription, and its key downstream effector, the transcription factor E2F1. Providing a direct mechanism for this suppression, we confirmed that MEN1703 treatment resulted in the downregulation of both MYC and E2F1 proteins in MM1.S cells (Fig. 32). Protein translation-related gene sets were markedly reduced, reflecting a broader shutdown of anabolism. Notably, western blot analysis confirmed a reduction in phosphorylation of ribosomal protein S6 at Ser235/236 upon MEN1703 treatment (Fig. 32). This site is a known mTOR effector and a direct substrate of PIM kinases. This validates that MEN1703 impairs signaling associated with protein translation and MYC/E2F oncogenic axis. These transcriptional programs are essential for MM survival and proliferation and are frequently activated in highrisk MM [366].

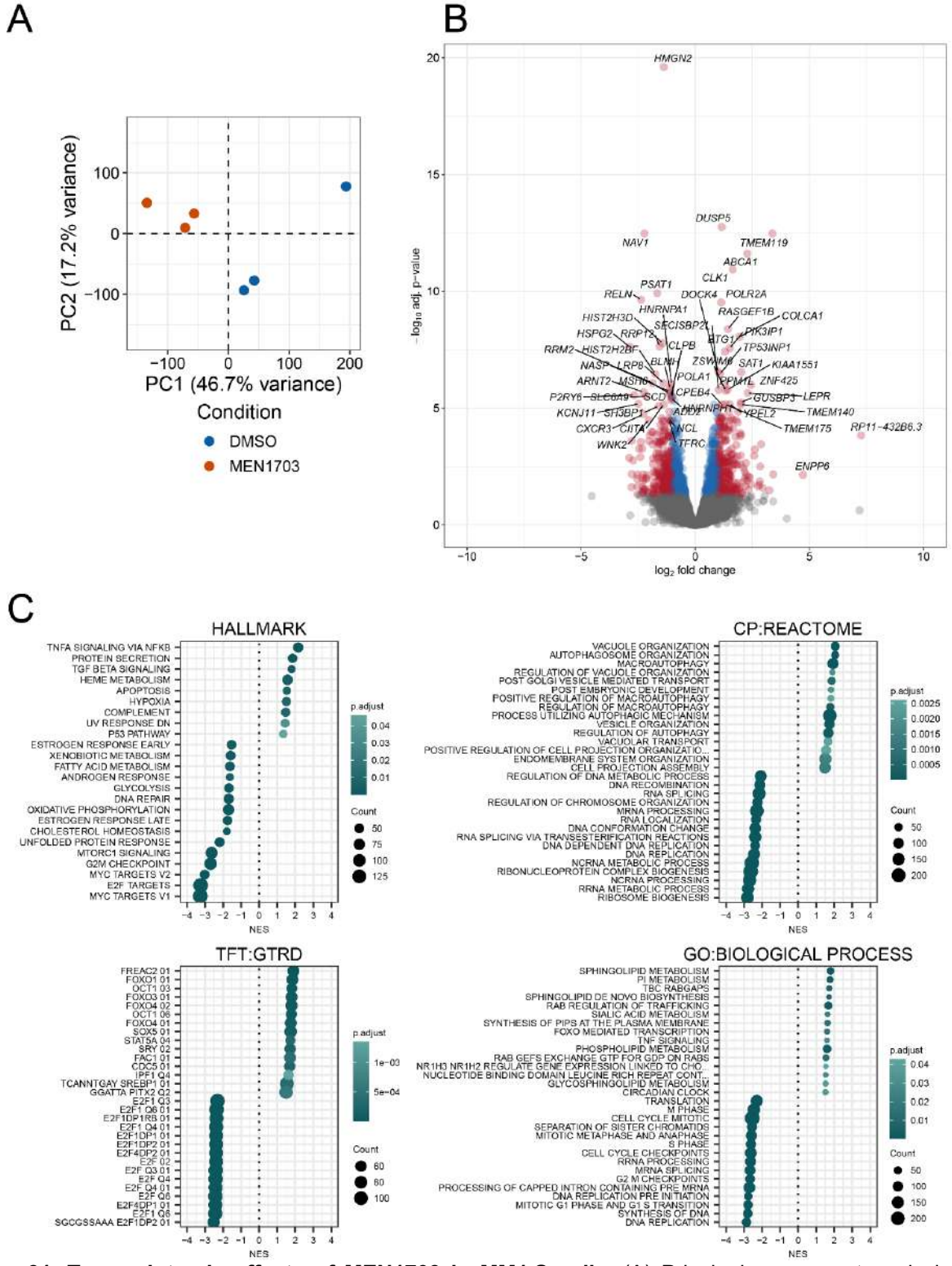
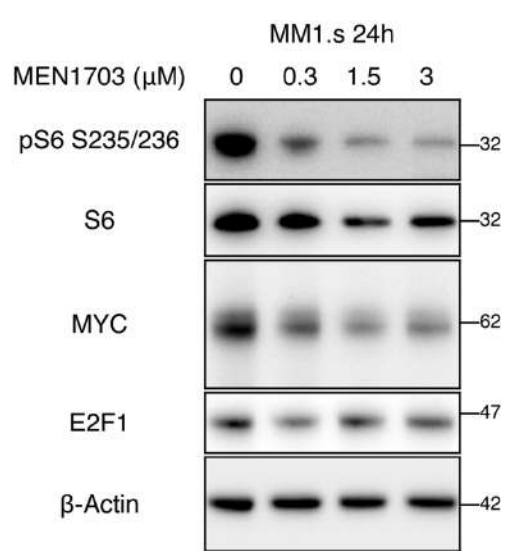


Fig. 31. Transcriptomic effects of MEN1703 in MM1.S cells. (A) Principal component analysis of RNAseq counts detected in MM1.S cells treated with DMSO or MEN1703 (1.5  $\mu$ M, 24 h). (B) Volcano plot of differentially expressed genes. Red dots indicate significantly differentially expressed genes with FDR < 0.05 and absolute log<sub>2</sub> fold change > 0.5; blue dots are FDR-significant but with smaller fold changes ( $\leq$  0.5); gray dots are not statistically significant. (C) Gene set enrichment analysis (GSEA) showing top positively and negatively enriched pathways across four curated gene set databases. NES - Normalized Enrichment Score.



**Fig. 32. MEN1703 reduces MYC, E2F1 and phosphorylation of S6 in MM1.S cells.** Western blot analysis of MM1.S cells treated with increasing concentrations of MEN1703 (0, 0.3, 1.5, 3 µM) for 24 h.

MEN1703 upregulated pro-apoptotic and tumor suppressive pathways, including the p53 signaling pathway, FOXO target genes, and apoptosis-related genes (Fig. 31C). These changes are consistent with PIM inhibition triggering cell death and growth arrest. Additionally, inflammatory and catabolic responses such as TNFα/NF-κB signaling, autophagy, and lysosomal activity were induced, possibly reflecting adaptive or compensatory stress mechanisms. The unfolded protein response (UPR) was suppressed, suggesting impaired proteostasis regulation under MEN1703 treatment.

Together, these findings support a model in which PIM inhibition disrupts proliferative and transcriptional networks sustained by MYC, while simultaneously activating apoptosis and suppressing key survival programs such as protein translation and DNA repair.

### 3.5.2 MEN1703 suppresses DNA repair gene networks

To understand the mechanisms underlying MEN1703-induced cell death, we performed a more detailed analysis of RNA-seq data from MM1.S cells treated with MEN1703. Given the phenotypic evidence of apoptosis, we specifically interrogated the transcriptional status of DNA repair pathways at a timepoint before apoptosis initiation (24 h).

We focused on curated child terms of the Gene Ontology category DNA repair (GO:0006281). Gene set enrichment analysis (GSEA) revealed broad suppression of multiple DNA repair programs, including mismatch repair, base-excision repair, nucleotide-excision repair, double-

strand break repair, recombinational repair, and interstrand crosslink repair (Fig. 33A). The downregulation of these gene sets suggests that PIM inhibition might interfere with DNA repair capacity at multiple levels.

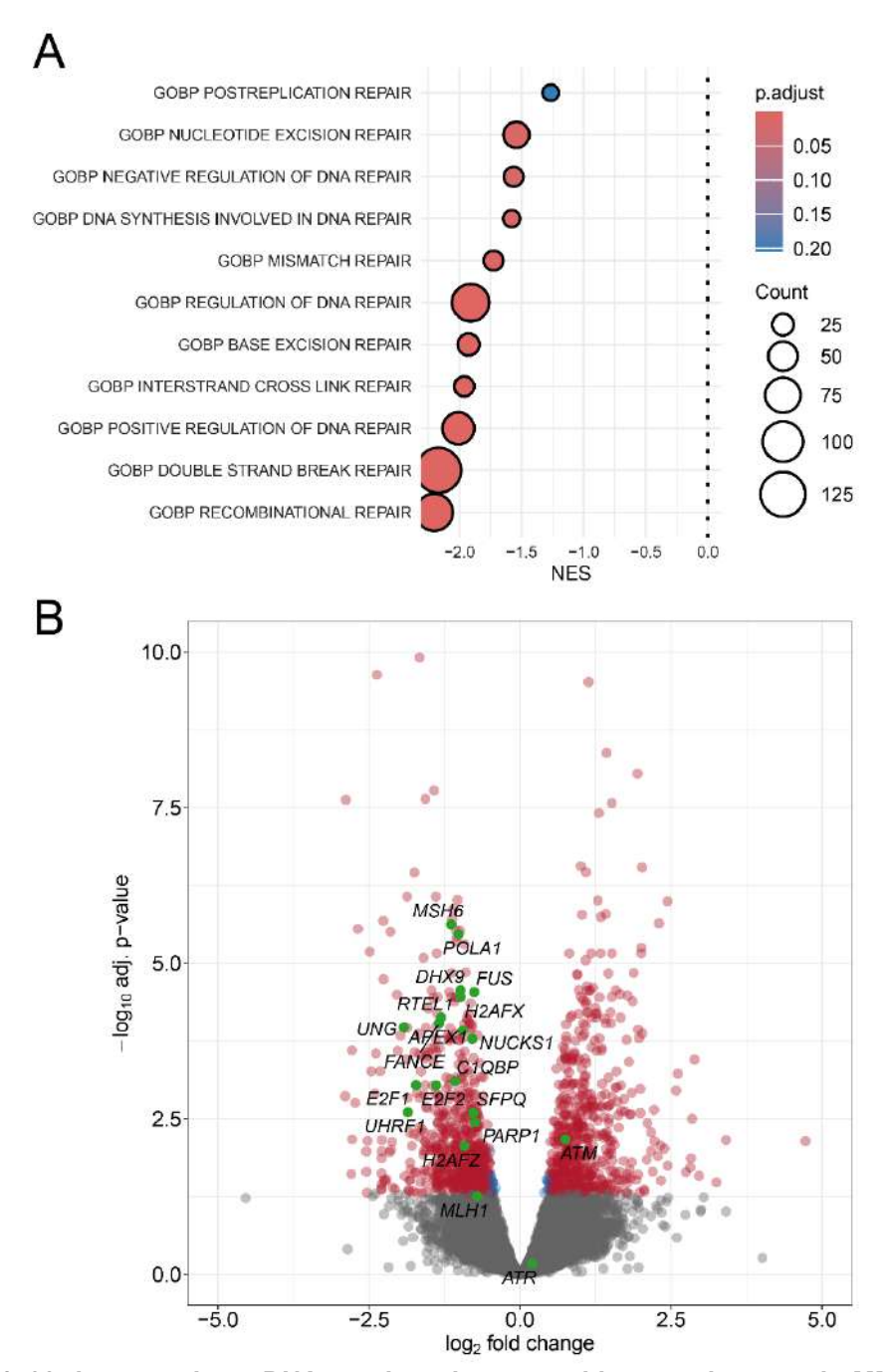


**Fig. 33. MEN1703 downregulates DNA repair pathways and key repair genes in MM1.S cells.** (A) Dot plot showing GSEA results for GO:BP gene sets that are part of the parent category DNA repair (GO:0006281). Normalized enrichment scores (NES) are shown on the x-axis. (B) Volcano plot of differentially expressed genes following MEN1703 treatment. Significantly upregulated (red), downregulated (blue), and non-significant (gray) genes are shown. Curated leading edge DNA repair genes are highlighted in green and labeled with gene symbols.

To further explore specific regulators, we examined the differential expression of key leading edge DNA repair genes. Several critical components of DNA surveillance and repair were significantly downregulated following MEN1703 treatment (Fig. 33B). These include *MSH6* (mismatch repair), *FANCE* (Fanconi pathway), *UNG*, *APEX1* (base excision repair), *RTEL1* (replication fork stability), and *PARP1* (single-strand break repair and chromatin signaling). The repression of *PARP1* is particularly notable given its role in coordinating repair of replication-associated damage and the existence of FDA-approved PARP inhibitors for cancer treatment. Interestingly, *ATM* transcript levels were modestly upregulated, while *ATR* expression remained unchanged. This may reflect a compensatory upregulation of ATM-dependent signaling in response to PIM inhibition and associated genomic stress involving double strand breaks.

To directly assess DNA damage induced by PIM inhibition, we performed a comet assay in JJN3 cells treated with MEN1703 (Fig. 34) We have selected this cell line since MM1.S cells are more sensitive to the conditions of comet assay and due to this fragility we experienced technical limitations, prompting us to use JJN3 instead. The comet assay quantitatively measures DNA strand breaks by assessing the migration of fragmented DNA from the nucleus ("comet tail") relative to intact DNA ("comet head"). MEN1703 treatment resulted in a significant increase in DNA fragmentation, as reflected by a higher comet tail-to-head ratio compared to DMSO-treated controls (p = 0.0074). These findings corroborate our transcriptomic data and support the conclusion that MEN1703 compromises DNA repair capacity, leading to accumulation of DNA strand breaks in MM cells.

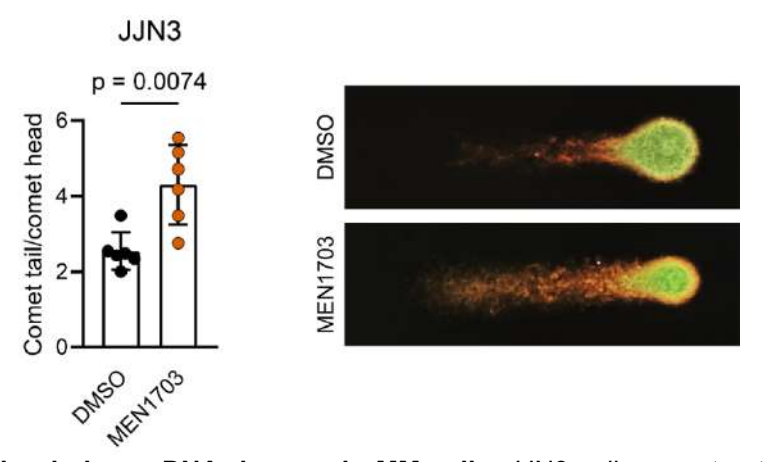


Fig. 34. PIM inhibition induces DNA damage in MM cells. JJN3 cells were treated with MEN1703 (1.5  $\mu$ M) or DMSO for 24 hours and subjected to a comet assay. Comet tail and head length were quantified manually using ImageJ. Statistical significance was assessed using Welch's unpaired t-test. Representative fluorescence images show increased DNA fragmentation in MEN1703-treated cells compared to DMSO. Experiments performed in collaboration with Ewa Kurtz.

# 3.6 *In vivo* validation of MEN1703 efficacy in a disseminated MM model

To assess whether the *in vitro* effects of MEN1703 translate into *in vivo* efficacy, we utilized a luciferase-tagged disseminated multiple myeloma model (Fig. 35). NSG mice were intravenously injected with 1×10<sup>6</sup> MM1.S-luc cells and monitored by bioluminescence imaging (BLI). Mice were randomized on day 7 based on BLI signal intensity to ensure comparable tumor burden across treatment groups. They were subsequently treated with MEN1703 at 50 mg/kg *per os* once daily (QD) or vehicle control (H<sub>2</sub>O) for three weeks. Tumor burden was monitored weekly using BLI.

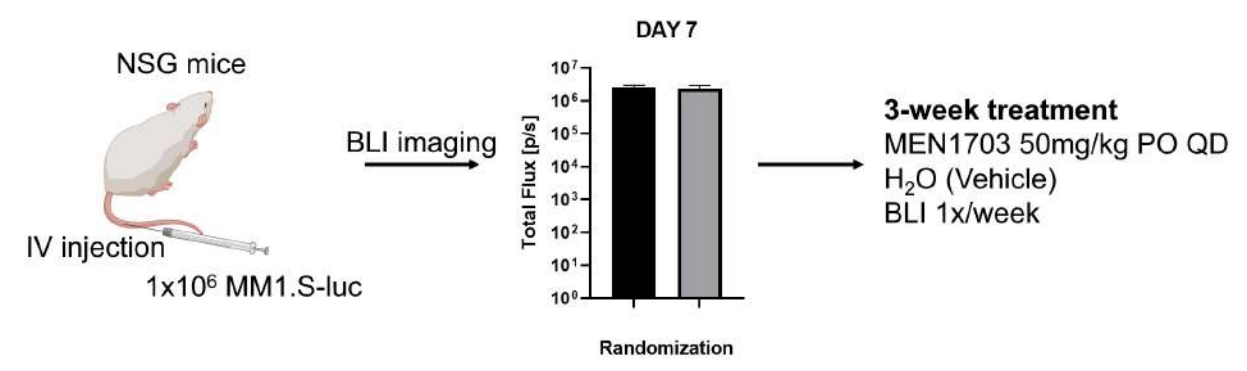
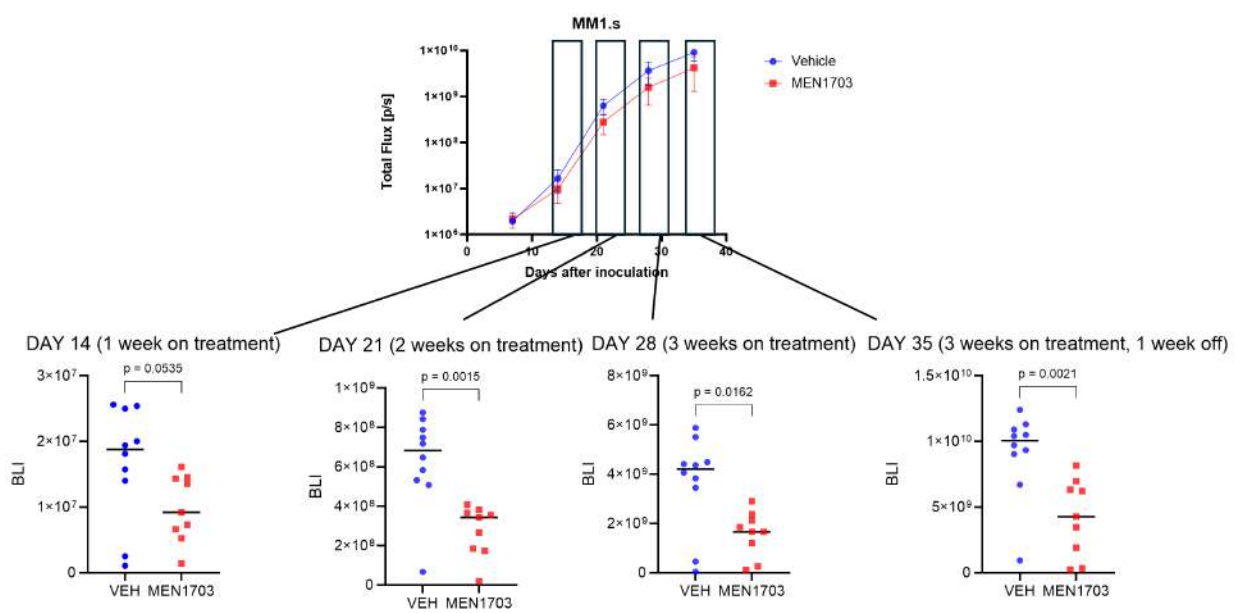


Fig. 35. *In vivo* study design to assess MEN1703 activity in MM1.S-luc model. IV - intravenous, BLI - bioluminescence, PO - *per os* (oral delivery), QD - *quaque die* (once a day).

BLI signal increased in both groups, but MEN1703-treated mice showed significantly slower tumor progression (Fig. 36). A difference in tumor burden began to emerge by day 14 (p = 0.0535), reached statistical significance by day 21 (p = 0.0015), and persisted throughout day 28 (p = 0.0162) and day 35 (p = 0.0021). These results demonstrate that MEN1703 delays MM progression *in vivo*. Notably, suppression of tumor burden was sustained even after treatment cessation, consistent with durable anti-myeloma effects. These *in vivo* data reinforce our *in vitro* findings and support the therapeutic potential of MEN1703 in MM.



**Fig. 36. MEN1703** suppresses **MM** progression *in vivo*. NSG mice were intravenously injected with 1×10<sup>6</sup> MM1.S-luc cells and randomized on day 7 based on BLI signal. Mice were treated with MEN1703 (50 mg/kg PO QD) or vehicle for 21 days. Tumor burden was monitored weekly using bioluminescence imaging. Top: BLI signal over time. Bottom: Quantified BLI signal on days 14, 21, 28, and 35. Horizontal bars represent group medians. Statistical significance determined using Mann-Whitney test. Experiment performed in collaboration with Dr. Zofia Pilch.

To validate target engagement by MEN1703 *in vivo*, we assessed phosphorylation of ribosomal protein S6 at serine 235/236. NSG mice were inoculated intravenously with 1×10<sup>6</sup> MM1.S-luc cells and randomized by BLI signal. Animals were then treated with MEN1703 (50 mg/kg PO QD) or vehicle for 3 days (Fig. 37A).

Following treatment, human MM cells were isolated from mouse bone marrow using magnetic bead-based CD138+ selection, and pS6 levels were measured by immunoblotting. MEN1703-treated mice exhibited a marked reduction in pS6 S235/236 levels compared to vehicle controls, while total S6 levels remained unchanged (Fig. 37B). Densitometric quantification confirmed a significant decrease in the ratio of pS6 to total S6 upon MEN1703 treatment (p = 0.0079) (Fig. 37C).

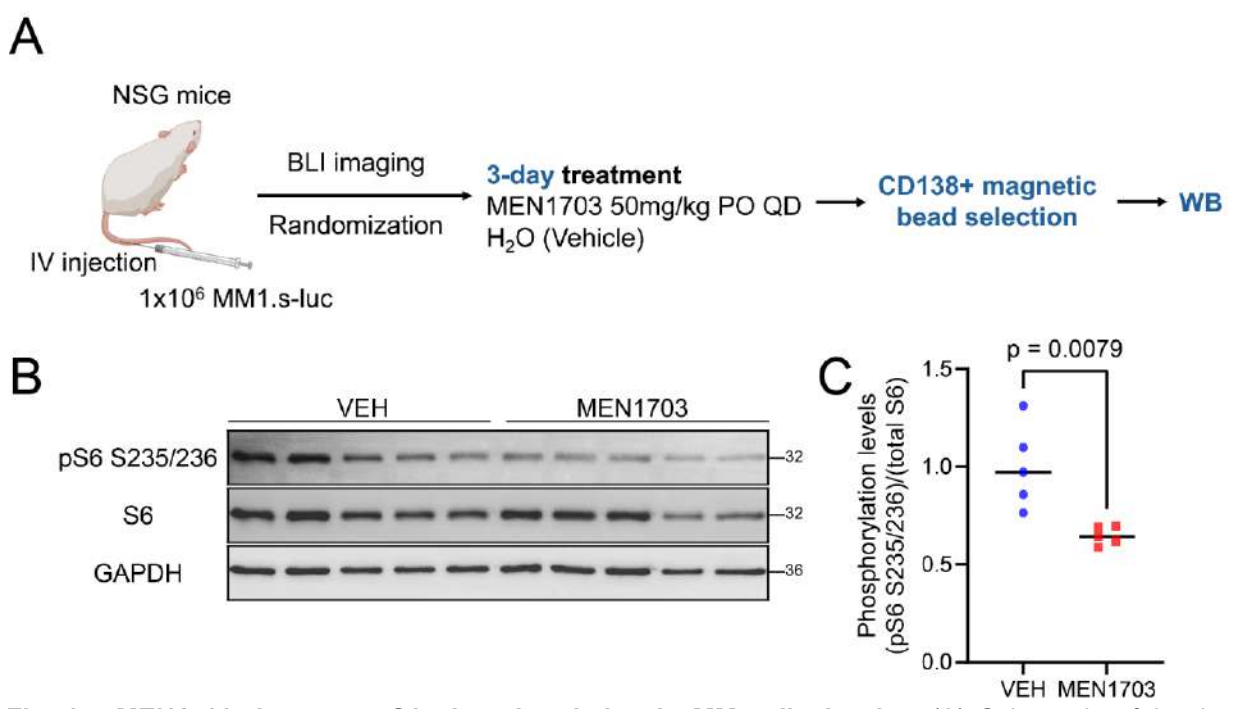


**Fig. 37. MEN1703 decreases S6 phosphorylation in MM cells** *in vivo.* (A) Schematic of *in vivo* experimental setup. (B) Western blot showing pS6 S235/236 and total S6 in vehicle- and MEN1703-treated mice. GAPDH was used as a loading control. (C) Densitometric quantification of pS6 normalized to total S6. Each point represents one mouse. Statistical significance determined using Mann-Whitney test. Experiment performed in collaboration with Drs. Zofia Pilch, Dominika Nowis and Ewa Kurtz.

These findings confirm that MEN1703 effectively engages its intracellular target *in vivo*, leading to suppression of a key PIM substrate and indicating on-target activity in MM cells growing in murine bone marrow.

# 3.7 PIM inhibition synergizes with proteasome inhibition in MM

MEN1703 primarily slowed disease progression rather than inducing MM regression. These findings suggest that PIM inhibition alone may not be sufficient for durable therapeutic responses in the clinical setting. Previous studies have reported synergy between PIM kinase and proteasome inhibitors [375]. To explore this, we treated JJN3 cells, which display lower sensitivity to bortezomib than MM1.S, with increasing concentrations of MEN1703 and bortezomib. The combinatorial treatment resulted in enhanced growth inhibition compared to either agent alone, with ZIP synergy scores reaching ~40, indicating strong synergistic interaction (Fig. 38A-B). These results support further *in vivo* testing and could guide rational design of clinical combination regimens.

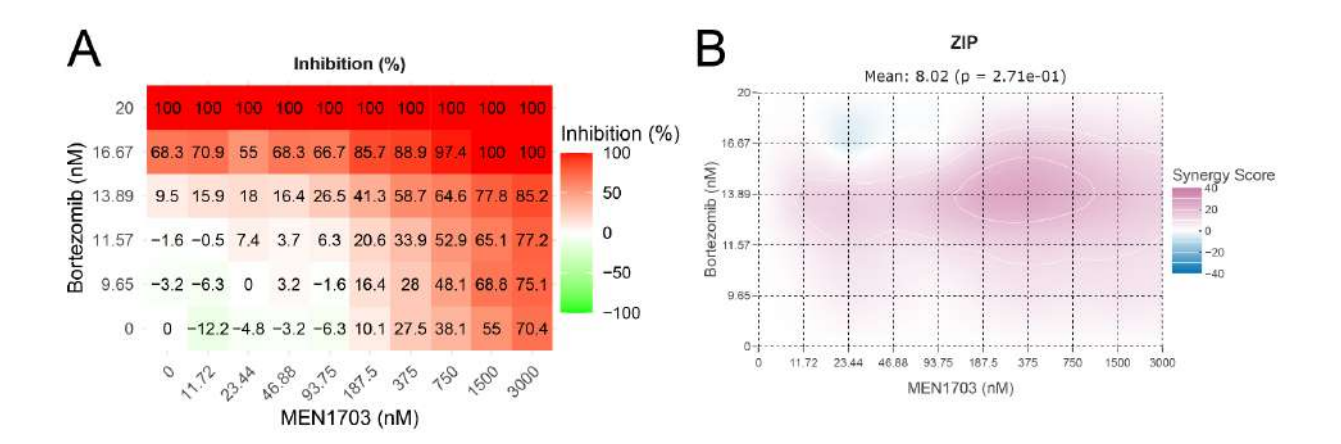


**Fig. 38. MEN1703 synergizes with bortezomib in JJN3 cells.** (A) Heatmap showing percent inhibition of JJN3 cell viability following 72 h treatment with indicated doses of MEN1703 and bortezomib. (B) ZIP synergy analysis reveals synergistic interaction across multiple dose combinations. Data were analyzed using SynergyFinder.

# 4 Functions of PIM kinases in MM microenvironment

### 4.1 Stromal expression of PIM kinases in MM bone marrow

During immunohistochemical analysis of multiple MM and HD bone marrow samples, we observed frequent expression of PIM kinases (particularly PIM3) in non-neoplastic cells adjacent to malignant plasma cells (Fig. 39).

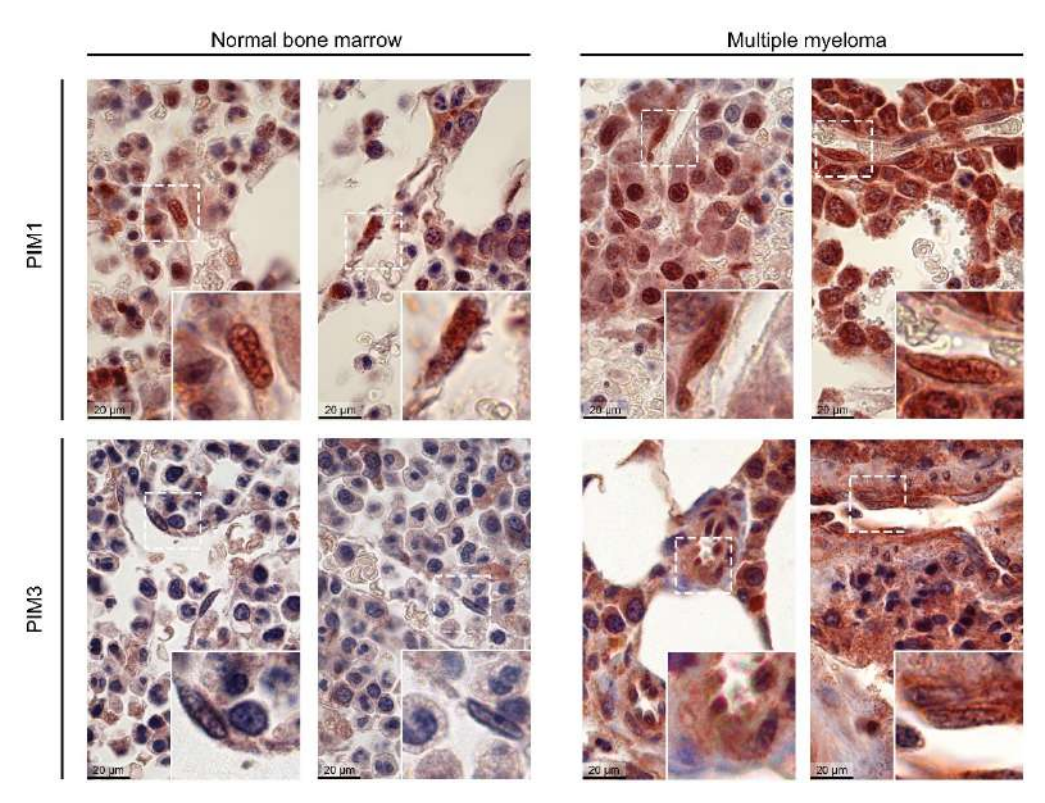
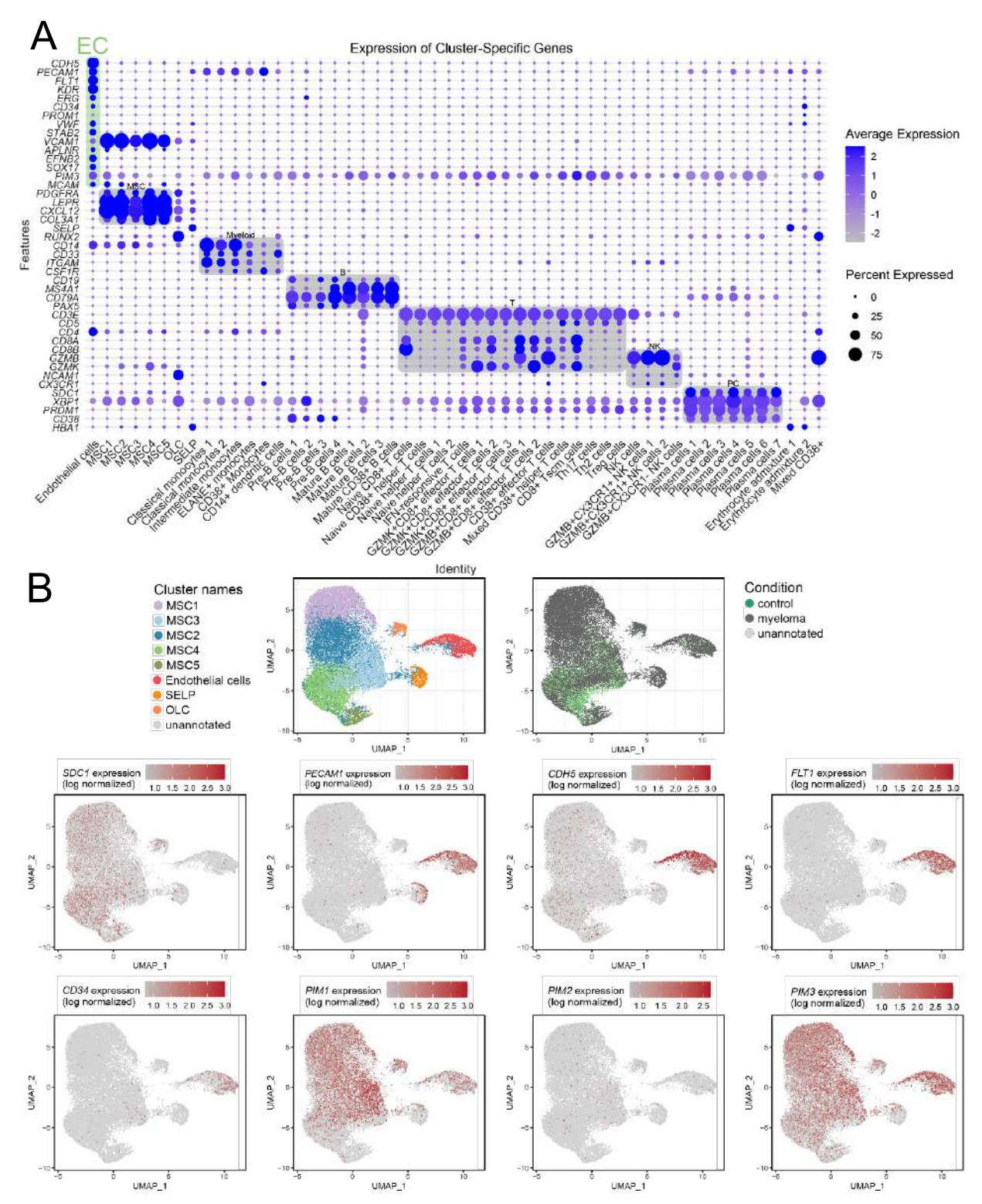


Fig. 39. PIM1 and PIM3 protein expression in non-PC bone marrow cells.

This finding aligned with our recent study of single-cell RNA-seq data [221], where *PIM3* was broadly expressed across non-MM stromal populations, in addition to MM cells (Fig. 40A). Based on the morphology and spatial distribution of these cells, we hypothesized they were of endothelial or mesenchymal origin. We therefore focused our analysis on stromal subsets within the scRNAseq dataset (Fig. 40B). *PIM1* was predominantly expressed by mesenchymal stromal cell subtype MSC2, while *PIM3* showed high expression in endothelial cells (Fig. 40B). *PIM2* transcripts were not detected (Figs. 40B, 41).



**Fig. 40.** scRNA-seq analysis of *PIM* kinase expression in the multiple myeloma (MM) microenvironment. (A) Dot plot showing the expression of *PIM3* across all major cell clusters identified in the MM microenvironment. (B) UMAP projections of the isolated stromal cell subset, showing cluster identification based on marker genes and the corresponding expression of PIM kinases. MSC, mesenchymal stromal cell; OLC, osteolineage cells; SELP, P-selectin-positive cell.

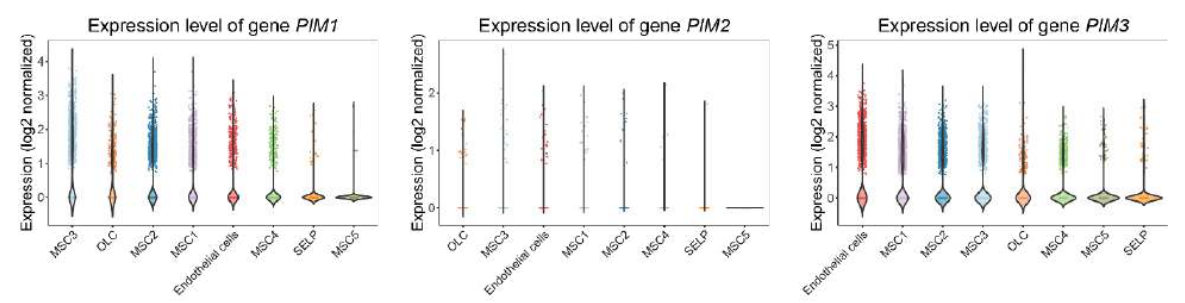
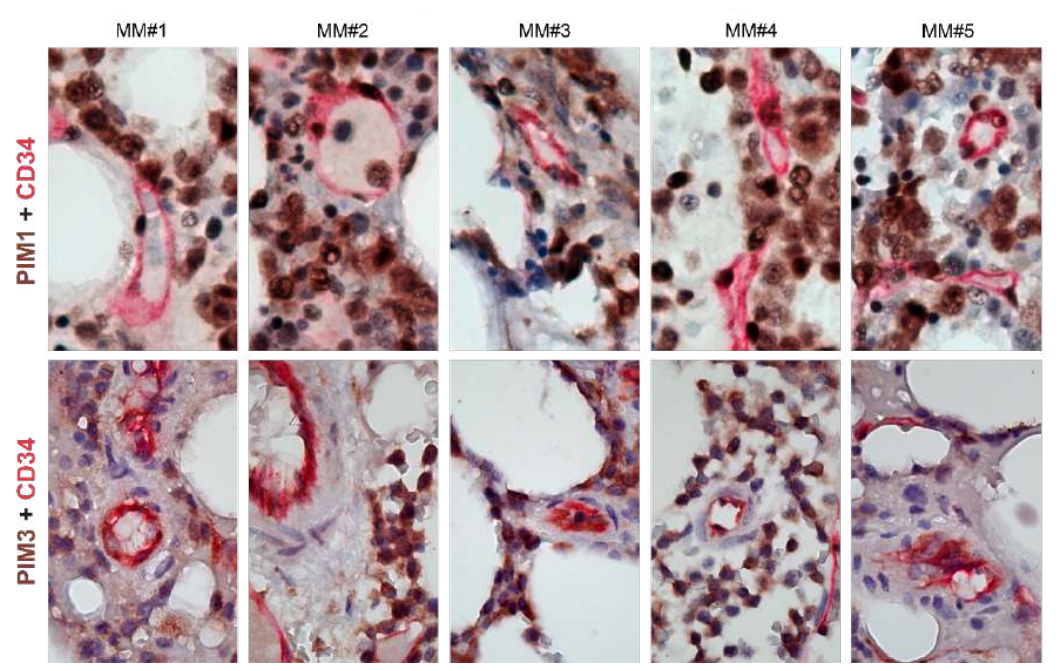


Fig. 41. Cell type-specific expression of PIM1, PIM2, and PIM3 in the MM stromal compartment.

To validate these observations, we performed double immunohistochemistry for PIM1/CD34 and PIM3/CD34 in TMAs of MM and HD BM trephine biopsies (Fig. 42). These experiments confirmed that MMECs (CD34<sup>+</sup>, pink) express high levels of PIM1 and PIM3 at the protein level, supporting a potential role for PIM kinases in the myeloma vascular niche.



**Fig. 42. PIM1 and PIM3** are highly expressed in the MM vascular niche. Dual-color immunohistochemistry (IHC) for PIM1 (brown, top row) or PIM3 (brown, bottom row) with the endothelial cell marker CD34 (pink). Representative images from five different MM patient bone marrow biopsies show strong expression of PIM1 and PIM3 protein within the CD34-positive vascular endothelium.

Prompted by these findings, we quantified PIM1, PIM2, and PIM3 protein expression in ECs in HD and MM BM samples. ECs were identified based on morphology and annotated by a board-certified pathologist. PIM3 protein expression was markedly higher in MM-associated endothelial cells compared to HD controls (Fig. 43). PIM1 was detected in both MM and HD endothelial cells at similar levels, whereas PIM2 was not highly expressed in endothelial cells from either group.

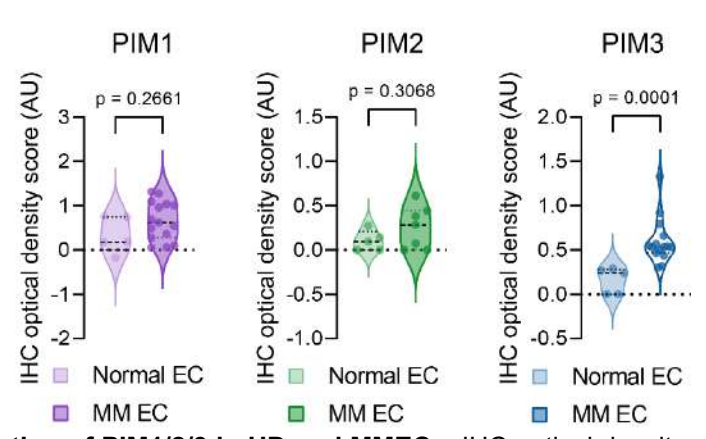


Fig. 43. IHC quantification of PIM1/2/3 in HD and MMECs. IHC optical density scores determined via IHC Profiler, quantified within regions of interest (ROIs) containing cells displaying EC morphology for each case.

### 4.2 Factors influencing PIM expression in MMECs

To investigate signals regulating PIM expression in MMECs, we used HUVEC-TERT2 (TERT2-immortalized Human Umbilical Vein Endothelial Cell), an established model for studying endothelial responses to cytokine cues and vessel formation *in vitro*. Upon stimulation with VEGFA<sub>165</sub>, a key angiogenic factor elevated in the MM microenvironment [218,224,234,376], we observed robust induction of both PIM1 and PIM3 proteins (Fig. 44). PIM1 expression increased rapidly following stimulation but declined over time, consistent with a transient early response. In contrast, PIM3 expression rose more gradually and remained sustained. These results suggest that VEGFA signaling is sufficient to drive PIM kinase expression in ECs.

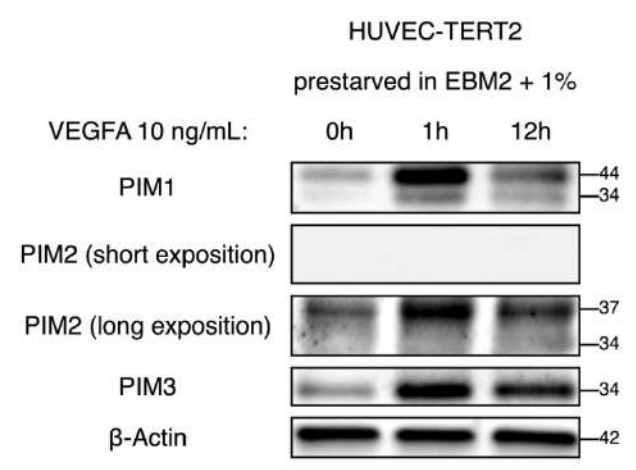


Fig. 44. The effect of VEGFA stimulation of HUVEC-TERT2 cells on PIM kinase expression. HUVEC-TERT2 cells were prestarved in EBM2 containing 1% FBS overnight (for 16 h).

PIM3 expression in HUVEC-TERT2 cells was also induced by stimulation with other proangiogenic cytokines, including FGF2, IGF1, and EGF (Fig. 45). This suggests that PIM3 induction in ECs is not limited to VEGFA signaling but represents a broader response to various angiogenic stimuli. These findings hint at an important role for PIM3 in endothelial cell activation or angiogenesis.

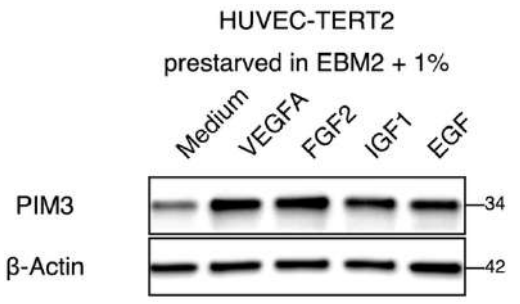
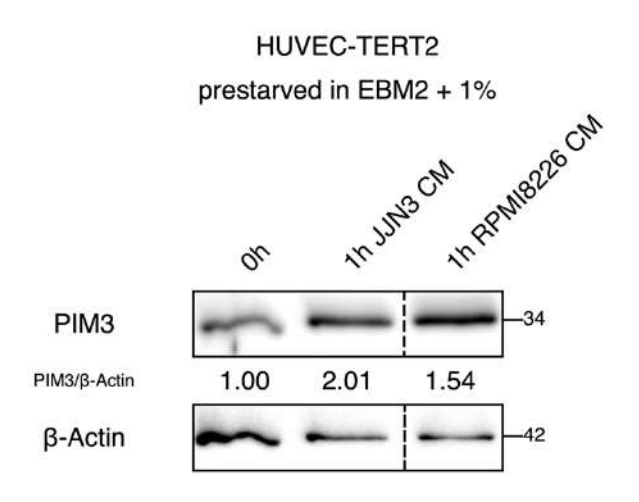


Fig. 45. PIM3 kinase expression in HUVEC-TERT2 cells stimulated with proangiogenic cytokines. Immunoblot analysis of PIM3 levels in HUVEC-TERT2 cells. The cells were prestarved in EBM2 containing 1% FBS overnight (for 16 h). Cells were stimulated for 1 hour with 10 ng/mL Vascular Endothelial Growth Factor A (VEGFA), Fibroblast Growth Factor 2 (FGF2), Insulin-like Growth Factor 1 (IGF1), or Epidermal Growth Factor (EGF). β-actin served as a loading control.

To test whether MM cells can directly induce PIM expression in endothelial cells via paracrine signaling, we stimulated HUVEC-TERT2 cells with conditioned medium (CM) collected from JJN3 and RPMI8226 MM cells, two cell lines expressing *VEGFA*. Exposure to the MM CM significantly increased PIM3 protein levels in HUVECs (Fig. 46). These findings support a model in which MM cells promote endothelial PIM3 expression through secretion of angiogenic mediators.



**Fig. 46. PIM3** protein is upregulated in **HUVEC-TERT2** cells by **MM-derived** conditioned medium **(CM)**. Western blot showing PIM3 levels in HUVEC-TERT2 cells at baseline (0h) and after 1 hour of stimulation with CM from JJN3 or RPMI8226 cells. β-actin serves as a loading control.

## 4.3 Transcriptional and functional consequences of pan-PIM inhibition in ECs

### 4.3.1 PIM kinase inhibition impairs angiogenic functions of ECs

To assess the functional relevance of PIM kinase activity in endothelial cells, we tested the effect of pan-PIM inhibition using MEN1703 at  $1.5\,\mu\text{M}$  (the same concentration previously used in MM cell assays). Treatment of HUVEC-TERT2 cells with MEN1703 led to a marked reduction in endothelial cell proliferation, migration, and their ability to form capillary-like structures in Matrigel (Fig. 47). Importantly, no MEN1703-dependent apoptosis induction was observed at the selected 24 h timepoint (Fig. 47A).

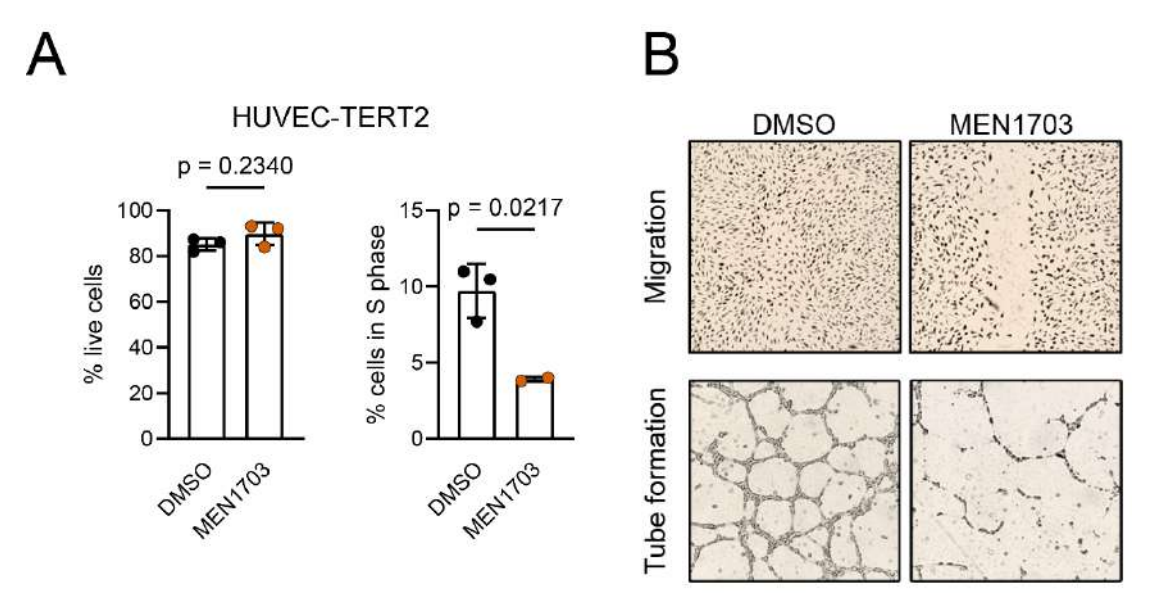


Fig. 47. MEN1703 impairs angiogenic functions of HUVEC-TERT2 endothelial cells without inducing apoptosis. HUVEC-TERT2 cells were treated with 1.5  $\mu$ M MEN1703 for 24 h to evaluate the impact of PIM kinase inhibition on endothelial cell function. Cell viability (A) was determined as described in 2.2.1.11. Cell proliferation was determined using Hoechst staining as explained in 2.2.1.21. Migration and tube formation (B) were studied as described in 2.2.1.15 and 2.2.1.16.

### 4.3.2 Transcriptomic response to PIM kinase inhibition in ECs

To investigate the transcriptional impact of pan-PIM kinase inhibition in endothelial cells, we performed bulk RNA-seq on HUVEC-TERT2 cells treated with MEN1703 (1.5  $\mu$ M) or DMSO for 24 hours. Principal component analysis (PCA) revealed a clear separation between control

and MEN1703-treated samples along the first principal component, which explained 40.6% of total variance (Fig. 48A).

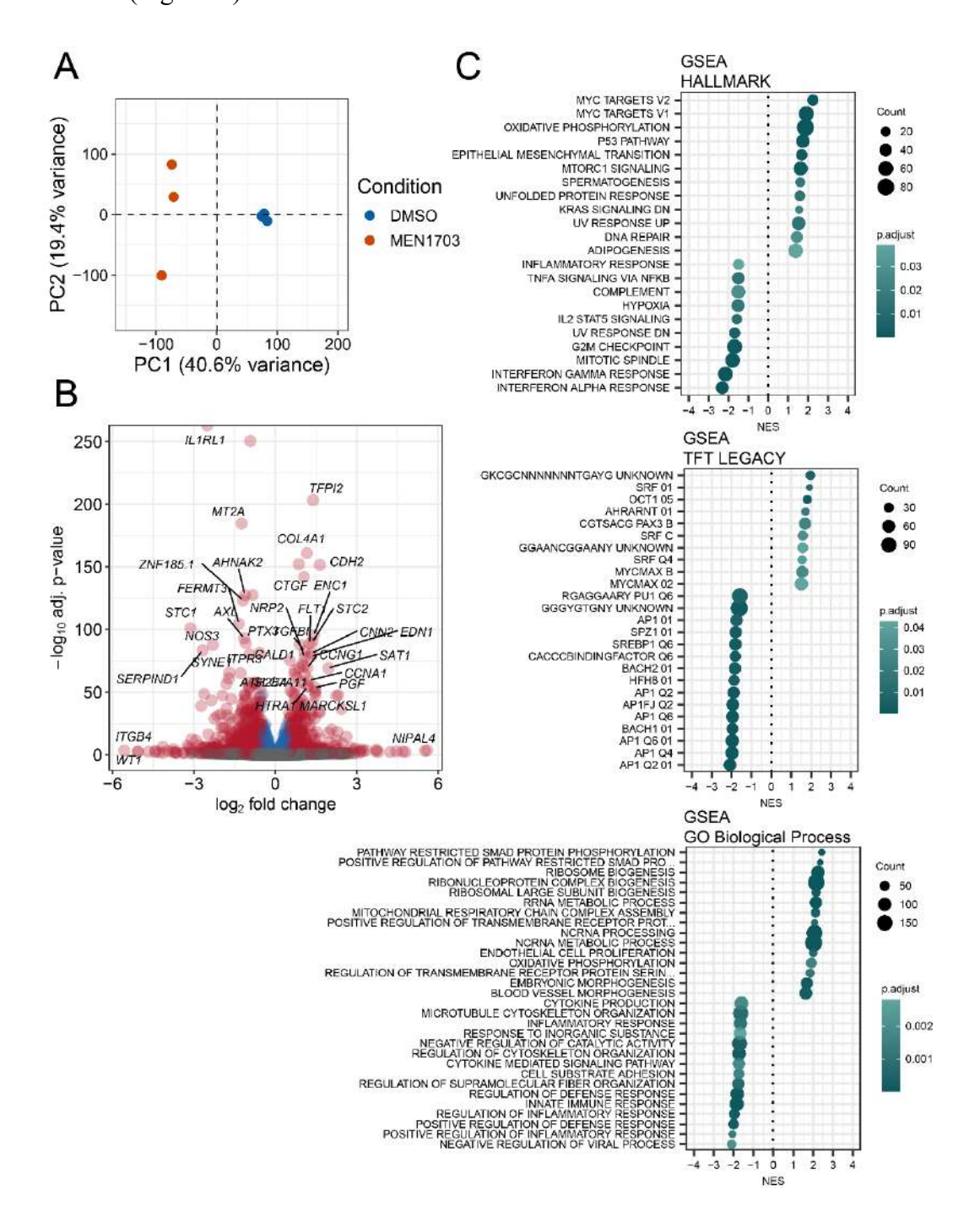


Fig. 48. Transcriptomic response to PIM kinase inhibition in HUVEC-TERT2 cells. (A) Principal component analysis (PCA) of bulk RNA-seq data from HUVEC-TERT2 cells treated with DMSO or MEN1703 (1.5  $\mu$ M, 24 h). (B) Volcano plot showing differentially expressed genes. Red dots indicate significantly differentially expressed genes with FDR < 0.05 and absolute log2 fold change > 0.5; blue dots are FDR-significant but with smaller fold changes ( $\leq$  0.5); gray dots are not statistically significant. (C) Graphical summary of Gene Set Enrichment Analysis (GSEA) showing top positively and negatively enriched pathways across four curated gene set databases. NES - Normalized Enrichment Score.

Principal component analysis showed distinct transcriptional profiles between DMSO- and MEN1703-treated endothelial cells (Fig. 48A). Differential expression analysis revealed broad gene expression changes after PIM inhibition (Fig. 48B). Transcripts linked to angiogenesis, endothelial activation, and migration, including *STC1*, *ITGB4*, and *AXL*, were among the most strongly downregulated.

Gene set enrichment analysis (GSEA) using the HALLMARK, TFT LEGACY, and GO Biological Process databases identified consistent enrichment of MYC-regulated, oxidative phosphorylation, and unfolded protein response pathways, suggesting activation of adaptive stress programs upon MEN1703 treatment (Fig. 48C). Conversely, pathways related to inflammatory signaling, cytokine responses, cell adhesion, and cytoskeletal organization were suppressed.

These findings indicate that PIM kinase inhibition disrupts transcriptional programs sustaining endothelial activation and angiogenic signaling.

### 4.3.3 MEN1703 reverses the MM-associated EC transcriptional state

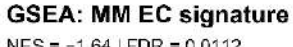
In a recent study [221], our group identified a transcriptional signature specific to MMECs, based on direct comparison with HD ECs (Table 28). This MMEC signature was defined by differential gene expression analysis using the Benjamini-Hochberg procedure for multiple testing correction, with selection criteria of log<sub>2</sub> fold change > 1 and adjusted p-value < 0.05. A total of 53 genes met these thresholds. The MMEC gene set included markers of epithelial-mesenchymal plasticity (EMP), cytoskeletal remodeling, and angiogenesis, such as *VIM*, *SERPINE1*, *EMP1*, and *STC1*.

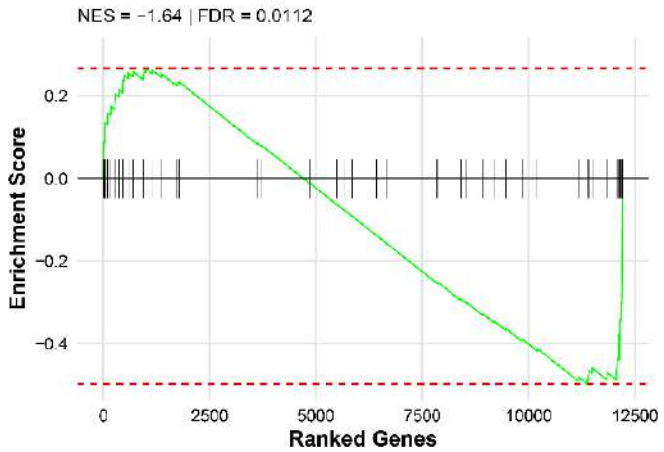
To test whether PIM inhibition could reverse this transcriptional phenotype, we used GSEA on our RNA-seq dataset described in 4.3.2. Our analysis revealed significant negative enrichment of the MMEC signature following MEN1703 treatment, indicating suppression of genes typically upregulated in MM-associated ECs (Fig. 49). This highlights a potential microenvironment-modifying effect of PIM inhibition and supports the role of PIM kinases in driving the endothelial reprogramming characteristic of MM.

Table 28. MMEC gene signature extracted from Garbicz et al. [221].

Gene	P- value	Log <sub>2</sub> fold change	Adjusted p-value
PXDC1	0.000	1.667	0.000
SERPINE1	0.000	2.836	0.001
VIM	0.000	1.833	0.002
LMNA	0.000	1.238	0.002
STC1	0.000	4.613	0.002
LUZP1	0.000	1.096	0.003
MIR4435- 2HG	0.000	1.530	0.005
EMP1	0.000	1.517	0.006
HSP90AB1	0.000	1.340	0.006
ADAMTS9	0.000	1.647	0.006
TUBB4B	0.000	1.707	0.006
ATP13A3	0.000	2.730	0.006
TUBB6	0.000	2.109	0.008
AKAP13	0.000	1.347	0.009
ATP2B1	0.000	1.234	0.010
EHD4	0.000	1.810	0.010
ITGA5	0.000	1.527	0.010
PODXL	0.000	3.008	0.010
MIR22HG	0.000	1.233	0.010
SNX9	0.000	1.426	0.013
ANXA2	0.000	1.200	0.016
EFNB1	0.000	1.646	0.016
TUBA1C	0.000	2.318	0.016
TM4SF1	0.000	1.385	0.017
NOP16	0.000	2.040	0.018

SQLE	0.000	2.107	0.018
NFATC2	0.000	1.515	0.018
PMP22	0.000	1.789	0.025
ACR	0.000	2.299	0.026
PSMD11	0.000	1.959	0.027
DDX21	0.000	1.110	0.028
SH3BGRL3	0.000	1.520	0.028
HS3ST1	0.000	2.003	0.028
PSMD12	0.000	1.465	0.029
USP12	0.000	1.724	0.030
LRRFIP2	0.000	1.377	0.031
PLPP3	0.000	1.182	0.032
ITGAV	0.000	1.256	0.033
METRNL	0.000	1.662	0.033
PLEKHM2	0.000	1.276	0.034
PGF	0.000	2.221	0.035
PSMD2	0.000	2.104	0.035
B3GNT5	0.000	1.825	0.040
PNP	0.000	1.217	0.041
FJX1	0.000	2.267	0.041
COL4A1	0.000	1.718	0.042
ARPC5L	0.000	1.033	0.044
SRP14	0.000	1.081	0.045
MSN	0.001	1.298	0.047
MYADM	0.001	1.366	0.047
SLK	0.001	1.545	0.049
NUTF2	0.001	1.247	0.050
CD276	0.001	1.475	0.050





**Fig. 49. PIM inhibition with MEN1703 reverses the MMEC transcriptional signature.** GSEA plot showing a significant negative enrichment of the "MMEC signature" gene set in endothelial cells following treatment with MEN1703.

### 4.3.4 PIM inhibition disrupts actin cytoskeletal architecture in ECs

To validate the transcriptional evidence pointing to cytoskeletal remodeling and impaired endothelial activation upon PIM inhibition, we performed a series of orthogonal functional assays in HUVEC-TERT2 cells treated with MEN1703 for 24 hours (Fig. 50).

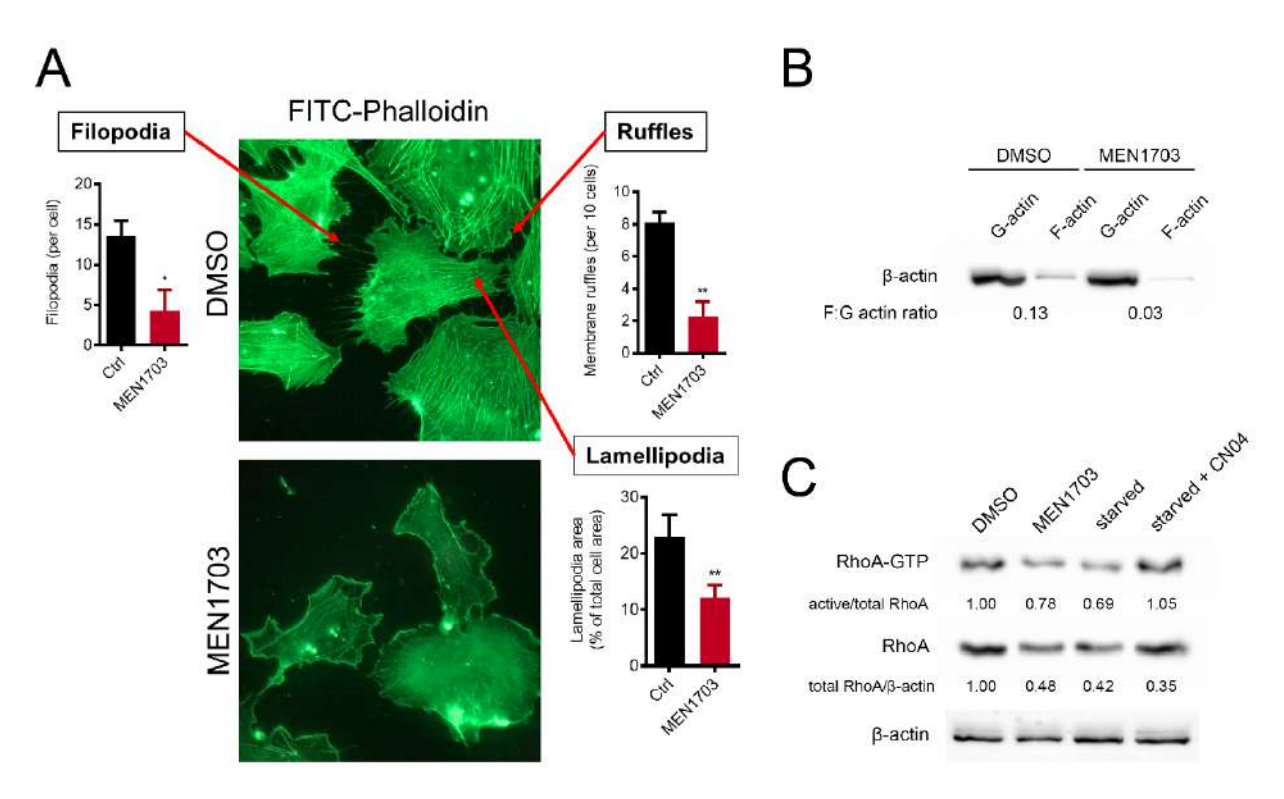


**Fig. 50. PIM** inhibition disrupts actin cytoskeletal architecture and RhoA signaling in endothelial cells. (A) Representative FITC-phalloidin staining of HUVEC-TERT2 cells treated with DMSO or MEN1703 (1.5 μM, 24 h). Quantification of filopodia (per cell), membrane ruffles (per 10 cells), and lamellipodia area (as % of total cell area). (B) F-/G-actin fractionation assay. Western blot of actin in polymerized (F-actin) and monomeric (G-actin) fractions from HUVEC-TERT2 cells treated with DMSO or MEN1703. (C) RhoA activity assay. GTP-bound (active) RhoA levels were assessed by pulldown and western blot. Starvation and CN04 (RhoA activator) were used as negative and positive controls, respectively. Densitometric quantification of active/total and total/ $\beta$ -actin RhoA ratios is shown below the bands.

Phalloidin staining (Fig. 50A) revealed a striking loss of organized actin structures in PIM-inhibited cells compared to DMSO controls. In untreated cells, prominent stress fibers, membrane ruffles, and lamellipodia were observed. In contrast, MEN1703-treated ECs displayed diffuse cortical actin staining and lacked well-defined F-actin stress fibers and protrusive structures. These changes suggest disrupted actin polymerization and cytoskeletal contractility.

To quantify these observations biochemically, we performed F/G-actin fractionation assays. PIM inhibitor-treated cells showed a decreased F-actin to G-actin ratio, confirming a shift toward monomeric actin (Fig. 50B). Finally, to probe the upstream signaling events involved in actin remodeling, we assessed the activity of RhoA, a small GTPase that plays a central role in regulating stress fiber formation and endothelial barrier function [377]. Using a GTP-RhoA pulldown assay, we found that MEN1703 treatment markedly reduced levels of active (GTP-bound) RhoA (Fig. 50C). These changes suggest that PIM kinase activity may support RhoA-mediated cytoskeletal signaling, either directly or via upstream regulatory nodes. Taken together, these data provide mechanistic support for the role of PIM kinases in maintaining actin cytoskeletal integrity in endothelial cells.

### 4.4 Establishment of BM EC isolation and culture conditions

To create a patient-relevant *ex vivo* model for studying the MM vascular niche, we developed and optimized a protocol to reliably isolate and culture both early outgrowth endothelial cells (EOCs) and mature endothelial cells (ECs) from bone marrow aspirates of MM patients and HD (Fig. 51A). The full protocol is described in the Materials and Methods section (2.2.1.8). To assess their angiogenic potential, tube formation assays in Matrigel were performed (Fig. 51B). The BMEC60 cell line and two MM-derived EC populations (MMEC1 and MMEC2) showed robust tube formation with characteristic tip cell-like structures (Fig. 51C), confirming functional endothelial identity. In contrast, bone marrow stromal cell cultures (BMSC1 and BMSC2) exhibited minimal tube formation. Flow cytometry further validated the endothelial phenotype, since the cells expressed high surface levels of CD31, VEGFR1, and CD144 (VE-cadherin) (Fig. 51D). These results confirm both the purity and angiogenic competence of the isolated MM endothelial cells.

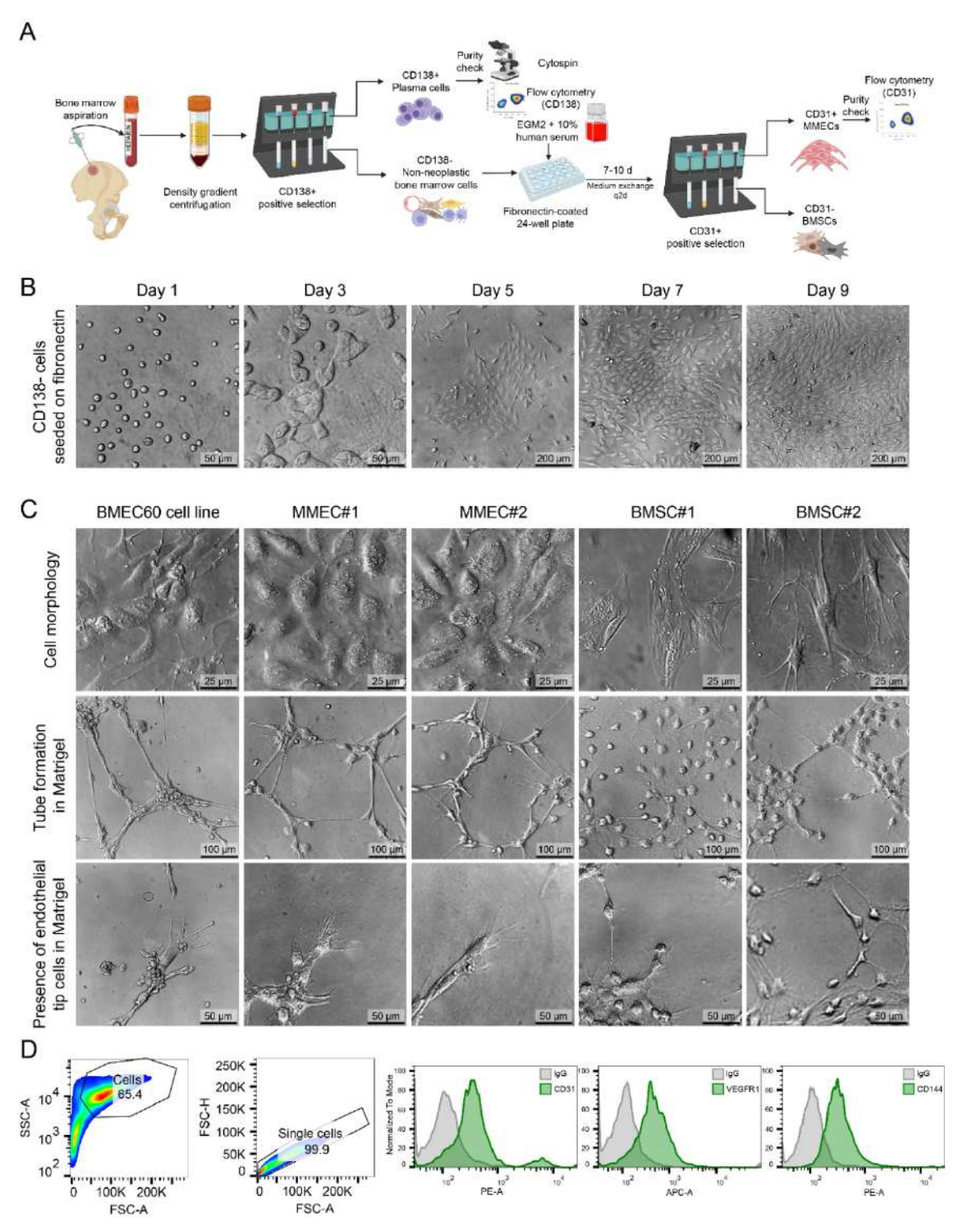


Fig. 51. Isolation and characterization of endothelial progenitor cells (EPCs) and mature endothelial cells (ECs) from bone marrow of MM patients. (A) Schematic workflow depicting the isolation of BM ECs. (B) Bright-field images showing morphological changes of CD138<sup>-</sup> bone marrow cells over a 9-day culture period, culminating in the formation of a cobblestone-like monolayer consistent with endothelial phenotype. (C) Bright-field images of BMEC60, MMEC1, MMEC2, and stromal cells BMSC1, BMSC2 in Matrigel tube formation assays. MMECs and BMEC60 formed organized tube networks with tip cell-like extensions, while BMSCs showed low angiogenic activity. (D) Flow cytometry data showing gating strategy and expression of endothelial markers CD31, VEGFR1, and CD144 (VEcadherin) compared to IgG controls, confirming endothelial identity.

To determine whether the cultured MM-derived ECs resemble *in situ* bone marrow ECs from MM patients, we analyzed the expression of a selected gene panel by real-time quantitative PCR (Fig. 52A). RNA was isolated from EOCs emerging by day 5 of culture on fibronectin-coated plates, as well as from magnetically enriched mature endothelial cells (CD31<sup>+</sup>) and the remaining CD31<sup>-</sup> mesenchymal fraction. Two endothelial cell lines (BMEC60 and HUVEC) served as positive controls.

EOCs displayed high expression of PTPRC (encoding CD45), while PTPRC expression was nearly absent in the CD31<sup>+</sup> and CD31<sup>-</sup> fractions, consistent with the presence of very early endothelial progenitor cells (EPCs) [378]. Both EOCs and CD31<sup>+</sup> cells expressed key endothelial markers including CD34, PECAMI (CD31), CDH5 (VE-cadherin), FLT1, and KDR (VEGFR2), with a trend towards lower expression levels in the respective CD31<sup>-</sup> populations. PROMI (CD133), a marker of endothelial progenitors [379–381], was significantly enriched in EOCs compared to both CD31<sup>+</sup> and CD31<sup>-</sup> cells (Mann-Whitney test, p < 0.0001). Furthermore, both EOCs and CD31<sup>+</sup> cells expressed transcripts characteristic of bone marrow EC subtypes: type H EC genes (APLNR, EFNB2, SOX17, FLT1) and type L EC markers (STAB2, VCAMI) [382]. To assess their functional relevance, we tested whether these ECs support MM cell survival and proliferation  $ex\ vivo$  (Fig. 52B). While CD138<sup>+</sup> MM cells failed to expand in basal medium alone, conditioned media from MM-derived CD31<sup>+</sup> ECs, BMEC60 cells, and CD31<sup>-</sup> stromal cells (positive control) supported MM cell growth (p < 0.001).

### 4.5 Investigation of MM-EC crosstalk in vitro

To investigate the molecular mechanisms underlying the support provided by endothelial cells to MM cells, we analyzed the effect of BMEC60-derived CM on key signaling pathways in MM1.S cells. MM1.S were prestarved in OptiMEM for 24 h before stimulation. MM cells were exposed to CM collected from BMEC60 endothelial cells after either 12 hours or 3 days of culture, and lysates were analyzed by western blot following 1- and 6-hour incubations (Fig. 53). Exposure to BMEC60 CM resulted in marked upregulation of PIM2 expression and MAPK pathway activity. In contrast, we have observed no activation of PI3K/AKT, suggesting that PIM2 induction may occur independently of PI3K/AKT/mTOR survival signaling.

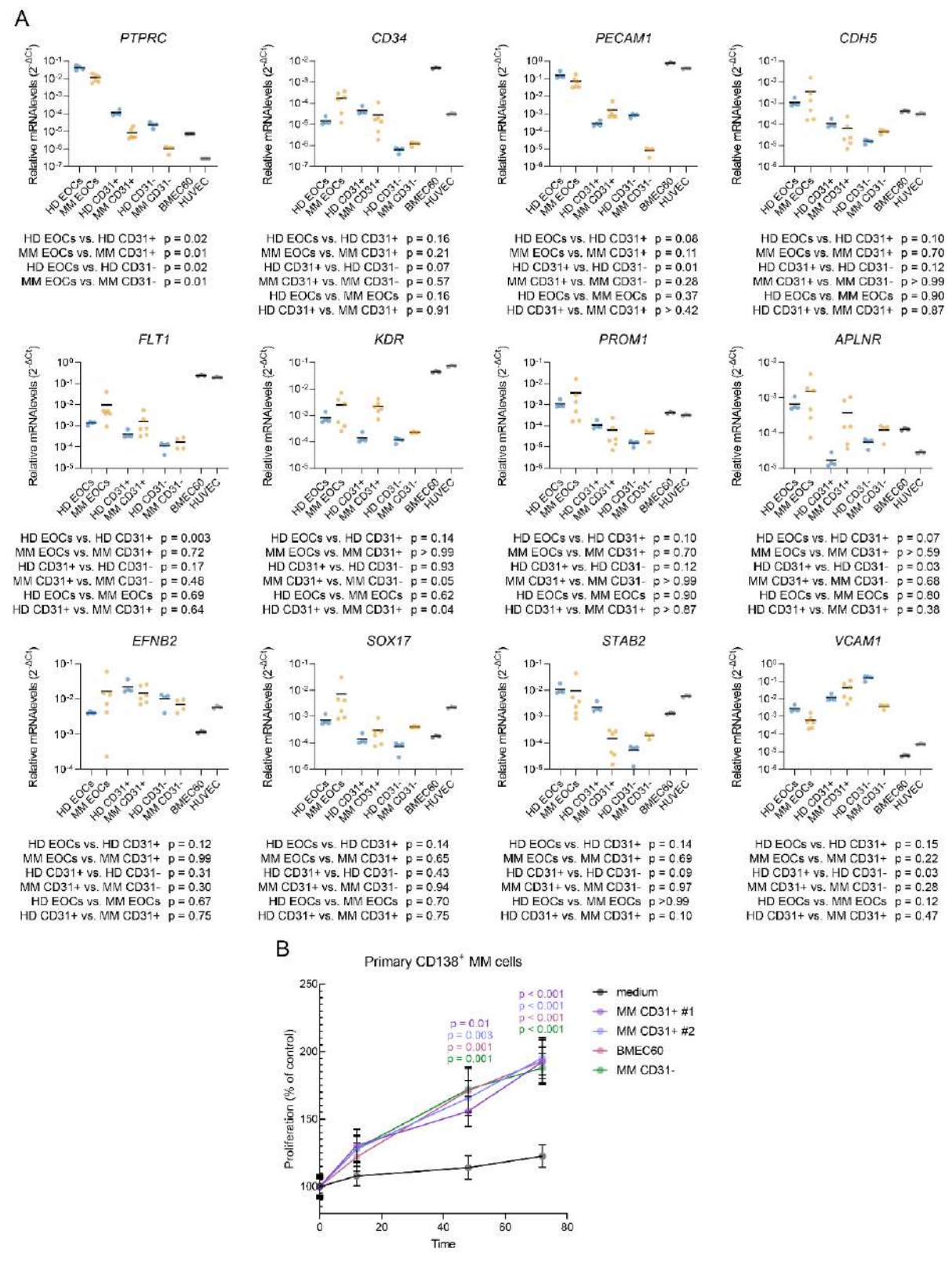
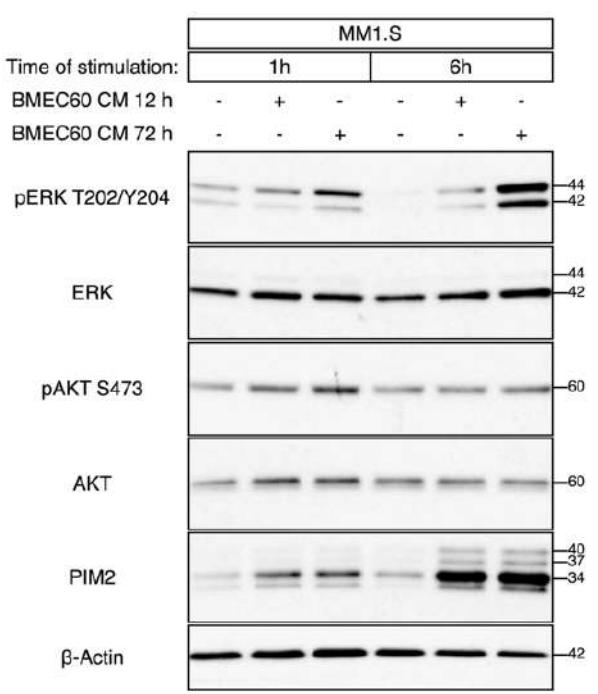


Fig. 52. Characterization of endothelial and stromal cell populations and their influence on MM cell proliferation. (A) qPCR analysis of endothelial and mesenchymal marker expression across HD-and MM-derived early outgrowth cells (EOCs), CD31<sup>+</sup> and CD31<sup>-</sup> fractions, and endothelial cell lines. (B) Proliferation of primary CD138<sup>+</sup> MM cells cultured with conditioned media from MM CD31<sup>+</sup> cells, MM CD31<sup>-</sup> cells, and BMEC60. Proliferation measured at 12, 48, and 72 hours.



**Fig. 53. BMEC-derived conditioned media induces PIM2 expression in MM1.S cells.** Western blot analysis of MM1.S cells prestarved in OptiMEM for 72 h and stimulated with conditioned media (CM) from BMEC60 endothelial cells for 1 h or 6 h. CM was collected from BMEC60 cells after either 12 h or 3 days of culture, as indicated.

Given the observed upregulation of PIM2 in MM1.S cells following stimulation with BMEC-derived conditioned media, we hypothesized that PIM kinases may be critical effectors of the paracrine prosurvival signals released by MM endothelial cells. To test this, we assessed whether pharmacologic inhibition of PIM kinases using MEN1703 could abrogate the protective effect of MMEC-derived CM on MM cell viability. Primary CD138+ MM cells were cultured for 48 h in the presence of either OptiMEM or MMEC-CM (diluted 1:1 with OptiMEM), with either MEN1703 or DMSO added at the time of seeding. Treatment with MEN1703 significantly reduced MM cell survival compared to DMSO-treated controls, indicating that the paracrine support conferred by endothelial-derived soluble factors is at least partially PIM-dependent.

#### Primary CD138<sup>+</sup> (48 h)

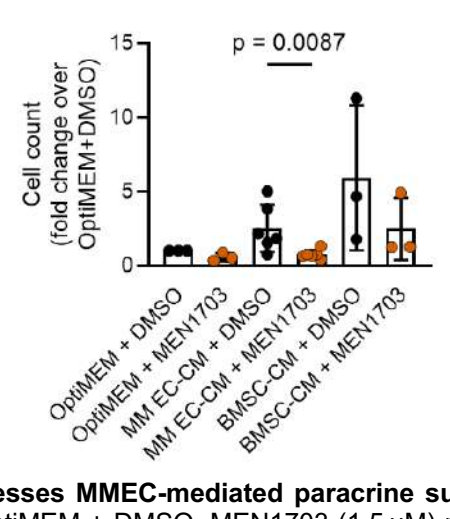


Fig. 54. PIM inhibition suppresses MMEC-mediated paracrine support of MM cell survival. Cell count was normalized to the OptiMEM + DMSO. MEN1703 (1.5  $\mu$ M) reduced MM cell count in MMEC-CM compared to DMSO (p = 0.0087, Mann-Whitney test). Each dot represents one biological replicate; bars show mean  $\pm$  SD.

## 5 Conclusions

## 5.1 Main results

The overarching goal of this thesis was to define how PIM kinases support the biology of multiple myeloma (MM) at two levels:

- 1. **Tumor-intrinsic:** how PIM kinases sustain malignant plasma cell survival and proliferation.
- 2. **Tumor-extrinsic:** how PIM kinases in the bone marrow (BM) niche, especially in endothelial cells (ECs), contribute to a microenvironment that supports MM survival.

The work demonstrates that PIM kinases are important nodes linking oncogenic transcription (MYC/E2F axis), anabolic output (mTOR/S6), stress management (DNA repair), and vascular support (endothelial activation and cytoskeletal dynamics). This dual role spans both MM cells themselves and the MM-associated vasculature and therefore presents a promising therapeutic opportunity.

### **5.1.1 PIMs in MM**

First, at the tumor-intrinsic level, we demonstrated that all three PIM paralogs (PIM1, PIM2, and PIM3) are upregulated in MM. Analysis of large-scale transcriptomic datasets from primary MM samples and MM cell lines revealed that *PIM2* is the most abundantly expressed paralog (Fig. 11). Compared to normal plasma cells, *PIMs* were significantly overexpressed in MM samples across independent datasets. Single-cell RNA-seq data confirmed *PIM2* enrichment in malignant plasma cells and implicated PIM kinases in disease progression, particularly in advanced MM stages (Fig. 12). Importantly, we conducted, to our knowledge, the first independent study assessing PIM1/2/3 protein expression in tissue microarrays of MM and HD bone marrow samples (Fig. 15). This analysis validated transcriptomic data and revealed the subcellular localization of PIM kinases *in situ* within malignant plasma cells.

CRISPR/Cas9 dependency analyses across MM cell lines identified *PIM2* as one of the strongest and most selective myeloma vulnerabilities, with a dependency profile comparable to core MM oncogenes such as *MYC* and *IRF4*. Notably, this dependency is unusually specific to myeloma relative to other hematologic malignancies (Fig. 8).

Consistent with its functional importance, high expression of *PIM1*, *PIM2*, and *PIM3* in patient samples correlates with inferior overall survival (OS) and progression-free survival (PFS), and *PIM2* and *PIM3* remain independent predictors of poor OS in multivariate Cox regression even after adjustment for established MM risk factors (Fig. 16-17).

Mechanistically, we identified a specific epigenetic mechanism for *PIM2* overexpression: its association with the acquisition of super-enhancers in malignant plasma cells, regulatory structures absent in their normal counterparts (Fig. 18-19). We further provide evidence for BRD4-dependent control, as BET bromodomain inhibition with JQ1 significantly downregulated *PIM2* (and, to a lesser degree, *PIM1* and *PIM3*), which is characteristic of super-enhancer-driven genes (Fig. 20).

We next examined the *in vitro* effects of PIM kinase inhibition across a panel of established MM cell lines (Fig. 21). Five pan-PIM inhibitors were evaluated: MEN1703, INCB053914, PIM447, AZD1208, and SGI1776. MEN1703 and INCB053914 showed the greatest potency, with submicromolar GI<sub>50</sub> values in several MM cell lines. Drug response varied across genetic backgrounds, with moderately reduced sensitivity to MEN1703 observed in MAF- or FGFR3-translocated lines. On the other hand, CCND1-translocated cell lines exhibited increased MEN1703 sensitivity. Notably, MEN1703 efficacy did not correlate with FLT3 expression, excluding this kinase as a potential secondary target of MEN1703 in MM (Fig. 22).

Time-course analysis revealed that MEN1703 induced a sustained anti-proliferative effect in MM cell lines over 12 days, with no evidence of resistance or rebound growth (Fig. 27). In contrast, PIM447 failed to durably suppress proliferation. Pharmacologic inhibition with MEN1703 induced robust apoptosis in MM cell lines, with increased Annexin V positivity, caspase 3/7, 8, and 9 activation, and PARP cleavage (Fig. 24-25).

We validated these findings in primary patient-derived MM cells. Treatment with MEN1703 selectively induced apoptosis in CD138<sup>+</sup> malignant plasma cells while sparing non-malignant

CD138<sup>-</sup> bone marrow cells (Fig. 26). Notably, MEN1703 retained its pro-apoptotic effects in co-culture with bone marrow stromal cells, indicating its ability to overcome microenvironment-mediated resistance. Apoptosis induction was further confirmed by caspase-3/7 activity assays. In contrast, PIM447 showed minimal efficacy when applied to the same primary samples in parallel.

Genetically, doxycycline-inducible shRNA knockdown showed that PIM2 is the major driver of MM cell proliferation and S6 phosphorylation, whereas PIM1 and PIM3 have weaker individual effects (Fig. 29). However, simultaneous knockdown of *PIM1/2/3* (sh3xPIM) produces a far stronger cytostatic and cytotoxic effect, suppressing proliferation to ~25% of control by day 9 and increasing cell death (Fig. 30). This indicates functional redundancy among PIM paralogs and suggests that full therapeutic benefit likely requires pan-PIM imhibition.

Mechanistically, MEN1703 disrupted multiple oncogenic transcriptional programs. Bulk RNA-seq in MM1.S cells revealed robust downregulation of MYC and E2F targets, DNA replication and repair genes, and ribosome biogenesis pathways (Fig. 31). Upregulated pathways included p53 signaling, FOXO targets, and inflammatory responses. Western blotting confirmed reduced MYC and E2F1 protein levels as well as phosphorylation of ribosomal protein S6 (Ser235/236), a direct downstream substrate of PIMs, confirming target engagement and inhibition of mTOR-dependent protein synthesis pathway (Fig. 32).

MEN1703 also drives accumulation of DNA damage and represses multiple DNA repair modules, including mismatch repair, Fanconi anemia pathway, base excision repair, and PARP1-associated replication stress responses (Fig. 33). A comet assay in JJN3 cells showed increased DNA fragmentation after treatment, indicating accumulation of DNA strand breaks (Fig. 34).

*In vivo*, MEN1703 delayed MM progression in a disseminated luciferase-labeled xenograft model in NSG mice (Fig. 36). Mice treated with 50 mg/kg MEN1703 daily exhibited significantly lower tumor burden by bioluminescence imaging. Phospho-S6 levels were reduced in CD138<sup>+</sup> MM cells harvested from bone marrow of treated animals, confirming on-target activity (Fig. 37). Tumor suppression persisted even after treatment cessation, although the efficacy of MEN1703 as single agent was moderate.

Finally, MEN1703 synergized with bortezomib in *in vitro* cytotoxicity assays (Fig. 38). Combination treatment enhanced growth inhibition in JJN3 cells. These results suggest that dual inhibition of PIM and proteasome activity could be clinically relevant.

### 5.1.2 PIMs in ECs

This thesis extends the role of PIM kinases beyond MM cells and into the tumor microenvironment, with a focus on the vascular niche. MM-associated endothelial cells (MMECs) are functionally distinct from their healthy counterparts, exhibiting enhanced angiogenic capacity, abnormal inflammatory and EMT (epithelial-mesenchymal transition) gene expression patterns, and active support of cancer cell survival [221]. Immunohistochemical (IHC) studies showed that PIM1 and PIM3 are strongly expressed in MMECs, as demonstrated by double IHCs for PIM1/CD34 and PIM3/CD34 on MM marrow biopsies (Fig. 42-43).

Mechanistically, PIM expression in ECs is dynamic and responsive to angiogenic cues. Stimulation of ECs with pro-angiogenic cytokines such as VEGFA or FGF2 increased PIM3 protein levels (Fig. 45), and conditioned medium from MM cells similarly induced PIM3 in HUVEC-TERT2 cells (Fig. 46), implicating myeloma-derived soluble factors in endothelial PIM activation.

Functionally, PIM kinases were essential for EC angiogenic activity. Inhibition with MEN1703 impaired capillary tube formation and disrupted F-actin architecture, suggesting a role in cytoskeletal remodeling and EC motility (Fig. 47). This was linked with decreased F-actin/G-actin ratio and lower RhoA GTPase activity in MEN1703-treated cells (Fig. 50). These changes imply impaired motility and barrier remodeling, which are required for sprouting angiogenesis and endothelial-mediated trafficking of tumor-supportive factors. Transcriptomic profiling of MEN1703-treated ECs showed downregulation of genes involved in angiogenesis, endothelial activation, adhesion, and cytokine/inflammatory signaling, alongside induction of stress response programs such as unfolded protein response and oxidative phosphorylation (Fig. 48). MEN1703 also reversed a MMEC-specific transcriptional signature, indicating that PIM inhibition could "de-program" the tumor/cytokine-activated endothelium (Fig. 49).

We also demonstrated that MMECs exert a prosurvival effect on MM cells via secreted factors (Fig. 53-54). This paracrine support was blocked by PIM kinase inhibition, suggesting that PIM activity in ECs is required to maintain a tumor-promoting microenvironment and EC-MM crosstalk.

## 5.2 Impact

This work enhances our understanding of the role of PIM kinases in MM by demonstrating their essential contribution to both tumor-intrinsic survival and microenvironmental support.

For the first time, PIM1/2/3 protein expression was independently validated in tissue microarrays of MM and healthy donor bone marrow (Fig. 15). This confirmed earlier transcriptomic findings and revealed spatial localization of PIMs within malignant plasma cells. Notably, their expression was largely restricted to plasma cells (both normal and malignant) providing a strong rationale for therapeutic targeting and suggesting a favorable therapeutic window. This alone has clinical implications: it points to PIM levels (especially PIM2 and PIM3) as potential biomarkers for high-risk disease and as rational guides in patient stratification for PIM-targeted therapies.

Our findings support further clinical development of MEN1703. This potent pan-PIM inhibitor consistently outperformed other clinical-stage compounds in preclinical MM models. MEN1703 selectively induced apoptosis in primary patient-derived MM cells while sparing non-malignant counterparts and remained effective even in stromal co-cultures, suggesting it can overcome microenvironmental resistance (Fig. 26). Notably, MEN1703 showed increased sensitivity in *CCND1*-translocated MM and in cases with high MYC/E2F1 transcriptional activity (Fig. 21, 23). These associations warrant mechanistic validation and testing across a broader cell line panel. Such efforts may guide biomarker-driven clinical trials and enable precision use of MEN1703 in MM [383]. The observed synergy with bortezomib (Fig. 38) strongly supports combination strategies that exploit protein homeostasis, translation, and DNA repair.

This is the first study to perform inducible, simultaneous silencing of all three PIM kinases (*PIM1*, *PIM2*, and *PIM3*) in MM cells, enabling both short- and long-term time-course experiments (Fig. 30). This genetic tool helps distinguish true on-target effects of PIM inhibition from potential off-target activities of small molecules (including MEN1703), and it will be useful

for dissecting paralog redundancy, kinase-independent PIM functions, and adaptive resistance mechanisms. In JJN3 cells - completely resistant to PIM447 and most other pan-PIM inhibitors - sh3xPIM partially recapitulated the cytotoxic effects observed with MEN1703, suggesting that PIM inhibition alone is sufficient to impair survival in these otherwise refractory cells. While this does not exclude the possibility that MEN1703 has additional off-target effects contributing to its superior efficacy, the genetic data support a substantial on-target component. These findings open the door to further studies investigating how MEN1703 differs functionally from other pan-PIM inhibitors like PIM447. It has been previously proposed that PIM kinases may also exert kinase-independent functions, and that ATP-competitive inhibitors can stabilize their targets, paradoxically enhancing non-catalytic activity [384]. This phenomenon has fueled interest in developing PIM-targeting proteolysis-targeting chimeras (PROTACs). Future work exploring MEN1703-like compounds or PROTAC-based PIM degraders may offer a promising path toward more complete functional inhibition of this pathway [385].

Mechanistic insights revealed that MEN1703 disrupts MYC- and E2F1-driven transcriptional programs, impairs mTOR activity, and suppresses multiple DNA repair pathways (Fig. 31-34). These effects were durable, with treatment leading to prolonged tumor suppression in mouse models, even after drug dosing cessation (Fig. 36). Furthermore, combination therapy with bortezomib resulted in synergy, pointing to the clinical potential of combined therapy. It will be insightful to test whether MEN1703 synergizes with other standards of care used for MM treatment, as well as novel inhibitors targeting DNA repair, MYC or PI3K/AKT/mTOR.

A major advance of this study is the demonstration that PIM kinases are not only crucial for MM cell survival but also for maintaining a tumor-supportive vascular niche. MEN1703 impaired angiogenic function of MMECs, reversed their pro-angiogenic transcriptional state, and blocked paracrine support for MM cells. These findings highlight a dual mechanism of therapeutic action: targeting both the malignant clone and its microenvironment.

Beyond cancer, PIM kinases (particularly PIM3) may play important roles in vascular diseases such as diabetes, hypertension, atherosclerosis, hemangiomas, and neovascular eye diseases like wet age-related macular degeneration. Their function in ECs remains incompletely understood. Identifying PIM interaction partners in ECs and dissecting their impact on actin cytoskeleton dynamics could provide novel biological insights. An *in vivo* conditional PIM3 knockout using

a VE-Cadherin-Cre driver would be a valuable tool to study endothelial-specific roles in physiology and pathology, however no such strain has been generated yet.

Together, these results provide a compelling rationale for the clinical advancement of potent, selective PIM inhibitors like MEN1703 in MM.

## 5.3 Discussion

Our data show that all three *PIM* paralogs are overexpressed in MM, with *PIM2* consistently the most abundant. This aligns with prior studies showing PIM2 upregulation in malignant plasma cells and its induction by bone marrow cytokines such as IL-6, BAFF, and APRIL via the JAK/STAT and NF-κB pathways [302,386,387]. PIM2's anti-apoptotic function through phosphorylation of BAD and stabilization of BCL2 family proteins is well established [388]. Additionally, PIM2 reprograms MM cell metabolism and suppresses the DNA damage response (DDR), favoring survival under metabolic and genotoxic stress [302]. Our results confirm and extend these findings, showing that MEN1703 downregulates MYC/E2F1 programs, impairs mTOR signaling, and disrupts DNA repair capacity in MM (Fig. 31-34).

Functionally, we show that MEN1703 induces durable anti-MM activity in cell lines and primary samples (Fig. 26), including those resistant to PIM447 and other clinical-stage compounds. This is significant given the limited clinical success of earlier PIM inhibitors. For example, PIM447 showed only cytostatic effects in MM patients despite preclinical efficacy, and clinical development was halted [389,390]. SGI-1776 and AZD1208 failed due to cardiac toxicity or lack of efficacy [391,392]. Our findings suggest that MEN1703 may overcome some of these limitations.

Importantly, our inducible shRNA experiments targeting all three *PIM* paralogs partially recapitulated the cytotoxic effects of MEN1703, supporting an on-target mechanism of action. Although MEN1703 may still act on additional kinases (e.g., FLT3 [307,393]), its efficacy in FLT3-negative MM argues against off-target FLT3 dependence. Prior reports suggest that ATP-competitive PIM inhibitors may paradoxically stabilize the protein and preserve non-catalytic functions [384]. This supports the development of PROTAC degraders, which could eliminate

both kinase-dependent and independent functions of PIMs and offer a more durable and sustained signaling blockade, preventing kinome re-wiring [394].

A key finding of this work is that the therapeutic potential of PIM inhibition extends beyond the malignant plasma cells to disrupt the supportive tumor microenvironment (TME). We demonstrated that MMECs overexpress PIM3 and display enhanced angiogenic capacity. This observation, which confirms prior studies linking PIM1/3 to vascular biology [271,272,395], establishes the MM vasculature as a PIM-dependent entity and a viable target for MEN1703. In addition, the link between PIMs and actin dynamics has already been discussed in previous studies demonstrating that these kinases phosphorylate actin capping proteins and wave regulatory complex [396,397], which however does not explain the upstream changes in RhoA activity we have observed in ECs.

This impact of PIM inhibitors on the TME might not be limited to angiogenesis. The established role of PIM kinases in MM bone disease further broadens their functional relevance [398,399]. PIM2 is reported to promote osteoclast activity while simultaneously suppressing osteoblast differentiation, directly driving the bone resorption and skeletal lesions characteristic of MM [166]. This dual activity in both malignant plasma cells and the microenvironment highlights the value of targeting PIM kinases as part of a strategy to modify tumor biology and niche interactions.

## 5.4 Limitations

Most mechanistic work was performed in established MM cell lines (e.g., MM1.S, JJN3, RPMI8226, U266) and immortalized endothelial cells (HUVEC-TERT2). While these are standard and reproducible systems, they only approximate the complexity of patient tumors and the human marrow niche. MM cell lines reflect advanced disease and long-term *in vitro* selection; HUVEC-TERT2 cells are macrovascular/umbilical-derived and not bona fide bone-marrow sinusoidal endothelium. This could over- or under-estimate PIM contributions to true marrow EC function and MM-EC crosstalk in situ. The observation that MEN1703 kills primary CD138<sup>+</sup> MM cells while sparing CD138<sup>-</sup> cells is reassuring, but the number of primary samples tested is limited. The findings should be validated using primary HD BM ECs or MMECs.

Without that, we cannot exclude the possibility that some EC phenotypes are specific to HUVEC-TERT2 biology.

Much of the transcriptional and functional profiling after MEN1703 treatment was done at a single dose (1.5  $\mu$ M) and one early timepoint (24 h for ECs; 24 h and 96-120 h windows for MM cells). This provides a snapshot but not the full kinetic trajectory of stress responses, compensatory signaling, or emergent resistance mechanisms. We do not yet know whether MM cells can recover from MEN1703 exposure if drug pressure is relaxed *in vitro*, nor do we know how ECs remodel over longer intervals. We may be overestimating the durability of some effects (e.g., suppression of pro-angiogenic transcription in ECs) or underestimating others (e.g., adaptive survival programs in MM cells that rewire after 48–72 h).

While we linked PIM inhibition to RhoA inactivation, actin depolymerization, and loss of lamellipodia/stress fibers in ECs, the precise molecular intermediates remain undefined. We did not map phosphorylation targets downstream of PIM in ECs, identify direct PIM substrates in cytoskeletal complexes, or address whether PIM acts through canonical angiogenic pathways (VEGFR2, PI3K/AKT, Src).

## 5.5 Outlook

Several priority questions emerge directly from this work.

### 1. Can we stratify patients for PIM-targeted therapy?

PIM2 and PIM3 expression correlates with inferior survival and remains independently prognostic in multivariate analyses, suggesting these kinases may serve as biomarkers of aggressive disease. MEN1703 sensitivity is associated with MYC/E2F1 transcriptional programs and possibly CCND1 translocation status. A logical next step is to formulate a biomarker panel (PIM2/PIM3 or MYC/E2F1 expression, MYC or CCND1 rearrangements) that could predict response to MEN1703 or related PIM inhibitors. This would enable rational, biomarker-guided early-phase clinical trials rather than unselected enrollment.

# 2. How durable is PIM pathway suppression, and what are the resistance mechanisms?

The *in vivo* xenograft data show durable tumor suppression even after MEN1703 withdrawal, with sustained, albeit moderate reduction of tumor burden. However, MM is notorious for adaptive resistance to therapies. Time-course multi-omics (transcriptome, phosphoproteome, chromatin accessibility) under prolonged MEN1703 exposure will be critical to uncover bypass pathways. Generation of MEN1703-resistant cell lines could also offer a possibility to study the rewiring leading up to PIM inhibitor resistance. Special attention should be given to the PI3K/AKT and MAPK pathways, which share some of the phosphorylation sites with PIMs [400,401].

### 3. How important are off-target effects for the efficacy of MEN1703?

Very few small-molecule kinase inhibitors are truly selective, because most bind conserved ATP pockets shared across many kinases [402]. MEN1703 is no exception: in addition to PIM1/2/3, it also inhibits kinases such as Haspin, CK1/2, DYRK1A/B, CLK1/4, HIPK1/3, and PKCɛ, some of which are involved in cell cycle control, survival signaling, RNA processing, DNA damage responses, and cytoskeletal/angiogenic behavior [393]. This poly-kinase profile might enhance the anti-myeloma and anti-angiogenic effects we observe, beyond PIM inhibition alone. Although it is not feasible to functionally dissect every off-target, mass spectrometry-based CETSA could help define which of these proteins are actually engaged by MEN1703 in cells, and selected candidates could then be tested functionally using siRNA or shRNA knockdown in the triple *PIM* knockdown (3×shPIM) background generated in this study.

# 4. Which drug classes should be combined with MEN1703 to achieve maximal MM burden reduction?

The observed synergy with bortezomib argues for combination trials. Rational next combinations include newer proteasome inhibitors (carfilzomib), IMiDs, alkylators, and PARP inhibitors (given MEN1703-associated suppression of DNA repair and PARP1 expression). Such studies should incorporate pharmacodynamic readouts (pS6, MYC/E2F1 suppression, DNA damage markers) and track toxicity in hematopoietic progenitors to define the therapeutic window.

### 5. How does PIM3 reprogram the BM endothelium?

We now know that MM-derived factors induce PIM3 in ECs, and that PIM inhibition reverses angiogenic behavior, RhoA activity, and MM-associated transcriptional signatures. Direct PIM3 substrates should be mapped using phosphoproteomics or co-

immunoprecipitation coupled with mass spectrometry. In addition, functional PIM3 genetic perturbations (either knockdown or knockout) should be tested in ECs to determine the on-target mechanism of action of MEN1703 in these cells. Given the downregulation of AP1 targets expression, chromatin accessibility studies should be performed to determine the potential mechanism behind these effects. Of note, PIMs have been linked with endothelial epigenetic regulation via the H3S10 mark [403], therefore the proposed studies should include a H3S10 ChIP-seq as well.

# 6. What is the composite outcome of PIM inhibition in *in vivo* syngeneic MM models? Our current in vivo data are derived from xenograft models, which, while valuable, are immunocompromised. PIM kinases are known to be expressed in various immune populations, including T-cells [404] and macrophages [285]. Furthermore, induction of DNA damage in tumor cells sets off a number of innate immunity pathways, such as cGAS/STING [405], which can influence the adaptive anti-tumor immunity. Finally, reprogramming tumor-associated endothelial cells helps the immune system mount an effective anti-tumor immune response [406]. It is therefore unknown whether MEN1703's efficacy in vivo is enhanced or limited by its effects on immune effector or suppressor cells. The critical next step is to test MEN1703 in immunocompetent, syngeneic MM models (e.g., 5TGM1 or Vk\*Myc). Key analyses should include not only survival and tumor burden, but also in-depth immunophenotyping (e.g., by flow or mass cytometry or single cell RNA-seq) of the bone marrow and spleen to assess changes in T-cell populations (CD8<sup>+</sup>, CD4<sup>+</sup>, Tregs), macrophage polarization, and myeloid-derived suppressor cells. This approach will reveal the net in vivo effect of PIM inhibition and provide a strong rationale for or against combination with immune checkpoint inhibitors or other anti-MM immunotherapies.

Taken together, this work highlights how systematic investigation of less-characterized kinase families can uncover critical disease mechanisms. We have shown that PIM kinases are important regulators of plasma cell survival and vascular niche adaptation. By dissecting these functions in both tumor-intrinsic and stromal contexts, the results of this thesis advance our understanding of MM pathobiology and identifies PIM inhibition as a rational therapeutic approach. These findings should serve as a foundation for continued preclinical and clinical exploration of PIM-targeting strategies in MM.

## 6 References

- 1. Siegel, R.L.; Miller, K.D.; Wagle, N.S.; Jemal, A. Cancer Statistics, 2023. *CA. Cancer J. Clin.* **2023**, *73*, 17–48, doi:10.3322/caac.21763.
- 2. Gupta, S.; Master, S.; Graham, C. Extramedullary Multiple Myeloma: A Patient-Focused Review of the Pathogenesis of Bone Marrow Escape. *World J. Oncol.* **2022**, *13*, 311–319, doi:10.14740/wjon1521.
- 3. Yadav, U.; Kumar, S.K.; Baughn, L.B.; Dispenzieri, A.; Greipp, P.; Ketterling, R.; Jevremovic, D.; Buadi, F.K.; Dingli, D.; Lacy, M.Q.; et al. Impact of Cytogenetic Abnormalities on the Risk of Disease Progression in Solitary Bone Plasmacytomas. *Blood* **2023**, *142*, 1871–1878, doi:10.1182/blood.2023021187.
- 4. Nakamoto-Matsubara, R.; Nardi, V.; Horick, N.; Fukushima, T.; Han, R.S.; Shome, R.; Ochi, K.; Panaroni, C.; Fulzele, K.; Rexha, F.; et al. Integration of Clinical Outcomes and Molecular Features in Extramedullary Disease in Multiple Myeloma. *Blood Cancer J.* **2024**, *14*, 224, doi:10.1038/s41408-024-01190-9.
- 5. Sanchorawala, V. Systemic Light Chain Amyloidosis. *N. Engl. J. Med.* **2024**, *390*, 2295–2307, doi:10.1056/NEJMra2304088.
- 6. Bender, S.; Ayala, M.V.; Bonaud, A.; Javaugue, V.; Carrion, C.; Oblet, C.; Rinsant, A.; Kaaki, S.; Oruc, Z.; Boyer, F.; et al. Immunoglobulin Light-Chain Toxicity in a Mouse Model of Monoclonal Immunoglobulin Light-Chain Deposition Disease. *Blood* **2020**, *136*, 1645–1656, doi:10.1182/blood.2020005980.
- 7. Bonaud, A.; Bender, S.; Touchard, G.; Lacombe, C.; Srour, N.; Delpy, L.; Oblet, C.; Druilhe, A.; Quellard, N.; Javaugue, V.; et al. A Mouse Model Recapitulating Human Monoclonal Heavy Chain Deposition Disease Evidences the Relevance of Proteasome Inhibitor Therapy. *Blood* **2015**, *126*, 757–765, doi:10.1182/blood-2015-03-630277.
- 8. Cook, G.; Rovira, M. Poems Syndrome and Disease Produced by Other Monoclonal IGs. In *The EBMT Handbook: Hematopoietic Cell Transplantation and Cellular Therapies*; Sureda, A., Corbacioglu, S., Greco, R., Kröger, N., Carreras, E., Eds.; Springer: Cham (CH), 2024 ISBN 978-3-031-44079-3.
- 9. Heaney, J.L.J.; Campbell, J.P.; Griffin, A.E.; Birtwistle, J.; Shemar, M.; Child, J.A.; Gregory, W.M.; Cairns, D.A.; Morgan, G.; Jackson, G.; et al. Diagnosis and Monitoring for Light Chain Only and Oligosecretory Myeloma Using Serum Free Light Chain Tests. *Br. J. Haematol.* **2017**, *178*, 220–230, doi:10.1111/bjh.14753.
- 10. Go, R.S.; Rajkumar, S.V. How I Manage Monoclonal Gammopathy of Undetermined Significance. *Blood* **2018**, *131*, 163–173, doi:10.1182/blood-2017-09-807560.
- 11. Rajkumar, S.V.; Kumar, S.; Lonial, S.; Mateos, M.V. Smoldering Multiple Myeloma Current Treatment Algorithms. *Blood Cancer J.* **2022**, *12*, 1–7, doi:10.1038/s41408-022-00719-0.
- 12. Skerget, S.; Penaherrera, D.; Chari, A.; Jagannath, S.; Siegel, D.S.; Vij, R.; Orloff, G.; Jakubowiak, A.; Niesvizky, R.; Liles, D.; et al. Comprehensive Molecular Profiling of Multiple Myeloma Identifies Refined Copy Number and Expression Subtypes. *Nat. Genet.* **2024**, *56*, 1878–1889, doi:10.1038/s41588-024-01853-0.
- 13. Solly, S. Remarks on the Pathology of Mollities Ossium; with Cases. *Medico-Chir. Trans.* **1844**, *27*, 435-498.8.
- 14. Macintyre, W. Case of Mollities and Fragilitas Ossium, Accompanied with Urine Strongly Charged with Animal Matter. *Medico-Chir. Trans.* **1850**, *33*, 211–232.

- 15. Jones, H.B. On a New Substance Occurring in the Urine of a Patient with Mollities Ossium. *Philos. Trans. R. Soc. Lond.* **1847**, *138*, 55–62, doi:10.1098/rstl.1848.0003.
- 16. v. Rustizky, J. Multiples Myelom. *Dtsch. Z. Für Chir.* **1873**, *3*, 162–172, doi:10.1007/BF02911073.
- 17. Kahler, O. Zur Symptomatologie Des Multiplen Myeloms: Beobachtung von Albumosurie. *Prag Med Wochenschr* **1889**, *13*, 33–45.
- 18. GESCHICKTER, C.F.; COPELAND, M.M. MULTIPLE MYELOMA. *Arch. Surg.* **1928**, *16*, 807–863, doi:10.1001/archsurg.1928.01140040002001.
- 19. Korngold, L.; Lipari, R. Multiple-Myeloma Proteins. III. The Antigenic Relationship of Bence Jones Proteins to Normal Gammaglobulin and Multiple-Myeloma Serum Proteins. *Cancer* **1956**, *9*, 262–272, doi:10.1002/1097-0142(195603/04)9:2%3C262::aid-cncr2820090210%3E3.0.co;2-b.
- 20. Mussap, M.; Dolci, A.; Graziani, M.S. Inaccurate Definition of Bence Jones Proteinuria in the EFLM Urinalysis Guideline 2023. *Clin. Chem. Lab. Med. CCLM* **2024**, *62*, e251–e252, doi:10.1515/cclm-2024-1001.
- 21. Zhou, L.; Yu, Q.; Wei, G.; Wang, L.; Huang, Y.; Hu, K.; Hu, Y.; Huang, H. Measuring the Global, Regional, and National Burden of Multiple Myeloma from 1990 to 2019. *BMC Cancer* 2021, 21, 606, doi:10.1186/s12885-021-08280-y.
- 22. Kumar, S.K.; Dispenzieri, A.; Lacy, M.Q.; Gertz, M.A.; Buadi, F.K.; Pandey, S.; Kapoor, P.; Dingli, D.; Hayman, S.R.; Leung, N.; et al. Continued Improvement in Survival in Multiple Myeloma: Changes in Early Mortality and Outcomes in Older Patients. *Leukemia* **2014**, *28*, 1122–1128, doi:10.1038/leu.2013.313.
- 23. Landgren, O.; Kyle, R.A.; Rajkumar, S.V. From Myeloma Precursor Disease to Multiple Myeloma: New Diagnostic Concepts and Opportunities for Early Intervention. *Clin. Cancer Res. Off. J. Am. Assoc. Cancer Res.* **2011**, *17*, 1243–1252, doi:10.1158/1078-0432.CCR-10-1822.
- 24. Landgren, O.; Shim, Y.K.; Michalek, J.; Costello, R.; Burton, D.; Ketchum, N.; Calvo, K.R.; Caporaso, N.; Raveche, E.; Middleton, D.; et al. Agent Orange Exposure and Monoclonal Gammopathy of Undetermined Significance: An Operation Ranch Hand Veteran Cohort Study. *JAMA Oncol.* **2015**, *1*, 1061–1068, doi:10.1001/jamaoncol.2015.2938.
- 25. Went, M.; Cornish, A.J.; Law, P.J.; Kinnersley, B.; Van Duin, M.; Weinhold, N.; Försti, A.; Hansson, M.; Sonneveld, P.; Goldschmidt, H.; et al. Search for Multiple Myeloma Risk Factors Using Mendelian Randomization. *Blood Adv.* **2020**, *4*, 2172–2179, doi:10.1182/bloodadvances.2020001502.
- 26. Lindqvist, E.K.; Goldin, L.R.; Landgren, O.; Blimark, C.; Mellqvist, U.-H.; Turesson, I.; Wahlin, A.; Björkholm, M.; Kristinsson, S.Y. Personal and Family History of Immune-Related Conditions Increase the Risk of Plasma Cell Disorders: A Population-Based Study. *Blood* **2011**, *118*, 6284–6291, doi:10.1182/blood-2011-04-347559.
- 27. Kumar, S.K.; Rajkumar, V.; Kyle, R.A.; Van Duin, M.; Sonneveld, P.; Mateos, M.-V.; Gay, F.; Anderson, K.C. Multiple Myeloma. *Nat. Rev. Dis. Primer* **2017**, *3*, 17046, doi:10.1038/nrdp.2017.46.
- 28. Hoffman, R.; Benz, E.J.; Silberstein, L.E.; Heslop, H.; Weitz, J.; Salama, M.E.; Abutalib, S.A. *Hematology*; 8th ed.; Elsevier, 2022; p. 2476; ISBN 978-0-323-73388-5.
- 29. Rajkumar, S.V.; Dimopoulos, M.A.; Palumbo, A.; Blade, J.; Merlini, G.; Mateos, M.-V.; Kumar, S.; Hillengass, J.; Kastritis, E.; Richardson, P.; et al. International Myeloma

- Working Group Updated Criteria for the Diagnosis of Multiple Myeloma. *Lancet Oncol.* **2014**, *15*, e538-548, doi:10.1016/S1470-2045(14)70442-5.
- 30. Pelon, M.; Krzeminski, P.; Tracz-Gaszewska, Z.; Misiewicz-Krzeminska, I. Factors Determining the Sensitivity to Proteasome Inhibitors of Multiple Myeloma Cells. *Front. Pharmacol.* **2024**, *15*, 1351565, doi:10.3389/fphar.2024.1351565.
- 31. Bird, S.; Pawlyn, C. IMiD Resistance in Multiple Myeloma: Current Understanding of the Underpinning Biology and Clinical Impact. *Blood* **2023**, *142*, 131–140, doi:10.1182/blood.2023019637.
- 32. Jureczek, J.; Kałwak, K.; Dzięgiel, P. Antibody-Based Immunotherapies for the Treatment of Hematologic Malignancies. *Cancers* **2024**, *16*, 4181, doi:10.3390/cancers16244181.
- 33. Swan, D.; Madduri, D.; Hocking, J. CAR T-cell Therapy in Multiple Myeloma: Current Status and Future Challenges. *Blood Cancer J.* **2024**, *14*, 206, doi:10.1038/s41408-024-01191-8.
- 34. Bolli, N.; Biancon, G.; Moarii, M.; Gimondi, S.; Li, Y.; De Philippis, C.; Maura, F.; Sathiaseelan, V.; Tai, Y.-T.; Mudie, L.; et al. Analysis of the Genomic Landscape of Multiple Myeloma Highlights Novel Prognostic Markers and Disease Subgroups. *Leukemia* **2018**, *32*, 2604–2616, doi:10.1038/s41375-018-0037-9.
- 35. Mikhael, J.R.; Dingli, D.; Roy, V.; Reeder, C.B.; Buadi, F.K.; Hayman, S.R.; Dispenzieri, A.; Fonseca, R.; Sher, T.; Kyle, R.A.; et al. Management of Newly Diagnosed Symptomatic Multiple Myeloma: Updated Mayo Stratification of Myeloma and Risk-Adapted Therapy (mSMART) Consensus Guidelines 2013. *Mayo Clin. Proc.* **2013**, *88*, 360–376, doi:10.1016/j.mayocp.2013.01.019.
- 36. Inobe, T.; Fishbain, S.; Prakash, S.; Matouschek, A. Defining the Geometry of the Two-Component Proteasome Degron. *Nat. Chem. Biol.* **2011**, *7*, 161–167, doi:10.1038/nchembio.521.
- 37. Obeng, E.A.; Carlson, L.M.; Gutman, D.M.; Harrington, W.J.; Lee, K.P.; Boise, L.H. Proteasome Inhibitors Induce a Terminal Unfolded Protein Response in Multiple Myeloma Cells. *Blood* **2006**, *107*, 4907–4916, doi:10.1182/blood-2005-08-3531.
- 38. Hetz, C.; Zhang, K.; Kaufman, R.J. Mechanisms, Regulation and Functions of the Unfolded Protein Response. *Nat. Rev. Mol. Cell Biol.* **2020**, *21*, 421–438, doi:10.1038/s41580-020-0250-z.
- 39. Richardson, P.G.; Barlogie, B.; Berenson, J.; Singhal, S.; Jagannath, S.; Irwin, D.; Rajkumar, S.V.; Srkalovic, G.; Alsina, M.; Alexanian, R.; et al. A Phase 2 Study of Bortezomib in Relapsed, Refractory Myeloma. *N. Engl. J. Med.* **2003**, *348*, 2609–2617, doi:10.1056/NEJMoa030288.
- 40. Richardson, P.G.; Sonneveld, P.; Schuster, M.; Irwin, D.; Stadtmauer, E.; Facon, T.; Harousseau, J.-L.; Ben-Yehuda, D.; Lonial, S.; Goldschmidt, H.; et al. Extended Follow-up of a Phase 3 Trial in Relapsed Multiple Myeloma: Final Time-to-Event Results of the APEX Trial. *Blood* **2007**, *110*, 3557–3560, doi:10.1182/blood-2006-08-036947.
- 41. Iuliano, L.; Dalla, E.; Picco, R.; Mallavarapu, S.; Minisini, M.; Malavasi, E.; Brancolini, C. Proteotoxic Stress-Induced Apoptosis in Cancer Cells: Understanding the Susceptibility and Enhancing the Potency. *Cell Death Discov.* **2022**, *8*, 407, doi:10.1038/s41420-022-01202-2.
- 42. Dimopoulos, M.A.; Anagnostopoulos, A.; Weber, D. Treatment of Plasma Cell Dyscrasias With Thalidomide and Its Derivatives. *J. Clin. Oncol.* **2003**, *21*, 4444–4454, doi:10.1200/JCO.2003.07.200.

- 43. Vacca, A.; Scavelli, C.; Montefusco, V.; Di Pietro, G.; Neri, A.; Mattioli, M.; Bicciato, S.; Nico, B.; Ribatti, D.; Dammacco, F.; et al. Thalidomide Downregulates Angiogenic Genes in Bone Marrow Endothelial Cells of Patients With Active Multiple Myeloma. *J. Clin. Oncol.* **2005**, *23*, 5334–5346, doi:10.1200/JCO.2005.03.723.
- 44. De Logu, F.; Trevisan, G.; Marone, I.M.; Coppi, E.; Padilha Dalenogare, D.; Titiz, M.; Marini, M.; Landini, L.; Souza Monteiro De Araujo, D.; Li Puma, S.; et al. Oxidative Stress Mediates Thalidomide-Induced Pain by Targeting Peripheral TRPA1 and Central TRPV4. *BMC Biol.* **2020**, *18*, 197, doi:10.1186/s12915-020-00935-9.
- 45. Heras Martinez, H.M.; Barragan, E.; Marichev, K.O.; Chávez-Flores, D.; Bugarin, A. Phthalimides as Anti-Inflammatory Agents. *Future Med. Chem.* **2025**, *17*, 125–142, doi:10.1080/17568919.2024.2437979.
- 46. Luptakova, K.; Rosenblatt, J.; Glotzbecker, B.; Mills, H.; Stroopinsky, D.; Kufe, T.; Vasir, B.; Arnason, J.; Tzachanis, D.; Zwicker, J.I.; et al. Lenalidomide Enhances Anti-Myeloma Cellular Immunity. *Cancer Immunol. Immunother. CII* **2012**, *62*, 39–49, doi:10.1007/s00262-012-1308-3.
- 47. Hsu, A.K.; Quach, H.; Tai, T.; Prince, H.M.; Harrison, S.J.; Trapani, J.A.; Smyth, M.J.; Neeson, P.; Ritchie, D.S. The Immunostimulatory Effect of Lenalidomide on NK-Cell Function Is Profoundly Inhibited by Concurrent Dexamethasone Therapy. *Blood* **2011**, *117*, 1605–1613, doi:10.1182/blood-2010-04-278432.
- 48. Hayashi, T.; Hideshima, T.; Akiyama, M.; Podar, K.; Yasui, H.; Raje, N.; Kumar, S.; Chauhan, D.; Treon, S.P.; Richardson, P.; et al. Molecular Mechanisms Whereby Immunomodulatory Drugs Activate Natural Killer Cells: Clinical Application. *Br. J. Haematol.* **2005**, *128*, 192–203, doi:10.1111/j.1365-2141.2004.05286.x.
- 49. Krönke, J.; Udeshi, N.D.; Narla, A.; Grauman, P.; Hurst, S.N.; McConkey, M.; Svinkina, T.; Heckl, D.; Comer, E.; Li, X.; et al. Lenalidomide Causes Selective Degradation of IKZF1 and IKZF3 in Multiple Myeloma Cells. *Science* **2014**, *343*, 301–305, doi:10.1126/science.1244851.
- 50. Barankiewicz, J.; Szumera-Ciećkiewicz, A.; Salomon-Perzyński, A.; Wieszczy, P.; Malenda, A.; Garbicz, F.; Prochorec-Sobieszek, M.; Misiewicz-Krzemińska, I.; Juszczyński, P.; Lech-Marańda, E. The CRBN, CUL4A and DDB1 Expression Predicts the Response to Immunomodulatory Drugs and Survival of Multiple Myeloma Patients. *J. Clin. Med.* **2021**, *10*, 2683, doi:10.3390/jcm10122683.
- 51. Görgün, G.; Calabrese, E.; Soydan, E.; Hideshima, T.; Perrone, G.; Bandi, M.; Cirstea, D.; Santo, L.; Hu, Y.; Tai, Y.-T.; et al. Immunomodulatory Effects of Lenalidomide and Pomalidomide on Interaction of Tumor and Bone Marrow Accessory Cells in Multiple Myeloma. *Blood* **2010**, *116*, 3227–3237, doi:10.1182/blood-2010-04-279893.
- 52. Bjorklund, C.C.; Lu, L.; Kang, J.; Hagner, P.R.; Havens, C.G.; Amatangelo, M.; Wang, M.; Ren, Y.; Couto, S.; Breider, M.; et al. Rate of CRL4(CRBN) Substrate Ikaros and Aiolos Degradation Underlies Differential Activity of Lenalidomide and Pomalidomide in Multiple Myeloma Cells by Regulation of c-Myc and IRF4. *Blood Cancer J.* **2015**, *5*, e354, doi:10.1038/bcj.2015.66.
- 53. Lopez-Girona, A.; Heintel, D.; Zhang, L.-H.; Mendy, D.; Gaidarova, S.; Brady, H.; Bartlett, J.B.; Schafer, P.H.; Schreder, M.; Bolomsky, A.; et al. Lenalidomide Downregulates the Cell Survival Factor, Interferon Regulatory Factor-4, Providing a Potential Mechanistic Link for Predicting Response. *Br. J. Haematol.* **2011**, *154*, 325–336, doi:10.1111/j.1365-2141.2011.08689.x.

- 54. Neri, P.; Barwick, B.G.; Jung, D.; Patton, J.C.; Maity, R.; Tagoug, I.; Stein, C.K.; Tilmont, R.; Leblay, N.; Ahn, S.; et al. ETV4-Dependent Transcriptional Plasticity Maintains MYC Expression and Results in IMiD Resistance in Multiple Myeloma. *Blood Cancer Discov.* **2024**, *5*, 56–73, doi:10.1158/2643-3230.BCD-23-0061.
- 55. Sperling, A.S.; Guerra, V.A.; Kennedy, J.A.; Yan, Y.; Hsu, J.I.; Wang, F.; Nguyen, A.T.; Miller, P.G.; McConkey, M.E.; Quevedo Barrios, V.A.; et al. Lenalidomide Promotes the Development of TP53-Mutated Therapy-Related Myeloid Neoplasms. *Blood* **2022**, *140*, 1753–1763, doi:10.1182/blood.2021014956.
- 56. Rajkumar, S.V.; Jacobus, S.; Callander, N.S.; Fonseca, R.; Vesole, D.H.; Williams, M.E.; Abonour, R.; Siegel, D.S.; Katz, M.; Greipp, P.R.; et al. Lenalidomide plus High-Dose Dexamethasone versus Lenalidomide plus Low-Dose Dexamethasone as Initial Therapy for Newly Diagnosed Multiple Myeloma: An Open-Label Randomised Controlled Trial. *Lancet Oncol.* **2010**, *11*, 29–37, doi:10.1016/S1470-2045(09)70284-0.
- 57. Kyle, R.A.; Rajkumar, S.V. Multiple Myeloma. *Blood* **2008**, *111*, 2962–2972, doi:10.1182/blood-2007-10-078022.
- 58. Weikum, E.R.; Knuesel, M.T.; Ortlund, E.A.; Yamamoto, K.R. Glucocorticoid Receptor Control of Transcription: Precision and Plasticity via Allostery. *Nat. Rev. Mol. Cell Biol.* **2017**, *18*, 159–174, doi:10.1038/nrm.2016.152.
- 59. Sharma, S.; Lichtenstein, A. Dexamethasone-Induced Apoptotic Mechanisms in Myeloma Cells Investigated by Analysis of Mutant Glucocorticoid Receptors. *Blood* **2008**, *112*, 1338–1345, doi:10.1182/blood-2007-11-124156.
- 60. Zhao, J.-J.; Chu, Z.-B.; Hu, Y.; Lin, J.; Wang, Z.; Jiang, M.; Chen, M.; Wang, X.; Kang, Y.; Zhou, Y.; et al. Targeting the miR-221-222/PUMA/BAK/BAX Pathway Abrogates Dexamethasone Resistance in Multiple Myeloma. *Cancer Res.* **2015**, *75*, 4384–4397, doi:10.1158/0008-5472.CAN-15-0457.
- 61. Singh, R.; Letai, A.; Sarosiek, K. Regulation of Apoptosis in Health and Disease: The Balancing Act of BCL-2 Family Proteins. *Nat. Rev. Mol. Cell Biol.* **2019**, *20*, 175–193, doi:10.1038/s41580-018-0089-8.
- 62. Friedenberg, W.R.; Kyle, R.A.; Knospe, W.H.; Bennett, J.M.; Tsiatis, A.A.; Oken, M.M. High-dose Dexamethasone for Refractory or Relapsing Multiple Myeloma. *Am. J. Hematol.* **1991**, *36*, 171–175, doi:10.1002/ajh.2830360303.
- 63. Neri, P.; Nijhof, I. Evidence-Based Mechanisms of Synergy with IMiD Agent-Based Combinations in Multiple Myeloma. *Crit. Rev. Oncol. Hematol.* **2023**, *188*, 104041, doi:10.1016/j.critrevonc.2023.104041.
- 64. Giliberto, M.; Thimiri Govinda Raj, D.B.; Cremaschi, A.; Skånland, S.S.; Gade, A.; Tjønnfjord, G.E.; Schjesvold, F.; Munthe, L.A.; Taskén, K. Ex Vivo Drug Sensitivity Screening in Multiple Myeloma Identifies Drug Combinations That Act Synergistically. *Mol. Oncol.* 2022, *16*, 1241–1258, doi:10.1002/1878-0261.13191.
- 65. Costa, L.J.; Banerjee, R.; Mian, H.; Weisel, K.; Bal, S.; Derman, B.A.; Htut, M.M.; Nagarajan, C.; Rodriguez, C.; Richter, J.; et al. International Myeloma Working Group Immunotherapy Committee Recommendation on Sequencing Immunotherapy for Treatment of Multiple Myeloma. *Leukemia* **2025**, 1–12, doi:10.1038/s41375-024-02482-6.
- 66. Dimopoulos, M.A.; Oriol, A.; Nahi, H.; San-Miguel, J.; Bahlis, N.J.; Usmani, S.Z.; Rabin, N.; Orlowski, R.Z.; Suzuki, K.; Plesner, T.; et al. Overall Survival With Daratumumab, Lenalidomide, and Dexamethasone in Previously Treated Multiple Myeloma (POLLUX):

- A Randomized, Open-Label, Phase III Trial. *J. Clin. Oncol.* **2023**, *41*, 1590–1599, doi:10.1200/JCO.22.00940.
- 67. Sonneveld, P.; Dimopoulos, M.A.; Boccadoro, M.; Quach, H.; Ho, P.J.; Beksac, M.; Hulin, C.; Antonioli, E.; Leleu, X.; Mangiacavalli, S.; et al. Daratumumab, Bortezomib, Lenalidomide, and Dexamethasone for Multiple Myeloma. *N. Engl. J. Med.* **2024**, *390*, 301–313, doi:10.1056/NEJMoa2312054.
- 68. Spencer, A.; Moreau, P.; Mateos, M.-V.; Goldschmidt, H.; Suzuki, K.; Levin, M.-D.; Sonneveld, P.; Orlowski, R.Z.; Yoon, S.-S.; Usmani, S.Z.; et al. Daratumumab for Patients with Myeloma with Early or Late Relapse after Initial Therapy: Subgroup Analysis of CASTOR and POLLUX. *Blood Adv.* **2024**, *8*, 388–398, doi:10.1182/bloodadvances.2023010579.
- 69. Martin, T.; Usmani, S.Z.; Berdeja, J.G.; Agha, M.; Cohen, A.D.; Hari, P.; Avigan, D.; Deol, A.; Htut, M.; Lesokhin, A.; et al. Ciltacabtagene Autoleucel, an Anti-B-Cell Maturation Antigen Chimeric Antigen Receptor T-Cell Therapy, for Relapsed/Refractory Multiple Myeloma: CARTITUDE-1 2-Year Follow-Up. *J. Clin. Oncol. Off. J. Am. Soc. Clin. Oncol.* 2023, 41, 1265–1274, doi:10.1200/JCO.22.00842.
- 70. Moreau, P.; Garfall, A.L.; Donk, N.W.C.J. van de; Nahi, H.; San-Miguel, J.F.; Oriol, A.; Nooka, A.K.; Martin, T.; Rosinol, L.; Chari, A.; et al. Teclistamab in Relapsed or Refractory Multiple Myeloma. *N. Engl. J. Med.* **2022**, *387*, 495–505, doi:10.1056/NEJMoa2203478.
- 71. Chari, A.; Minnema, M.C.; Berdeja, J.G.; Oriol, A.; Donk, N.W.C.J. van de; Rodríguez-Otero, P.; Askari, E.; Mateos, M.-V.; Costa, L.J.; Caers, J.; et al. Talquetamab, a T-Cell-Redirecting GPRC5D Bispecific Antibody for Multiple Myeloma. *N. Engl. J. Med.* **2022**, 387, 2232–2244, doi:10.1056/NEJMoa2204591.
- 72. Maude, S.L.; Frey, N.; Shaw, P.A.; Aplenc, R.; Barrett, D.M.; Bunin, N.J.; Chew, A.; Gonzalez, V.E.; Zheng, Z.; Lacey, S.F.; et al. Chimeric Antigen Receptor T Cells for Sustained Remissions in Leukemia. *N. Engl. J. Med.* **2014**, *371*, 1507–1517, doi:10.1056/NEJMoa1407222.
- 73. Munshi, N.C.; Anderson, L.D.; Shah, N.; Madduri, D.; Berdeja, J.; Lonial, S.; Raje, N.; Lin, Y.; Siegel, D.; Oriol, A.; et al. Idecabtagene Vicleucel in Relapsed and Refractory Multiple Myeloma. *N. Engl. J. Med.* **2021**, *384*, 705–716, doi:10.1056/NEJMoa2024850.
- 74. San-Miguel, J.; Dhakal, B.; Yong, K.; Spencer, A.; Anguille, S.; Mateos, M.-V.; Larrea, C.F. de; Martínez-López, J.; Moreau, P.; Touzeau, C.; et al. Cilta-Cel or Standard Care in Lenalidomide-Refractory Multiple Myeloma. *N. Engl. J. Med.* **2023**, *389*, 335–347, doi:10.1056/NEJMoa2303379.
- 75. Harrison, S.J.; Touzeau, C.; Kint, N.; Li, K.; Nguyen, T.; Mayeur-Rousse, C.; Rahman, M.; Bris, Y.L.; Er, J.; Eugene-Lamer, J.; et al. CAR+ T-Cell Lymphoma after Cilta-Cel Therapy for Relapsed or Refractory Myeloma. *N. Engl. J. Med.* **2025**, *392*, 677–685, doi:10.1056/NEJMoa2309728.
- 76. Mohan, M.; Monge, J.; Shah, N.; Luan, D.; Forsberg, M.; Bhatlapenumarthi, V.; Balev, M.; Patwari, A.; Cheruvalath, H.; Bhutani, D.; et al. Teclistamab in Relapsed Refractory Multiple Myeloma: Multi-Institutional Real-World Study. *Blood Cancer J.* **2024**, *14*, 1–6, doi:10.1038/s41408-024-01003-z.
- 77. Lesokhin, A.M.; Tomasson, M.H.; Arnulf, B.; Bahlis, N.J.; Miles Prince, H.; Niesvizky, R.; Rodríguez-Otero, P.; Martinez-Lopez, J.; Koehne, G.; Touzeau, C.; et al. Elranatamab in Relapsed or Refractory Multiple Myeloma: Phase 2 MagnetisMM-3 Trial Results. *Nat. Med.* **2023**, *29*, 2259–2267, doi:10.1038/s41591-023-02528-9.

- 78. Goebeler, M.-E.; Bargou, R.C. T Cell-Engaging Therapies BiTEs and Beyond. *Nat. Rev. Clin. Oncol.* **2020**, *17*, 418–434, doi:10.1038/s41571-020-0347-5.
- 79. Lesokhin, A.M.; Tomasson, M.H.; Arnulf, B.; Bahlis, N.J.; Miles Prince, H.; Niesvizky, R.; Rodríguez-Otero, P.; Martinez-Lopez, J.; Koehne, G.; Touzeau, C.; et al. Elranatamab in Relapsed or Refractory Multiple Myeloma: Phase 2 MagnetisMM-3 Trial Results. *Nat. Med.* **2023**, *29*, 2259–2267, doi:10.1038/s41591-023-02528-9.
- 80. Dhakal, B.; Shah, N.; Kansagra, A.; Kumar, A.; Lonial, S.; Garfall, A.; Cowan, A.; Poudyal, B.S.; Costello, C.; Gay, F.; et al. ASTCT Clinical Practice Recommendations for Transplantation and Cellular Therapies in Multiple Myeloma. *Transplant. Cell. Ther.* **2022**, *28*, 284–293, doi:10.1016/j.jtct.2022.03.019.
- 81. Attal, M.; Lauwers-Cances, V.; Hulin, C.; Leleu, X.; Caillot, D.; Escoffre, M.; Arnulf, B.; Macro, M.; Belhadj, K.; Garderet, L.; et al. Lenalidomide, Bortezomib, and Dexamethasone with Transplantation for Myeloma. *N. Engl. J. Med.* **2017**, *376*, 1311–1320, doi:10.1056/NEJMoa1611750.
- 82. Malard, F.; Neri, P.; Bahlis, N.J.; Terpos, E.; Moukalled, N.; Hungria, V.T.M.; Manier, S.; Mohty, M. Multiple Myeloma. *Nat. Rev. Dis. Primer* **2024**, *10*, 1–21, doi:10.1038/s41572-024-00529-7.
- 83. Shapiro-Shelef, M.; Calame, K. Regulation of Plasma-Cell Development. *Nat. Rev. Immunol.* **2005**, *5*, 230–242, doi:10.1038/nri1572.
- 84. Gatto, D.; Brink, R. The Germinal Center Reaction. *J. Allergy Clin. Immunol.* **2010**, *126*, 898–907; quiz 908–909, doi:10.1016/j.jaci.2010.09.007.
- 85. Bakkus, M.H.; Heirman, C.; Van Riet, I.; Van Camp, B.; Thielemans, K. Evidence That Multiple Myeloma Ig Heavy Chain VDJ Genes Contain Somatic Mutations but Show No Intraclonal Variation. *Blood* **1992**, *80*, 2326–2335.
- 86. Sahota, S.S.; Leo, R.; Hamblin, T.J.; Stevenson, F.K. Myeloma VL and VH Gene Sequences Reveal a Complementary Imprint of Antigen Selection in Tumor Cells. *Blood* **1997**, *89*, 219–226.
- 87. González, D.; Van Der Burg, M.; García-Sanz, R.; Fenton, J.A.; Langerak, A.W.; González, M.; Van Dongen, J.J.M.; San Miguel, J.F.; Morgan, G.J. Immunoglobulin Gene Rearrangements and the Pathogenesis of Multiple Myeloma. *Blood* **2007**, *110*, 3112–3121, doi:10.1182/blood-2007-02-069625.
- 88. Van Riet, I.; Heirman, C.; Lacor, P.; Waele, M.D.; Thielemans, K.; Van Camp, B. Detection of Monoclonal B Lymphocytes in Bone Marrow and Peripheral Blood of Multiple Myeloma Patients by Immunoglobulin Gene Rearrangement Studies. *Br. J. Haematol.* **1989**, *73*, 289–295, doi:10.1111/j.1365-2141.1989.tb07742.x.
- 89. Billadeau, D.; Ahmann, G.; Greipp, P.; Van Ness, B. The Bone Marrow of Multiple Myeloma Patients Contains B Cell Populations at Different Stages of Differentiation That Are Clonally Related to the Malignant Plasma Cell. *J. Exp. Med.* **1993**, *178*, 1023–1031, doi:10.1084/jem.178.3.1023.
- 90. Hemminki, K.; Försti, A.; Houlston, R.; Sud, A. Epidemiology, Genetics and Treatment of Multiple Myeloma and Precursor Diseases. *Int. J. Cancer* **2021**, *149*, 1980–1996, doi:10.1002/ijc.33762.
- 91. Lu, F.; Martin, K.A.; Soldan, S.S.; Kossenkov, A.V.; Wickramasinghe, P.; Vladimirova, O.; De Leo, A.; Lin, C.; Nefedova, Y.; Lieberman, P.M. Defective Epstein-Barr Virus Genomes and Atypical Viral Gene Expression in B-Cell Lines Derived from Multiple Myeloma Patients. *J. Virol.* **2021**, *95*, 10.1128/jvi.00088-21, doi:10.1128/jvi.00088-21.

- 92. Rodríguez-García, A.; Mennesson, N.; Hernandez-Ibarburu, G.; Morales, M.L.; Garderet, L.; Bouchereau, L.; Allain-Maillet, S.; Piver, E.; Marbán, I.; Rubio, D.; et al. Impact of Viral Hepatitis Therapy in Multiple Myeloma and Other Monoclonal Gammopathies Linked to Hepatitis B or C Viruses. *Haematologica* **2024**, *109*, 272–282, doi:10.3324/haematol.2023.283096.
- 93. Barley, K.; Parekh, A.; Salam, S.; Mendu, D.R.; Shukla, R.P.; Vatti, D.; Verina, D.; Stauffer, C.; Salib, C.; El Jamal, S.; et al. Regression of Smoldering Myeloma with Treatment of Gaucher Disease. *Blood Adv.* **2024**, *8*, 1634–1638, doi:10.1182/bloodadvances.2023012304.
- 94. Da Vià, M.C.; Ziccheddu, B.; Maeda, A.; Bagnoli, F.; Perrone, G.; Bolli, N. A Journey Through Myeloma Evolution: From the Normal Plasma Cell to Disease Complexity. *HemaSphere* **2020**, *4*, e502, doi:10.1097/HS9.0000000000000502.
- 95. Maura, F.; Bolli, N.; Angelopoulos, N.; Dawson, K.J.; Leongamornlert, D.; Martincorena, I.; Mitchell, T.J.; Fullam, A.; Gonzalez, S.; Szalat, R.; et al. Genomic Landscape and Chronological Reconstruction of Driver Events in Multiple Myeloma. *Nat. Commun.* **2019**, *10*, 3835, doi:10.1038/s41467-019-11680-1.
- 96. Rustad, E.H.; Yellapantula, V.; Leongamornlert, D.; Bolli, N.; Ledergor, G.; Nadeu, F.; Angelopoulos, N.; Dawson, K.J.; Mitchell, T.J.; Osborne, R.J.; et al. Timing the Initiation of Multiple Myeloma. *Nat. Commun.* **2020**, *11*, 1917, doi:10.1038/s41467-020-15740-9.
- 97. Corre, J.; Munshi, N.; Avet-Loiseau, H. Genetics of Multiple Myeloma: Another Heterogeneity Level? *Blood* **2015**, *125*, 1870–1876, doi:10.1182/blood-2014-10-567370.
- 98. Bergsagel, P.L.; Kuehl, W.M. Molecular Pathogenesis and a Consequent Classification of Multiple Myeloma. *J. Clin. Oncol.* **2005**, *23*, 6333–6338, doi:10.1200/JCO.2005.05.021.
- 99. Carrasco, D.R.; Tonon, G.; Huang, Y.; Zhang, Y.; Sinha, R.; Feng, B.; Stewart, J.P.; Zhan, F.; Khatry, D.; Protopopova, M.; et al. High-Resolution Genomic Profiles Define Distinct Clinico-Pathogenetic Subgroups of Multiple Myeloma Patients. *Cancer Cell* **2006**, *9*, 313–325, doi:10.1016/j.ccr.2006.03.019.
- 100. Bolli, N.; Maura, F.; Minvielle, S.; Gloznik, D.; Szalat, R.; Fullam, A.; Martincorena, I.; Dawson, K.J.; Samur, M.K.; Zamora, J.; et al. Genomic Patterns of Progression in Smoldering Multiple Myeloma. *Nat. Commun.* **2018**, *9*, 3363, doi:10.1038/s41467-018-05058-y.
- 101. Chesi, M.; Brents, L.A.; Ely, S.A.; Bais, C.; Robbiani, D.F.; Mesri, E.A.; Kuehl, W.M.; Bergsagel, P.L. Activated Fibroblast Growth Factor Receptor 3 Is an Oncogene That Contributes to Tumor Progression in Multiple Myeloma. *Blood* **2001**, *97*, 729–736, doi:10.1182/blood.v97.3.729.
- 102. Katsarou, A.; Trasanidis, N.; Ponnusamy, K.; Kostopoulos, I.V.; Alvarez-Benayas, J.; Papaleonidopoulou, F.; Keren, K.; Sabbattini, P.M.R.; Feldhahn, N.; Papaioannou, M.; et al. MAF Functions as a Pioneer Transcription Factor That Initiates and Sustains Myelomagenesis. *Blood Adv.* **2023**, 7, 6395–6410, doi:10.1182/bloodadvances.2023009772.
- 103. Barwick, B.G.; Neri, P.; Bahlis, N.J.; Nooka, A.K.; Dhodapkar, M.V.; Jaye, D.L.; Hofmeister, C.C.; Kaufman, J.L.; Gupta, V.A.; Auclair, D.; et al. Multiple Myeloma Immunoglobulin Lambda Translocations Portend Poor Prognosis. *Nat. Commun.* **2019**, *10*, 1911, doi:10.1038/s41467-019-09555-6.
- 104. Delmore, J.E.; Issa, G.C.; Lemieux, M.E.; Rahl, P.B.; Shi, J.; Jacobs, H.M.; Kastritis, E.; Gilpatrick, T.; Paranal, R.M.; Qi, J.; et al. BET Bromodomain Inhibition as a Therapeutic Strategy to Target C-Myc. *Cell* **2011**, *146*, 904–917, doi:10.1016/j.cell.2011.08.017.

- 105. Jovanović, K.K.; Roche-Lestienne, C.; Ghobrial, I.M.; Facon, T.; Quesnel, B.; Manier, S. Targeting MYC in Multiple Myeloma. *Leukemia* **2018**, *32*, 1295–1306, doi:10.1038/s41375-018-0036-x.
- 106. Rustad, E.H.; Yellapantula, V.D.; Glodzik, D.; Maclachlan, K.H.; Diamond, B.; Boyle, E.M.; Ashby, C.; Blaney, P.; Gundem, G.; Hultcrantz, M.; et al. Revealing the Impact of Structural Variants in Multiple Myeloma. *Blood Cancer Discov.* **2020**, *1*, 258–273, doi:10.1158/2643-3230.BCD-20-0132.
- 107. Walker, B.A.; Wardell, C.P.; Brioli, A.; Boyle, E.; Kaiser, M.F.; Begum, D.B.; Dahir, N.B.; Johnson, D.C.; Ross, F.M.; Davies, F.E.; et al. Translocations at 8q24 Juxtapose MYC with Genes That Harbor Superenhancers Resulting in Overexpression and Poor Prognosis in Myeloma Patients. *Blood Cancer J.* **2014**, 4, e191–e191, doi:10.1038/bcj.2014.13.
- 108. Barwick, B.G.; Gupta, V.A.; Vertino, P.M.; Boise, L.H. Cell of Origin and Genetic Alterations in the Pathogenesis of Multiple Myeloma. *Front. Immunol.* **2019**, *10*, 1121, doi:10.3389/fimmu.2019.01121.
- 109. Wang, Y.; Xu, J.; Xu, B.; Li, P.; Yang, Y.; Wang, W.; Xu, T.; Maihemaiti, A.; Lan, T.; Wang, P.; et al. The Prognostic Role of 1q21 Gain/Amplification in Newly Diagnosed Multiple Myeloma: The Faster, the Worse. *Cancer* **2023**, *129*, 1005–1016, doi:10.1002/cncr.34641.
- 110. Walker, B.A.; Boyle, E.M.; Wardell, C.P.; Murison, A.; Begum, D.B.; Dahir, N.M.; Proszek, P.Z.; Johnson, D.C.; Kaiser, M.F.; Melchor, L.; et al. Mutational Spectrum, Copy Number Changes, and Outcome: Results of a Sequencing Study of Patients With Newly Diagnosed Myeloma. *J. Clin. Oncol.* **2015**, *33*, 3911–3920, doi:10.1200/JCO.2014.59.1503.
- 111. Chapman, M.A.; Lawrence, M.S.; Keats, J.J.; Cibulskis, K.; Sougnez, C.; Schinzel, A.C.; Harview, C.L.; Brunet, J.-P.; Ahmann, G.J.; Adli, M.; et al. Initial Genome Sequencing and Analysis of Multiple Myeloma. *Nature* **2011**, *471*, 467–472, doi:10.1038/nature09837.
- 112. Boyle, E.M.; Deshpande, S.; Tytarenko, R.; Ashby, C.; Wang, Y.; Bauer, M.A.; Johnson, S.K.; Wardell, C.P.; Thanendrarajan, S.; Zangari, M.; et al. The Molecular Make up of Smoldering Myeloma Highlights the Evolutionary Pathways Leading to Multiple Myeloma. *Nat. Commun.* **2021**, *12*, 293, doi:10.1038/s41467-020-20524-2.
- 113. Sacco, A.; Federico, C.; Todoerti, K.; Ziccheddu, B.; Palermo, V.; Giacomini, A.; Ravelli, C.; Maccarinelli, F.; Bianchi, G.; Belotti, A.; et al. Specific Targeting of the KRAS Mutational Landscape in Myeloma as a Tool to Unveil the Elicited Antitumor Activity. *Blood* 2021, *138*, 1705–1720, doi:10.1182/blood.2020010572.
- 114. Van Andel, H.; Kocemba, K.A.; De Haan-Kramer, A.; Mellink, C.H.; Piwowar, M.; Broijl, A.; Van Duin, M.; Sonneveld, P.; Maurice, M.M.; Kersten, M.J.; et al. Loss of CYLD Expression Unleashes Wnt Signaling in Multiple Myeloma and Is Associated with Aggressive Disease. *Oncogene* **2017**, *36*, 2105–2115, doi:10.1038/onc.2016.368.
- 115. Maclachlan, K.H.; Rustad, E.H.; Derkach, A.; Zheng-Lin, B.; Yellapantula, V.; Diamond, B.; Hultcrantz, M.; Ziccheddu, B.; Boyle, E.M.; Blaney, P.; et al. Copy Number Signatures Predict Chromothripsis and Clinical Outcomes in Newly Diagnosed Multiple Myeloma. *Nat. Commun.* **2021**, *12*, 5172, doi:10.1038/s41467-021-25469-8.
- 116. Oben, B.; Froyen, G.; Maclachlan, K.H.; Leongamornlert, D.; Abascal, F.; Zheng-Lin, B.; Yellapantula, V.; Derkach, A.; Geerdens, E.; Diamond, B.T.; et al. Whole-Genome

- Sequencing Reveals Progressive versus Stable Myeloma Precursor Conditions as Two Distinct Entities. *Nat. Commun.* **2021**, *12*, 1861, doi:10.1038/s41467-021-22140-0.
- 117. Flynt, E.; Bisht, K.; Sridharan, V.; Ortiz, M.; Towfic, F.; Thakurta, A. Prognosis, Biology, and Targeting of TP53 Dysregulation in Multiple Myeloma. *Cells* **2020**, *9*, 287, doi:10.3390/cells9020287.
- 118. Schmidt, T.M.; Fonseca, R.; Usmani, S.Z. Chromosome 1q21 Abnormalities in Multiple Myeloma. *Blood Cancer J.* **2021**, *11*, 1–11, doi:10.1038/s41408-021-00474-8.
- 119. Walker, B.A.; Wardell, C.P.; Murison, A.; Boyle, E.M.; Begum, D.B.; Dahir, N.M.; Proszek, P.Z.; Melchor, L.; Pawlyn, C.; Kaiser, M.F.; et al. APOBEC Family Mutational Signatures Are Associated with Poor Prognosis Translocations in Multiple Myeloma. *Nat. Commun.* **2015**, *6*, 6997, doi:10.1038/ncomms7997.
- 120. Grasedieck, S.; Panahi, A.; Jarvis, M.C.; Borzooee, F.; Harris, R.S.; Larijani, M.; Avet-Loiseau, H.; Samur, M.; Munshi, N.; Song, K.; et al. Redefining High Risk Multiple Myeloma with an APOBEC/Inflammation-Based Classifier. *Leukemia* **2024**, *38*, 1172–1177, doi:10.1038/s41375-024-02210-0.
- 121. Maura, F.; Petljak, M.; Lionetti, M.; Cifola, I.; Liang, W.; Pinatel, E.; Alexandrov, L.B.; Fullam, A.; Martincorena, I.; Dawson, K.J.; et al. Biological and Prognostic Impact of APOBEC-Induced Mutations in the Spectrum of Plasma Cell Dyscrasias and Multiple Myeloma Cell Lines. *Leukemia* **2018**, *32*, 1043–1047, doi:10.1038/leu.2017.345.
- 122. Maura, F.; Rustad, E.H.; Yellapantula, V.; Łuksza, M.; Hoyos, D.; Maclachlan, K.H.; Diamond, B.T.; Greenbaum, B.D.; Morgan, G.; Lesokhin, A.; et al. Role of AID in the Temporal Pattern of Acquisition of Driver Mutations in Multiple Myeloma. *Leukemia* **2020**, *34*, 1476–1480, doi:10.1038/s41375-019-0689-0.
- 123. Hoang, P.H.; Cornish, A.J.; Dobbins, S.E.; Kaiser, M.; Houlston, R.S. Mutational Processes Contributing to the Development of Multiple Myeloma. *Blood Cancer J.* **2019**, 9, 60, doi:10.1038/s41408-019-0221-9.
- 124. Gupta, V.A.; Barwick, B.G.; Matulis, S.M.; Shirasaki, R.; Jaye, D.L.; Keats, J.J.; Oberlton, B.; Joseph, N.S.; Hofmeister, C.C.; Heffner, L.T.; et al. Venetoclax Sensitivity in Multiple Myeloma Is Associated with B-Cell Gene Expression. *Blood* **2021**, *137*, 3604–3615, doi:10.1182/blood.2020007899.
- 125. Yang, Y.; Bolomsky, A.; Oellerich, T.; Chen, P.; Ceribelli, M.; Häupl, B.; Wright, G.W.; Phelan, J.D.; Huang, D.W.; Lord, J.W.; et al. Oncogenic RAS Commandeers Amino Acid Sensing Machinery to Aberrantly Activate mTORC1 in Multiple Myeloma. *Nat. Commun.* **2022**, *13*, 5469, doi:10.1038/s41467-022-33142-x.
- 126. Cordas Dos Santos, D.M.; Toenges, R.; Bertamini, L.; Alberge, J.-B.; Ghobrial, I.M. New Horizons in Our Understanding of Precursor Multiple Myeloma and Early Interception. *Nat. Rev. Cancer* **2024**, *24*, 867–886, doi:10.1038/s41568-024-00755-x.
- 127. Kawano, Y.; Moschetta, M.; Manier, S.; Glavey, S.; Görgün, G.T.; Roccaro, A.M.; Anderson, K.C.; Ghobrial, I.M. Targeting the Bone Marrow Microenvironment in Multiple Myeloma. *Immunol. Rev.* **2015**, *263*, 160–172, doi:10.1111/imr.12233.
- 128. Giannakoulas, N.; Ntanasis-Stathopoulos, I.; Terpos, E. The Role of Marrow Microenvironment in the Growth and Development of Malignant Plasma Cells in Multiple Myeloma. *Int. J. Mol. Sci.* **2021**, *22*, 4462, doi:10.3390/ijms22094462.
- 129. De Jong, M.M.E.; Kellermayer, Z.; Papazian, N.; Tahri, S.; Hofste Op Bruinink, D.; Hoogenboezem, R.; Sanders, M.A.; Van De Woestijne, P.C.; Bos, P.K.; Khandanpour, C.; et al. The Multiple Myeloma Microenvironment Is Defined by an Inflammatory Stromal Cell Landscape. *Nat. Immunol.* **2021**, *22*, 769–780, doi:10.1038/s41590-021-00931-3.

- 130. Reagan, M.R.; Liaw, L.; Rosen, C.J.; Ghobrial, I.M. Dynamic Interplay between Bone and Multiple Myeloma: Emerging Roles of the Osteoblast. *Bone* **2015**, *75*, 161–169, doi:10.1016/j.bone.2015.02.021.
- 131. Abe, M.; Hiura, K.; Wilde, J.; Shioyasono, A.; Moriyama, K.; Hashimoto, T.; Kido, S.; Oshima, T.; Shibata, H.; Ozaki, S.; et al. Osteoclasts Enhance Myeloma Cell Growth and Survival via Cell-Cell Contact: A Vicious Cycle between Bone Destruction and Myeloma Expansion. *Blood* **2004**, *104*, 2484–2491, doi:10.1182/blood-2003-11-3839.
- 132. Garbicz, F.; Kaszkowiak, M.; Dudkiewicz-Garbicz, J.; Dorfman, D.M.; Ostrowska, J.; Barankiewicz, J.; Salomon-Perzyński, A.; Lech-Marańda, E.; Nguyen, T.; Juszczyński, P.; et al. Characterization and Experimental Use of Multiple Myeloma Bone Marrow Endothelial Cells and Progenitors. *Int. J. Mol. Sci.* **2024**, *25*, 12047, doi:10.3390/ijms252212047.
- 133. Nakamura, K.; Smyth, M.J.; Martinet, L. Cancer Immunoediting and Immune Dysregulation in Multiple Myeloma. *Blood* **2020**, *136*, 2731–2740, doi:10.1182/blood.2020006540.
- 134. Hideshima, T.; Anderson, K.C. Signaling Pathway Mediating Myeloma Cell Growth and Survival. *Cancers* **2021**, *13*, 216, doi:10.3390/cancers13020216.
- 135. Hideshima, T.; Mitsiades, C.; Tonon, G.; Richardson, P.G.; Anderson, K.C. Understanding Multiple Myeloma Pathogenesis in the Bone Marrow to Identify New Therapeutic Targets. *Nat. Rev. Cancer* **2007**, *7*, 585–598, doi:10.1038/nrc2189.
- 136. Neri, P.; Bahlis, N.J. Targeting of Adhesion Molecules as a Therapeutic Strategy in Multiple Myeloma. *Curr. Cancer Drug Targets* 12, 776–796, doi:10.2174/156800912802429337.
- 137. Bou Zerdan, M.; Nasr, L.; Kassab, J.; Saba, L.; Ghossein, M.; Yaghi, M.; Dominguez, B.; Chaulagain, C.P. Adhesion Molecules in Multiple Myeloma Oncogenesis and Targeted Therapy. *Int. J. Hematol. Oncol.* **2022**, *11*, IJH39, doi:10.2217/ijh-2021-0017.
- 138. Alrasheed, N.; Lee, L.; Ghorani, E.; Henry, J.Y.; Conde, L.; Chin, M.; Galas-Filipowicz, D.; Furness, A.J.S.; Chavda, S.J.; Richards, H.; et al. Marrow-Infiltrating Regulatory T Cells Correlate with the Presence of Dysfunctional CD4+PD-1+ Cells and Inferior Survival in Patients with Newly Diagnosed Multiple Myeloma. *Clin. Cancer Res.* **2020**, 26, 3443–3454, doi:10.1158/1078-0432.CCR-19-1714.
- 139. Beyer, M.; Kochanek, M.; Giese, T.; Endl, E.; Weihrauch, M.R.; Knolle, P.A.; Classen, S.; Schultze, J.L. In Vivo Peripheral Expansion of Naive CD4+CD25highFoxP3+ Regulatory T Cells in Patients with Multiple Myeloma. *Blood* **2006**, *107*, 3940–3949, doi:10.1182/blood-2005-09-3671.
- 140. Guillerey, C.; Harjunpää, H.; Carrié, N.; Kassem, S.; Teo, T.; Miles, K.; Krumeich, S.; Weulersse, M.; Cuisinier, M.; Stannard, K.; et al. TIGIT Immune Checkpoint Blockade Restores CD8+ T-Cell Immunity against Multiple Myeloma. *Blood* **2018**, *132*, 1689–1694, doi:10.1182/blood-2018-01-825265.
- 141. Guillerey, C.; Ferrari De Andrade, L.; Vuckovic, S.; Miles, K.; Ngiow, S.F.; Yong, M.C.R.; Teng, M.W.L.; Colonna, M.; Ritchie, D.S.; Chesi, M.; et al. Immunosurveillance and Therapy of Multiple Myeloma Are CD226 Dependent. *J. Clin. Invest.* **2015**, *125*, 2077–2089, doi:10.1172/JCI77181.
- 142. Minnie, S.A.; Kuns, R.D.; Gartlan, K.H.; Zhang, P.; Wilkinson, A.N.; Samson, L.; Guillerey, C.; Engwerda, C.; MacDonald, K.P.A.; Smyth, M.J.; et al. Myeloma Escape after Stem Cell Transplantation Is a Consequence of T-Cell Exhaustion and Is Prevented by TIGIT Blockade. *Blood* **2018**, *132*, 1675–1688, doi:10.1182/blood-2018-01-825240.

- 143. Guillerey, C.; Nakamura, K.; Vuckovic, S.; Hill, G.R.; Smyth, M.J. Immune Responses in Multiple Myeloma: Role of the Natural Immune Surveillance and Potential of Immunotherapies. *Cell. Mol. Life Sci.* **2016**, *73*, 1569–1589, doi:10.1007/s00018-016-2135-z.
- 144. Moscvin, M.; Evans, B.; Bianchi, G. Dissecting Molecular Mechanisms of Immune Microenvironment Dysfunction in Multiple Myeloma and Precursor Conditions. *J. Cancer Metastasis Treat.* **2023**, doi:10.20517/2394-4722.2022.110.
- 145. John, M.; Helal, M.; Duell, J.; Mattavelli, G.; Stanojkovska, E.; Afrin, N.; Leipold, A.M.; Steinhardt, M.J.; Zhou, X.; Žihala, D.; et al. Spatial Transcriptomics Reveals Profound Subclonal Heterogeneity and T-Cell Dysfunction in Extramedullary Myeloma. *Blood* **2024**, *144*, 2121–2135, doi:10.1182/blood.2024024590.
- 146. Mishra, A.K.; Schmidt, T.M.; Martell, E.B.; Chen, A.S.; Dogru, R.E.; Hematti, P.; Callander, N.S. PD1+TIGIT+2B4+KLRG1+ Cells Might Underlie T Cell Dysfunction in Patients Treated with BCMA-Directed Chimeric Antigen Receptor T Cell Therapy. *Transplant. Cell. Ther.* **2024**, *30*, 191–202, doi:10.1016/j.jtct.2023.11.014.
- 147. Friedrich, M.J.; Neri, P.; Kehl, N.; Michel, J.; Steiger, S.; Kilian, M.; Leblay, N.; Maity, R.; Sankowski, R.; Lee, H.; et al. The Pre-Existing T Cell Landscape Determines the Response to Bispecific T Cell Engagers in Multiple Myeloma Patients. *Cancer Cell* **2023**, 41, 711-725.e6, doi:10.1016/j.ccell.2023.02.008.
- 148. Bailur, J.K.; McCachren, S.S.; Doxie, D.B.; Shrestha, M.; Pendleton, K.; Nooka, A.K.; Neparidze, N.; Parker, T.L.; Bar, N.; Kaufman, J.L.; et al. Early Alterations in Stemlike/Marrow-Resident T Cells and Innate and Myeloid Cells in Preneoplastic Gammopathy. *JCI Insight* **2019**, *4*, e127807, doi:10.1172/jci.insight.127807.
- 149. Tian, E.; Zhan, F.; Walker, R.; Rasmussen, E.; Ma, Y.; Barlogie, B.; Shaughnessy, J.D. The Role of the Wnt-Signaling Antagonist DKK1 in the Development of Osteolytic Lesions in Multiple Myeloma. *N. Engl. J. Med.* **2003**, *349*, 2483–2494, doi:10.1056/NEJMoa030847.
- 150. Noonan, K.; Marchionni, L.; Anderson, J.; Pardoll, D.; Roodman, G.D.; Borrello, I. A Novel Role of IL-17–Producing Lymphocytes in Mediating Lytic Bone Disease in Multiple Myeloma. *Blood* **2010**, *116*, 3554–3563, doi:10.1182/blood-2010-05-283895.
- 151. Peng, R.; Dong, Y.; Zheng, M.; Kang, H.; Wang, P.; Zhu, M.; Song, K.; Wu, W.; Li, F. IL-17 Promotes Osteoclast-Induced Bone Loss by Regulating Glutamine-Dependent Energy Metabolism. *Cell Death Dis.* **2024**, *15*, 1–12, doi:10.1038/s41419-024-06475-2.
- 152. Lutz, R.; Grünschläger, F.; Simon, M.; Awwad, M.H.S.; Bauer, M.; Yousefian, S.; Beumer, N.; Jopp-Saile, L.; Sedlmeier, A.; Solé-Boldo, L.; et al. Multiple Myeloma Long-Term Survivors Exhibit Sustained Immune Alterations Decades after First-Line Therapy. *Nat. Commun.* **2024**, *15*, 10396, doi:10.1038/s41467-024-54543-0.
- 153. Mateos, M.-V.; Blacklock, H.; Schjesvold, F.; Oriol, A.; Simpson, D.; George, A.; Goldschmidt, H.; Larocca, A.; Chanan-Khan, A.; Sherbenou, D.; et al. Pembrolizumab plus Pomalidomide and Dexamethasone for Patients with Relapsed or Refractory Multiple Myeloma (KEYNOTE-183): A Randomised, Open-Label, Phase 3 Trial. *Lancet Haematol.* **2019**, *6*, e459–e469, doi:10.1016/S2352-3026(19)30110-3.
- 154. Rosenblatt, J.; Avigan, D. Targeting the PD-1/PD-L1 Axis in Multiple Myeloma: A Dream or a Reality? *Blood* **2017**, *129*, 275–279, doi:10.1182/blood-2016-08-731885.
- 155. Teitelbaum, S.L.; Ross, F.P. Genetic Regulation of Osteoclast Development and Function. *Nat. Rev. Genet.* **2003**, *4*, 638–649, doi:10.1038/nrg1122.

- 156. Edwards, C.M.; Zhuang, J.; Mundy, G.R. The Pathogenesis of the Bone Disease of Multiple Myeloma. *Bone* **2008**, *42*, 1007–1013, doi:10.1016/j.bone.2008.01.027.
- 157. Bataille, R.; Chappard, D.; Marcelli, C.; Dessauw, P.; Baldet, P.; Sany, J.; Alexandre, C. Recruitment of New Osteoblasts and Osteoclasts Is the Earliest Critical Event in the Pathogenesis of Human Multiple Myeloma. *J. Clin. Invest.* **1991**, *88*, 62–66, doi:10.1172/JCI115305.
- 158. Valentin-Opran, A.; Charhon, S.A.; Meunier, P.J.; Edouard, C.M.; Arlot, M.E. Quantitative Histology of Myeloma-Induced Bone Changes. *Br. J. Haematol.* **1982**, *52*, 601–610, doi:10.1111/j.1365-2141.1982.tb03936.x.
- 159. Trotter, T.N.; Li, M.; Pan, Q.; Peker, D.; Rowan, P.D.; Li, J.; Zhan, F.; Suva, L.J.; Javed, A.; Yang, Y. Myeloma Cell–Derived Runx2 Promotes Myeloma Progression in Bone. *Blood* **2015**, *125*, 3598–3608, doi:10.1182/blood-2014-12-613968.
- 160. Abe, M.; Hiura, K.; Wilde, J.; Shioyasono, A.; Moriyama, K.; Hashimoto, T.; Kido, S.; Oshima, T.; Shibata, H.; Ozaki, S.; et al. Osteoclasts Enhance Myeloma Cell Growth and Survival via Cell-Cell Contact: A Vicious Cycle between Bone Destruction and Myeloma Expansion. *Blood* **2004**, *104*, 2484–2491, doi:10.1182/blood-2003-11-3839.
- 161. Long, F. Building Strong Bones: Molecular Regulation of the Osteoblast Lineage. *Nat. Rev. Mol. Cell Biol.* **2012**, *13*, 27–38, doi:10.1038/nrm3254.
- 162. Adamik, J.; Galson, D.L.; Roodman, G.D. Osteoblast Suppression in Multiple Myeloma Bone Disease. *J. Bone Oncol.* **2018**, *13*, 62–70, doi:10.1016/j.jbo.2018.09.001.
- 163. Edwards, C.M.; Zhuang, J.; Mundy, G.R. The Pathogenesis of the Bone Disease of Multiple Myeloma. *Bone* **2008**, *42*, 1007–1013, doi:10.1016/j.bone.2008.01.027.
- 164. McDonald, M.M.; Reagan, M.R.; Youlten, S.E.; Mohanty, S.T.; Seckinger, A.; Terry, R.L.; Pettitt, J.A.; Simic, M.K.; Cheng, T.L.; Morse, A.; et al. Inhibiting the Osteocyte-Specific Protein Sclerostin Increases Bone Mass and Fracture Resistance in Multiple Myeloma. *Blood* **2017**, *129*, 3452–3464, doi:10.1182/blood-2017-03-773341.
- 165. Kaiser, M.F.; Heider, U.; Mieth, M.; Zang, C.; von Metzler, I.; Sezer, O. The Proteasome Inhibitor Bortezomib Stimulates Osteoblastic Differentiation of Human Osteoblast Precursors via Upregulation of Vitamin D Receptor Signalling. *Eur. J. Haematol.* **2013**, 90, 263–272, doi:10.1111/ejh.12069.
- 166. Teramachi, J.; Hiasa, M.; Oda, A.; Harada, T.; Nakamura, S.; Amachi, R.; Tenshin, H.; Iwasa, M.; Fujii, S.; Kagawa, K.; et al. Pim-2 Is a Critical Target for Treatment of Osteoclastogenesis Enhanced in Myeloma. *Br. J. Haematol.* **2018**, *180*, 581–585, doi:10.1111/bjh.14388.
- 167. Beider, K.; Bitner, H.; Leiba, M.; Gutwein, O.; Koren-Michowitz, M.; Ostrovsky, O.; Abraham, M.; Wald, H.; Galun, E.; Peled, A.; et al. Multiple Myeloma Cells Recruit Tumor-Supportive Macrophages through the CXCR4/CXCL12 Axis and Promote Their Polarization toward the M2 Phenotype. *Oncotarget* **2014**, *5*, 11283–11296, doi:10.18632/oncotarget.2207.
- 168. Chen, H.; Li, M.; Sanchez, E.; Soof, C.M.; Bujarski, S.; Ng, N.; Cao, J.; Hekmati, T.; Zahab, B.; Nosrati, J.D.; et al. JAK1/2 Pathway Inhibition Suppresses M2 Polarization and Overcomes Resistance of Myeloma to Lenalidomide by Reducing TRIB1, MUC1, CD44, CXCL12, and CXCR4 Expression. *Br. J. Haematol.* **2020**, *188*, 283–294, doi:10.1111/bjh.16158.
- 169. Gutiérrez-González, A.; Martínez-Moreno, M.; Samaniego, R.; Arellano-Sánchez, N.; Salinas-Muñoz, L.; Relloso, M.; Valeri, A.; Martínez-López, J.; Corbí, Á.L.; Hidalgo, A.;

- et al. Evaluation of the Potential Therapeutic Benefits of Macrophage Reprogramming in Multiple Myeloma. *Blood* **2016**, *128*, 2241–2252, doi:10.1182/blood-2016-01-695395.
- 170. Sun, J.; Park, C.; Guenthner, N.; Gurley, S.; Zhang, L.; Lubben, B.; Adebayo, O.; Bash, H.; Chen, Y.; Maksimos, M.; et al. Tumor-Associated Macrophages in Multiple Myeloma: Advances in Biology and Therapy. *J. Immunother. Cancer* **2022**, *10*, e003975, doi:10.1136/jitc-2021-003975.
- 171. Görgün, G.T.; Whitehill, G.; Anderson, J.L.; Hideshima, T.; Maguire, C.; Laubach, J.; Raje, N.; Munshi, N.C.; Richardson, P.G.; Anderson, K.C. Tumor-Promoting Immune-Suppressive Myeloid-Derived Suppressor Cells in the Multiple Myeloma Microenvironment in Humans. *Blood* **2013**, *121*, 2975–2987, doi:10.1182/blood-2012-08-448548.
- 172. Akhmetzyanova, I.; Aaron, T.; Galbo, P.; Tikhonova, A.; Dolgalev, I.; Tanaka, M.; Aifantis, I.; Zheng, D.; Zang, X.; Fooksman, D. Tissue-Resident Macrophages Promote Early Dissemination of Multiple Myeloma via IL-6 and TNFα. *Blood Adv.* **2021**, *5*, 3592–3608, doi:10.1182/bloodadvances.2021005327.
- 173. Opperman, K.S.; Vandyke, K.; Clark, K.C.; Coulter, E.A.; Hewett, D.R.; Mrozik, K.M.; Schwarz, N.; Evdokiou, A.; Croucher, P.I.; Psaltis, P.J.; et al. Clodronate-Liposome Mediated Macrophage Depletion Abrogates Multiple Myeloma Tumor Establishment In Vivo. *Neoplasia N. Y. N* **2019**, *21*, 777–787, doi:10.1016/j.neo.2019.05.006.
- 174. Sun, J.; Corradini, S.; Azab, F.; Shokeen, M.; Muz, B.; Miari, K.E.; Maksimos, M.; Diedrich, C.; Asare, O.; Alhallak, K.; et al. IL-10R Inhibition Reprograms Tumor-Associated Macrophages and Reverses Drug Resistance in Multiple Myeloma. *Leukemia* **2024**, *38*, 2355–2365, doi:10.1038/s41375-024-02391-8.
- 175. Ramachandran, I.R.; Martner, A.; Pisklakova, A.; Condamine, T.; Chase, T.; Vogl, T.; Roth, J.; Gabrilovich, D.; Nefedova, Y. Myeloid-Derived Suppressor Cells Regulate Growth of Multiple Myeloma by Inhibiting T Cells in Bone Marrow. *J. Immunol.* **2013**, *190*, 3815–3823, doi:10.4049/jimmunol.1203373.
- 176. Giallongo, C.; Tibullo, D.; Parrinello, N.L.; La Cava, P.; Di Rosa, M.; Bramanti, V.; Di Raimondo, C.; Conticello, C.; Chiarenza, A.; Palumbo, G.A.; et al. Granulocyte-like Myeloid Derived Suppressor Cells (G-MDSC) Are Increased in Multiple Myeloma and Are Driven by Dysfunctional Mesenchymal Stem Cells (MSC). *Oncotarget* **2016**, *7*, 85764–85775, doi:10.18632/oncotarget.7969.
- 177. Favaloro, J.; Liyadipitiya, T.; Brown, R.; Yang, S.; Suen, H.; Woodland, N.; Nassif, N.; Hart, D.; Fromm, P.; Weatherburn, C.; et al. Myeloid Derived Suppressor Cells Are Numerically, Functionally and Phenotypically Different in Patients with Multiple Myeloma. *Leuk. Lymphoma* **2014**, *55*, 2893–2900, doi:10.3109/10428194.2014.904511.
- 178. Chauhan, D.; Singh, A.V.; Brahmandam, M.; Carrasco, R.; Bandi, M.; Hideshima, T.; Bianchi, G.; Podar, K.; Tai, Y.-T.; Mitsiades, C.; et al. Functional Interaction of Plasmacytoid Dendritic Cells with Multiple Myeloma Cells: A Therapeutic Target. *Cancer Cell* **2009**, *16*, 309–323, doi:10.1016/j.ccr.2009.08.019.
- 179. Wolf, N.K.; Kissiov, D.U.; Raulet, D.H. Roles of Natural Killer Cells in Immunity to Cancer, and Applications to Immunotherapy. *Nat. Rev. Immunol.* **2023**, *23*, 90–105, doi:10.1038/s41577-022-00732-1.
- 180. Li, X.; Chen, M.; Wan, Y.; Zhong, L.; Han, X.; Chen, X.; Xiao, F.; Liu, J.; Zhang, Y.; Zhu, D.; et al. Single-cell Transcriptome Profiling Reveals the Key Role of ZNF683 in Natural Killer Cell Exhaustion in Multiple Myeloma. *Clin. Transl. Med.* **2022**, *12*, e1065, doi:10.1002/ctm2.1065.

- 181. Cheng, Y.; Sun, F.; Alapat, D.V.; Wanchai, V.; Mery, D.; Siegel, E.R.; Xu, H.; Johnson, S.; Guo, W.; Bailey, C.; et al. Multi-Omics Reveal Immune Microenvironment Alterations in Multiple Myeloma and Its Precursor Stages. *Blood Cancer J.* **2024**, *14*, 194, doi:10.1038/s41408-024-01172-x.
- 182. Blanquart, E.; Ekren, R.; Rigaud, B.; Joubert, M.-V.; Baylot, V.; Daunes, H.; Cuisinier, M.; Villard, M.; Carrié, N.; Mazzotti, C.; et al. NK Cells with Adhesion Defects and Reduced Cytotoxic Functions Are Associated with a Poor Prognosis in Multiple Myeloma. *Blood* **2024**, *144*, 1271–1283, doi:10.1182/blood.2023023529.
- 183. Martínez-Sánchez, M.V.; Periago, A.; Legaz, I.; Gimeno, L.; Mrowiec, A.; Montes-Barqueros, N.R.; Campillo, J.A.; Bolarin, J.M.; Bernardo, M.V.; López-Álvarez, M.R.; et al. Overexpression of KIR Inhibitory Ligands (HLA-I) Determines That Immunosurveillance of Myeloma Depends on Diverse and Strong NK Cell Licensing. *OncoImmunology* **2016**, *5*, e1093721, doi:10.1080/2162402X.2015.1093721.
- 184. D'Souza, C.; Prince, H.M.; Neeson, P.J. Understanding the Role of T-Cells in the Antimyeloma Effect of Immunomodulatory Drugs. *Front. Immunol.* **2021**, *12*, 632399, doi:10.3389/fimmu.2021.632399.
- 185. Verkleij, C.P.M.; Frerichs, K.A.; Broekmans, M.E.C.; Duetz, C.; O'Neill, C.A.; Bruins, W.S.C.; Homan-Weert, P.M.; Minnema, M.C.; Levin, M.-D.; Broijl, A.; et al. NK Cell Phenotype Is Associated With Response and Resistance to Daratumumab in Relapsed/Refractory Multiple Myeloma. *HemaSphere* **2023**, 7, e881, doi:10.1097/HS9.00000000000000881.
- 186. Vu, S.H.; Pham, H.H.; Pham, T.T.P.; Le, T.T.; Vo, M.-C.; Jung, S.-H.; Lee, J.-J.; Nguyen, X.-H. Adoptive NK Cell Therapy a Beacon of Hope in Multiple Myeloma Treatment. *Front. Oncol.* **2023**, *13*, 1275076, doi:10.3389/fonc.2023.1275076.
- 187. Bhat, S.; Viswanathan, P.; Chandanala, S.; Prasanna, S.J.; Seetharam, R.N. Expansion and Characterization of Bone Marrow Derived Human Mesenchymal Stromal Cells in Serum-Free Conditions. *Sci. Rep.* **2021**, *11*, 3403, doi:10.1038/s41598-021-83088-1.
- 188. Shiozawa, Y.; Havens, A.; Pienta, K.; Taichman, R. The Bone Marrow Niche: Habitat to Hematopoietic and Mesenchymal Stem Cells, and Unwitting Host to Molecular Parasites. *Leukemia* **2008**, *22*, 941–950, doi:10.1038/leu.2008.48.
- 189. Crippa, S.; Bernardo, M.E. Mesenchymal Stromal Cells: Role in the BM Niche and in the Support of Hematopoietic Stem Cell Transplantation. *HemaSphere* **2018**, *2*, e151, doi:10.1097/HS9.000000000000151.
- 190. Omatsu, Y.; Sugiyama, T.; Kohara, H.; Kondoh, G.; Fujii, N.; Kohno, K.; Nagasawa, T. The Essential Functions of Adipo-Osteogenic Progenitors as the Hematopoietic Stem and Progenitor Cell Niche. *Immunity* **2010**, *33*, 387–399, doi:10.1016/j.immuni.2010.08.017.
- 191. Sugiyama, T.; Kohara, H.; Noda, M.; Nagasawa, T. Maintenance of the Hematopoietic Stem Cell Pool by CXCL12-CXCR4 Chemokine Signaling in Bone Marrow Stromal Cell Niches. *Immunity* **2006**, *25*, 977–988, doi:10.1016/j.immuni.2006.10.016.
- 192. Di Staulo, A.M.; Ayemoba, C.E.; Petenkaya, A.; Zhang, S.; Maryanovich, M.; Chronis, K.; Pinho, S. Vascular Cell Adhesion Molecule-1 Regulates Bone Marrow Mesenchymal Stem Cell Maintenance and Niche Function. *Blood* 2023, 142, 1328, doi:10.1182/blood-2023-178444.
- 193. Kim, J.; Denu, R.A.; Dollar, B.A.; Escalante, L.E.; Kuether, J.P.; Callander, N.S.; Asimakopoulos, F.; Hematti, P. Macrophages and Mesenchymal Stromal Cells Support Survival and Proliferation of Multiple Myeloma Cells. *Br. J. Haematol.* **2012**, *158*, 336–346, doi:10.1111/j.1365-2141.2012.09154.x.

- 194. Corre, J.; Mahtouk, K.; Attal, M.; Gadelorge, M.; Huynh, A.; Fleury-Cappellesso, S.; Danho, C.; Laharrague, P.; Klein, B.; Rème, T.; et al. Bone Marrow Mesenchymal Stem Cells Are Abnormal in Multiple Myeloma. *Leukemia* **2007**, *21*, 1079–1088, doi:10.1038/sj.leu.2404621.
- 195. Reagan, M.R.; Ghobrial, I.M. Multiple Myeloma Mesenchymal Stem Cells: Characterization, Origin, and Tumor-Promoting Effects. *Clin. Cancer Res.* **2012**, *18*, 342–349, doi:10.1158/1078-0432.CCR-11-2212.
- 196. Boueya, I.L.; Sandhow, L.; Albuquerque, J.R.P.; Znaidi, R.; Passaro, D. Endothelial Heterogeneity in Bone Marrow: Insights across Development, Adult Life and Leukemia. *Leukemia* **2025**, *39*, 8–24, doi:10.1038/s41375-024-02453-x.
- 197. Boueya, I.L.; Sandhow, L.; Albuquerque, J.R.P.; Znaidi, R.; Passaro, D. Endothelial Heterogeneity in Bone Marrow: Insights across Development, Adult Life and Leukemia. *Leukemia* **2025**, *39*, 8–24, doi:10.1038/s41375-024-02453-x.
- 198. Perlin, J.R.; Sporrij, A.; Zon, L.I. Blood on the Tracks: Hematopoietic Stem Cell-Endothelial Cell Interactions in Homing and Engraftment. *J. Mol. Med. Berl. Ger.* **2017**, 95, 809–819, doi:10.1007/s00109-017-1559-8.
- 199. Kusumbe, A.P.; Ramasamy, S.K.; Adams, R.H. Coupling of Angiogenesis and Osteogenesis by a Specific Vessel Subtype in Bone. *Nature* **2014**, *507*, 323–328, doi:10.1038/nature13145.
- 200. Ramasamy, S.K.; Kusumbe, A.P.; Wang, L.; Adams, R.H. Endothelial Notch Activity Promotes Angiogenesis and Osteogenesis in Bone. *Nature* **2014**, *507*, 376–380, doi:10.1038/nature13146.
- 201. Xu, C.; Gao, X.; Wei, Q.; Nakahara, F.; Zimmerman, S.E.; Mar, J.; Frenette, P.S. Stem Cell Factor Is Selectively Secreted by Arterial Endothelial Cells in Bone Marrow. *Nat. Commun.* **2018**, *9*, 2449, doi:10.1038/s41467-018-04726-3.
- 202. Ito, T.; Hamazaki, Y.; Takaori-Kondo, A.; Minato, N. Bone Marrow Endothelial Cells Induce Immature and Mature B Cell Egress in Response to Erythropoietin. *Cell Struct. Funct.* **2017**, *42*, 149–157, doi:10.1247/csf.17018.
- 203. Coutu, D.L.; Kokkaliaris, K.D.; Kunz, L.; Schroeder, T. Three-Dimensional Map of Nonhematopoietic Bone and Bone-Marrow Cells and Molecules. *Nat. Biotechnol.* **2017**, *35*, 1202–1210, doi:10.1038/nbt.4006.
- 204. Itkin, T.; Gur-Cohen, S.; Spencer, J.A.; Schajnovitz, A.; Ramasamy, S.K.; Kusumbe, A.P.; Ledergor, G.; Jung, Y.; Milo, I.; Poulos, M.G.; et al. Distinct Bone Marrow Blood Vessels Differentially Regulate Haematopoiesis. *Nature* **2016**, *532*, 323–328, doi:10.1038/nature17624.
- 205. Bixel, M.G.; Kusumbe, A.P.; Ramasamy, S.K.; Sivaraj, K.K.; Butz, S.; Vestweber, D.; Adams, R.H. Flow Dynamics and HSPC Homing in Bone Marrow Microvessels. *Cell Rep.* **2017**, *18*, 1804–1816, doi:10.1016/j.celrep.2017.01.042.
- 206. Spencer, J.A.; Ferraro, F.; Roussakis, E.; Klein, A.; Wu, J.; Runnels, J.M.; Zaher, W.; Mortensen, L.J.; Alt, C.; Turcotte, R.; et al. Direct Measurement of Local Oxygen Concentration in the Bone Marrow of Live Animals. *Nature* **2014**, *508*, 269–273, doi:10.1038/nature13034.
- 207. Marsch, W.Ch.; Gross, U.M. Frequency and Pathomorphology of Extramedullary Manifestations in Plasma Cell Myeloma of the Skeleton. *Pathol. Res. Pract.* **1978**, *163*, 115–127, doi:10.1016/S0344-0338(78)80080-6.
- 208. Salama, M.E.; Lange, H.; Tripp, S.R.; Kohan, J.; Landis, N.D.; Krueger, J.S.; Potts, S.J. AngioMap Is a Novel Image Analysis Algorithm for Assessment of Plasma Cell

- Distribution within Bone Marrow Vascular Niche. *Appl. Immunohistochem. Mol. Morphol. AIMM* **2014**, *22*, 550–554, doi:10.1097/PAI.0b013e318294cb61.
- 209. Wong, K.F.; Chan, J.K.; Chu, Y.C. Multiple Myeloma with Tadpolelike Cells and Rosette Formation. *Am. J. Clin. Pathol.* **1992**, *98*, 630–632, doi:10.1093/ajcp/98.6.630.
- 210. Folkman, J. Tumor Angiogenesis: Therapeutic Implications. *N. Engl. J. Med.* **1971**, *285*, 1182–1186, doi:10.1056/NEJM197111182852108.
- 211. Folkman, J. Angiogenesis: An Organizing Principle for Drug Discovery? *Nat. Rev. Drug Discov.* **2007**, *6*, 273–286, doi:10.1038/nrd2115.
- 212. Folkman, J.; Langer, R.; Linhardt, R.J.; Haudenschild, C.; Taylor, S. Angiogenesis Inhibition and Tumor Regression Caused by Heparin or a Heparin Fragment in the Presence of Cortisone. *Science* **1983**, *221*, 719–725, doi:10.1126/science.6192498.
- 213. Giuliani, N.; Colla, S.; Morandi, F.; Rizzoli, V. Angiopoietin-1 and Myeloma-Induced Angiogenesis. *Leuk. Lymphoma* **2005**, *46*, 29–33, doi:10.1080/1042-8190400001022.
- 214. Giatromanolaki, A.; Bai, M.; Margaritis, D.; Bourantas, K.L.; Koukourakis, M.I.; Sivridis, E.; Gatter, K.C. Hypoxia and Activated VEGF/Receptor Pathway in Multiple Myeloma. *Anticancer Res.* **2010**, *30*, 2831–2836.
- 215. Giuliani, N.; Storti, P.; Bolzoni, M.; Palma, B.D.; Bonomini, S. Angiogenesis and Multiple Myeloma. *Cancer Microenviron.* **2011**, *4*, 325–337, doi:10.1007/s12307-011-0072-9.
- 216. Palano, M.T.; Giannandrea, D.; Platonova, N.; Gaudenzi, G.; Falleni, M.; Tosi, D.; Lesma, E.; Citro, V.; Colombo, M.; Saltarella, I.; et al. Jagged Ligands Enhance the Pro-Angiogenic Activity of Multiple Myeloma Cells. *Cancers* **2020**, *12*, 2600, doi:10.3390/cancers12092600.
- 217. Barchnicka, A.; Olejniczak-Nowakowska, M.; Krupa-Kotara, K.; Grosicki, S. The Importance of Antiangiogenic Effect in Multiple Myeloma Treatment.
- 218. Vacca, A.; Ria, R.; Ribatti, D.; Semeraro, F.; Djonov, V.; Di Raimondo, F.; Dammacco, F. A Paracrine Loop in the Vascular Endothelial Growth Factor Pathway Triggers Tumor Angiogenesis and Growth in Multiple Myeloma. *Haematologica* **2003**, *88*, 176–185.
- 219. Vacca, A. Endothelial Cells in the Bone Marrow of Patients with Multiple Myeloma. *Blood* **2003**, *102*, 3340–3348, doi:10.1182/blood-2003-04-1338.
- 220. De Jong, M.M.E.; Kellermayer, Z.; Papazian, N.; Tahri, S.; Hofste Op Bruinink, D.; Hoogenboezem, R.; Sanders, M.A.; Van De Woestijne, P.C.; Bos, P.K.; Khandanpour, C.; et al. The Multiple Myeloma Microenvironment Is Defined by an Inflammatory Stromal Cell Landscape. *Nat. Immunol.* **2021**, *22*, 769–780, doi:10.1038/s41590-021-00931-3.
- 221. Garbicz, F.; Kaszkowiak, M.; Dudkiewicz-Garbicz, J.; Dorfman, D.M.; Ostrowska, J.; Barankiewicz, J.; Salomon-Perzyński, A.; Lech-Marańda, E.; Nguyen, T.; Juszczyński, P.; et al. Characterization and Experimental Use of Multiple Myeloma Bone Marrow Endothelial Cells and Progenitors. *Int. J. Mol. Sci.* 2024, 25, 12047, doi:10.3390/ijms252212047.
- 222. Moschetta, M.; Mishima, Y.; Kawano, Y.; Manier, S.; Paiva, B.; Palomera, L.; Aljawai, Y.; Calcinotto, A.; Unitt, C.; Sahin, I.; et al. Targeting Vasculogenesis to Prevent Progression in Multiple Myeloma. *Leukemia* **2016**, *30*, 1103–1115, doi:10.1038/leu.2016.3.
- 223. Zhu, D.; Wang, Z.; Zhao, J.-J.; Calimeri, T.; Meng, J.; Hideshima, T.; Fulciniti, M.; Kang, Y.; Ficarro, S.; Tai, Y.-T.; et al. The Cyclophilin A-CD147 Complex Promotes Bone Marrow Colonization of B-Cell Malignancies: Implications for Therapy. *Nat. Med.* **2015**, *21*, 572–580, doi:10.1038/nm.3867.

- 224. Dankbar, B.; Padró, T.; Leo, R.; Feldmann, B.; Kropff, M.; Mesters, R.M.; Serve, H.; Berdel, W.E.; Kienast, J. Vascular Endothelial Growth Factor and Interleukin-6 in Paracrine Tumor-Stromal Cell Interactions in Multiple Myeloma. *Blood* **2000**, *95*, 2630–2636.
- 225. Antonio G. Solimando; Matteo C. Da Vià; Patrizia Leone; Paola Borrelli; Giorgio A. Croci; Paula Tabares; Andreas Brandl; Giuseppe Di Lernia; Francesco P. Bianchi; Silvio Tafuri; et al. Halting the Vicious Cycle within the Multiple Myeloma Ecosystem: Blocking JAM-A on Bone Marrow Endothelial Cells Restores Angiogenic Homeostasis and Suppresses Tumor Progression. *Haematologica* **2020**, *106*, 1943–1956, doi:10.3324/haematol.2019.239913.
- 226. Lamanuzzi, A.; Saltarella, I.; Desantis, V.; Frassanito, M.A.; Leone, P.; Racanelli, V.; Nico, B.; Ribatti, D.; Ditonno, P.; Prete, M.; et al. Inhibition of mTOR Complex 2 Restrains Tumor Angiogenesis in Multiple Myeloma. *Oncotarget* **2018**, *9*, 20563–20577, doi:10.18632/oncotarget.25003.
- 227. Braunstein, M.; Özçelik, T.; Bağişlar, S.; Vakil, V.; Smith, E.L.; Dai, K.; Akyerli, C.B.; Batuman, O.A. Endothelial Progenitor Cells Display Clonal Restriction in Multiple Myeloma. *BMC Cancer* **2006**, *6*, 161, doi:10.1186/1471-2407-6-161.
- 228. Bisping, G.; Leo, R.; Wenning, D.; Dankbar, B.; Padró, T.; Kropff, M.; Scheffold, C.; Kröger, M.; Mesters, R.M.; Berdel, W.E.; et al. Paracrine Interactions of Basic Fibroblast Growth Factor and Interleukin-6 in Multiple Myeloma. *Blood* **2003**, *101*, 2775–2783, doi:10.1182/blood-2002-09-2907.
- 229. Kuric, M.; Beck, S.; Schneider, D.; Rindt, W.; Evers, M.; Meißner-Weigl, J.; Zeck, S.; Krug, M.; Herrmann, M.; Hartmann, T.N.; et al. Modeling Myeloma Dissemination In Vitro with hMSC-Interacting Subpopulations of INA-6 Cells and Their Aggregation/Detachment Dynamics. *Cancer Res. Commun.* **2024**, *4*, 1150–1164, doi:10.1158/2767-9764.CRC-23-0411.
- 230. Tjin, E.P.M.; Derksen, P.W.B.; Kataoka, H.; Spaargaren, M.; Pals, S.T. Multiple Myeloma Cells Catalyze Hepatocyte Growth Factor (HGF) Activation by Secreting the Serine Protease HGF-Activator. *Blood* **2004**, *104*, 2172–2175, doi:10.1182/blood-2003-12-4386.
- 231. Standal, T.; Hjorth-Hansen, H.; Rasmussen, T.; Dahl, I.M.S.; Lenhoff, S.; Brenne, A.-T.; Seidel, C.; Baykov, V.; Waage, A.; Børset, M.; et al. Osteopontin Is an Adhesive Factor for Myeloma Cells and Is Found in Increased Levels in Plasma from Patients with Multiple Myeloma. *Haematologica* **2004**, *89*, 174–182.
- 232. Li, Y.-Y.; Zhang, L.-Y.; Xiang, Y.-H.; Li, D.; Zhang, J. Matrix Metalloproteinases and Tissue Inhibitors in Multiple Myeloma: Promote or Inhibit? *Front. Oncol.* **2023**, *13*, 1127407, doi:10.3389/fonc.2023.1127407.
- 233. Umezu, T.; Tadokoro, H.; Azuma, K.; Yoshizawa, S.; Ohyashiki, K.; Ohyashiki, J.H. Exosomal miR-135b Shed from Hypoxic Multiple Myeloma Cells Enhances Angiogenesis by Targeting Factor-Inhibiting HIF-1. *Blood* **2014**, *124*, 3748–3757, doi:10.1182/blood-2014-05-576116.
- 234. Pour, L.; Svachova, H.; Adam, Z.; Almasi, M.; Buresova, L.; Buchler, T.; Kovarova, L.; Nemec, P.; Penka, M.; Vorlicek, J.; et al. Levels of Angiogenic Factors in Patients with Multiple Myeloma Correlate with Treatment Response. *Ann. Hematol.* **2010**, *89*, 385–389, doi:10.1007/s00277-009-0834-3.
- 235. Indraccolo, S. Interferon-Alpha as Angiogenesis Inhibitor: Learning from Tumor Models. *Autoimmunity* **2010**, *43*, 244–247, doi:10.3109/08916930903510963.

- 236. Bruno, T.; Corleone, G.; Catena, V.; Cortile, C.; De Nicola, F.; Fabretti, F.; Gumenyuk, S.; Pisani, F.; Mengarelli, A.; Passananti, C.; et al. AATF/Che-1 Localizes to Paraspeckles and Suppresses R-loops Accumulation and Interferon Activation in Multiple Myeloma. *EMBO J.* **2022**, *41*, e109711, doi:10.15252/embj.2021109711.
- 237. Pugh, C.W.; Ratcliffe, P.J. Regulation of Angiogenesis by Hypoxia: Role of the HIF System. *Nat. Med.* **2003**, *9*, 677–684, doi:10.1038/nm0603-677.
- 238. Colla, S.; Tagliaferri, S.; Morandi, F.; Lunghi, P.; Donofrio, G.; Martorana, D.; Mancini, C.; Lazzaretti, M.; Mazzera, L.; Ravanetti, L.; et al. The New Tumor-Suppressor Gene Inhibitor of Growth Family Member 4 (ING4) Regulates the Production of Proangiogenic Molecules by Myeloma Cells and Suppresses Hypoxia-Inducible Factor-1 α (HIF-1α) Activity: Involvement in Myeloma-Induced Angiogenesis. *Blood* **2007**, *110*, 4464–4475, doi:10.1182/blood-2007-02-074617.
- 239. Ribatti, D.; Tamma, R.; Vacca, A. Mast Cells and Angiogenesis in Human Plasma Cell Malignancies. *Int. J. Mol. Sci.* **2019**, *20*, 481, doi:10.3390/ijms20030481.
- 240. Sun, M.; Xiao, Q.; Wang, X.; Yang, C.; Chen, C.; Tian, X.; Wang, S.; Li, H.; Qiu, S.; Shu, J.; et al. Tumor-Associated Macrophages Modulate Angiogenesis and Tumor Growth in a Xenograft Mouse Model of Multiple Myeloma. *Leuk. Res.* **2021**, *110*, 106709, doi:10.1016/j.leukres.2021.106709.
- 241. Tanaka, Y.; Abe, M.; Hiasa, M.; Oda, A.; Amou, H.; Nakano, A.; Takeuchi, K.; Kitazoe, K.; Kido, S.; Inoue, D.; et al. Myeloma Cell-Osteoclast Interaction Enhances Angiogenesis Together with Bone Resorption: A Role for Vascular Endothelial Cell Growth Factor and Osteopontin. *Clin. Cancer Res. Off. J. Am. Assoc. Cancer Res.* 2007, 13, 816–823, doi:10.1158/1078-0432.CCR-06-2258.
- 242. Wang, L.; Du, F.; Zhang, H.M.; Zhang, W.J.; Wang, H.X. Changes in Circulating Endothelial Progenitor Cells Predict Responses of Multiple Myeloma Patients to Treatment with Bortezomib and Dexamethasone. *Braz. J. Med. Biol. Res.* **2015**, *48*, 736–742, doi:10.1590/1414-431X20154558.
- 243. Ria, R.; Vacca, A.; Russo, F.; Cirulli, T.; Massaia, M.; Tosi, P.; Cavo, M.; Guidolin, D.; Ribatti, D.; Dammacco, F. A VEGF-Dependent Autocrine Loop Mediates Proliferation and Capillarogenesis in Bone Marrow Endothelial Cells of Patients with Multiple Myeloma. *Thromb. Haemost.* **2004**, *92*, 1438–1445, doi:10.1160/TH04-06-0334.
- 244. Ferrucci, A.; Moschetta, M.; Frassanito, M.A.; Berardi, S.; Catacchio, I.; Ria, R.; Racanelli, V.; Caivano, A.; Solimando, A.G.; Vergara, D.; et al. A HGF/cMET Autocrine Loop Is Operative in Multiple Myeloma Bone Marrow Endothelial Cells and May Represent a Novel Therapeutic Target. *Clin. Cancer Res.* 2014, 20, 5796–5807, doi:10.1158/1078-0432.CCR-14-0847.
- 245. Roccaro, A.M.; Hideshima, T.; Raje, N.; Kumar, S.; Ishitsuka, K.; Yasui, H.; Shiraishi, N.; Ribatti, D.; Nico, B.; Vacca, A.; et al. Bortezomib Mediates Antiangiogenesis in Multiple Myeloma via Direct and Indirect Effects on Endothelial Cells. *Cancer Res.* **2006**, 66, 184–191, doi:10.1158/0008-5472.CAN-05-1195.
- 246. Wu, J.; Chu, E.; Kang, Y. PIM Kinases in Multiple Myeloma. *Cancers* **2021**, *13*, 4304, doi:10.3390/cancers13174304.
- 247. Cohen, P.; Cross, D.; Jänne, P.A. Kinase Drug Discovery 20 Years after Imatinib: Progress and Future Directions. *Nat. Rev. Drug Discov.* **2021**, *20*, 551–569, doi:10.1038/s41573-021-00195-4.
- 248. Brault, L.; Gasser, C.; Bracher, F.; Huber, K.; Knapp, S.; Schwaller, J. PIM Serine/Threonine Kinases in the Pathogenesis and Therapy of Hematologic Malignancies

- and Solid Cancers. *Haematologica* **2010**, *95*, 1004–1015, doi:10.3324/haematol.2009.017079.
- 249. Juszczyński, P. Kinazy PIM jako cel terapeutyczny w nowotworach układów krwiotwórczego i chłonnego. **2014**.
- 250. Bullock, A.N.; Debreczeni, J.; Amos, A.L.; Knapp, S.; Turk, B.E. Structure and Substrate Specificity of the Pim-1 Kinase\*. *J. Biol. Chem.* **2005**, *280*, 41675–41682, doi:10.1074/jbc.M510711200.
- 251. Hanahan, D.; Weinberg, R.A. The Hallmarks of Cancer. *Cell* **2000**, *100*, 57–70, doi:10.1016/S0092-8674(00)81683-9.
- 252. Hanahan, D. Hallmarks of Cancer: New Dimensions. *Cancer Discov.* **2022**, *12*, 31–46, doi:10.1158/2159-8290.CD-21-1059.
- 253. Lu, J.; Zavorotinskaya, T.; Dai, Y.; Niu, X.-H.; Castillo, J.; Sim, J.; Yu, J.; Wang, Y.; Langowski, J.L.; Holash, J.; et al. Pim2 Is Required for Maintaining Multiple Myeloma Cell Growth through Modulating TSC2 Phosphorylation. *Blood* **2013**, *122*, 1610–1620, doi:10.1182/blood-2013-01-481457.
- 254. Kim, O.; Jiang, T.; Xie, Y.; Guo, Z.; Chen, H.; Qiu, Y. Synergism of Cytoplasmic Kinases in IL6-Induced Ligand-Independent Activation of Androgen Receptor in Prostate Cancer Cells. *Oncogene* **2004**, *23*, 1838–1844, doi:10.1038/sj.onc.1207304.
- 255. Ruppert, S.M.; Chehtane, M.; Zhang, G.; Hu, H.; Li, X.; Khaled, A.R. JunD/AP-1-Mediated Gene Expression Promotes Lymphocyte Growth Dependent on Interleukin-7 Signal Transduction. *PloS One* **2012**, *7*, e32262, doi:10.1371/journal.pone.0032262.
- 256. An, N.; Kraft, A.S.; Kang, Y. Abnormal Hematopoietic Phenotypes in Pim Kinase Triple Knockout Mice. *J. Hematol. Oncol. J Hematol Oncol* **2013**, *6*, 12, doi:10.1186/1756-8722-6-12.
- 257. An, N.; Kraft, A.S.; Kang, Y. Abnormal Hematopoietic Phenotypes in Pim Kinase Triple Knockout Mice. *J. Hematol. Oncol. J Hematol Oncol* **2013**, *6*, 12, doi:10.1186/1756-8722-6-12.
- 258. Domen, J.; van der Lugt, N.M.; Acton, D.; Laird, P.W.; Linders, K.; Berns, A. Pim-1 Levels Determine the Size of Early B Lymphoid Compartments in Bone Marrow. *J. Exp. Med.* **1993**, *178*, 1665–1673, doi:10.1084/jem.178.5.1665.
- 259. Haas, M.; Caron, G.; Chatonnet, F.; Manenti, S.; Alaterre, E.; Devin, J.; Delaloy, C.; Bertolin, G.; Viel, R.; Pignarre, A.; et al. PIM2 Kinase Has a Pivotal Role in Plasmablast Generation and Plasma Cell Survival, Opening up Novel Treatment Options in Myeloma. *Blood* **2022**, *139*, 2316–2337, doi:10.1182/blood.2021014011.
- 260. Peperzak, V.; Veraar, E.A.M.; Keller, A.M.; Xiao, Y.; Borst, J. The Pim Kinase Pathway Contributes to Survival Signaling in Primed CD8+ T Cells upon CD27 Costimulation. *J. Immunol. Baltim. Md* 1950 **2010**, 185, 6670–6678, doi:10.4049/jimmunol.1000159.
- 261. Clements, A.N.; Warfel, N.A. Targeting PIM Kinases to Improve the Efficacy of Immunotherapy. *Cells* **2022**, *11*, 3700, doi:10.3390/cells11223700.
- 262. Tahvanainen, J.; Kyläniemi, M.K.; Kanduri, K.; Gupta, B.; Lähteenmäki, H.; Kallonen, T.; Rajavuori, A.; Rasool, O.; Koskinen, P.J.; Rao, K.V.S.; et al. Proviral Integration Site for Moloney Murine Leukemia Virus (PIM) Kinases Promote Human T Helper 1 Cell Differentiation. *J. Biol. Chem.* **2013**, *288*, 3048–3058, doi:10.1074/jbc.M112.361709.
- 263. Aho, T.L.T.; Lund, R.J.; Ylikoski, E.K.; Matikainen, S.; Lahesmaa, R.; Koskinen, P.J. Expression of Human Pim Family Genes Is Selectively Up-Regulated by Cytokines Promoting T Helper Type 1, but Not T Helper Type 2, Cell Differentiation. *Immunology* **2005**, *116*, 82–88, doi:10.1111/j.1365-2567.2005.02201.x.

- 264. Li, Z.; Lin, F.; Zhuo, C.; Deng, G.; Chen, Z.; Yin, S.; Gao, Z.; Piccioni, M.; Tsun, A.; Cai, S.; et al. PIM1 Kinase Phosphorylates the Human Transcription Factor FOXP3 at Serine 422 to Negatively Regulate Its Activity under Inflammation. *J. Biol. Chem.* **2014**, *289*, 26872–26881, doi:10.1074/jbc.M114.586651.
- 265. Deng, G.; Nagai, Y.; Xiao, Y.; Li, Z.; Dai, S.; Ohtani, T.; Banham, A.; Li, B.; Wu, S.-L.; Hancock, W.; et al. Pim-2 Kinase Influences Regulatory T Cell Function and Stability by Mediating Foxp3 Protein N-Terminal Phosphorylation. *J. Biol. Chem.* **2015**, *290*, 20211–20220, doi:10.1074/jbc.M115.638221.
- 266. Liu, Y.; Shang, Y.; Yan, Z.; Li, H.; Wang, Z.; Liu, Z.; Li, Z. Pim1 Kinase Positively Regulates Myoblast Behaviors and Skeletal Muscle Regeneration. *Cell Death Dis.* **2019**, 10, 773, doi:10.1038/s41419-019-1993-3.
- 267. Cottage, C.T.; Bailey, B.; Fischer, K.M.; Avitabile, D.; Collins, B.; Tuck, S.; Quijada, P.; Gude, N.; Alvarez, R.; Muraski, J.; et al. Cardiac Progenitor Cell Cycling Stimulated by Pim-1 Kinase. *Circ. Res.* **2010**, *106*, 891–901, doi:10.1161/CIRCRESAHA.109.208629.
- 268. Zhang, P.; Wang, H.; Min, X.; Wang, Y.; Tang, J.; Cheng, J.; Li, D.; Chen, X.; Cheng, F.; Wang, N.; et al. Pim-3 Is Expressed in Endothelial Cells and Promotes Vascular Tube Formation. *J. Cell. Physiol.* **2009**, *220*, 82–90, doi:10.1002/jcp.21733.
- 269. Zippo, A.; De Robertis, A.; Bardelli, M.; Galvagni, F.; Oliviero, S. Identification of Flk-1 Target Genes in Vasculogenesis: Pim-1 Is Required for Endothelial and Mural Cell Differentiation in Vitro. *Blood* **2004**, *103*, 4536–4544, doi:10.1182/blood-2003-11-3827.
- 270. Chen, M.; Yi, B.; Zhu, N.; Wei, X.; Zhang, G.-X.; Huang, S.; Sun, J. Pim1 Kinase Promotes Angiogenesis through Phosphorylation of Endothelial Nitric Oxide Synthase at Ser-633. *Cardiovasc. Res.* **2016**, *109*, 141–150, doi:10.1093/cvr/cvv250.
- 271. Santio, N.M.; Ganesh, K.; Kaipainen, P.P.; Halme, A.; Seyednasrollah, F.; Arbash, E.; Hänninen, S.; Kivelä, R.; Carpen, O.; Saharinen, P. Endothelial Pim3 Kinase Protects the Vascular Barrier during Lung Metastasis. *Nat. Commun.* **2024**, *15*, 10514, doi:10.1038/s41467-024-54445-1.
- 272. Yang, H.; Wang, Y.; Qian, H.; Zhang, P.; Huang, C. Pim Protein Kinase-3 Is Regulated by TNF-α and Promotes Endothelial Cell Sprouting. *Mol. Cells* **2011**, *32*, 235–241, doi:10.1007/s10059-011-1026-z.
- 273. Spirli, A.; Cheval, L.; Debonneville, A.; Penton, D.; Ronzaud, C.; Maillard, M.; Doucet, A.; Loffing, J.; Staub, O. The Serine-threonine Kinase PIM3 Is an Aldosterone-regulated Protein in the Distal Nephron. *Physiol. Rep.* **2019**, *7*, e14177, doi:10.14814/phy2.14177.
- 274. Konietzko, U.; Kauselmann, G.; Scafidi, J.; Staubli, U.; Mikkers, H.; Berns, A.; Schweizer, M.; Waltereit, R.; Kuhl, D. Pim Kinase Expression Is Induced by LTP Stimulation and Required for the Consolidation of Enduring LTP. *EMBO J.* **1999**, *18*, 3359–3369, doi:10.1093/emboj/18.12.3359.
- 275. Park, Y.; Obiang-Obounou, B.W.; Lee, K.; Choi, J.; Jang, B. AZD1208, a pan-Pim Kinase Inhibitor, Inhibits Adipogenesis and Induces Lipolysis in 3T3-L1 Adipocytes. *J. Cell. Mol. Med.* **2018**, *22*, 2488–2497, doi:10.1111/jcmm.13559.
- 276. Kim, K.; Kim, J.H.; Youn, B.U.; Jin, H.M.; Kim, N. Pim-1 Regulates RANKL-Induced Osteoclastogenesis via NF-κB Activation and NFATc1 Induction. *J. Immunol. Baltim. Md* 1950 **2010**, 185, 7460–7466, doi:10.4049/jimmunol.1000885.
- 277. Warfel, N.A.; Kraft, A.S. PIM Kinase (and Akt) Biology and Signaling in Tumors. *Pharmacol. Ther.* **2015**, *151*, 41–49, doi:10.1016/j.pharmthera.2015.03.001.
- 278. Szydłowski, M.; Prochorec-Sobieszek, M.; Szumera-Ciećkiewicz, A.; Derezińska, E.; Hoser, G.; Wasilewska, D.; Szymańska-Giemza, O.; Jabłońska, E.; Białopiotrowicz, E.;

- Sewastianik, T.; et al. Expression of PIM Kinases in Reed-Sternberg Cells Fosters Immune Privilege and Tumor Cell Survival in Hodgkin Lymphoma. *Blood* **2017**, *130*, 1418–1429, doi:10.1182/blood-2017-01-760702.
- 279. Aho, T.L.T.; Sandholm, J.; Peltola, K.J.; Mankonen, H.P.; Lilly, M.; Koskinen, P.J. Pim-1 Kinase Promotes Inactivation of the pro-Apoptotic Bad Protein by Phosphorylating It on the Ser112 Gatekeeper Site. *FEBS Lett.* **2004**, *571*, 43–49, doi:10.1016/j.febslet.2004.06.050.
- 280. Zhang, Y.; Wang, Z.; Li, X.; Magnuson, N.S. Pim Kinase-Dependent Inhibition of c-Myc Degradation. *Oncogene* **2008**, *27*, 4809–4819, doi:10.1038/onc.2008.123.
- 281. Theo Cuypers, H.; Selten, G.; Quint, W.; Zijlstra, M.; Maandag, E.R.; Boelens, W.; van Wezenbeek, P.; Melief, C.; Berns, A. Murine Leukemia Virus-Induced T-Cell Lymphomagenesis: Integration of Proviruses in a Distinct Chromosomal Region. *Cell* **1984**, *37*, 141–150, doi:10.1016/0092-8674(84)90309-X.
- 282. Möröy, T.; Verbeek, S.; Ma, A.; Achacoso, P.; Berns, A.; Alt, F. E Mu N- and E Mu L-Myc Cooperate with E Mu Pim-1 to Generate Lymphoid Tumors at High Frequency in Double-Transgenic Mice. *Oncogene* **1991**, *6*, 1941–1948.
- 283. Szydłowski, M.; Garbicz, F.; Jabłońska, E.; Górniak, P.; Komar, D.; Pyrzyńska, B.; Bojarczuk, K.; Prochorec-Sobieszek, M.; Szumera-Ciećkiewicz, A.; Rymkiewicz, G.; et al. Inhibition of PIM Kinases in DLBCL Targets MYC Transcriptional Program and Augments the Efficacy of Anti-CD20 Antibodies. *Cancer Res.* **2021**, *81*, 6029–6043, doi:10.1158/0008-5472.CAN-21-1023.
- 284. Nihira, K.; Ando, Y.; Yamaguchi, T.; Kagami, Y.; Miki, Y.; Yoshida, K. Pim-1 Controls NF-kappaB Signalling by Stabilizing RelA/P65. *Cell Death Differ.* **2010**, *17*, 689–698, doi:10.1038/cdd.2009.174.
- 285. Szydlowski, M.; Pawlak, M.; Garbicz, F.; Górniak, P.; Żurańska, J.; Król, M.; Taciak, B.; Białasek, M.; Szumera-Ciećkiewicz, A.; Sokół, K.; et al. Hodgkin Lymphoma Reed-Sternberg Cells Induce Immunosuppressive and Pro-Angiogenic Phenotype of Tumor-Associated Macrophages in a Paracrine Manner. *Blood* **2020**, *136*, 30–30, doi:10.1182/blood-2020-134886.
- 286. Zhu, N.; Ramirez, L.M.; Lee, R.L.; Magnuson, N.S.; Bishop, G.A.; Gold, M.R. CD40 Signaling in B Cells Regulates the Expression of the Pim-1 Kinase via the NF-Kappa B Pathway. *J. Immunol. Baltim. Md* 1950 **2002**, 168, 744–754, doi:10.4049/jimmunol.168.2.744.
- 287. Lu, J.; Zavorotinskaya, T.; Dai, Y.; Niu, X.-H.; Castillo, J.; Sim, J.; Yu, J.; Wang, Y.; Langowski, J.L.; Holash, J.; et al. Pim2 Is Required for Maintaining Multiple Myeloma Cell Growth through Modulating TSC2 Phosphorylation. *Blood* **2013**, *122*, 1610–1620, doi:10.1182/blood-2013-01-481457.
- 288. Zhang, F.; Beharry, Z.M.; Harris, T.E.; Lilly, M.B.; Smith, C.D.; Mahajan, S.; Kraft, A.S. PIM1 Protein Kinase Regulates PRAS40 Phosphorylation and mTOR Activity in FDCP1 Cells. *Cancer Biol. Ther.* **2009**, *8*, 846–853, doi:10.4161/cbt.8.9.8210.
- 289. Tamburini, J.; Green, A.S.; Bardet, V.; Chapuis, N.; Park, S.; Willems, L.; Uzunov, M.; Ifrah, N.; Dreyfus, F.; Lacombe, C.; et al. Protein Synthesis Is Resistant to Rapamycin and Constitutes a Promising Therapeutic Target in Acute Myeloid Leukemia. *Blood* **2009**, *114*, 1618–1627, doi:10.1182/blood-2008-10-184515.
- 290. Yang, J.; Wang, J.; Chen, K.; Guo, G.; Xi, R.; Rothman, P.B.; Whitten, D.; Zhang, L.; Huang, S.; Chen, J.-L. eIF4B Phosphorylation by Pim Kinases Plays a Critical Role in

- Cellular Transformation by Abl Oncogenes. *Cancer Res.* **2013**, *73*, 4898–4908, doi:10.1158/0008-5472.CAN-12-4277.
- 291. Song, J.H.; An, N.; Chatterjee, S.; Kistner-Griffin, E.; Mahajan, S.; Mehrotra, S.; Kraft, A.S. Deletion of Pim Kinases Elevates the Cellular Levels of Reactive Oxygen Species and Sensitizes to K-Ras-Induced Cell Killing. *Oncogene* **2015**, *34*, 3728–3736, doi:10.1038/onc.2014.306.
- 292. Gu, J.J.; Wang, Z.; Reeves, R.; Magnuson, N.S. PIM1 Phosphorylates and Negatively Regulates ASK1-Mediated Apoptosis. *Oncogene* **2009**, *28*, 4261–4271, doi:10.1038/onc.2009.276.
- 293. Morishita, D.; Katayama, R.; Sekimizu, K.; Tsuruo, T.; Fujita, N. Pim Kinases Promote Cell Cycle Progression by Phosphorylating and Down-Regulating p27Kip1 at the Transcriptional and Posttranscriptional Levels. *Cancer Res.* **2008**, *68*, 5076–5085, doi:10.1158/0008-5472.CAN-08-0634.
- 294. Morishita, D.; Katayama, R.; Sekimizu, K.; Tsuruo, T.; Fujita, N. Pim Kinases Promote Cell Cycle Progression by Phosphorylating and Down-Regulating p27Kip1 at the Transcriptional and Posttranscriptional Levels. *Cancer Res.* **2008**, *68*, 5076–5085, doi:10.1158/0008-5472.CAN-08-0634.
- 295. Cen, B.; Mahajan, S.; Zemskova, M.; Beharry, Z.; Lin, Y.-W.; Cramer, S.D.; Lilly, M.B.; Kraft, A.S. Regulation of Skp2 Levels by the Pim-1 Protein Kinase. *J. Biol. Chem.* **2010**, 285, 29128–29137, doi:10.1074/jbc.M110.137240.
- 296. Bachmann, M.; Kosan, C.; Xing, P.X.; Montenarh, M.; Hoffmann, I.; Möröy, T. The Oncogenic Serine/Threonine Kinase Pim-1 Directly Phosphorylates and Activates the G2/M Specific Phosphatase Cdc25C. *Int. J. Biochem. Cell Biol.* **2006**, *38*, 430–443, doi:10.1016/j.biocel.2005.10.010.
- 297. Bachmann, M.; Hennemann, H.; Xing, P.X.; Hoffmann, I.; Möröy, T. The Oncogenic Serine/Threonine Kinase Pim-1 Phosphorylates and Inhibits the Activity of Cdc25C-Associated Kinase 1 (C-TAK1): A Novel Role for Pim-1 at the G2/M Cell Cycle Checkpoint. *J. Biol. Chem.* **2004**, *279*, 48319–48328, doi:10.1074/jbc.M404440200.
- 298. Casillas, A.L.; Chauhan, S.S.; Toth, R.K.; Sainz, A.G.; Clements, A.N.; Jensen, C.C.; Langlais, P.R.; Miranti, C.K.; Cress, A.E.; Warfel, N.A. Direct Phosphorylation and Stabilization of HIF-1α by PIM1 Kinase Drives Angiogenesis in Solid Tumors. *Oncogene* **2021**, 40, 5142–5152, doi:10.1038/s41388-021-01915-1.
- 299. Din, S.; Mason, M.; Völkers, M.; Johnson, B.; Cottage, C.T.; Wang, Z.; Joyo, A.Y.; Quijada, P.; Erhardt, P.; Magnuson, N.S.; et al. Pim-1 Preserves Mitochondrial Morphology by Inhibiting Dynamin-Related Protein 1 Translocation. *Proc. Natl. Acad. Sci. U. S. A.* 2013, *110*, 5969–5974, doi:10.1073/pnas.1213294110.
- 300. Yang, T.; Ren, C.; Qiao, P.; Han, X.; Wang, L.; Lv, S.; Sun, Y.; Liu, Z.; Du, Y.; Yu, Z. PIM2-Mediated Phosphorylation of Hexokinase 2 Is Critical for Tumor Growth and Paclitaxel Resistance in Breast Cancer. *Oncogene* **2018**, *37*, 5997–6009, doi:10.1038/s41388-018-0386-x.
- 301. Warfel, N.A.; Sainz, A.G.; Song, J.H.; Kraft, A.S. PIM Kinase Inhibitors Kill Hypoxic Tumor Cells by Reducing Nrf2 Signaling and Increasing Reactive Oxygen Species. *Mol. Cancer Ther.* **2016**, *15*, 1637–1647, doi:10.1158/1535-7163.MCT-15-1018.
- 302. Ramachandran, J.; Santo, L.; Siu, K.T.; Panaroni, C.; Raje, N. Pim2 Is Important for Regulating DNA Damage Response in Multiple Myeloma Cells. *Blood Cancer J.* **2016**, 6, e462, doi:10.1038/bcj.2016.73.

- 303. Hogan, C.; Hutchison, C.; Marcar, L.; Milne, D.; Saville, M.; Goodlad, J.; Kernohan, N.; Meek, D. Elevated Levels of Oncogenic Protein Kinase Pim-1 Induce the P53 Pathway in Cultured Cells and Correlate with Increased Mdm2 in Mantle Cell Lymphoma. *J. Biol. Chem.* **2008**, *283*, 18012–18023, doi:10.1074/jbc.M709695200.
- 304. Xie, Y.; Xu, K.; Linn, D.E.; Yang, X.; Guo, Z.; Shimelis, H.; Nakanishi, T.; Ross, D.D.; Chen, H.; Fazli, L.; et al. The 44-kDa Pim-1 Kinase Phosphorylates BCRP/ABCG2 and Thereby Promotes Its Multimerization and Drug-Resistant Activity in Human Prostate Cancer Cells. *J. Biol. Chem.* **2008**, *283*, 3349–3356, doi:10.1074/jbc.M707773200.
- 305. Xie, Y.; Burcu, M.; Linn, D.E.; Qiu, Y.; Baer, M.R. Pim-1 Kinase Protects P-Glycoprotein from Degradation and Enables Its Glycosylation and Cell Surface Expression. *Mol. Pharmacol.* **2010**, *78*, 310–318, doi:10.1124/mol.109.061713.
- 306. Agrawal, S.; Koschmieder, S.; Bäumer, N.; Reddy, N.G.P.; Berdel, W.E.; Müller-Tidow, C.; Serve, H. Pim2 Complements Flt3 Wild-Type Receptor in Hematopoietic Progenitor Cell Transformation. *Leukemia* **2008**, *22*, 78–86, doi:10.1038/sj.leu.2404988.
- 307. Czardybon, W.; Windak, R.; Gołas, A.; Gałęzowski, M.; Sabiniarz, A.; Dolata, I.; Salwińska, M.; Guzik, P.; Zawadzka, M.; Gabor-Worwa, E.; et al. A Novel, Dual Pan-PIM/FLT3 Inhibitor SEL24 Exhibits Broad Therapeutic Potential in Acute Myeloid Leukemia. *Oncotarget* **2018**, *9*, 16917–16931, doi:10.18632/oncotarget.24747.
- 308. Rampal, R.K.; Pinzon-Ortiz, M.; Somasundara, A.V.H.; Durham, B.; Koche, R.; Spitzer, B.; Mowla, S.; Krishnan, A.; Li, B.; An, W.; et al. Therapeutic Efficacy of Combined JAK1/2, Pan-PIM, and CDK4/6 Inhibition in Myeloproliferative Neoplasms. *Clin. Cancer Res. Off. J. Am. Assoc. Cancer Res.* **2021**, *27*, 3456–3468, doi:10.1158/1078-0432.CCR-20-4898.
- 309. Mazzacurati, L.; Collins, R.J.; Pandey, G.; Lambert-Showers, Q.T.; Amin, N.E.; Zhang, L.; Stubbs, M.C.; Epling-Burnette, P.K.; Koblish, H.K.; Reuther, G.W. The Pan-PIM Inhibitor INCB053914 Displays Potent Synergy in Combination with Ruxolitinib in Models of MPN. *Blood Adv.* **2019**, *3*, 3503–3514, doi:10.1182/bloodadvances.2019000260.
- 310. Lim, J.T.; Singh, N.; Leuvano, L.A.; Calvert, V.S.; Petricoin, E.F.; Teachey, D.T.; Lock, R.B.; Padi, M.; Kraft, A.S.; Padi, S.K.R. PIM Kinase Inhibitors Block the Growth of Primary T-Cell Acute Lymphoblastic Leukemia: Resistance Pathways Identified by Network Modeling Analysis. *Mol. Cancer Ther.* **2020**, *19*, 1809–1821, doi:10.1158/1535-7163.MCT-20-0160.
- 311. Lahera, A.; Vela-Martín, L.; Fernández-Navarro, P.; Llamas, P.; López-Lorenzo, J.L.; Cornago, J.; Santos, J.; Fernández-Piqueras, J.; Villa-Morales, M. PIM1 Is a Potential Therapeutic Target for the Leukemogenic Effects Mediated by JAK/STAT Pathway Mutations in T-ALL/LBL. *Npj Precis. Oncol.* **2024**, *8*, 1–13, doi:10.1038/s41698-024-00638-2.
- 312. De Smedt, R.; Peirs, S.; Morscio, J.; Matthijssens, F.; Roels, J.; Reunes, L.; Lintermans, B.; Goossens, S.; Lammens, T.; Van Roy, N.; et al. Pre-Clinical Evaluation of Second Generation PIM Inhibitors for the Treatment of T-Cell Acute Lymphoblastic Leukemia and Lymphoma. *Haematologica* **2019**, *104*, e17–e20, doi:10.3324/haematol.2018.199257.
- 313. Kuang, X.; Xiong, J.; Wang, W.; Li, X.; Lu, T.; Fang, Q.; Wang, J. PIM Inhibitor SMI-4a Induces Cell Apoptosis in B-Cell Acute Lymphocytic Leukemia Cells via the HO-1-Mediated JAK2/STAT3 Pathway. *Life Sci.* **2019**, *219*, 248–256, doi:10.1016/j.lfs.2019.01.022.

- 314. Chen, J.-L.; Limnander, A.; Rothman, P.B. Pim-1 and Pim-2 Kinases Are Required for Efficient Pre–B-Cell Transformation by v-Abl Oncogene. *Blood* **2008**, *111*, 1677–1685, doi:10.1182/blood-2007-04-083808.
- 315. Minieri, V.; De Dominici, M.; Nevalainen, M.T.; Calabretta, B. Targeting the STAT5 Pathway in Ph+ Acute Lymphoblastic Leukemia. *Oncotarget* **2018**, *9*, 36726–36727, doi:10.18632/oncotarget.26412.
- 316. Chen, L.S.; Redkar, S.; Bearss, D.; Wierda, W.G.; Gandhi, V. Pim Kinase Inhibitor, SGI-1776, Induces Apoptosis in Chronic Lymphocytic Leukemia Cells. *Blood* **2009**, *114*, 4150–4157, doi:10.1182/blood-2009-03-212852.
- 317. Decker, S.; Finter, J.; Forde, A.J.; Kissel, S.; Schwaller, J.; Mack, T.S.; Kuhn, A.; Gray, N.; Follo, M.; Jumaa, H.; et al. PIM Kinases Are Essential for Chronic Lymphocytic Leukemia Cell Survival (PIM2/3) and CXCR4-Mediated Microenvironmental Interactions (PIM1). *Mol. Cancer Ther.* **2014**, *13*, 1231–1245, doi:10.1158/1535-7163.MCT-13-0575-T.
- 318. Bialopiotrowicz, E.; Gorniak, P.; Pula, B.; Noyszewska-Kania, M.; Makuch-Lasica, H.; Nowak, G.; Szydlowski, M.; Jablonska, E.; Sewastianik, T.; Polak, A.; et al. Microenvironment-Induced Expression of PIM Kinases Supports Chronic Lymphocytic Leukemia Cells Survival and Promotes CXCR4-mTOR Pathway Dependent Migration. *Blood* **2016**, *128*, 3239, doi:10.1182/blood.V128.22.3239.3239.
- 319. Decker, S.; Saleem, S.; Kissel, S.; Zwick, A.; Aumann, K.; Zirlik, K.; Duyster, J.; Dierks, C. The Pan-PIM Kinase Inhibitor LGB321 Strongly Increases Ibrutinib Effects in CLL, By Blocking Anti-Apoptotic Pathways and Microenvironmental Interactions. *Blood* **2018**, *132*, 1840, doi:10.1182/blood-2018-99-114424.
- 320. Hogan, C.; Hutchison, C.; Marcar, L.; Milne, D.; Saville, M.; Goodlad, J.; Kernohan, N.; Meek, D. Elevated Levels of Oncogenic Protein Kinase Pim-1 Induce the P53 Pathway in Cultured Cells and Correlate with Increased Mdm2 in Mantle Cell Lymphoma. *J. Biol. Chem.* **2008**, *283*, 18012–18023, doi:10.1074/jbc.M709695200.
- 321. HSI, E.D.; JUNG, S.-H.; LAI, R.; JOHNSON, J.L.; COOK, J.R.; JONES, D.; DEVOS, S.; CHESON, B.D.; DAMON, L.E.; SAID, J. Ki67 and PIM1 Expression Predict Outcome in Mantle Cell Lymphoma Treated with High Dose Therapy, Stem Cell Transplantation and Rituximab: A Cancer and Leukemia Group B 59909 Correlative Science Study. *Leuk. Lymphoma* **2008**, *49*, 2081–2090, doi:10.1080/10428190802419640.
- 322. Mensah, A.A.; Ghiringhelli, A.; Sartori, G.; Spriano, F.; Tarantelli, C.; Cascione, L.; Rinaldi, A.; Arribas, A.A.; Bellarosa, D.; Binaschi, M.; et al. Abstract C144: MEN1703/SEL24, a Potent PIM Inhibitor, Demonstrates Promising Anti-Tumour Activity in Activated B Cell like Diffuse Large B Cell Lymphoma, Mantle Cell Lymphoma and Marginal Zone Lymphoma Cells. *Mol. Cancer Ther.* **2023**, *22*, C144, doi:10.1158/1535-7163.TARG-23-C144.
- 323. Yang, Q.; Chen, L.S.; Neelapu, S.S.; Miranda, R.N.; Medeiros, L.J.; Gandhi, V. Transcription and Translation Are Primary Targets of Pim Kinase Inhibitor SGI-1776 in Mantle Cell Lymphoma. *Blood* **2012**, *120*, 3491–3500, doi:10.1182/blood-2012-02-412643.
- 324. Schatz, J.H.; Oricchio, E.; Wolfe, A.L.; Jiang, M.; Linkov, I.; Maragulia, J.; Shi, W.; Zhang, Z.; Rajasekhar, V.K.; Pagano, N.C.; et al. Targeting Cap-Dependent Translation Blocks Converging Survival Signals by AKT and PIM Kinases in Lymphoma. *J. Exp. Med.* **2011**, *208*, 1799–1807, doi:10.1084/jem.20110846.

- 325. Szydłowski, M.; Dębek, S.; Prochorec-Sobieszek, M.; Szołkowska, M.; Tomirotti, A.M.; Juszczyński, P.; Szumera-Ciećkiewicz, A. PIM Kinases Promote Survival and Immune Escape in Primary Mediastinal Large B-Cell Lymphoma through Modulation of JAK-STAT and NF-κB Activity. *Am. J. Pathol.* **2021**, *191*, 567–574, doi:10.1016/j.ajpath.2020.12.001.
- 326. Chapuy, B.; Stewart, C.; Dunford, A.J.; Kim, J.; Kamburov, A.; Redd, R.A.; Lawrence, M.S.; Roemer, M.G.M.; Li, A.J.; Ziepert, M.; et al. Molecular Subtypes of Diffuse Large B Cell Lymphoma Are Associated with Distinct Pathogenic Mechanisms and Outcomes. *Nat. Med.* **2018**, *24*, 679–690, doi:10.1038/s41591-018-0016-8.
- 327. Peters, T.L.; Li, L.; Tula-Sanchez, A.A.; Pongtornpipat, P.; Schatz, J.H. Control of Translational Activation by PIM Kinase in Activated B-Cell Diffuse Large B-Cell Lymphoma Confers Sensitivity to Inhibition by PIM447. *Oncotarget* **2016**, *7*, 63362–63373, doi:10.18632/oncotarget.11457.
- 328. Kuo, H.-P.; Ezell, S.A.; Hsieh, S.; Schweighofer, K.J.; Cheung, L.W.; Wu, S.; Sirisawad, M.; Eckert, K.; Liang, Y.; Hsu, J.; et al. The Role of PIM1 in the Ibrutinib-Resistant ABC Subtype of Diffuse Large B-Cell Lymphoma.
- 329. Szydłowski, M.; Garbicz, F.; Jabłońska, E.; Górniak, P.; Komar, D.; Pyrzyńska, B.; Bojarczuk, K.; Prochorec-Sobieszek, M.; Szumera-Ciećkiewicz, A.; Rymkiewicz, G.; et al. Inhibition of PIM Kinases in DLBCL Targets MYC Transcriptional Program and Augments the Efficacy of Anti-CD20 Antibodies. *Cancer Res.* **2021**, *81*, 6029–6043, doi:10.1158/0008-5472.CAN-21-1023.
- 330. Gómez-Abad, C.; Pisonero, H.; Blanco-Aparicio, C.; Roncador, G.; González-Menchén, A.; Martinez-Climent, J.A.; Mata, E.; Rodríguez, M.E.; Muñoz-González, G.; Sánchez-Beato, M.; et al. PIM2 Inhibition as a Rational Therapeutic Approach in B-Cell Lymphoma. *Blood* **2011**, *118*, 5517–5527, doi:10.1182/blood-2011-03-344374.
- 331. Brault, L.; Menter, T.; Obermann, E.C.; Knapp, S.; Thommen, S.; Schwaller, J.; Tzankov, A. PIM Kinases Are Progression Markers and Emerging Therapeutic Targets in Diffuse Large B-Cell Lymphoma. *Br. J. Cancer* **2012**, *107*, 491–500, doi:10.1038/bjc.2012.272.
- 332. Haas, M.; Caron, G.; Chatonnet, F.; Manenti, S.; Alaterre, E.; Devin, J.; Delaloy, C.; Bertolin, G.; Viel, R.; Pignarre, A.; et al. PIM2 Kinase Has a Pivotal Role in Plasmablast Generation and Plasma Cell Survival, Opening up Novel Treatment Options in Myeloma. *Blood* **2022**, *139*, 2316–2337, doi:10.1182/blood.2021014011.
- 333. Keane, N.A.; Reidy, M.; Natoni, A.; Raab, M.S.; O'Dwyer, M. Targeting the Pim Kinases in Multiple Myeloma. *Blood Cancer J.* **2015**, *5*, e325–e325, doi:10.1038/bcj.2015.46.
- 334. Asano, J.; Nakano, A.; Oda, A.; Amou, H.; Hiasa, M.; Takeuchi, K.; Miki, H.; Nakamura, S.; Harada, T.; Fujii, S.; et al. The Serine/Threonine Kinase Pim-2 Is a Novel Anti-Apoptotic Mediator in Myeloma Cells. *Leukemia* **2011**, *25*, 1182–1188, doi:10.1038/leu.2011.60.
- 335. Haas, M.; Caron, G.; Chatonnet, F.; Manenti, S.; Alaterre, E.; Devin, J.; Delaloy, C.; Bertolin, G.; Viel, R.; Pignarre, A.; et al. PIM2 Kinase Has a Pivotal Role in Plasmablast Generation and Plasma Cell Survival, Opening up Novel Treatment Options in Myeloma. *Blood* **2022**, *139*, 2316–2337, doi:10.1182/blood.2021014011.
- 336. Haas, M.; Cherfa, S.; Nguyen, L.; Bourgoin, M.; Caron, G.; Dessauge, E.; Marchand, T.; Delpy, L.; Auberger, P.; Moreaux, J.; et al. PIM2 Inhibition Promotes MCL1 Dependency in Plasma Cells Involving Integrated Stress Response-Driven NOXA Expression. *Nat. Commun.* **2025**, *16*, 256, doi:10.1038/s41467-024-55572-5.

- 337. Liu, Z.; Guo, Y.; Liu, X.; Cao, P.; Liu, H.; Dong, X.; Ding, K.; Fu, R. Pim-2 Kinase Regulates Energy Metabolism in Multiple Myeloma. *Cancers* **2022**, *15*, 67, doi:10.3390/cancers15010067.
- 338. Ramachandran, J.; Santo, L.; Siu, K.T.; Panaroni, C.; Raje, N. Pim2 Is Important for Regulating DNA Damage Response in Multiple Myeloma Cells. *Blood Cancer J.* **2016**, *6*, e462, doi:10.1038/bcj.2016.73.
- 339. Hiasa, M.; Teramachi, J.; Oda, A.; Amachi, R.; Harada, T.; Nakamura, S.; Miki, H.; Fujii, S.; Kagawa, K.; Watanabe, K.; et al. Pim-2 Kinase Is an Important Target of Treatment for Tumor Progression and Bone Loss in Myeloma. *Leukemia* **2015**, *29*, 207–217, doi:10.1038/leu.2014.147.
- 340. Teramachi, J.; Hiasa, M.; Oda, A.; Harada, T.; Nakamura, S.; Amachi, R.; Tenshin, H.; Iwasa, M.; Fujii, S.; Kagawa, K.; et al. Pim-2 Is a Critical Target for Treatment of Osteoclastogenesis Enhanced in Myeloma. *Br. J. Haematol.* **2018**, *180*, 581–585, doi:10.1111/bjh.14388.
- 341. Cervantes-Gomez, F.; Chen, L.S.; Orlowski, R.Z.; Gandhi, V. Biological Effects of the Pim Kinase Inhibitor, SGI-1776, in Multiple Myeloma. *Clin. Lymphoma Myeloma Leuk.* **2013**, doi:10.1016/j.clml.2013.05.019.
- 342. Bellon, M.; Nicot, C. Targeting Pim Kinases in Hematological Cancers: Molecular and Clinical Review. *Mol. Cancer* **2023**, *22*, 18, doi:10.1186/s12943-023-01721-1.
- 343. Koblish, H.; Li, Y.-L.; Shin, N.; Hall, L.; Wang, Q.; Wang, K.; Covington, M.; Marando, C.; Bowman, K.; Boer, J.; et al. Preclinical Characterization of INCB053914, a Novel Pan-PIM Kinase Inhibitor, Alone and in Combination with Anticancer Agents, in Models of Hematologic Malignancies. *PloS One* **2018**, *13*, e0199108, doi:10.1371/journal.pone.0199108.
- 344. Patel, M.R.; Donnellan, W.; Byrne, M.; Asch, A.S.; Zeidan, A.M.; Baer, M.R.; Fathi, A.T.; Kuykendall, A.T.; Zheng, F.; Walker, C.; et al. Phase 1/2 Study of the Pan-PIM Kinase Inhibitor INCB053914 Alone or in Combination With Standard-of-Care Agents in Patients With Advanced Hematologic Malignancies. *Clin. Lymphoma Myeloma Leuk.* **2023**, *23*, 674–686, doi:10.1016/j.clml.2023.05.002.
- 345. Cortes, J.; Tamura, K.; DeAngelo, D.J.; de Bono, J.; Lorente, D.; Minden, M.; Uy, G.L.; Kantarjian, H.; Chen, L.S.; Gandhi, V.; et al. Phase I Studies of AZD1208, a Proviral Integration Moloney Virus Kinase Inhibitor in Solid and Haematological Cancers. *Br. J. Cancer* **2018**, *118*, 1425–1433, doi:10.1038/s41416-018-0082-1.
- 346. Paíno, T.; Garcia-Gomez, A.; González-Méndez, L.; San-Segundo, L.; Hernández-García, S.; López-Iglesias, A.-A.; Algarín, E.M.; Martín-Sánchez, M.; Corbacho, D.; Ortiz-de-Solorzano, C.; et al. The Novel Pan-PIM Kinase Inhibitor, PIM447, Displays Dual Antimyeloma and Bone-Protective Effects, and Potently Synergizes with Current Standards of Care. *Clin. Cancer Res.* **2017**, *23*, 225–238, doi:10.1158/1078-0432.CCR-16-0230.
- 347. Paíno, T.; González-Méndez, L.; San-Segundo, L.; Corchete, L.A.; Hernández-García, S.; Díaz-Tejedor, A.; Algarín, E.M.; Mogollón, P.; Martín-Sánchez, M.; Gutiérrez, N.C.; et al. Protein Translation Inhibition Is Involved in the Activity of the Pan-PIM Kinase Inhibitor PIM447 in Combination with Pomalidomide-Dexamethasone in Multiple Myeloma. *Cancers* **2020**, *12*, 2743, doi:10.3390/cancers12102743.
- 348. Raab, M.S.; Thomas, S.K.; Ocio, E.M.; Guenther, A.; Goh, Y.-T.; Talpaz, M.; Hohmann, N.; Zhao, S.; Xiang, F.; Simon, C.; et al. The First-in-Human Study of the Pan-PIM Kinase

- Inhibitor PIM447 in Patients with Relapsed and/or Refractory Multiple Myeloma. *Leukemia* **2019**, *33*, 2924–2933, doi:10.1038/s41375-019-0482-0.
- 349. Iida, S.; Sunami, K.; Minami, H.; Hatake, K.; Sekiguchi, R.; Natsume, K.; Ishikawa, N.; Rinne, M.L.; Taniwaki, M. A Phase I, Dose-Escalation Study of Oral PIM447 in Japanese Patients with Relapsed and/or Refractory Multiple Myeloma. *Int. J. Hematol.* **2021**, doi:10.1007/s12185-021-03096-9.
- 350. Mascarenhas, J.O.; Rampal, R.; El Chaer, F.; Gupta, V.; Shimoda, K.; Kiladjian, J.-J.; Passamonti, F.; Bose, P.; Scandura, J.M.; Mesa, R.; et al. A Phase 1/2 Study of Nuvisertib (TP-3654), an Investigational Selective PIM1 Kinase Inhibitor, in Combination with JAK Inhibitors Ruxolitinib or Momelotinib in Patients with Myelofibrosis. *Blood* **2024**, *144*, 6629, doi:10.1182/blood-2024-200268.
- 351. Martinelli, G.; Santoro, A.; Gambacorti-Passerini, C.; Vives Polo, S.; Solomon, S.R.; Mukherjee, S.; Levy, M.Y.; Wierzbowska, A.; Calbacho, M.; Angelosanto, N.; et al. Phase 1/2 Study of SEL24/MEN1703, a First-in-Class Dual PIM/FLT3 Kinase Inhibitor, in Patients with IDH1/2-Mutated Acute Myeloid Leukemia: The DIAMOND-01 Trial. *J. Clin. Oncol.* **2022**, *40*, 7024–7024, doi:10.1200/JCO.2022.40.16 suppl.7024.
- 352. Martinelli, G.; Santoro, A.; Gambacorti-Passerini, C.; Polo, S.V.; Solomon, S.R.; Mukherjee, S.; Lech-Maranda, E.; Levy, M.Y.; Wierzbowska, A.; Calbacho-Robles, M.; et al. AML-389 Phase 1/2 Study of SEL24/MEN1703, a First-in-Class Dual PIM/FLT3 Kinase Inhibitor, in Patients With IDH1/2-Mutated Acute Myeloid Leukemia: The DIAMOND-01 Trial. *Clin. Lymphoma Myeloma Leuk.* **2022**, *22*, S243–S244, doi:10.1016/S2152-2650(22)01282-4.
- 353. Szydłowski, M.; Garbicz, F.; Jabłońska, E.; Górniak, P.; Komar, D.; Pyrzyńska, B.; Bojarczuk, K.; Prochorec-Sobieszek, M.; Szumera-Ciećkiewicz, A.; Rymkiewicz, G.; et al. Inhibition of PIM Kinases in DLBCL Targets MYC Transcriptional Program and Augments the Efficacy of Anti-CD20 Antibodies. *Cancer Res.* **2021**, *81*, 6029–6043, doi:10.1158/0008-5472.CAN-21-1023.
- 354. Ryvu Therapeutics SA An Open Label, Phase 2 Clinical Trial of MEN1703 as Monotherapy and in Combination With Glofitamab in Patients With Relapsed or Refractory Aggressive B-Cell Non-Hodgkin Lymphoma; clinicaltrials.gov, 2025;
- 355. Gulla', A.; Anderson, K.C. Multiple Myeloma: The (r)Evolution of Current Therapy and a Glance into the Future. *Haematologica* **2020**, *105*, 2358–2367, doi:10.3324/haematol.2020.247015.
- 356. Rees, M.J.; D'Agostino, M.; Leypoldt, L.B.; Kumar, S.; Weisel, K.C.; Gay, F. Navigating High-Risk and Ultrahigh-Risk Multiple Myeloma: Challenges and Emerging Strategies. *Am. Soc. Clin. Oncol. Educ. Book* **2024**, *44*, e433520, doi:10.1200/EDBK 433520.
- 357. Paul, B.; Anwer, F.; Raza, S.; Mammadzadeh, A.; Khasawneh, B.; Shatnawi, S.; McGuirk, J.; Ahmed, N.; Mahmoudjafari, Z.; Mushtaq, M.; et al. Comparative Meta-Analysis of Triplet vs. Quadruplet Induction Regimens in Newly Diagnosed, Treatment Naïve, Multiple Myeloma. *Cancers* **2024**, *16*, 2938, doi:10.3390/cancers16172938.
- 358. Jafari, R.; Almqvist, H.; Axelsson, H.; Ignatushchenko, M.; Lundbäck, T.; Nordlund, P.; Molina, D.M. The Cellular Thermal Shift Assay for Evaluating Drug Target Interactions in Cells. *Nat. Protoc.* **2014**, *9*, 2100–2122, doi:10.1038/nprot.2014.138.
- 359. Fink, S.; Zugelder, L.; Roth, B.; Brandt, E.; Meloche, S.; Izsvák, Z.; Bargou, R.C.; Stühmer, T. A Simple Approach for Multi-Targeted shRNA-Mediated Inducible Knockdowns Using Sleeping Beauty Vectors. *PLOS ONE* **2018**, *13*, e0205585, doi:10.1371/journal.pone.0205585.

- 360. Chomczynski, P.; Sacchi, N. Single-Step Method of RNA Isolation by Acid Guanidinium Thiocyanate-Phenol-Chloroform Extraction. *Anal. Biochem.* **1987**, *162*, 156–159, doi:10.1006/abio.1987.9999.
- 361. Tsherniak, A.; Vazquez, F.; Montgomery, P.G.; Weir, B.A.; Kryukov, G.; Cowley, G.S.; Gill, S.; Harrington, W.F.; Pantel, S.; Krill-Burger, J.M.; et al. Defining a Cancer Dependency Map. *Cell* **2017**, *170*, 564-576.e16, doi:10.1016/j.cell.2017.06.010.
- 362. Aguilar, S.V.; Aguilar, O.; Allan, R.; Amir, E.A.D.; Angeli, V.; Artyomov, M.N.; Asinovski, N.; Astarita, J.; Austen, K.F.; Bajpai, G.; et al. ImmGen at 15. *Nat. Immunol.* **2020**, *21*, 700–703, doi:10.1038/s41590-020-0687-4.
- 363. Human Cell Atlas Available online: https://www.humancellatlas.org/ (accessed on 29 September 2023).
- 364. THE TABULA SAPIENS CONSORTIUM The Tabula Sapiens: A Multiple-Organ, Single-Cell Transcriptomic Atlas of Humans. *Science* **2022**, *376*, eabl4896, doi:10.1126/science.abl4896.
- 365. Jang, J.S.; Li, Y.; Mitra, A.K.; Bi, L.; Abyzov, A.; van Wijnen, A.J.; Baughn, L.B.; Van Ness, B.; Rajkumar, V.; Kumar, S.; et al. Molecular Signatures of Multiple Myeloma Progression through Single Cell RNA-Seq. *Blood Cancer J.* **2019**, *9*, 1–10, doi:10.1038/s41408-018-0160-x.
- 366. Silva, A.S.; Canevarolo, R.; Sudalagunta, P.R.; Meads, M.; Silva, M.; zhao, X.; Magaletti, D.; Alugubelli, R.R.; Avila, G.D.; Persi, E.; et al. Epigenetic Plasticity Drives Carcinogenesis and Multi-Therapy Resistance in Multiple Myeloma 2025.
- 367. Gygi, S.P.; Rochon, Y.; Franza, B.R.; Aebersold, R. Correlation between Protein and mRNA Abundance in Yeast. *Mol. Cell. Biol.* **1999**, *19*, 1720–1730.
- 368. Misiewicz-Krzeminska, I.; de Ramón, C.; Corchete, L.A.; Krzeminski, P.; Rojas, E.A.; Isidro, I.; García-Sanz, R.; Martínez-López, J.; Oriol, A.; Bladé, J.; et al. Quantitative Expression of Ikaros, IRF4, and PSMD10 Proteins Predicts Survival in VRD-Treated Patients with Multiple Myeloma. *Blood Adv.* **2020**, *4*, 6023–6033, doi:10.1182/bloodadvances.2020002711.
- 369. Budczies, J.; Klauschen, F.; Sinn, B.V.; Győrffy, B.; Schmitt, W.D.; Darb-Esfahani, S.; Denkert, C. Cutoff Finder: A Comprehensive and Straightforward Web Application Enabling Rapid Biomarker Cutoff Optimization. *PloS One* **2012**, 7, e51862, doi:10.1371/journal.pone.0051862.
- 370. Chapuy, B.; McKeown, M.R.; Lin, C.Y.; Monti, S.; Roemer, M.G.M.; Qi, J.; Rahl, P.B.; Sun, H.H.; Yeda, K.T.; Doench, J.G.; et al. Discovery and Characterization of Super-Enhancer-Associated Dependencies in Diffuse Large B Cell Lymphoma. *Cancer Cell* **2013**, *24*, 777–790, doi:10.1016/j.ccr.2013.11.003.
- 371. Jia, Y.; Zhou, J.; Tan, T.K.; Chung, T.-H.; Wong, R.W.J.; Chooi, J.-Y.; Lim, J.S.L.; Sanda, T.; Ooi, M.; De Mel, S.; et al. Myeloma-Specific Superenhancers Affect Genes of Biological and Clinical Relevance in Myeloma. *Blood Cancer J.* **2021**, *11*, 32, doi:10.1038/s41408-021-00421-7.
- 372. Lovén, J.; Hoke, H.A.; Lin, C.Y.; Lau, A.; Orlando, D.A.; Vakoc, C.R.; Bradner, J.E.; Lee, T.I.; Young, R.A. Selective Inhibition of Tumor Oncogenes by Disruption of Super-Enhancers. *Cell* **2013**, *153*, 320–334, doi:10.1016/j.cell.2013.03.036.
- 373. Whyte, W.A.; Orlando, D.A.; Hnisz, D.; Abraham, B.J.; Lin, C.Y.; Kagey, M.H.; Rahl, P.B.; Lee, T.I.; Young, R.A. Master Transcription Factors and Mediator Establish Super-Enhancers at Key Cell Identity Genes. *Cell* **2013**, *153*, 307–319, doi:10.1016/j.cell.2013.03.035.

- 374. Kruidering, M.; Evan, G.I. Caspase-8 in Apoptosis: The Beginning of "the End"? *IUBMB Life* **2000**, *50*, 85–90, doi:10.1080/713803693.
- 375. Paíno, T.; Garcia-Gomez, A.; González-Méndez, L.; San-Segundo, L.; Hernández-García, S.; López-Iglesias, A.-A.; Algarín, E.M.; Martín-Sánchez, M.; Corbacho, D.; Ortiz-de-Solorzano, C.; et al. The Novel Pan-PIM Kinase Inhibitor, PIM447, Displays Dual Antimyeloma and Bone-Protective Effects, and Potently Synergizes with Current Standards of Care. *Clin. Cancer Res.* **2017**, *23*, 225–238, doi:10.1158/1078-0432.CCR-16-0230.
- 376. Giatromanolaki, A.; Bai, M.; Margaritis, D.; Bourantas, K.L.; Koukourakis, M.I.; Sivridis, E.; Gatter, K.C. Hypoxia and Activated VEGF/Receptor Pathway in Multiple Myeloma. *Anticancer Res.* **2010**, *30*, 2831–2836.
- 377. Yao, L.; Romero, M.J.; Toque, H.A.; Yang, G.; Caldwell, R.B.; Caldwell, R.W. The Role of RhoA/Rho Kinase Pathway in Endothelial Dysfunction. *J. Cardiovasc. Dis. Res.* **2010**, *1*, 165–170, doi:10.4103/0975-3583.74258.
- 378. Hur, J.; Yoon, C.-H.; Kim, H.-S.; Choi, J.-H.; Kang, H.-J.; Hwang, K.-K.; Oh, B.-H.; Lee, M.-M.; Park, Y.-B. Characterization of Two Types of Endothelial Progenitor Cells and Their Different Contributions to Neovasculogenesis. *Arterioscler. Thromb. Vasc. Biol.* **2004**, *24*, 288–293, doi:10.1161/01.ATV.0000114236.77009.06.
- 379. Eggermann, J.; Kliche, S.; Jarmy, G.; Hoffmann, K.; Mayr-Beyrle, U.; Debatin, K.M.; Waltenberger, J.; Beltinger, C. Endothelial Progenitor Cell Culture and Differentiation in Vitro: A Methodological Comparison Using Human Umbilical Cord Blood. *Cardiovasc. Res.* **2003**, *58*, 478–486, doi:10.1016/s0008-6363(03)00252-9.
- 380. Kaplan, R.N.; Riba, R.D.; Zacharoulis, S.; Bramley, A.H.; Vincent, L.; Costa, C.; MacDonald, D.D.; Jin, D.K.; Shido, K.; Kerns, S.A.; et al. VEGFR1-Positive Haematopoietic Bone Marrow Progenitors Initiate the Pre-Metastatic Niche. *Nature* **2005**, 438, 820–827, doi:10.1038/nature04186.
- 381. Werner, N.; Kosiol, S.; Schiegl, T.; Ahlers, P.; Walenta, K.; Link, A.; Böhm, M.; Nickenig, G. Circulating Endothelial Progenitor Cells and Cardiovascular Outcomes. *N. Engl. J. Med.* **2005**, *353*, 999–1007, doi:10.1056/NEJMoa043814.
- 382. Iga, T.; Kobayashi, H.; Kusumoto, D.; Sanosaka, T.; Fujita, N.; Tai-Nagara, I.; Ando, T.; Takahashi, T.; Matsuo, K.; Hozumi, K.; et al. Spatial Heterogeneity of Bone Marrow Endothelial Cells Unveils a Distinct Subtype in the Epiphysis. *Nat. Cell Biol.* **2023**, *25*, 1415–1425, doi:10.1038/s41556-023-01240-7.
- 383. Tomasik, B.; Garbicz, F.; Braun, M.; Bieńkowski, M.; Jassem, J. Heterogeneity in Precision Oncology. *Camb. Prisms Precis. Med.* **2023**, 1–37, doi:10.1017/pcm.2023.23.
- 384. Torres-Ayuso, P.; Katerji, M.; Mehlich, D.; Lookingbill, S.A.; Sabbasani, V.R.; Liou, H.; Casillas, A.L.; Chauhan, S.S.; Serwa, R.; Rubin, M.R.; et al. PIM1 Targeted Degradation Prevents the Emergence of Chemoresistance in Prostate Cancer. *Cell Chem. Biol.* **2024**, *31*, 326-337.e11, doi:10.1016/j.chembiol.2023.10.023.
- 385. Torres-Ayuso, P.; Brognard, J. Defeating Kinases That Promote Tumorigenesis through Non-Catalytic Functions with PROTACs PIM Kinase as an Example. *Expert Opin. Ther. Targets* **2025**, *29*, 189–191, doi:10.1080/14728222.2025.2500418.
- 386. Enzler, T.; Bonizzi, G.; Silverman, G.J.; Otero, D.C.; Widhopf, G.F.; Anzelon-Mills, A.; Rickert, R.C.; Karin, M. Alternative and Classical NF-κB Signaling Retain Autoreactive B Cells in the Splenic Marginal Zone and Result in Lupus-like Disease. *Immunity* **2006**, 25, 403–415, doi:10.1016/j.immuni.2006.07.010.

- 387. Asano, J.; Nakano, A.; Oda, A.; Amou, H.; Hiasa, M.; Takeuchi, K.; Miki, H.; Nakamura, S.; Harada, T.; Fujii, S.; et al. The Serine/Threonine Kinase Pim-2 Is a Novel Anti-Apoptotic Mediator in Myeloma Cells. *Leukemia* **2011**, *25*, 1182–1188, doi:10.1038/leu.2011.60.
- 388. Macdonald, A.; Campbell, D.G.; Toth, R.; McLauchlan, H.; Hastie, C.J.; Arthur, J.S.C. Pim Kinases Phosphorylate Multiple Sites on Bad and Promote 14-3-3 Binding and Dissociation from Bcl-XL. *BMC Cell Biol.* **2006**, *7*, 1, doi:10.1186/1471-2121-7-1.
- 389. Raab, M.S.; Thomas, S.K.; Ocio, E.M.; Guenther, A.; Goh, Y.-T.; Talpaz, M.; Hohmann, N.; Zhao, S.; Xiang, F.; Simon, C.; et al. The First-in-Human Study of the Pan-PIM Kinase Inhibitor PIM447 in Patients with Relapsed and/or Refractory Multiple Myeloma. *Leukemia* **2019**, *33*, 2924–2933, doi:10.1038/s41375-019-0482-0.
- 390. Iida, S.; Sunami, K.; Minami, H.; Hatake, K.; Sekiguchi, R.; Natsume, K.; Ishikawa, N.; Rinne, M.; Taniwaki, M. A Phase I, Dose-Escalation Study of Oral PIM447 in Japanese Patients with Relapsed and/or Refractory Multiple Myeloma. *Int. J. Hematol.* **2021**, *113*, 797–806, doi:10.1007/s12185-021-03096-9.
- 391. Cortes, J.; Tamura, K.; DeAngelo, D.J.; de Bono, J.; Lorente, D.; Minden, M.; Uy, G.L.; Kantarjian, H.; Chen, L.S.; Gandhi, V.; et al. Phase I Studies of AZD1208, a Proviral Integration Moloney Virus Kinase Inhibitor in Solid and Haematological Cancers. *Br. J. Cancer* **2018**, *118*, 1425–1433, doi:10.1038/s41416-018-0082-1.
- 392. Astex Pharmaceuticals, Inc. Safety Study to Determine the Maximum Tolerated Dose, Pharmacokinetics and Pharmacodynamics of SGI-1776, a PIM Kinase Inhibitor, in Subjects With Hormone and Docetaxel Refractory Prostate Cancer and Relapsed/Refractory Non Hodgkin's Lymphoma; clinicaltrials.gov, 2024;
- 393. Czardybon, W.; Windak, R.; Dolata, I.; Salwińska, M.; Szydlowski, M.; Sewastianik, T.; Białopiotrowicz, E.; Mądro, E.; Lech-Marańda, E.; Budziszewska, B.K.; et al. Abstract 1749: Preclinical Characterization of SEL24-B489, a Dual PIM/FLT3 Inhibitor for the Treatment of Hematological Malignancies. *Cancer Res.* **2014**, *74*, 1749, doi:10.1158/1538-7445.AM2014-1749.
- 394. Burslem, G.M.; Smith, B.E.; Lai, A.C.; Jaime-Figueroa, S.; McQuaid, D.C.; Bondeson, D.P.; Toure, M.; Dong, H.; Qian, Y.; Wang, J.; et al. The Advantages of Targeted Protein Degradation over Inhibition: A RTK Case Study. *Cell Chem. Biol.* **2018**, *25*, 67-77.e3, doi:10.1016/j.chembiol.2017.09.009.
- 395. Xue, Z.; Han, M.; Sun, T.; Wu, Y.; Xing, W.; Mu, F.; Zhang, Z.; Liu, J.; Liang, X.; Ling, L.; et al. PIM1 Instigates Endothelial-to-Mesenchymal Transition to Aggravate Atherosclerosis. *Theranostics* **2025**, *15*, 745–765, doi:10.7150/thno.102597.
- 396. Jensen, C.C.; Clements, A.N.; Liou, H.; Ball, L.E.; Bethard, J.R.; Langlais, P.R.; Toth, R.K.; Chauhan, S.S.; Casillas, A.L.; Daulat, S.R.; et al. PIM1 Phosphorylates ABI2 to Enhance Actin Dynamics and Promote Tumor Invasion. *J. Cell Biol.* **2023**, *222*, e202208136, doi:10.1083/jcb.202208136.
- 397. Santio, N.M.; Vainio, V.; Hoikkala, T.; Mung, K.L.; Lång, M.; Vahakoski, R.; Zdrojewska, J.; Coffey, E.T.; Kremneva, E.; Rainio, E.-M.; et al. PIM1 Accelerates Prostate Cancer Cell Motility by Phosphorylating Actin Capping Proteins. *Cell Commun. Signal.* **2020**, *18*, 121, doi:10.1186/s12964-020-00618-6.
- 398. Seo, J.; Ko, R.; Kim, M.; Seo, J.; Lee, H.; Kim, D.; Jeong, W.; Kim, H.S.; Lee, S.Y. Pim1 Promotes the Maintenance of Bone Homeostasis by Regulating Osteoclast Function. *Exp. Mol. Med.* **2025**, *57*, 733–744, doi:10.1038/s12276-025-01421-4.

- 399. Paíno, T.; Garcia-Gomez, A.; González-Méndez, L.; San-Segundo, L.; Hernández-García, S.; López-Iglesias, A.-A.; Algarín, E.M.; Martín-Sánchez, M.; Corbacho, D.; Ortiz-de-Solorzano, C.; et al. The Novel Pan-PIM Kinase Inhibitor, PIM447, Displays Dual Antimyeloma and Bone-Protective Effects, and Potently Synergizes with Current Standards of Care. *Clin. Cancer Res.* **2017**, *23*, 225–238, doi:10.1158/1078-0432.CCR-16-0230.
- 400. Warfel, N.A.; Kraft, A.S. PIM Kinase (and Akt) Biology and Signaling in Tumors. *Pharmacol. Ther.* **2015**, *151*, 41–49, doi:10.1016/j.pharmthera.2015.03.001.
- 401. Cargnello, M.; Roux, P.P. Activation and Function of the MAPKs and Their Substrates, the MAPK-Activated Protein Kinases. *Microbiol. Mol. Biol. Rev.* **2011**, *75*, 50–83, doi:10.1128/mmbr.00031-10.
- 402. The Landscape of Kinase Inhibitors Available online: https://www.science.org/content/blog-post/landscape-kinase-inhibitors (accessed on 27 October 2025).
- 403. Zippo, A.; De Robertis, A.; Serafini, R.; Oliviero, S. PIM1-Dependent Phosphorylation of Histone H3 at Serine 10 Is Required for MYC-Dependent Transcriptional Activation and Oncogenic Transformation. *Nat. Cell Biol.* **2007**, *9*, 932–944, doi:10.1038/ncb1618.
- 404. Daenthanasanmak, A.; Wu, Y.; Iamsawat, S.; Nguyen, H.D.; Bastian, D.; Zhang, M.; Sofi, M.H.; Chatterjee, S.; Hill, E.G.; Mehrotra, S.; et al. PIM-2 Protein Kinase Negatively Regulates T Cell Responses in Transplantation and Tumor Immunity. *J. Clin. Invest.* **2018**, *128*, 2787–2801, doi:10.1172/JCI95407.
- 405. Li, T.; Chen, Z.J. The cGAS-cGAMP-STING Pathway Connects DNA Damage to Inflammation, Senescence, and Cancer. *J. Exp. Med.* **2018**, *215*, 1287–1299, doi:10.1084/jem.20180139.
- 406. Amersfoort, J.; Eelen, G.; Carmeliet, P. Immunomodulation by Endothelial Cells Partnering up with the Immune System? *Nat. Rev. Immunol.* **2022**, *22*, 576–588, doi:10.1038/s41577-022-00694-4.

# 7 Appendix

## 7.1 Bioethical committee approval

### Komisja Bioetyczna

#### przy Instytucie Hematologii i Transfuzjologii

ul. I. Gandhi 14, 02 – 776 Warszawa tel.: (022) 34 96 472

#### Opinia Nr 43/2016

z dnia 19.12.2016 r.

Na podstawie art. 29 ustawy z dnia 5 grudnia 1996 r. o zawodzie lekarza (Dz.U. z 1997r. Nr 28 poz. 152 z późn. zm.) oraz rozporządzenia Ministra Zdrowia i Opieki Społecznej z dnia 11 maja 1999r. w sprawie szczegółowych zasad powoływania i finansowania oraz trybu działania komisji bioetycznych (Dz.U. Nr 47, poz. 480 oraz Dz.U. z 2007 r. Nr 6, poz.46) Komisja Bioetyczna przy Instytucie Hematologii i Transfuzjologii w Warszawie na posiedzeniu w dn. 19.12.2016 r. przeanalizowała wniosek: "Inhibitory pan-PIM jako racjonalna strategia leczenia celowanego w szpiczaku mnogim zaburzająca jego interakcje z mikrośrodowiskiem".

Kierownik samodzielnej jednostki organizacyjnej: Prof. dr hab. med. Krzysztof Warzocha Opickun naukowy projektu: Prof. nadzw. dr hab. n. med. Przemysław Juszczyński – z-ca Kierownika Kliniki Hematologii Instytutu Hematologii i Transfuzjologii.

Kierownik projektu: Filip Garbicz – student kierunku lekarskiego Warszawskiego Uniwersytetu Medycznego

Finansowanie: Projekt realizowany w ramach projektu Diamentowy Grant (DI2015 007145) przez Ministerstwo Nauki i Szkolnictwa Wyższego

W wyniku przeprowadzonej dyskusji oraz glosowania komisja podjęla uchwałę o pozytywnym zaopiniowaniu w/w projektu badawczego.

Komisja zapoznała się z następującymi dokumentami:

- Wniosek do Komisji Bioetycznej z prośbą o wyrażenie zgody na prowadzenie badania.
- 2. Streszczenie programu badania.
- 3. Formularz: "Świadoma zgoda na udział w badaniu".
- 4. Formularz: "Informacja dla chorego na szpiczaka plazmocytowego".

Komisja działa zgodnie z zasadami Prawidłowego Prowadzenia Badań Klinicznych (GCP) opracowanymi w oparciu o Deklarację Helsińską. Od niniejszej opinii przysługuje odwołanie do Odwoławczej Komisji Bioetycznej przy Ministrze Zdrowia za pośrednictwem Komisji Bioetycznej przy Instytucie Hematologii i Transfuzjologii w Warszawie.

## Lista obecności członków Komisji Bioetycznej przy Instytucie Hematologii i Transfuzjologii na posiedzeniu w dniu 19.12.2016 r.

Lp.	Imię i nazwisko	podpis
1.	Prof. dr hab. med. Stanisław Maj	They.
2	Prof. dr hab. med. Bożena Mariańska	XIII
3	Prof. dr hab.med. Alfred Jerzy Meissner	Mulh
4	Prof. dr hab. med. Magdalena Łętowska	Muh
5	Dr med. Bernadetta Ceglarek	Se
6	Dr med. Jerzy Ratajczak	Protejush
7	Mgr Andrzej Kaliński	
8	Mgr farm. Bożena Wajdyk	ZHaipis/
9	Mgr Małgorzata Piątek	Margovela Signer
10	Ks. Eugeniusz Klimiński	Ext
11	Piel. Sylwia Siarkowska	Shislearly

KOMISJA BIOETYCZNA przy Instytucie Hematologii i Transfuzjologii 02-776 Warszawa, ul. Indiry Gandhi 14 tul. 022 34 36 384, fax 022 34 96 335

Przewodniczący
Prof. dr (hay). med. Stanisław Maj